UNIVERSITY OF KWAZULU-NATAL

Robust Equipment for the Measurement of Vapour-Liquid Equilibrium at High Temperatures and High Pressures

R.A. HARRIS

[B.Sc. (Eng), M.Sc. Eng.]

January, 2004

Robust Equipment for the Measurement of Vapour-Liquid Equilibrium at High Temperatures and High Pressures

Roger A. Harris

A thesis submitted in the
School of Chemical Engineering
University of KwaZulu-Natal
Durban

(All work performed in the
School of Chemical Engineering
University of Natal, Durban
South Africa
and
Department of Industrial Chemistry
University of Oldenburg
Germany)

In fulfillment of the requirements for the degree of
Doctor of Philosophy

January, 2004

"It is a capital mistake to theorise before one has data."

Sir Arthur Conan Doyle

DECLARATION

The work presented in this thesis was performed at the University of Natal, Durban and the University of Oldenburg, Germany from January 2001 to December 2003. The work was supervised by Professor D. Ramjugernath, Professor J.D. Raal and Professor T.M. Letcher.

This thesis is presented as the full requirement for the degree of Ph.D. in Chemical Engineering. All the work presented in this thesis is original unless otherwise stated and has not (in whole or part) been submitted previously to any tertiary institute as part of a degree.

_____

R.A. Harris

I hereby certify that I find this work to be suitable for submission for the degree of Ph.D. in Chemical Engineering.

_____

D. Ramjugernath

ACKNOWLEDGEMENTS

I would like to acknowledge the following people for their contribution to this work:

- Firstly, my supervisors, Professors D. Ramjugernath, J.D. Raal and T.M. Letcher, for their advice and assistance during this project.

- Professor Dr. J. Gmehling, Dr. Kai Fischer, Dr. J. Rarey and the staff and students at the DDBST and LTP (Oldenburg, Germany) for their friendship and assistance during my stay there. In particular Mr. M. Wilken, Mr. R. Wittig and Ms. S. Laue for their involvement in this work.

- The workshop staff, Mr. L. Henwood, K. Jack and K. Robertson, for their help in this project. In particular Mr. L. Henwood for his help in designing, constructing and commissioning the apparatus used in this work.

- NRF and SASOL for Financial support during my degree.

- My colleagues, Kasuren, Prathika, Tyrone, Scott, Minal, Nick, John-Roy, Warren and Nash in the Thermodynamics Research Unit for their ideas and friendship.

- On a personal note my parents, Quenten and Pearl, for years (which have been extended by my continued studying) of support and motivation.

- Michela Soukop (my fiancé) for love and patience during this lengthy period of study.

- Thanks to God for help rendered and prayers answered.

ABSTRACT

In this work VLE data was measured on three different pieces of equipment. Measurements were undertaken in the laboratory of Professor Gmehling in Oldenburg, Germany using two different static cells and in the Thermodynamics Research Unit (TRU), University of Natal, South Africa using a specially designed dynamic still. The three pieces of equipment used are as follows:

i.) Static apparatus of Rarey and Gmehling (1993),

ii.) Static apparatus of Kolbe and Gmehling (1985) as modified by Fischer and Wilken (2001), and,

iii.) Dynamic apparatus of Harris et al. (2003b).

In total 370 data points were measured; fourteen sets of VLE data and eight vapour pressure data sets were measured.

The work undertaken in Germany measured the systems hexane (1) + N-methylformamide (2), benzene (1) + N-methylformamide (2), chlorobenzene (1) + N-methylformamide (2) and acetonitrile (1) + N-methylformamide (2), at 363.15 K using the equipment of Rarey and Gmehling (1993). The systems CO_2 (1) + Napthalene (2) at T = 372.45 K, 403.85 K and 430.65 K and CO_2 (1) + Benzoic acid (2) at T = 403.28 K, 432.62 K and 458.37 K were measured on the equipment of Kolbe and Gmehling (1985) (as modified by Fischer and Wilken (2001)). Apart from the CO_2 (1) + Napthalene (2) system at T = 372.45 K, all the above-mentioned data are new data.

The equipment designed in the TRU was designed to operate between 300 and 700 K and between 1 kPa and 30 MPa. The equipment is of the dynamic recirculating VLE still type (DRVS) and is based on the principles of low-pressure stills. The still is constructed from uniquely machined Stainless-steel components and standard commercial Stainless-steel tubing and valves and is computer controlled to operate either isobarically or isothermally.

Vapour pressures were measured on the new equipment for n-heptane, n-decane, n-dodecane, n-hexadecane, 1-octadecene, 1-hexadecanol and d,l-menthol at low pressures and for acetone at high pressures. These vapour pressure measurements were used as test systems and ranged from 1.00 kPa to 1 000 kPa and from 308.33 K to 583.90 K. Cyclohexane (1) + ethanol (2) at 40 kPa and n-dodecane (1) + 1-octadecene (2) at 26.66 kPa were measured as two isobaric VLE test

systems. The VLE data measured for d,l-menthol (1) + l-isomenthol (2) at $T = 448.15$ K and n-dodecane (1) + 1-octadecene (2) at $P = 3.0$ kPa represent new data measured on the equipment.

All the VLE systems were modeled. Two data reduction methods were investigated:

i.) the combined (γ–ϕ) method, and,

ii.) the direct method (ϕ–ϕ) method.

Several different Gibbs excess models (Wilson, NRTL and UNIQUAC), equations of state (Peng-Robinson and virial) and mixing rules (Huron-Vidal, Wong-Sandler and Twu-Coon) were used in different combinations to find the best fit for the data. The Maher and Smith (1979) method was used to determine infinite dilution activity coefficients from the very smooth data of the N-methylformamide systems. Excess properties were determined for the CO_2 (1) + Napthalene (2) and the CO_2 (1) + Benzoic acid (2) systems.

Although the equipment of Harris et al. (2003b) was able to measure data at high temperatures and elevated pressures, the precission of the data was not as good as was expected. Measuring the system temperature at elevated temperatures was especially problematic. The problem is attributed to the large mass of Stainless-steel used in the construction of the apparatus. To rectify this problem it is suggested that the equipment be modified to be lighter in weight and only capable of measuring VLE at moderate pressures (less than 3 MPa).

TABLE OF CONTENTS

LIST OF FIGURES

LIST OF TABLES

NOMENCLATURE

LIST OF SYMBOLS

a,b	EOS parameters
A	Helmholtz free energy [J/mol]
B	Antoinne coefficient / Second virial coefficient (when accompanied by a subscript)
f	Fugacity
g	NRTL equation fitted parameter
G	Gibbs energy [J/mol]
H	Enthalpy [J/mol]
k	EOS interaction parameter
l	EOS interaction parameter
n	Number of moles
P	Pressure [kPa or MPa]
R	Universal gas constant
t	time
T	Temperature [K]
V	Volume (when accompanied by superscript) / molar volume
x	Liquid phase mole fraction
y	Vapour phase mole fraction
Z	Compressibility factor

GREEK LETTERS

α	NRTL interaction parameter / EOS temperature dependent parameter
δ	Residuals as in $\delta g = g - g^*$
ϕ	fugacity coefficient
γ	Activity coefficient

κ	EOS parameter
λ	Wilson equation fitted parameter
μ	Chemical potential
ω	Acentric factor

SUPERSCRIPTS

E	Excess property
id	ideal
l	Liquid phase
o	Standard state
sat	Saturated
v	Vapour phase
^	In solution property
-	Partial property
*	Experimental value

SUBSCRIPTS

c	Critical point
i, j	Molecular species
m	Mixture property
T	Total
r	Reduced property

ABBREVIATIONS

DRVS	Dynamic recirculating VLE still
EOS	Equation of State
GC	Gas Chromatograph
HPVLE	High pressure vapour-liquid equilibrium
IDAC	Infinite dilution activity coefficient
P-R	Peng-Robinson
TRU	Thermodynamics Research Unit
VLE	Vapour-liquid equilibrium

CHAPTER

ONE

INTRODUCTION

In the field of chemical engineering, two main processes are of fundamental importance. These are reaction and separation processes. Separation processes are costly and constitute the majority of equipment expenditure in chemical plants (Seader and Henley (1998)). They are extremely important as they separate a relatively low value raw chemical mixture into high purity or valuable end products. Most separation processes require mass transfer by diffusion, the driving force and direction of which is governed by thermodynamics with limitations dictated by equilibrium. Numerous methods of separating mixtures of varying complexity exist and as these processes constitute such huge capital and operation costs it is imperative to optimise them.

The optimization of these processes requires extensive knowledge of the chemicals involved. Data required includes values for the pure components such as vapour pressures, density and heat of vaporization and mixture properties such vapour-liquid equilibrium (VLE) and diffusivity data. One of the most important sets of data is the VLE data for the mixture. By nature VLE is so complex that, as yet, there is no reliable theory to accurately predict the data. At present the most effective prediction techniques (such as UNIFAC) are only as good (at best) as the data from which their parameters are derived.

The determination of VLE data is not an easy task nor is it a cheap one. It requires extremely expensive and precise equipment as well as experienced and thorough operators - a single VLE point can cost as much as $ 3 200 (Moser and Kistenmacher (1987) corrected for inflation (3%)). For the data to be useful it needs to be accurate and to extend its application to temperatures and pressures outside the measurement boundaries. Furthermore, it needs to be fitted (and modeled) by a thermodynamic relationship. To exacerbate the costs, current trends show an increased demand for measurements at high pressures and (or) high temperatures. The growth in industry of the use of supercritical fluid extraction requires data at extremely high pressures but usually rather low temperatures. With the increase in environmental responsibility within large corporations, chemical plants can no longer simply incinerate heavy distillation column bottoms.

In order to add value to these bottoms they need to be separated into their pure components. This requires VLE data at low pressures but extremely high temperatures.

As part of this study VLE data were measured in the laboratories of Professor J. Gmehling, University of Oldenburg, Germany. This work constitutes a collaboration between the Thermodynamics Research Unit of the University of KwaZulu-Natal, Durban and the Industrial Chemistry Department of the University of Oldenburg. The work was sponsored by the Forschungszentrum Jülich GmbH (Germany) and the National Research Foundation (South Africa). VLE measurements in Germany ranged from moderate pressures to supercritical measurements for CO_2. The moderate pressure work focused on previously unmeasured systems for industrially important chemicals. The high-pressure CO_2 systems provide valuable data for supercritical behaviour. All these results will eventually be used to further the predictive methods for determining VLE which are being developed and improved at the University of Oldenburg, Germany.

The other part of this study focuses on the design, construction and development of a robust equilibrium still. The aim of the design was to build a still, which would complement the existing apparatus of the Thermodynamics Research Unit (TRU), University of Natal, South Africa and provide a medium for measuring VLE across a broad range of temperatures and pressures.

As a whole, this study increases the knowledge of VLE thermodynamics, as many of the systems measured constitute new data. All the systems measured were regressed and fitted with thermodynamic expressions. Furthermore, the work done on designing and constructing new equipment serves to highlight shortfalls of current equipment as well as limitations of certain types of stills.

CHAPTER

TWO

REVIEW OF EQUIPMENT DEVELOPMENT

2.1 INTRODUCTION

The measurement of vapour-liquid equilibrium (VLE) data requires the use of very specialized, often very complicated, equipment. Furthermore, VLE is measured across a large range of pressures and temperatures. Pressures range from less than 1 kPa to more than 100 MPa and temperatures range from less than 200 K to sometimes greater than 600 K. The measurements themselves can be performed in many different ways with the data usually being expressed in one of three ways: as an isobar (constant pressure), as an isotherm (constant temperature) or as an isopleth (constant composition).

As VLE data are so extensive it is not so surprising that the equipment used to measure it is also extensive. For almost all new situations equipment has to be invented or modified to suit the purpose. It would far exceed the scope of this work to review all the different types of VLE apparatus currently in use. However, in this work three different pieces of equipment were used for the measurement of VLE over a considerable temperature and pressure range, and, as a review of equipment the development of these three pieces of equipment is followed. As in most scientific fields, progress is through the improvement or modification of existing ideas. The development of the equipment used in this work followed the same principle. The following is a description of the improvements and modifications were led to the equipment used in this work.

2.1.1 Equipment Classification

There are many different pieces of equipment available for the measurement of VLE data. Several methods of classification are commonly adopted. Figure 2-1 is a very simplified diagram of modern VLE equipment classification adapted from that of Raal and Mülhbauer (1998).

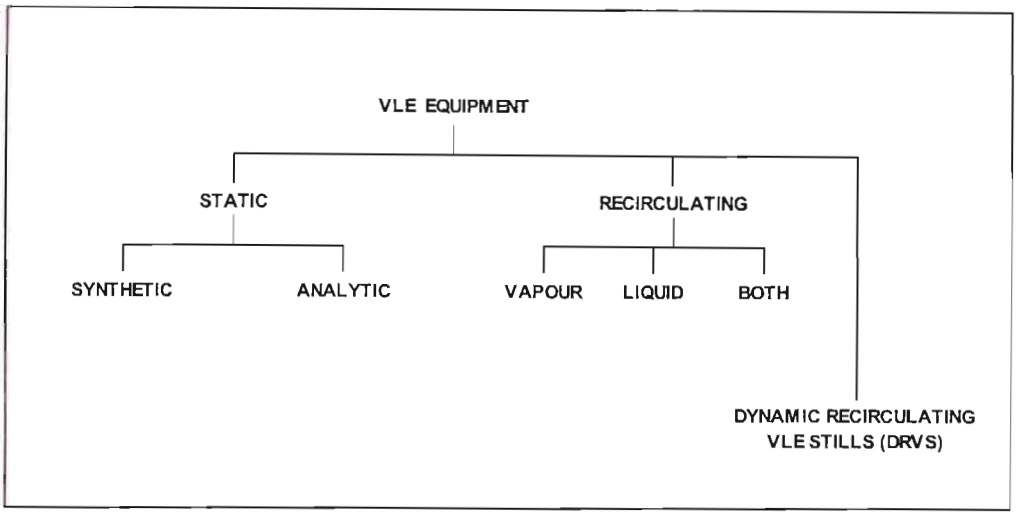

Figure 2-1: Modern VLE equipment classification.

The choice of VLE equipment is dependent on several variables. Most obvious are the pressure and temperature ranges. Further considerations are the systems to be measured (volatility, viscosity and thermal stability) as well as the amount of funding available for the construction and operation of the equipment.

Static Equipment

Static implies that the two phases are not recirculated and coexist in a closed, agitated cell. If the phases are sampled then the equipment is classed as an analytic device. If the phases are not sampled but rather their compositions are calculated (from knowledge of the overall composition of the system) then the device is classified as synthetic.

Static devices can be used for the measurement of high or low pressure VLE. The measurements are usually isothermal with the temperature being maintained by submersing the cell in a bath of oil, water or air. As the equilibrium temperature is dependent on the bath temperature, temperature ranges are restricted by the limits of the heating fluid.

Recirculating Equipment

Recirculating VLE devices recirculate either the vapour or liquid phase or both. Generally they are more complicated and require greater skill in operating. However, they make sampling of the

recirculated phase(s) easier and more reliable. As with the static cells they are cells submersed in a bath of oil, water or air. As such they face the same restrictions as those mentioned above.

Dynamic Recirculating VLE Stills (DRVS)

The DRVS is based on a different principle to the cells mentioned above. Usually DRVSs are comprised of a reboiler, equilibrium chamber and a condenser. Their salient features and operation are described in greater detail later but it is important to note that they are not immersed in a bath and are thus not restricted to the limitations of these fluids. Instead a heater is used to boil the contents of the reboiler and achieve the desired temperature.

2.1.2 Equipment used in this work

Three pieces of equipment were used to measure VLE in this work. Table 2-1 lists the equipment used, its classification and its measurement conditions.

Table 2-1 Equipment used in this work

Equipment	Type	Pressure	Temperature
Rarey and Gmehling (1993)	Static Synthetic	Moderate	Moderate
Kolbe and Gmehling (1986)[1]	Static Synthetic	High	Moderate to High
Harris et al (2003b)	DRVS	Low to Moderate	Moderate to Very High

The equipment of Rarey and Gmehling (1993) and Kolbe and Gmehling (1985) was used in the laboratories of Professor Gmehling, Oldenburg, Germany during a research visit in 2001 made possible by the collaboration between the Thermodynamics Research Unit (University of Natal) and the Department of Industrial Chemistry (University of Oldenburg). The collaboration was funded by the joint research and development project of the Forschungszentrum Jülich GmbH (Germany) and the National Research Foundation (South Africa). The equipment of Rarey and Gmehling was used to measure VLE at moderate temperatures and pressures while the equipment

[1] Modified equipment used in this work as modified by Fischer and Gmehling (1994) and Fischer and Wilken (2001).

of Kolbe and Gmehling (1985) with modifications by Fischer and Wilken (2001) was used for high-pressure – moderate-temperature measurements

The equipment of Harris et al. (2003b) was constructed and used at the University of Natal, Durban. It was used for high-temperature – low-pressure measurements.

2.2 STATIC EQUIPMENT

2.2.1 Features of Static Equipment

Static equipment experimental methods are mentioned in many equipment reviews (Hála et al. (1967), Malanowski (1982b), Marsh (1989), Raal and Mülhbauer (1994) and Raal and Mülhbauer (1998)). These reviews give excellent summaries of the important features of static pieces of equipment. Some of the most common and important features are as follows:

- An agitated equilibrium cell. The equilibrium cell must be isolated from all interferences and must contain the equilibrium mix without unobserved loss or addition of material. The contents of the cell are agitated so as to attain equilibrium rapidly. Agitation can be by stirring or shaking. Accurate temperature and pressure measurements are made in the cell.
- Isothermal bath. The equilibrium cell is kept at the equilibrium temperature by submersion in a bath. The heating fluid in the bath is usually air, water or oil. It is important that the temperature of the bath be accurately controlled and monitored.
- Vacuum system. Before measurements can commence the contents of the equilibrium cell must be evacuated. Some form of vacuum system or procedure is usually used.
- Injection pumps. The components to be measured need to be introduced to the cell via injection pumps.
- Phase sampling (optional).

Figure 2-2 below illustrates these important features.

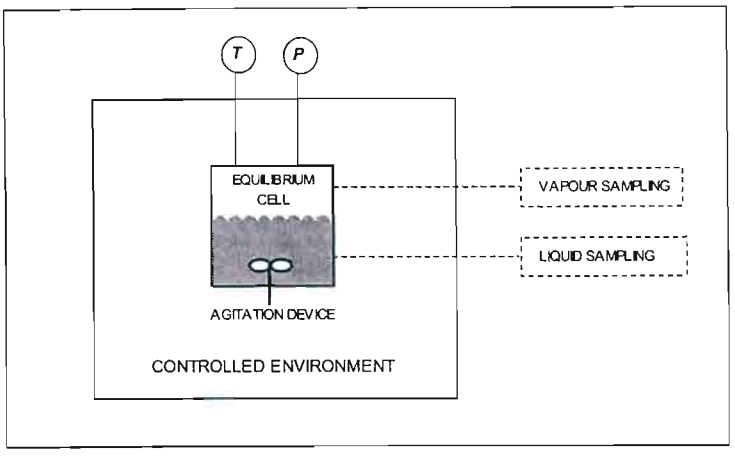

Figure 2-2: Schematic diagram of basic static equipment.

2.3 STATIC SYNTHETIC EQUIPMENT

Both pieces of static equipment, which were used in this work, were of the synthetic type. Thus, the discussion which follows, concentrates on this type of equipment only and follows the progression of this field of study in the past three decades. As explained previously synthetic equipment measures the overall composition to pressure (z_i-P) relationship. This data can then be used to calculate the liquid composition to pressure (x_i-P) relationship. The x_i-P data are calculated using mass balances and equilibrium relationships and is explained in detail in Chapter Three. As a consequence of measuring only z_i-P data the calculated x_i-y_i relationship is only as reliable as the calculation procedure used.

2.3.1 Features of Static Synthetic Equipment

Static synthetic equipment shares all the features mentioned previously with certain added criteria:

- There are no sampling facilities. The lack of sampling facilities implies that the true composition of any phase can only be calculated and never measured. Furthermore, the lack of sampling facilities greatly simplifies the construction of the still and infers that the time taken to measure a single point is greatly reduced as no sampling of the phases is necessary.
- Accurate measurement of the cell volume. As the cell volume is an important variable in calculating the phase compositions it is important that it be known accurately.

- Metered injection pumps. Knowledge of the overall composition (z_i) is essential for the calculation of phase compositions. As there is no sampling facility z_i must be calculated by accurately measuring the quantity of each component added to the cell via metered injection pumps.

Table 2-2 below lists some of the more common static synthetic designs.

Table 2-2 Common static synthetic designs

Author	Operation	T_{max} / K	P_{max} / MPa
Kohn (1961)	isothermal	-	10.4
Meskel-Lessavre et al. (1981)	isothermal	373	5
Konrad et al (1983)	isothermal	450	200
Rousseaux et al. (1983)	isothermal	573	60
Fontalba et al. (1984)	isothermal	433	45
Kolbe and Gmehling (1985)	isothermal	423	1
Ochiogrosso et al. (1986)	isothermal	535	70
Laugier et al. (1990)	isothermal	353	20

2.3.2 The Equipment of Kolbe and Gmehling (1985)

As mentioned previously the equipment of Kolbe and Gmehling (1985) is of the static synthetic type. The equipment, with modifications (Fischer and Gmehling (1994) and Fischer and Wilken (2001)) was used to measure isothermal data for mixtures of CO_2 + Naphthalene and CO_2 + Benzoic acid. The equipment used in this work is designed to operate up to 473.15 K and up to 21 MPa. Although developed during a period (mid 1980's) when much work was being done on static measurement techniques the design is based on the earlier work of Gibbs and van Ness (1972) and operates on the principles explained in that work. In order to explain the development of the equipment of Kolbe and Gmehling (1985) it is necessary to review the equipment of Gibbs and van Ness (1972).

The Equipment of Gibbs and van Ness (1972)

Gibbs and van Ness (1972) developed new apparatus for the measurement of isothermal z_i-P data. It was felt that while previous experimental techniques (Ljunglin and Van Ness (1962) and Van Ness et al. (1967a & b) were sufficiently accurate, they did not produce data rapidly enough. Measurements were slow as a separate experiment was required for each z_i-P data set. This was because pure degassed liquids were distilled directly into the equilibrium cell. Thus, each point required the cell to be cleaned and emptied. To speed up the experimental procedure, Gibbs and van Ness (1972), proposed that pure degassed liquids be fed into piston-cylinder devices. The pure liquids are stored in these devices and then injected into the equilibrium cell when needed. In this manner the composition can be changed in the cell without emptying and cleaning it. Accurate z_i data are obtained by forming mixtures of known composition in the cell and then varying it by adding volumetrically metered doses of pure component from the injection devices (the method is explained in more detail in Chapter Three). In this manner the complete composition range is covered in two runs. Generally 20 to 30 points were produced per binary system.

Figure 2-3 is a schematic diagram of the major components of the apparatus of Gibbs and van Ness (1972).

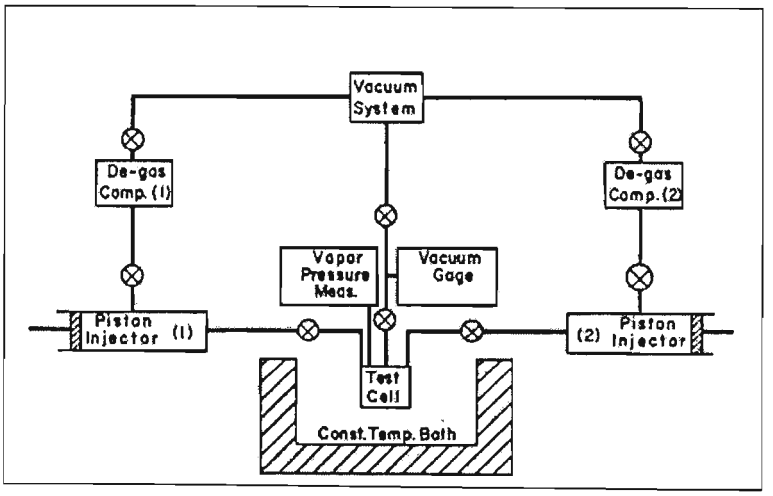

Figure 2-3: Schematic diagram of the apparatus of Gibbs and van Ness (1972).

The equilibrium cell is submerged in a constant temperature water bath with a temperature range of 273.15 to 348.15 K and a stability of ±0.01 K. Figure 2-4 illustrates a single piston injector and the equilibrium cell.

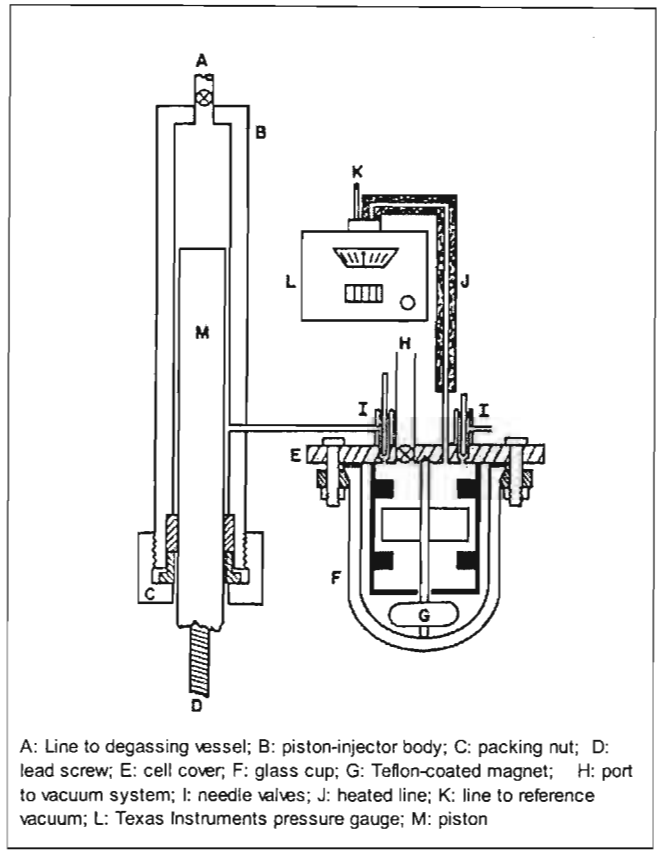

A: Line to degassing vessel; B: piston-injector body; C: packing nut; D: lead screw; E: cell cover; F: glass cup; G: Teflon-coated magnet; H: port to vacuum system; I: needle valves; J: heated line; K: line to reference vacuum; L: Texas Instruments pressure gauge; M: piston

Figure 2-4: Piston injector and equilibrium cell of Gibbs and van Ness (1972).

The Equipment of Kolbe and Gmehling (1985)

As stated above the apparatus of Kolbe and Gmehling (1985) is based on the principles of Gibbs and van Ness (1972). As such the equipment is designed to measure z_i-P data rapidly and accurately. As with the equipment of Gibbs and van Ness (1972) the pure components are stored in piston-injectors. Exactly known quantities of the pure components are added and thus the overall composition is known. The pressure is measured so that z_i-P data are obtained. The equipment is designed to measure temperatures up to 423.15 K and pressures between 100 and 1 000 kPa. Figure 2-5 is a schematic diagram of the equipment.

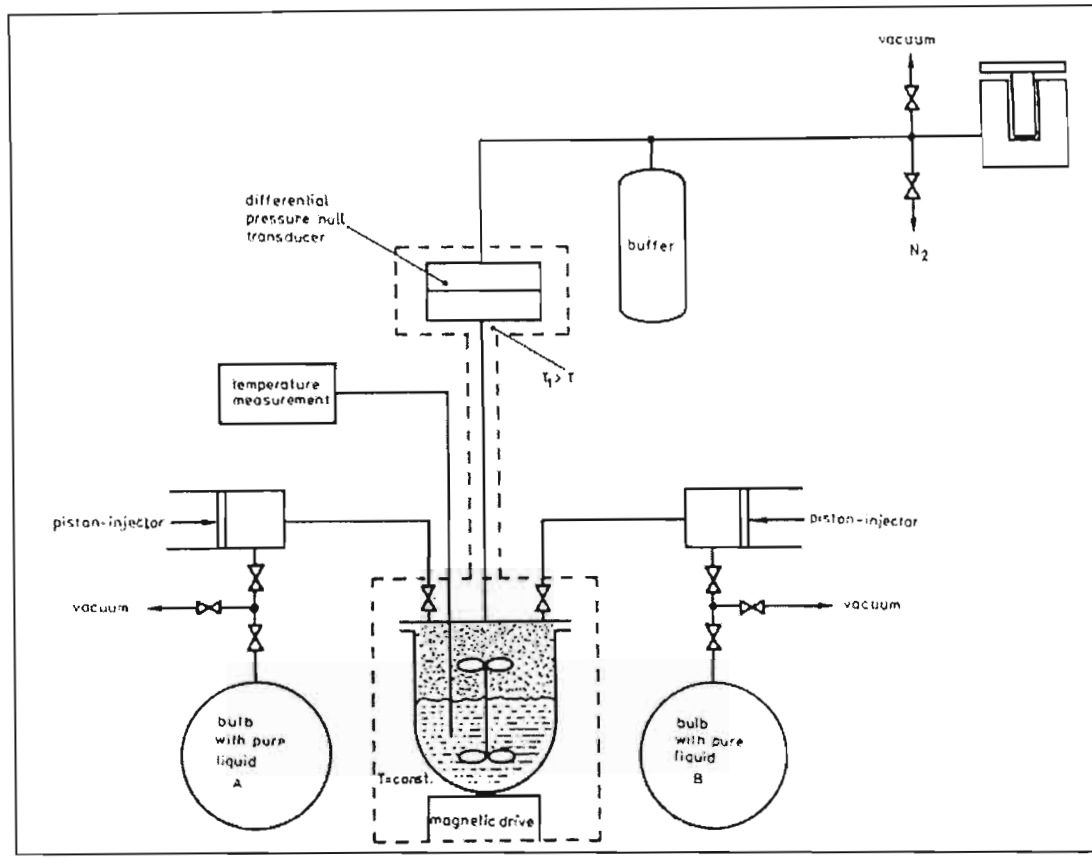

Figure 2-5: Schematic diagram of the apparatus of Kolbe and Gmehling (1985).

The magnetically stirred equilibrium cell is immersed in a thermostatted air bath. The temperature in the air bath can be set to 273.15 to 423.15 K and controlled to within 0.02 K. The temperature is measured with a Hewlett-Packard quartz thermometer and the pressure with a Desgranges and Hout (Type 8000), France, pressure balance. The dosage equipment (piston-injectors) were manufactured by Ruska Inc., Texas and consist of hand-driven pistons. The capacity of the piston-injectors is 0.1 *l* and the accuracy of dosage is ± 0.00001 *l*. The temperature of the pumps is controlled to within 0.5 K.

Figure 2-6 illustrates the equilibrium cell. The cell is made from thick-walled (5 mm) glass and has a volume of 0.18 *l* while the cell lid and valves are 316 SS. The lid is sealed to the cell with a Teflon gasket.

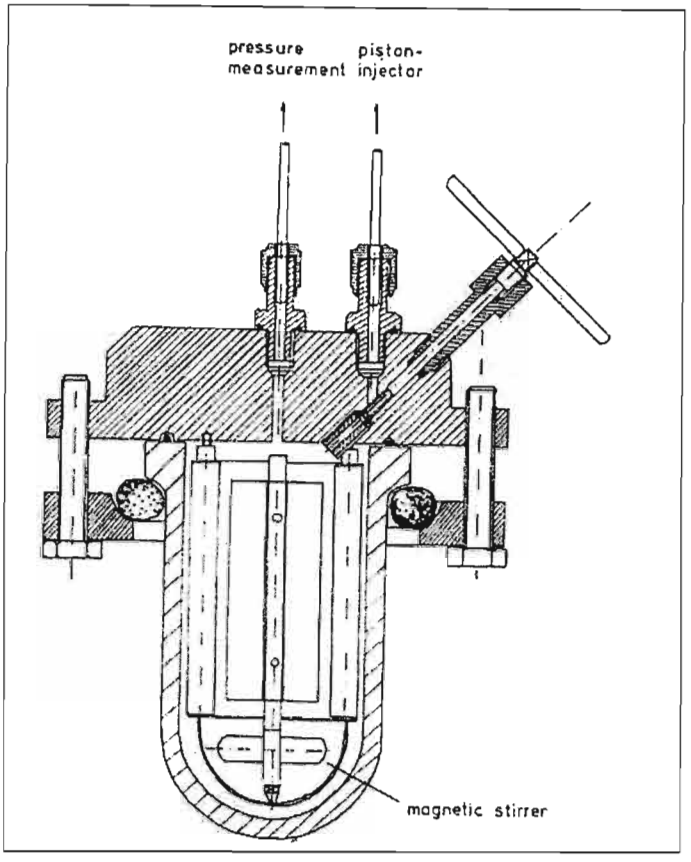

Figure 2-6: Equilibrium cell of Kolbe and Gmehling (1985).

Modifications of Fischer and Gmehling (1994)

Figure 2-7 is a schematic diagram of the equipment used by Fischer and Gmehling (1994). Several improvements were made to the equipment:

- The range of the equipment was extended to 12 MPa by replacing the glass equilibrium cell with a steel one.
- The internal electric motor and stirrer system were replaced with a rotating magnetic field induced by four solenoids.
- The liquid in the piston injectors is kept at a constant temperature ($T \pm 0.1$ K) and pressure ($P \pm 1$ kPa), which correlates to a mole fraction accuracy of $x \pm 0.0001$.

All measurements performed on this still were for subcritical fluids.

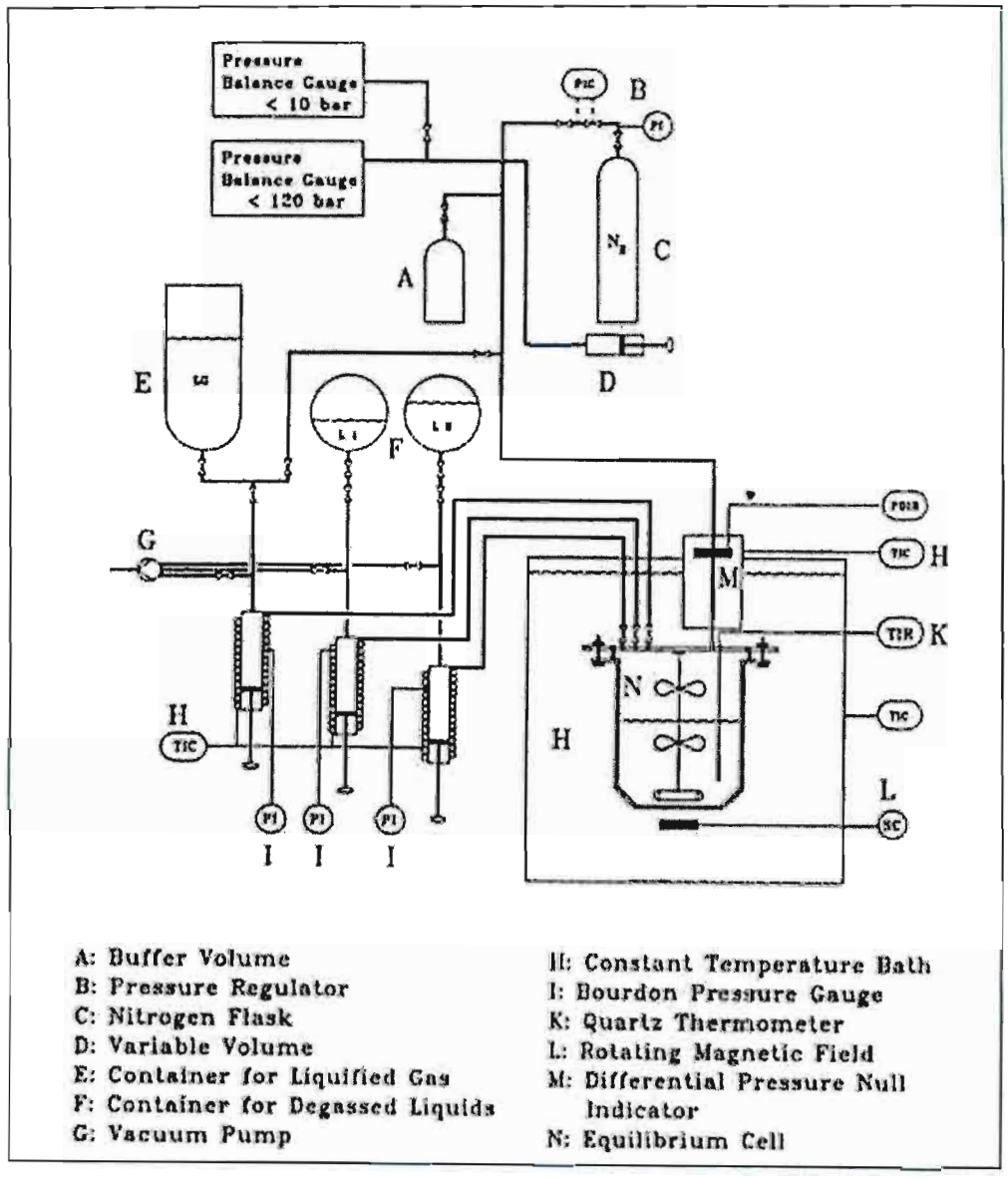

Figure 2-7: Schematic diagram of apparatus of Fischer and Gmehling (1994).

Equipment of Fischer and Wilken (2001)

Certain modifications needed to be made to the equipment so as to measure super-critical fluids as all previous measurements had been for sub-critical conditions. The modifications are detailed

by Fischer and Wilken (2001) and on the Laboratory for Thermophysical Properties GmbH. (LTP) web site. Modifications are as follows:

- Gasses used were stored in the manual piston injection pumps while solids were measured on a mass balance and introduced to the cell prior to experimentation.
- The steel cell was replaced with a titanium cell with sapphire windows.
- The pressure balance used was capable of measuring pressures in excess of 20 MPa.

The experimental set-up is illustrated in Figure 2-8.

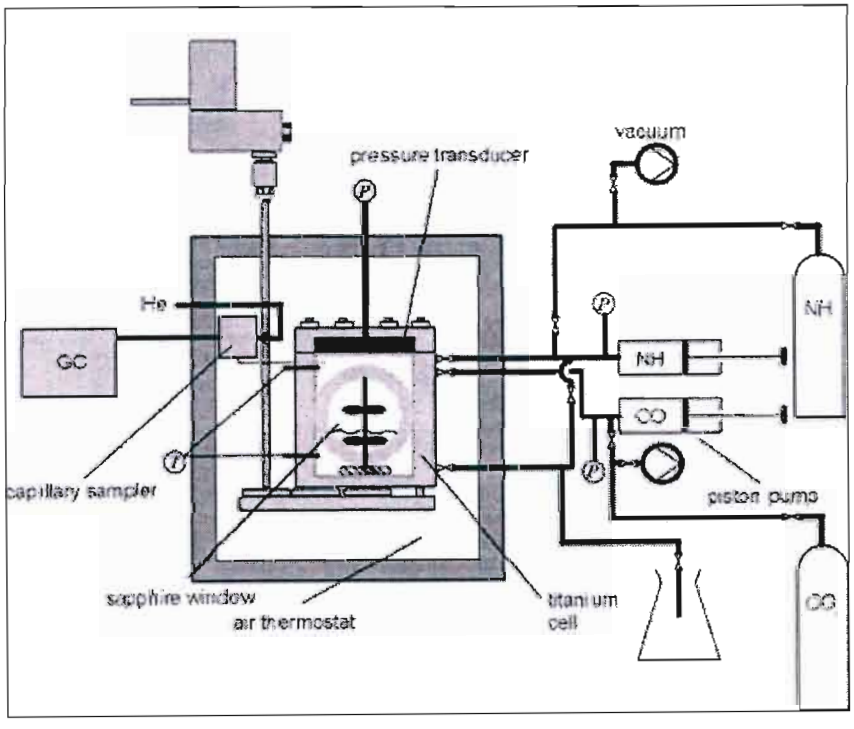

Figure 2-8: Experimental static apparatus of the LTP for high-pressure VLE measurement.

2.3.3 The equipment of Rarey and Gmehling (1993)

Equipment Development

As with the previously discussed apparatus, the equipment of Rarey and Gmehling (1993) is of the static synthetic type. It is computer-operated and is based on the principles of the apparatus of Gibbs and Van Ness (1972) which is discussed above.

General Principles

The equipment used in the measurements of Harris et al. (2003a) was developed by Rarey (1991) and is described by Rarey and Gmehling (1993) and Rarey et al. (1999). The general design of the static equipment is a thermostatted stirred equilibrium cell. This cell is kept at constant temperature by being submersed in a stirred high precision water bath. The cell is injected with known amounts of degassed liquids by an automated high-precision injection pump and allowed to equilibrate. Once equilibrium is reached the pressure of the system is recorded and the composition is changed. Through this method a number of vapour pressure (P) data points at constant temperature (T) are measured for a known overall composition (z_i). Figure 2-9 is a schematic diagram of the equipment.

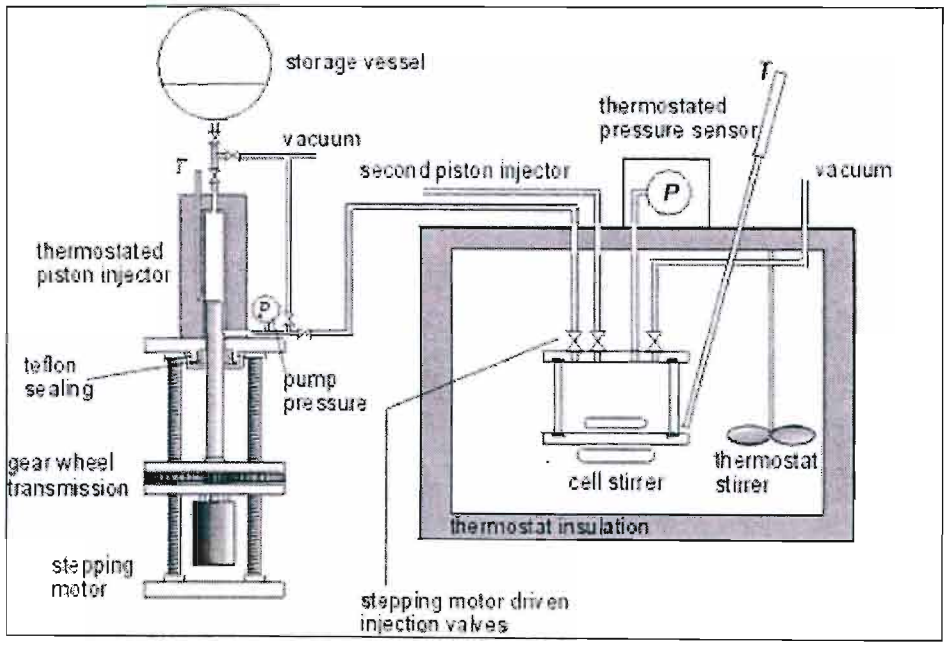

Figure 2-9: Schematic diagram of equipment from Rarey et al. (1999).

The most important features of this still are the automation of the entire equipment and the precision computer controlled injection piston pumps (Gaube (1988) - Figure 2-10). The automation of the equipment makes it possible to measure 40 to 60 VLE points for an isotherm in 3 to 4 days with only 3 to 4 hours of human labour required. The precision injection pump makes it possible to inject small quantities of pure component accurately and thus determine dilute condition VLE. The equipment is described in more detail in Chapter Four and the operation thereof in Chapter Five.

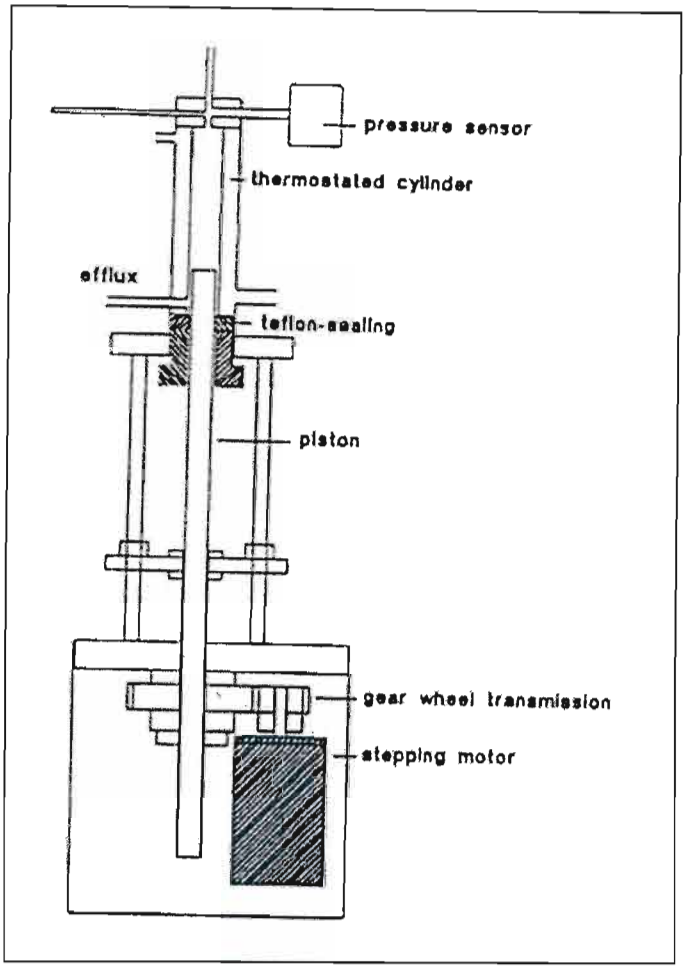

Figure 2-10: Schematic diagram of high-precision injection pump of Gaube (1988).

2.4 RECIRCULATING APPARATUS

2.4.2 Dynamic Equipment

The apparatus designed, constructed and used in this work (as discussed in Chapter Three) recirculates both the vapour and liquid phases, thus, only equipment with dual phase recirculation is discussed here. More detailed descriptions of recirculation equipment are given in some of the previously mentioned reviews.

General considerations

Figure 2-11 is a schematic diagram of the common high-pressure recirculating apparatus. Generally, an equilibrium cell is thermostatted in an air, water or oil bath. The cell is charged with a mixture and allowed to equilibrate. The two resulting phases are circulated and sampled and the pressure in the cell is recorded to produce the required VLE diagram. Table 2-3 lists some of the common phase recirculation high-pressure VLE apparatus from literature.

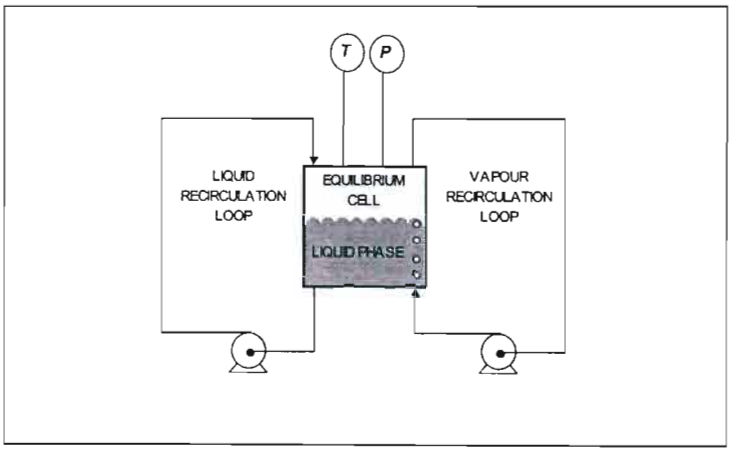

Figure 2-11 Schematic diagram of the common high-pressure recirculating apparatus.

Phase circulation

Both phases are circulated counter-currently (usually). The vapour enters through the bottom of the cell and bubbles through the liquid phase. The liquid enters at the top of the cell and falls to the liquid bulk flowing through the vapour.

Phase sampling

Dual phase circulation simplifies sampling. As there is both a liquid and vapour line, samples are obtained by diverting a part of the stream and isolating it. This isolated sample can then be fed to an analysing device. The added ease of sampling, however, is somewhat negated by the added complexity of phase circulation.

Table 2-3 Common phase recirculation high-pressure VLE apparatus

Author	Still	Operation	Recirculation	Eq. Time	T / K	P / MPA
Suzuki (1990)	R - V & L	Isothermal (AB)	mag. Pumps	8h (init)	334.15	12
Jenings (1989)	CCR - V & L	Isothermal (AB)	mag. Pumps	-	323.15	9
Kim (1989)	CCR - V & L	Isothermal (OB)	mag. Pumps	10 min	430.15	25
Shibata (1989)	CCR - V & L	Isothermal (O)	mag. Pumps	< 1h	422.15	34.5
D'Souza (1988)	CCR - V & L	Isothermal (O)	metering Pumps	-	353.15	17
Iomata	R - V & L	Isothermal & Isobaric (AB)	mag. Pumps	-	413.15	2.1
Morris (1985)	CCR - V & L	Isothermal (OB)	mag. Pumps	15 min	413.15	14.5
Behrens (1983)	CCR - V & L	Isothermal (OB)	mag. Pumps	4 - 8h	373.15	8
Hsu (1985)	R - V / L	Isothermal (AB)	mag. Pumps	2 - 6h	422.15	8
Kniesl (1988)	CCR - V & L	Isothermal & Isobaric (O)	mini-pump	1.5h	425.15	34.5
Wisniewska (1993)	Ebuliometer	Isothermal	L & cond. V	1h	500.15	3
Radosz (1984)	CCR - V & L	Isothermal & Isobaric (AB)	mag. Pumps	15 - 60min	533.15	35
King (1983)	V & L (ocas) R	Isothermal (AB)	air driven pumps	20min ?	773.15	50
Kuk (1983)	CCR - V & L	Isothermal & Isobaric (OB)	factory pumps	-	333.15	20.7
Kubota (1983)	R - V / L	Isothermal (CTB)	HP pump	2h	353.15	80
Muirbrook (1965)	CCR - V & L	Isothermal (CTB)	Vane pumps	-	303.15	103.4
Yorizane (1985)	R - V & L	Isothermal (CTB)	1 cell moveable	3 - 5h	298.15	12.1
Takashima (1986)	R - V, L_1 & L_2	Isothermal (AB)	mag. Pumps	-	308.15	10.3
Adams (1988)	CCR - V & L	Isothermal (AB)	mag. Pumps	5 - 10min	343.15	21.3

R: Recirculation
CCR: Counter current recirculation
V: Vapour
L: Liquid
(AB): Air bath
(OB): Oil Bath
(O): Oven
(CTB): Constant Temperature Bath

Dynamic recirculating VLE still (DRVS)

The DRVS is illustrated in Figure 2-12. The salient features are the equilibrium chamber, reboiler and dual phase recirculation. A binary mixture is placed in the reboiler. The mixture is superheated and the excess energy (superheat) supplies the pumping action that is used to transport the mixture to the equilibrium chamber where the mixture equilibrates and the liquid and vapour phases are disengaged. The liquid and vapour phases are then returned to the reboiler separately and sampled en route.

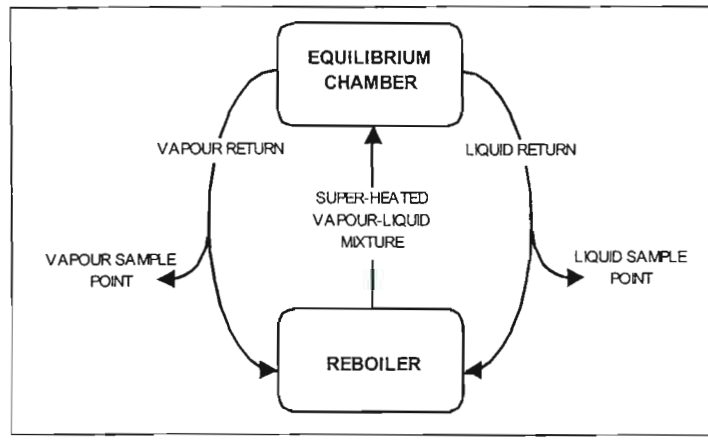

Figure 2-12: Schematic diagram of dynamic apparatus with reboiler.

Comparison of common recirculation apparatus and DRVS

Common Recirculating	DRVS
• Pumps. Requires pumps to recirculate the vapour and liquid phases. One of the challenges in designing recirculating equipment is to design pumps, which cause minimal disturbance to the equilibrium pressure when in operation.	• The design of the DRVS apparatus makes the use of recirculating pumps unnecessary. The liquid component is returned to the reboiler (circulated) by static head. The vapour component is condensed and then returned by static head.
• Degassing of liquids. Liquids need to be degassed before introducing them into the apparatus. Degassing of liquids requires all the dissolved gases to be removed from them prior to experimentation. If liquids are not degassed, the entrained gases can affect the equilibrium pressures.	• No degassing is required as the apparatus degasses the liquids during operation. In the equilibrium chamber the gases are separated from the liquids and follow the vapour stream. The gases, however, do not condense in the condenser as the condenser temperature is always above 263.15 K. The gases are

	thus evacuated via the vacuum pump. (More detail is given in Chapters Three and Four).
• Temperature restrictions. As explained previously, the temperature at which measurements can be made is limited by the thermostatting fluid (air, water or oil).	• There is no thermostatting fluid in this design so the temperature restrictions are due to the heaters in the reboiler and the MOC of the still only.
• Supercritical measurements. Common recirculating apparatus is superb for measuring supercritical fluids. The vapour phase containing non-condensable components is circulated by pumps.	• It is impossible to measure supercritical fluid mixtures in this type of still as the supercritical fluid will not condense and will thus not be recirculated.

2.4.3 DRVS

Malanowski (1982a), Abbott (1986), Marsh (1989) and Raal and Mülhbauer (1998) review DRVS equipment, specifically those used in low-pressure work. The following discussion gives a brief history on the development of this type of still.

Experimental apparatus of Othmer (1928)

One of the first experimental stills to incorporate the idea of a reboiler and be simple, compact and functional was that of Othmer (1928). The still (Figure 2-13) comprises a boiling vessel (reboiler) which is charged with a binary mixture. An electric heater brings the mixture to a boil and the vapour generated passes through the elliptical aperture (E) to the vapour tube. The vapour is condensed in the condenser (G) and collected in the receiver. Once the receiver is full the excess condensate returns to the reboiler.

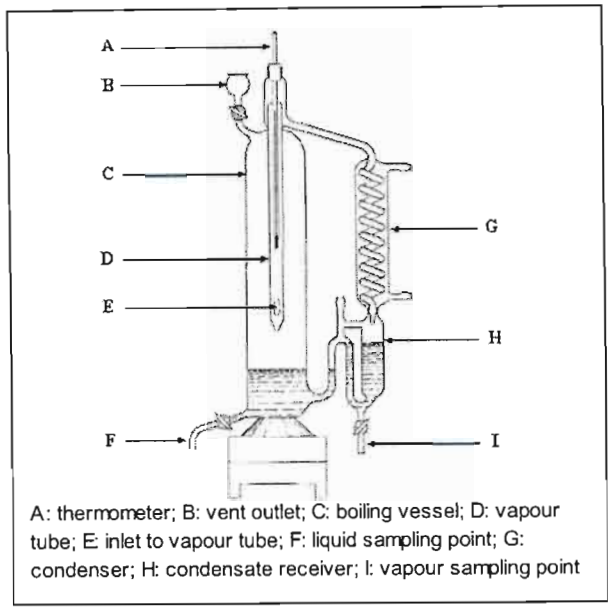

Figure 2-13: Experimental apparatus of Othmer (1928).

The still is run in this manner until equilibrium is reached (30 – 60 minutes). As the still is operated isobarically, the stability of the temperature reading can be used to assess when equilibrium has been reached. Once equilibrium is reached the boiling is stopped and liquid (F) and vapour samples (I) are withdrawn.

Possible sources of error for measurements performed with this still can be attributed to:

- Inaccurate temperature measurement. Measurement of either the liquid or vapour temperature is unacceptable (Raal and Mülhbauer (1998)).
- The design of the condensate receiver. The condensate receiver is too large in proportion to the reboiler and unless the contents are stirred there may be some composition gradient.
- Vapour condensation on the walls of the boiling vessel. If any vapour were to condensate on the walls of the boiling vessel it would change the equilibrium composition. The larger the relative volatility of the system being measured, the larger the possible error incurred. Similarly, if the walls of the vessel are heated, any drop of liquid which is splashed on the walls would evaporate thus resulting in the same problem.
- Not reaching true equilibrium. There is some doubt as to whether the vapour above a boiling liquid is in true equilibrium with it.

Although Othmer's (1928) still only has a vapour recirculation, its concept is important to the stills that follow. Malanowski (1982a) reports that it was the most popular design during the period 1930 to 1949 and that more than 150 papers were published detailing modifications on the original design. Analyses, however, imply that the data produced by these stills are usually inaccurate and thermodynamically inconsistent.

Experimental apparatus of Lee (1931)

Lee (1931) proposed the first still with recirculating vapour and liquid phases (Figure 2-14). A mixture is introduced into the boiling vessel and brought to the boil. The superheated mixture forces a mixture of vapour and liquid up the Cottrell* pump. The mixture comes into contact with the thermometer. The liquid returns directly to the reboiler while the vapour is condensed and the condensate returns to the reboiler via the receiver. Once equilibrium is reached liquid and vapour samples are taken from the boiling vessel and the condensate receiver respectively.

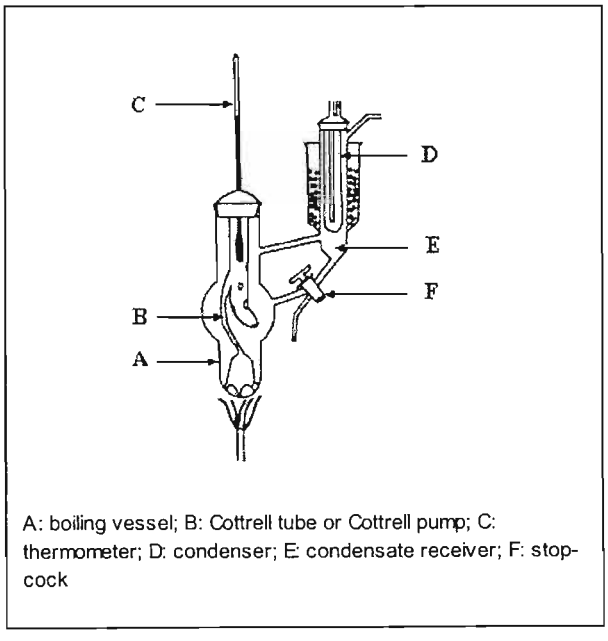

A: boiling vessel; B: Cottrell tube or Cottrell pump; C: thermometer; D: condenser; E: condensate receiver; F: stop-cock

Figure 2-14: Apparatus of Lee (1931).

Possible problems or sources of error for measurements performed with this still can be attributed to:

- The Cottrell tube. It is assumed that the Cottrell tube itself is sufficient for the attainment of equilibrium whereas Raal and Mülhbauer (1998) and Joseph et al. (2000) claim that this assumption is invalid. They feel that mass transfer in the Cottrell tube between the liquid and vapour phases is limited due to insufficient contact time and small interfacial areas. Thus, if the mixture exiting the Cottrell tube is not in equilibrium, repeated passes will not improve this condition.
- The disturbance of the equilibrium during sampling. The operation of the still is disturbed during the sampling of the liquid phase.
- The boiling vessel not being stirred. As in the previous design, the lack of stirring in the boiling vessel negatively affects the operation of the still.
- There is partial condensation on the walls of the apparatus as there is no insulation or vacuum jacket surrounding it.

Experimental apparatus of Gillespie (1946)

The still of Gillespie (1946) (Figure 2-15) has a boiling vessel equipped with both internal and external heaters. As described previously, the boiling vessel is charged with a liquid mixture and brought to the boil. As the solution boils a vapour-liquid mixture is forced up the Cottrell tube and discharged onto a thermometer. The mixture then flows into the disengagement chamber (D) where the vapour and liquid phases are separated. The liquid returns to the reboiler. The vapour phase flows through the concentric tubes to the condensers where it is condensed. The condensate returns to the reboiler via the condensate receiver. Once equilibrium is reached (two to three hours) the liquid and vapour phases are sampled from points J and H respectively. Two major developments in this still were the disengagement chamber and the sampling points, which allowed samples of the liquid and vapour to be removed for analysis.

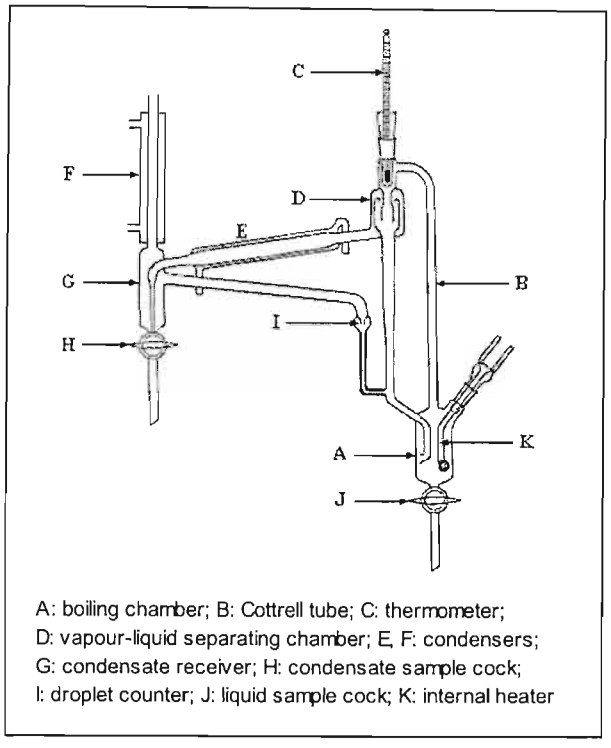

Figure 2-15: Experimental apparatus of Gillespie (1946).

Possible problems or sources of error for measurements performed with this still can be attributed to:

- The Cottrell tube. As in the previously discussed design, it is assumed that the Cottrell tube itself is sufficient for the attainment of equilibrium, which, as explained above, is problematic.
- The liquid sample being taken from the reboiler. The liquid sample should be taken directly after the disengagement chamber. By sampling the liquid phase from the reboiler it has already been reconstituted with the separated vapour phase.
- The time taken to equilibrate. The time taken to equilibrate is very long.
- No stirrers. To improve operation and to homogenize the sampled vapour phase there should be stirrers in the reboiler and condensate receiver respectively.
- The operation of the still was disturbed during the removal of liquid and vapour samples.

Experimental apparatus of Brown (1952)

The major improvement of the Brown (1952) still (Figure 2-16) over that of Gillespie (1946) is that Brown (1952) added a liquid trap and liquid sampling valve (E) before returning the liquid phase to the reboiler. Brown (1952) also added a condenser to cool the liquid phases before mixing it with the cooled vapour phase. Furthermore, due to the valve arrangement, obtaining liquid and vapour samples from this equipment do not disturb the operation of the still.

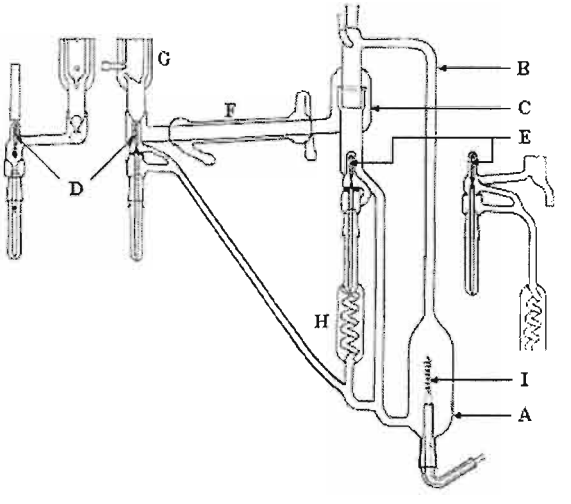

A: boiling chamber; B: Cottrell tube; C: vapour-liquid separator; D: vapour sampling valve; E: liquid sampling valve, F, G & H: condensers; I: internal heater

Figure 2-16: Experimental apparatus of Brown (1952).

Apart from these modifications mentioned above, the problems and errors discussed for the Gillespie (1946) still persisted in this apparatus.

Experimental apparatus of Yerazunis et al. (1964)

The modifications proposed by Yerazunis et al. (1964) eliminate some of the previously discussed deficiencies of the Brown (1952) still. The most important feature of the Yerazunis et al. (1964) still (Figure 2-17) is an equilibrium chamber packed with ¼-in. Fenske helices. (Heertjies (1960) first proposed passing the vapour-liquid mixture exiting the Cottrell tube through a packed column to ensure equilibrium was reached.) A further modification (suggested by Rose and Williams (1955)) is to use the separated vapour phase as a thermal barrier.

In the Yerazunis et al. (1964) still The vapour-liquid mixture exits the Cottrell tube and is forced downward over the packing in the equilibrium chamber. This packing provides a large surface area for the contacting phases and ensures that equilibrium is reached rapidly (30 to 45 minutes). The two phases separate and the liquid stream passes over a temperature sensor before returning to the reboiler. The vapour stream flows around the packed column before entering the condenser thus providing a thermal barrier to the equilibrium chamber.

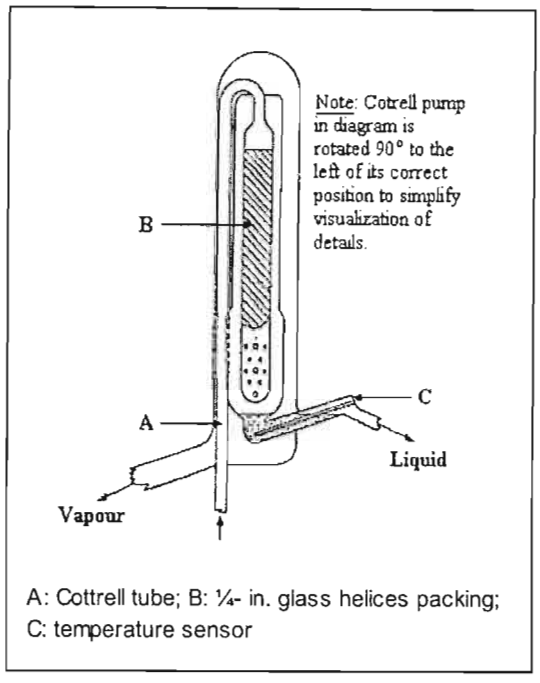

Figure 2-17: Experimental apparatus of Yerazunis et al. (1964).

Experimental apparatus of Rogalski and Malanowski (1980)

The Rogalski and Malanowski (1980) still (Figure 2-18) is an example of a well designed modern recirculation device (Abbott (1986) and was found to give consistent and reliable results (Hiaki (1994)). The still is similar to it predecessors. A liquid mixture is boiled in the boiling vessel (reboiler) and a mixture of vapour and liquid is transported by the Cottrell tube to the equilibrium chamber. Unlike the still of Yerazunis et al. (1964), this still does not have a packed equilibrium chamber as it incorrectly assumes that the Cottrell tube is always sufficient for the transported mixture to reach equilibrium. An advantage, however, is the thermal insulation of the equilibrium chamber by the vacuum jacket (F). As in previously discussed designs, the separated liquid phase is returned to the reboiler as is the condensed vapour. Liquid and vapour samples are

withdrawn through septa from the liquid container (M) and the condensate receiver (L) respectively. This allows for easy sampling without disrupting the operation of the still.

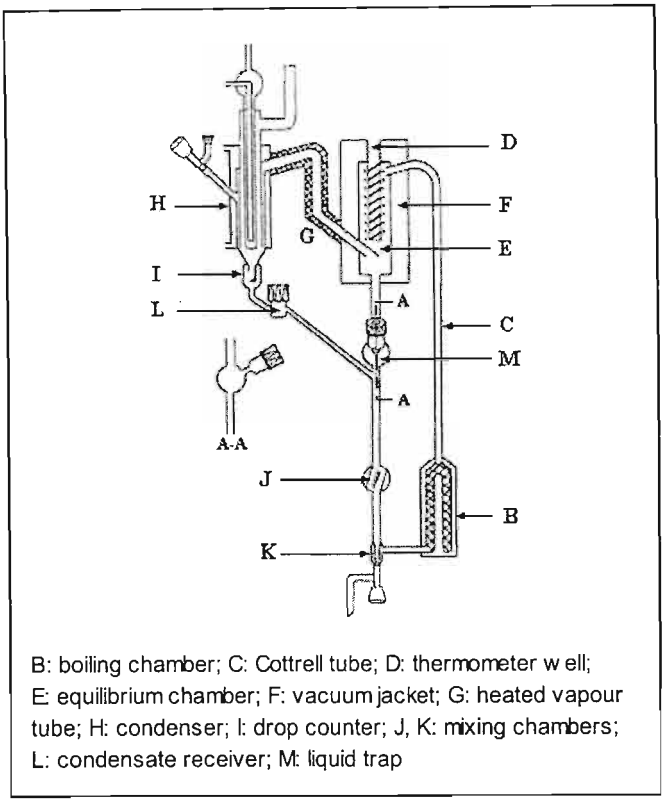

B: boiling chamber; C: Cottrell tube; D: thermometer well; E: equilibrium chamber; F: vacuum jacket; G: heated vapour tube; H: condenser; I: drop counter; J, K: mixing chambers; L: condensate receiver; M: liquid trap

Figure 2-18: Experimental apparatus of Rogalski and Malanowski (1980).

Experimental apparatus of Raal and Mülhbauer (1998)

The Raal and Mülhbauer (1998) still (Figure 2-19) incorporates all the features important to a well-designed still while eliminating most of the shortcomings discussed. Several authors discuss the features of the still as well as the results measured with it, e.g.: Joseph et al. (2000, 2001), Harris et al. (2002a) and Sewnarain (2002). Some of the important features of the still are as follows:

- The equilibrium chamber is packed with 3mm wire mesh cylinders. This packing creates a large surface area and ensures that equilibrium is reached as discussed previously. Most important is the open structure and the low pressure drop through the packing. The temperature sensor is embedded in the packing to measure the equilibrium temperature accurately.

- The isolated vapour and liquid phases are easily sampled before they are returned to the reboiler. The operation of the still is not disturbed during sampling.
- Mechanical stirring is incorporated in both the condensate receiver and the reboiler. Stirring of the contents of the condensate receiver is to ensure that the contents are a homogeneous mixture, which results in reproducible sampling. Stirring of the reboiler (not shown in Figure 2-19) ensures that the more volatile returning condensate is thoroughly mixed with the other liquid to prevent "flashing".
- The equilibrium chamber is insulated with a vacuum jacket to ensure minimal heat loss and, as result, that there is no condensation of the vapour phase. The Cottrell tube is also insulated with a vacuum jacket. This insulation ensures minimal heat loss but also prevents the transfer of superheat from the Cottrell tube to the surrounding equilibrium chamber.
- Both an external and an internal heater provide smooth, well-controlled boiling of the liquid mixture in the reboiler.
- The still can be operated either isobarically or isothermally. Operation is computer-aided.

Limitations associated with this still:

- As with all the designs discussed above, the still is made from glass and is limited to operating pressures below one atmosphere. Furthermore, as mentioned previously, liquid mixtures solidifying can shatter the glass. If liquid mixtures solidifying do not shatter the glass, melting these solids leads to local hot and cold spots on the glass, which in turn creates structural strain and breakage.
- Some of the fittings such as the drain valves are made from Teflon which melts at temperatures in excess of 493.15 K. However, structural strain can lead to breakage at temperatures as low as 453.15 K.

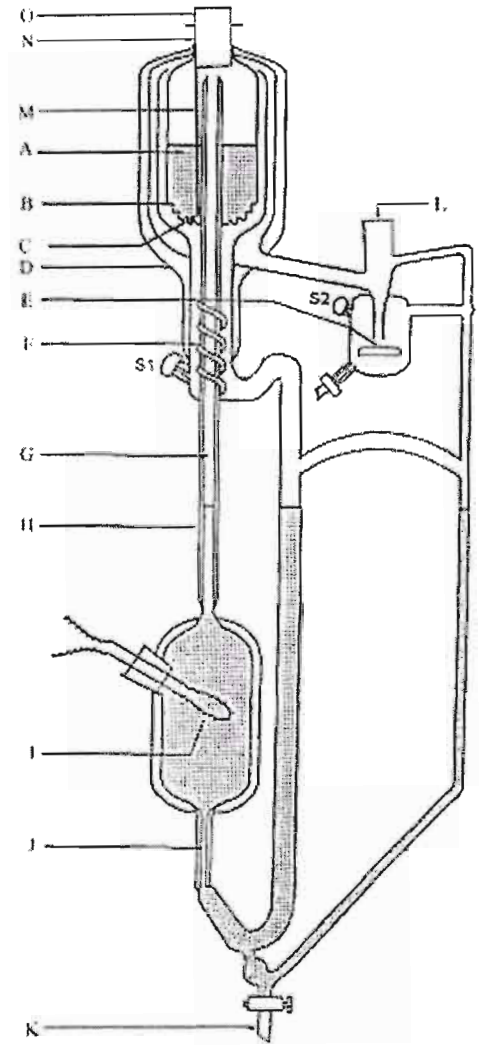

A: SS wire mesh packing; B: drain holes; C: Pt-100 bulb; D: vacuum jacket; E: magnetic stirrer; F: SS mixing spiral; G: insulated Cottrell pump; H: vacuum jacket; I: internal heater; J: capillary; K: drain valve; S1: liquid sampling point; S2: vapour sampling point; L: condenser (attached here);
M: glass tube housing Pt-100; N: taper opening; O: glass stopper

Figure 2-19: Experimental apparatus of Raal and Mülhbauer (1998).

Experimental apparatus of Raal (1998)

Raal (1998) designed a semi-opaque polyvinyl difluoride (PVDF) still (Figure 2-20) based on the concepts of the previously mentioned still to accommodate the measurement of mixtures containing fluorine. Although the still operates in the exact same manner as the previously

mentioned design, it is an example of a non-transparent still not made of glass. The new still had a maximum operating temperature of 430 K and a maximum pressure of 2 bar and produced very accurate results.

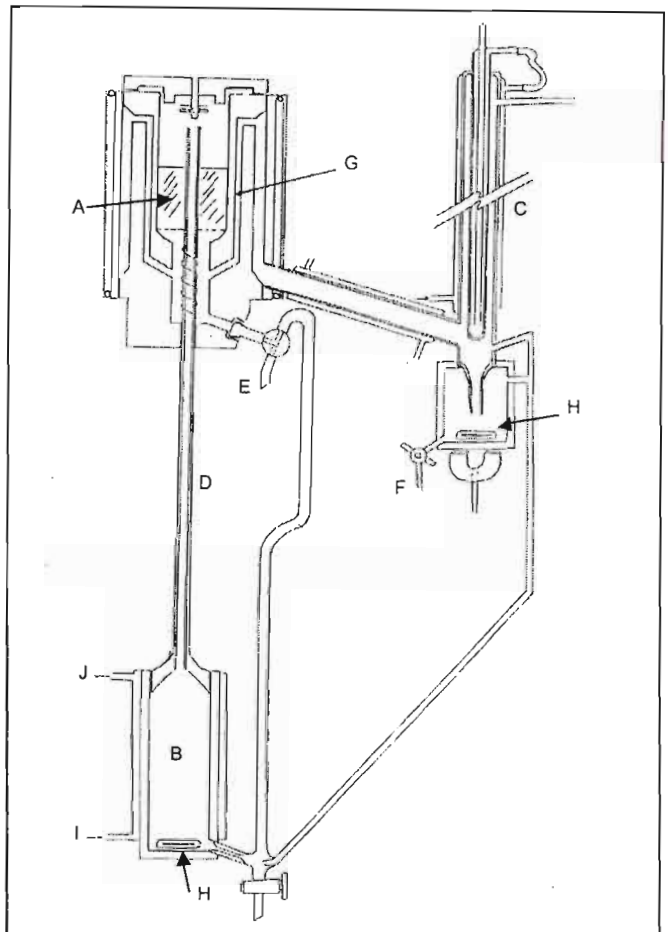

A: Packed equilibrium chamber; B: reboiler; C: condenser;
D: Cottrell tube; E: liquid sample port; F: vapour sample port;
G: vapour passages; H: magnetic stirrer; I: hot fluid in;
J: fluid out

Figure 2-20: Experimental apparatus of Raal (1998) made with PVDF.

Experimental apparatus of Wiśniewska et al. (1993)

Wiśniewska et al. (1993) developed a Stainless Steel (SS) still (Figure 2-21) to measure VLE at elevated pressures. The still is based on the design of Rogalski and Malanowski (1980). A liquid

mixture is boiled and transported up the Cottrell tube to the equilibrium chamber where the vapour-liquid mixture is expelled onto a thermometer well. The liquid and vapour phases are separated and returned to the boiling vessel. The liquid and vapour phases are sampled before being returned to the boiling vessel. The sampling procedure does not disturb the operation of the still. The entire still is constructed from SS except for a drop counter (3), which is thick-walled glass. The still is capable of operating at pressures up to 3 MPa and measurements have been made up to 471 K. As in the glass still of Rogalski and Malinowski (1980), it is assumed that the Cottrell tube is sufficient to allow the phases to equilibrate.

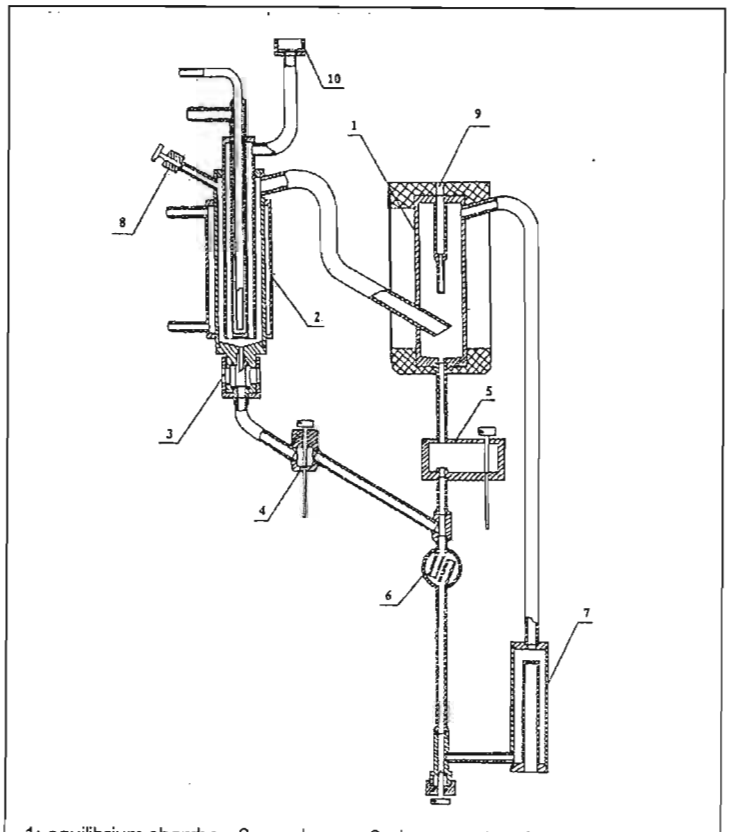

1: equilibrium chamber; 2: condenser; 3: drop counter; 4: vapour sampling valve; 5: liquid sampling valve; 6: mixing device; 7: Cottrell pump (electric heater and reboiler); 8: feed valve; 9: resistance thermometer; 10: pressure connection.

Figure 2-21 Experimental apparatus of Wiśniewska et al. (1993).

2.5 CONCLUSIONS

From the above discussion it is possible to see that the development of experimental equipment requires not just new insights but a thorough knowledge of previous designs; their salient points and their short-falls. The static synthetic apparatus and procedure is a good example of the development, progression and specialisation of equipment. Kolbe and Gmehling (1985) based their idea on that of Gibbs and Van Ness (1972). Gmehling and Fischer (1994) refined the apparatus and modified it for higher-pressure measurements by replacing the glass cell with a steel one. Fischer and Wilken (2001) have further modified the design to develop static synthetic equipment specifically suited to the measurement of supercritical systems. In a similar way the design of Rarey and Gmehling (1993) is an example of the static synthetic type apparatus with a highly developed control system that makes VLE experiments almost completely automated.

As above, the development and specialisation of the DRVSs has been discussed. In particular, the development of the equilibrium chamber to the most efficient design of Raal and Mülhbauer (1998) has been described. This design incorporates many ideas from previous designs and addresses the problems encountered in some designs. Some of the most pertinent specialisations, which were reviewed and used to inspire our design, were also discussed (Raal and Ramjugernath (1998) and Wiśniewska et al. (1993)).

In conclusion, this review gives a brief description of some the most used VLE equipment and follows the development of the equipment that was used in this work. There are many other designs, which are used with great success that were not mentioned here. For more details on other equipment the reader is referred to the reviews mentioned in this Chapter.

CHAPTER

THREE

DESCRIPTION OF EQUIPMENT USED IN THIS WORK

3.1 EQUIPMENT USED IN THIS WORK

As mentioned previously, three pieces of equipment were used to measure VLE in this work. Table 3-1 lists the equipment used and the pressure and temperature ranges of each.

Table 3-1 Equipment used in this work [3]

Equipment	T_{min} / K	T_{max} / K	P_{min} / kPa	P_{max} / kPa
Rarey and Gmehling (1993)	300	363	1	200
Kolbe and Gmehling (1985)[2]	300	473	10	21000
Harris et al (2003b)	300	600[3]	1	30000[3]

The equipment of Rarey and Gmehling (1993) and Kolbe and Gmehling (1985), with modifications, was used in the laboratories of Professor Gmehling, Oldenburg, Germany during a research visit in 2001 made possible by the collaboration between the Thermodynamics Research Unit (University of Natal) and the Department of Industrial Chemistry (University of Oldenburg). The collaboration was funded by the joint research and development project of the Forschungszentrum Jülich GmbH (Germany) and the National Research Foundation (South Africa).

[2] Modified equipment used in this work as modified by Fischer and Gmehling (1994) and Fischer and Wilken (2001).

[3] These are the design parameters. The maximum temperature and pressure at which the equipment was operated are lower as explained in Chapter Seven.

The equipment of Rarey and Gmehling was used to measure VLE at moderate temperatures and pressures while the equipment of Kolbe and Gmehling (1985) with modifications by Fischer and Wilken (2001) was used for high-pressure – moderate-temperature measurements. In Chapter Two the development of these pieces of equipment was documented. Chapter Three focuses on the details of the equipment used in this work.

The equipment of Harris et al. (2003b) was constructed and used at the University of Natal, Durban. It was used for high-temperature – low-pressure measurements. A detailed analysis of its construction and development is given in this Chapter.

3.2 STATIC APPARATUS USED AT THE UNIVERSITY OF OLDENBURG, GERMANY

3.2.1 Appararatus of Gmehling and Kolbe (1985) with modifications

The general concepts of the static synthetic type of apparatus have been discussed in Chapter Two. The principle of static synthetic measurements is to introduce precisely known amounts of the pure components into a thermoregulated equilibrium cell. This is done in a stepwise process, allowing the system to equilibrate between steps. From this procedure the system pressure is then determined as a function of composition. In Chapter Two the development of this piece of apparatus was discussed. The progression from a glass still to a steel one to the present titanium cell with sapphire windows was outlined. The details of the equipment used in this work are given below and illustrated in Figure 3-1.

Equilibrium cell

The equilibrium cell (approximately 0.11 *l*) is constructed from two pieces of titanium. The bottom part houses two sapphire windows that are fitted fore and aft to allow the observation of the chemical mixture. The top part, which is essentially a fitted cap, is sealed to the bottom part with a recessed Teflon gasket. Pressure measurement is with a pressure gauge (digital dynamometer type 21000 combined with pressure block type 410 from Desgranges & Huot, France); the sensor is fitted in the top of the equilibrium cell. Temperature measurement is with a Pt. 100 (model 1560, Hart Scientific); the sensor is embedded in the wall of the cell and is accurate to within ± 0.03 K. Specially constructed valves are fitted into the sides of the cell. The CO_2 is injected through these into the cell. The valves are constructed and fitted into the cell in

such away as to eradicate any dead space. The contents of the cell are agitated by a magnetic stirrer. The stirrer itself is a bar magnet encased in stainless-steel and is driven by a rotating magnetic field which is external to the cell.

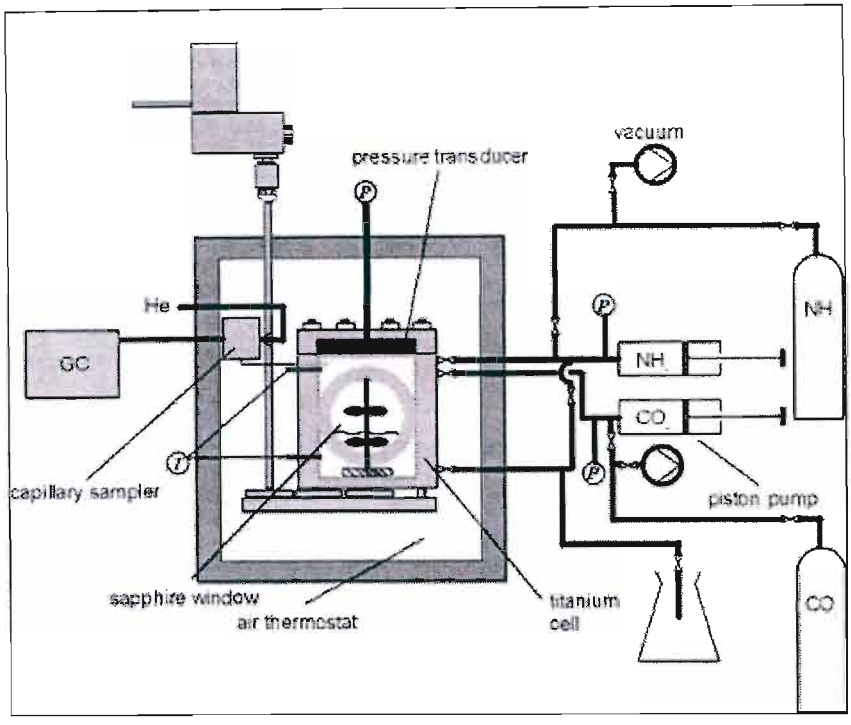

Figure 3-1: Experimental static apparatus of Kolbe and Gmehling (1985) with modifications (Fischer and Gmehling (1994) and Fischer and Wilken (2001)).

Auxiliary Equipment

The equilibrium cell is kept at the equilibrium temperature by being housed in an air thermostat. The air thermostat has a glass window and is lit inside so that the cell and its contents can be observed without disturbing the bath. CO_2 is injected into the cell with a manual piston pump. The volume change of the piston pump is read from an imbedded gauge. The displaced volume is a function of piston movement. The pump temperature and pressure are monitored with Pt. 100 resistance thermometer (model 1560, Hart Scientific) and a pressure sensor (model PDCR 911, Druck) respectively. The determination of the amount of CO_2 injected into the cell is discussed in Chapter Five.

3.2.2 The Equipment of Rarey and Gmehling (1993)

The development of the equipment of Rarey and Gmehling is discussed in Chapter Two. In principle this apparatus functions in the same way as the one described above. The most noticeable difference, however, is that the operation of this apparatus is completely automated. The general outlay of the equipment is illustrated in Figure 3-2.

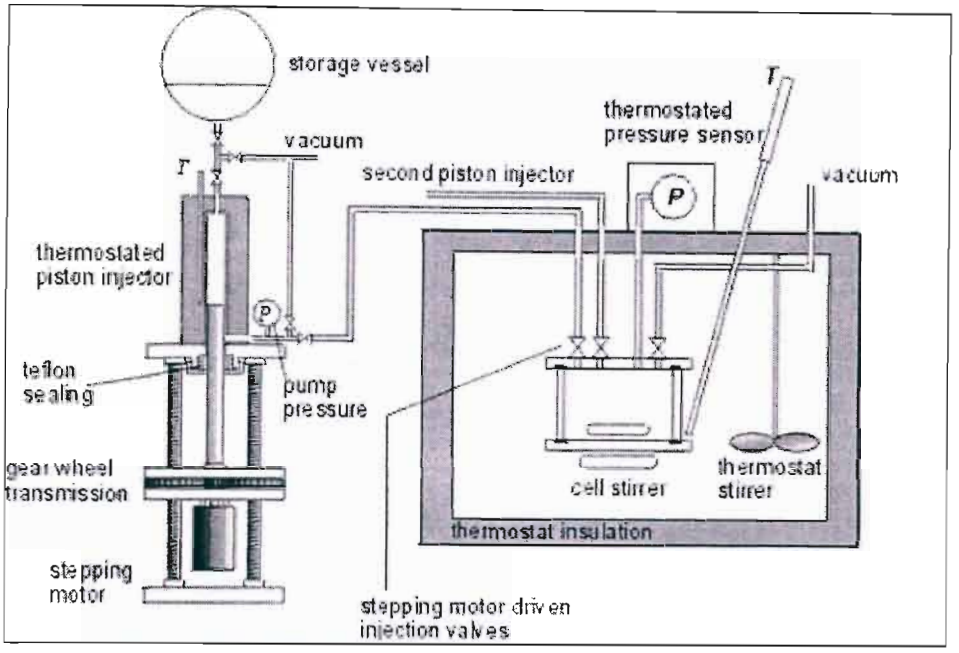

Figure 3-2: Schematic diagram of equipment from Rarey et al. (1999).

Equilibrium Cell

In principle the equilibrium cell (approximately 0.05 *l*) is very similar to the one described above. The cell is constructed from Stainless-steel but has no windows. The contents of the cell are agitated by magnetic stirrer and the cell is immersed in a constant temperature water bath. The piston pumps are connected to the cell through automated valves.

Temperature and pressure range and measurement

The equipment is suitable for measurements between 278.15 to 368.15 K and 0 to 300 kPa. Pressure (P) was measured inside the equilibrium cell using a Digiquartz pressure sensor (Model 245A, Paroscientific), which is accurate to within ± (20 Pa + 0.0001 P/Pa). Temperature (T) was

measured using a Pt 100 resistance thermometer (Model 1506, Hart Scientific), which was positioned in the water bath close to the cell and is accurate to within ± 0.03 K.

High-precision injection pump

The injection pump is based on the design of Gaube (1988). Figure 3-3 is a schematic diagram of the pump. The piston is moved by a stepper motor with the ratio of 1000 steps per rotation. The maximum injectable volume of the piston pump is roughly 0.032 *l* which equates to approximately 400 000 steps. The minimum injectable volume is roughly 0.00003 *l* with a precision of ± 2%. The piston pump is kept at constant temperature and the temperature is measured with a Pt 100 resistance thermometer (Model 1506, Hart Scientific). The pressure inside the pump is measured with a CEREBAR PMCAR1M2A0520-sensor with modified sealing. The calculation of the amount of pure component injected into the cell is described in Chapter Five.

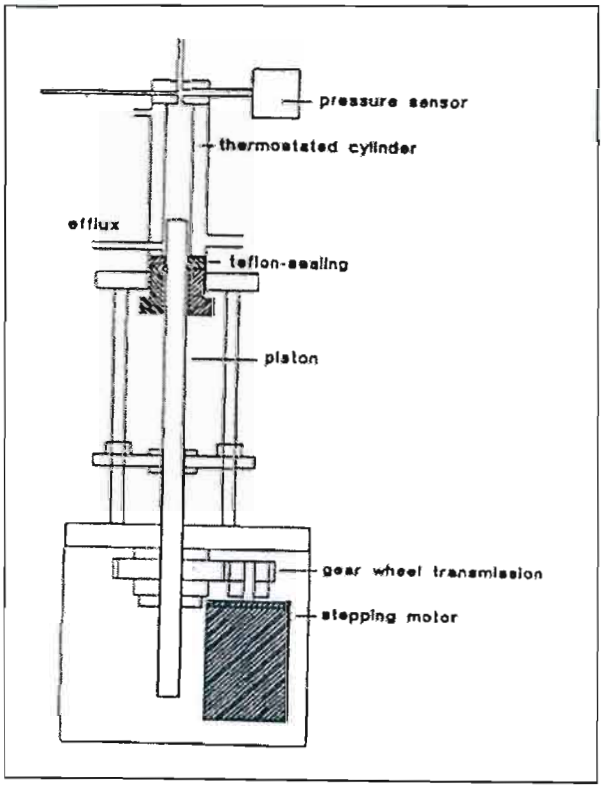

Figure 3-3: Schematic diagram of high-precision injection pump of Gaube (1988).

Apparatus Automation

The most useful benefit from automation of the equipment is that it makes it possible to measure 40 to 60 VLE points for an isotherm in 3 to 4 days with only 3 to 4 hours of human labour required. Furthermore, computer control of the precision injection pump makes it possible to measure data in the dilute regions. A PC controls the automation of the apparatus. All experimental variables are fed to the PC and it controls the injection of pure component based on the pressure readings from the cell. The operation of the apparatus is discussed in Chapter Five.

3.3 EQUIPMENT PRESENTLY IN USE AT THE UNIVERSITY OF NATAL

In the laboratories of the Thermodynamics Research Unit (TRU), University of Natal, Durban (UND) there are three main pieces of equipment for the measurement of VLE. Table 3-2 lists the equipment and gives special characteristics of each.

Table 3-2 Equipment used by the TRU (UND) for the measurement of VLE

Equipment	T_{min} / K	T_{max} / K	P_{min} / kPa	P_{max} / kPa
Raal and Mühlbauer (1998) [DRVS]	313.15	453.15	5	100
Raal and Mühlbauer (1998) [HP App.]	300	448.15	10	17500
Moodley (2003)	180	300	0	1000

Each of the above has certain limitations:

Ebulliometers and DRVS (Raal and Mühlbauer (1998))

The ebulliometers and DRVS (Raal and Mühlbauer (1998)) are constructed from glass and are thus not suitable for pressures exceeding atmospheric. Furthermore, they are fitted with Teflon valves, which reduce their operability at higher temperatures as they melt at elevated temperatures ($T > 493.15$K). During previous work (Harris (2001b)) with high boiling substances several problems arose with the equipment. It was found that at temperatures above 453.15 K certain fittings that form part of the sampling mechanism melted and thus it was impossible to exceed these temperatures unless for only limited time periods. The substances being measured were high-boiling complex hydrocarbons that had higher melting points (313.15 K $< M_{pt.} <$ *363.15 K)* than the ambient temperature. These chemicals proved very problematic:

- It was extremely troublesome to introduce the chemicals into the cell due to the fact that they had to be melted first and then maintained at a temperature higher than their melting point.
- If the equipment was allowed to cool the chemicals would solidify and prevent proper operation at startup.
- Often when the chemicals cooled and solidified, the volumetric change would cause the glass to crack.

Raal and Mühlbauer (1998) [HP Apparatus]

The equipment of Raal and Mühlbauer (1998) [HP Still] is designed for temperatures not exceeding T = 448.15 K and pressures not exceeding 17.5 MPa. The equipment is of the static type with both liquid and vapour sampling. The cell is constructed from Stainless-steel and has two sapphire windows. The cell is kept at the equilibrium temperature by being immersed in an insulated air bath. Ramjugernath (2000) added the refrigeration loop in the air bath regulating fluid system, which enables the equipment to measure data at 250 K. Equilibration takes approximately 1 to 2 hours and sampling of the two phases approximately 1 hour. The samples are vaporized and homogenized in specially designed jet mixers. Although the measurement of VLE at the equilibrium temperature is not too time consuming, heating the equipment up to the equilibrium temperature, however, takes some time.

Moodley et al. (2003)

The equipment of Moodley et al. is designed for the measurement of cryogenic VLE of refrigerants. The equipment is a single-phase recirculating apparatus; only the vapour phase is recirculated. Both phases are sampled and analysed by GC. The cell is constructed from thick-walled glass and is immersed in a thermostat bath. The bath is cooled by pumping nitrogen gas (which is cooled in a bath of solid CO_2 and acetone) through it. All valves, fittings and pumps have been specially designed for this purpose and thus are only suitable for very low temperatures. Seals and gaskets specifically suited for low temperature work were used. As the equipment is specifically made for low-temperature work it cannot be used for high-temperature work as the seals and gaskets will either be damaged or dislodged. The glass cell makes observance of the equilibrium mixture possible but limits the pressure range of the apparatus. The equipment is limited to T < 300 K and to P < 1000 kPa.

Aims and objectives for building new equipment

It was felt that while the equipment presently found in the laboratories at UND had a broad range of measurement potential there were certain areas, which could be expanded on. It was felt that temperature capabilities could be extended. In previous discussions it had been intimated that equipment to measure the VLE for high boiling hydrocarbons (such as distillation column bottoms from the petroleum industry) would be beneficial. Previous studies such as Sewnarian (2001) and Harris (2001a,b) had shown that the limits of the glass DRVS could prove restrictive in future studies. It was felt that if new equipment was to be built it would need to cover a considerable range of temperature and pressure capabilities so as to make it as versatile as possible.

The objectives of the new design were to build equipment which would:

- Operate between 300 and 700 K.
- Operate between 1 kPa and 30 MPa.
- Operate both isothermally and isobarically.
- Equilibriate rapidly.
- Allow for vapour and liquid sampling.

The need for equipment to measure high temperature VLE was confirmed when SASOL Ltd. requested the TRU to measure an isotherm at 523.15 K (Pillay (2002)). In retrospect, however, the initial aims of the project were too ambitious and attempting to meet all the above mentioned requirements proved to be difficult. In this Chapter the design and construction of the equipment is discussed. The problems resulting from the design are discussed in Chapter Seven.

3.4 DESIGN AND CONSTRUCTION OF NEW APPARATUS

3.4.1 General considerations

The new equipment was designed based on the principles of the still of Raal and Mülhbauer (1998) and Raal and Ramjugernath (1998). As mentioned previously the still was designed to operate between 300 and 700 K and between 1 kPa and 30 MPa. As glass is unable

to withstand these pressures the entire apparatus was constructed in stainless-steel (SS). SS is not the most robust metal but other factors need to be considered when choosing a material of construction (MOC):

- Most important is the strength of the material. As far as tensile strength is concerned, SS is not the best by weight. Metals such as tungsten have much greater tensile strength.
- Resistance to corrosion. SS is not resistant to acidic corrosion but as the still was designed for the purpose of measuring solvent VLE this was not deemed a serious setback as stainless-steel is fairly resistant to atmospheric oxidation and does not react with any of the well known solvents used in this work.
- Cost of materials. The cost of the materials used is a very important factor in deciding which MOC to use. Although there are other metals stronger than SS none of the stronger metals are cheaper than SS or as freely available.
- Ease of machining the chosen MOC. As all construction work for this project was undertaken in our workshop it was important to use a material that would not cause problems to the workshop, which could result in unnecessary delays. The workshop advised us to use SS as they felt that metals with a higher tensile strength such as tungsten could cause breakages to their machining equipment.

By considering all of the above factors the MOC chosen was 316 SS. 316 SS has good corrosion resistance and has good tensile strength and is a very common MOC in the processing industry. 316 SS has a maximum of 0.1 % carbon, approximately 16 to 18 % Chromium, 10 to 14 % Nickel and 2 to 3 % Molybdenum (Fontana (1986)). 316 SS has a tensile strength of 520 N/mm^2 and its design strength vs. temperature is plotted in Figure 3-4 (Sinnott (1998)). For the discussion on wall thickness used in the design of the apparatus it is important to note how the design stress decreases with temperature.

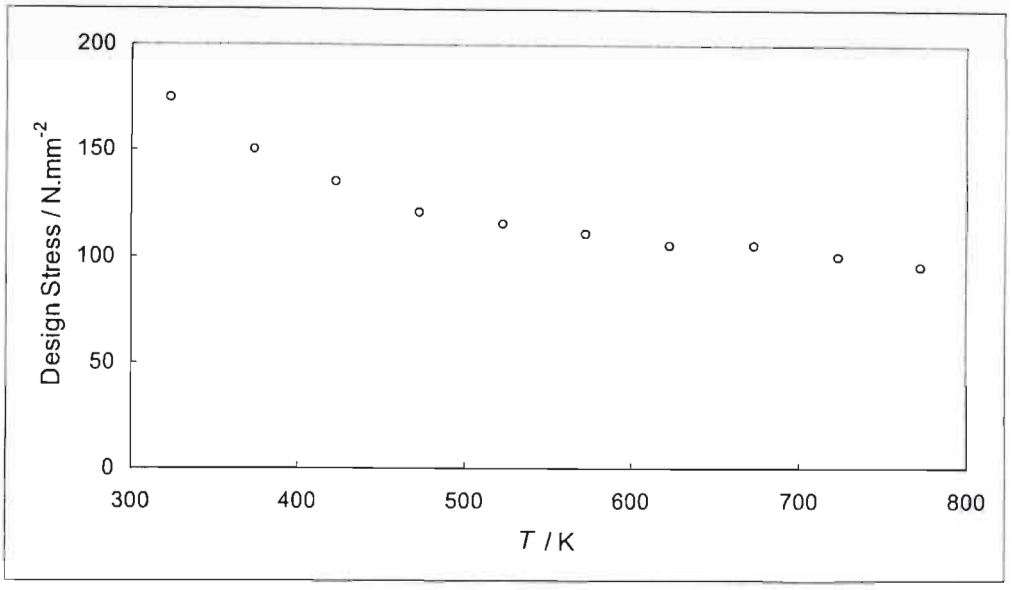

Figure 3-4: Design Stress vs. Temperature for 316 SS.

316 SS is resistant to rust which is important as no contamination is vital for accurate VLE measurements. Furthermore, 316 SS is an austenitic steel and nonmagnetic and cannot be hardened by heat treatment. Although hardening of the steel makes it stronger, it also makes it less ductile. As the still would be subject to larger temperature ranges the flanges would expand and contract. If the steel became hardedned by repeated heating and cooling it could possibly crack and this needed to be avoided at all costs as this would weaken the still (making it hazardous at high pressures) and allow for leaks.

As with the MOC, a general discussion of pressure vessel design is appropriate. Although all our designs are not technically pressure vessels[4] they were designed by referring to recommendations for pressure vessels (Sinnott (1998)) and with safety as the first concern. Pressure vessels can be divided into two classes depending on the wall thickness to vessel diameter ratio. Vessels with a ratio less than 1:10 are classed as thin-walled vessels and those with a ratio greater than 1:10 are classed as thick-walled vessels. Due to our intended maximum pressure (35 MPa), our vessels are classed as thick walled vessels.

[4] Pressure vessels are generally considered to be vessels with a diameter greater than 150mm and subject to a pressure difference greater than 100 kPa (Sinnott (1998)).

Thick-walled vessel design is a very complex science and the scope of this project did not allow for an in-depth study. However, it is important to note that although the components designed and manufactured for this study were machined from a solid billet (monobloc), there are more complex designs for thick-walled pressure vessels. The overall affect of these more complex designs is to create a vessel with a higher maximum pressure limit than a monobloc vessel with the same wall thickness. Sinnott (1998) lists three compound vessel designs:

i.) Shrink-fitted vessels. These vessels are made by shrinking one vessel over another. The outer vessel is made with an internal diameter slightly smaller than the outer diameter of the internal vessel. The outer vessel is then heated until it expands sufficiently to fit over the internal vessel. As the outer vessel cools it shrinks and places the inner under compression. This process can be repeated for more than one layer.

ii.) Multilayer vessels. These vessels are made by wrapping thin layers around a central tube. The thin layers are heated, fitted and allowed to tighten and then welded. This process gives the desired stress distribution in the compound wall.

iii.) Wound vessels. Cylindrical vessels can be reinforced by winding. Thin ribbons or wire are wound on the vessel under compression. The winding can be wound on hot to increase the prestressing.

These three methods can be used to increase the strength of pressure vessel, however, they require a great deal of expertise and experience in the field of pressure vessel design and manufacture. As mentioned previously, all our construction was done by our in-house workshop and it was not possible for them to construct any of the compound vessels described above. Thus, the monobloc design was adopted.

The general process of the DRVS was discussed and explained in Chapter Two. In principle the still requires three main unit operations:

i.) A reboiler. The chemical mixture is heated (boiled) in the reboiler and the superheated mixture is transported to the equilibrium chamber.

ii.) The equilibrium chamber. In the equilibrium chamber the superheated mixture equilibrates. The two phases are disengaged and the liquid phase is returned to the reboiler and the vapour phase is transported to the condenser. Both phases are sampled before they are returned to the reboiler.

iii.) The condenser. Although the design of the condenser is simple it is an important part of the DRSV used in this work. The function of the condenser is to condense the vapour phase and return it to the reboiler. As the condenser is situated above the reboiler, the condensed vapour phase returns to the reboiler by the hydrostatic head. This makes a vapour pump unnecessary and thus reduces costs and equipment complications.

In addition to these unit operations there are several auxillary components which are vital to the operation of the still. These include the heating of the reboiler, the cooling of the condenser and the maintaining of the pressure in the still. (To a lesser degree the equilibrium chamber is also heated but only for short periods to speed up the heating up of the equipment.) The general outlay of the apparatus and auxillary equipment is illustrated in Figure 3-5. Different hardware is used depending on whether the apparatus is being operated either at low pressures (P < 100 kPa) or at high pressures (P > 100 kPa). Figure 3-6 illustrates the general principles of the still itself.

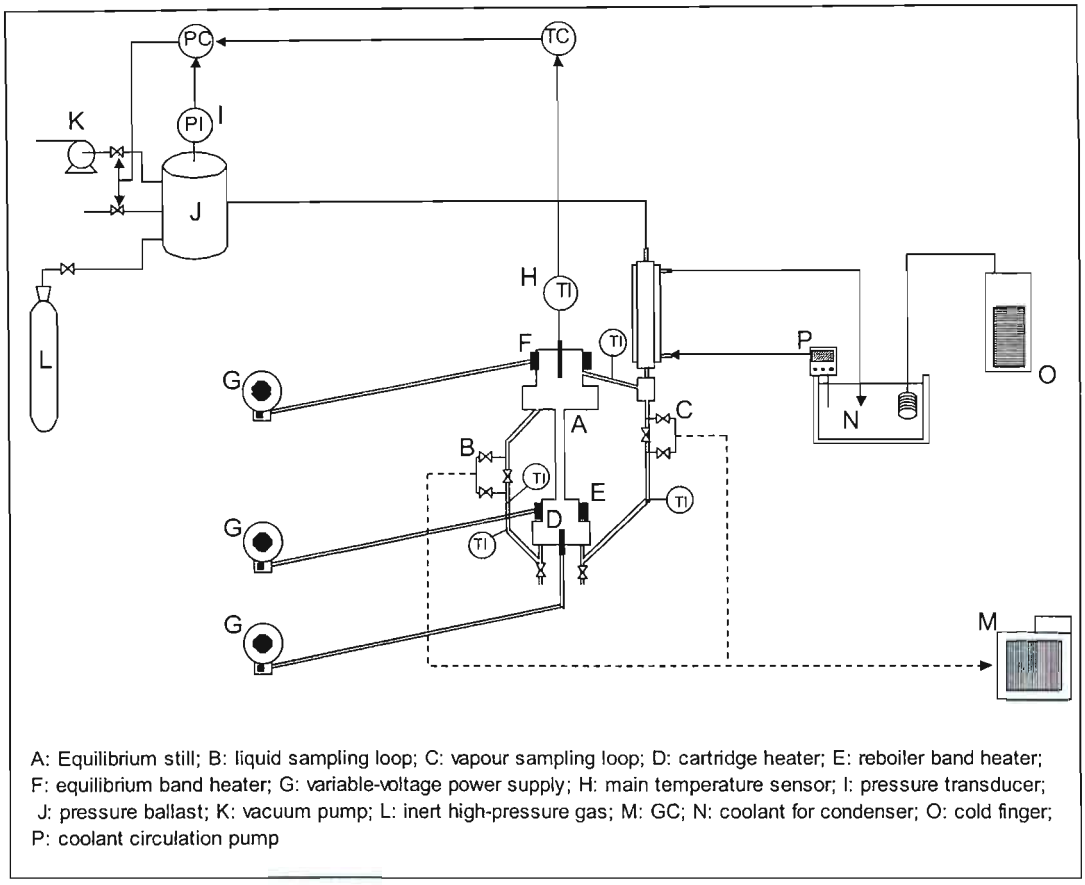

Figure 3-5: Schematic diagram of the equipment of Harris et al. (2003b).

Figure 3-6 illustrates the general principles of the still itself. A liquid mixture is charged into the reboiler. Both phases are sampled before they are returned to the reboiler.

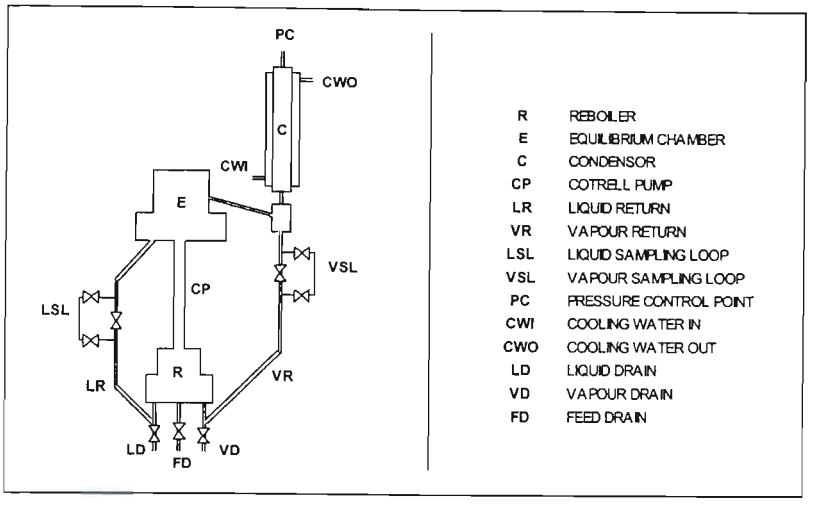

Figure 3-6: The still of Harris et al. (2003b).

The apparatus can be divided into six sections for discussion:

- The reboiler.
- The equilibrium chamber.
- The condenser.
- Thermal insulation.
- Temperature and pressure measurement.
- Vapour and liquid phase sampling.

3.4.2 The Reboiler

The general concept for the reboiler is taken directly from the DRVS designs of Raal and Mühlbauer (1998) and Raal and Ramjugernath (1998). The reboiler must provide a a chamber in which to heat and boil the mixture being measured. Boiling produces vapour bubbles and the reboiler must be designed in such a way that these vapour bubbles exit the reboiler via the Cottrell tube only. As these bubbles exit the reboiler they must propel slugs of superheated liquid up the Cottrell tube to the equilibrium chamber.

Originally the reboiler was designed as two machined pieces fitting together to give a cavity (Figure 3-7). The original design used only an external heater to heat the reboiler and boil the contents. This design was used for its simplicity and ease of manufacture. However, after careful consideration and inspection of the glass DRVS of Raal and Mühlbauer (1998) the reboiler was

re-designed to include a cartridge heater. It is believed that the best operation of a DRVS is achieved if the external heater is used to maintain the contents at boiling temperature and the cartridge heater is used to provide the energy to boil the mixture. The cartridge heater was included in our final design after discussions with the workshop and cartridge heater suppliers to assess what dimensions were feasible. (The smallest diameter for the heater is 6mm).

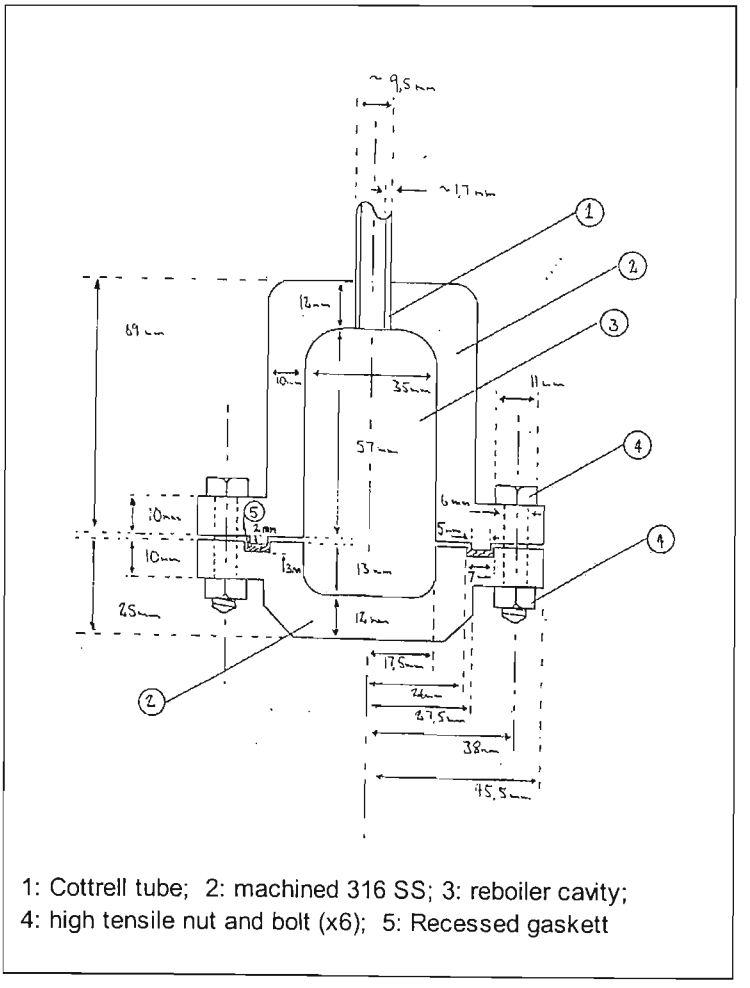

Figure 3-7: Original reboiler design.

The final reboiler design is represented schematically in Figure 3-8 and as technical diagram in Figure 3-9. The reboiler was constructed from a 316 SS billet. It was machined in the workshop of the School of Chemical Engineering, U.N.D. The reboiler comprises two halves, which are held together by six 6 mm high-tensile bolts. The two halves are sealed with a Supergraf® custom made gasket. The gasket is made from a graphite-based material and was chosen as it is

able to operate at a maximum temperature of 773.15 K, which exceeds our maximum design temperature. Furthermore, with an applied gasket stress of less than 10 N/mm^2 the gasket will seal up to 20 MPa. The reboiler was designed so as to accommodate two heaters. The external heater is a custom made 500 Watt band heater and the internal heater is a standard 250 Watt cartridge heater. The two heaters make smooth boiling and accurate control possible due to their different Wattages and designs. The external heater is on the outside of the reboiler and its energy is conducted through the thick metal walls to heat the equipment and the reboiler contents. As the cartridge heater fits into a cavity in a cylinder inside the reboiler its design is quite different to the rest of the reboiler. With the general shape of the reboiler the pressurized contents exert a force outwards onto the walls of the vessel. Equation 3-1 (Sinnott (1998)) was used to roughly approximate the wall thickness required for the vessel:

$$P = \frac{\sigma}{s_f}\left[\frac{K^2 - 1}{K^2}\right] \tag{3-1}$$

where σ is the stress limit of the MOC, s_f is a safety factor (s_f = 2 in our work) and $K = D_o / D_i$ with D_o = outer diameter and D_i = inner diameter. From the equation it is seen that the wall thickness is derived from the ratio of the outer and inner diameters of the vessel. As the cartridge cavity is a much smaller diameter it can have much thinner walls but still the same value for K. As the cartridge cavity has much thinner walls the effect of changing the power input to the cartridge heater manifests itself much quicker and allows the boiling to be controlled much easier than if there had only been an external heater.

The external corners of the vessel are rounded so as to reduce structural stresses on the vessel when the contents are pressurized.

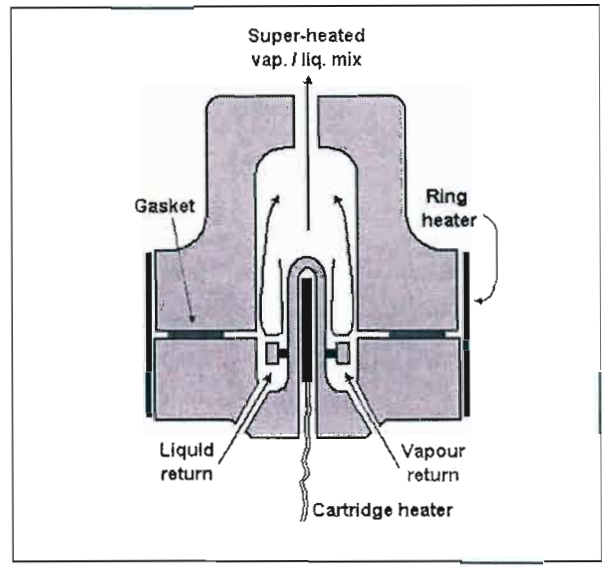

Figure 3-8: The reboiler of Harris et al. (2003b) [Schematic illustration].

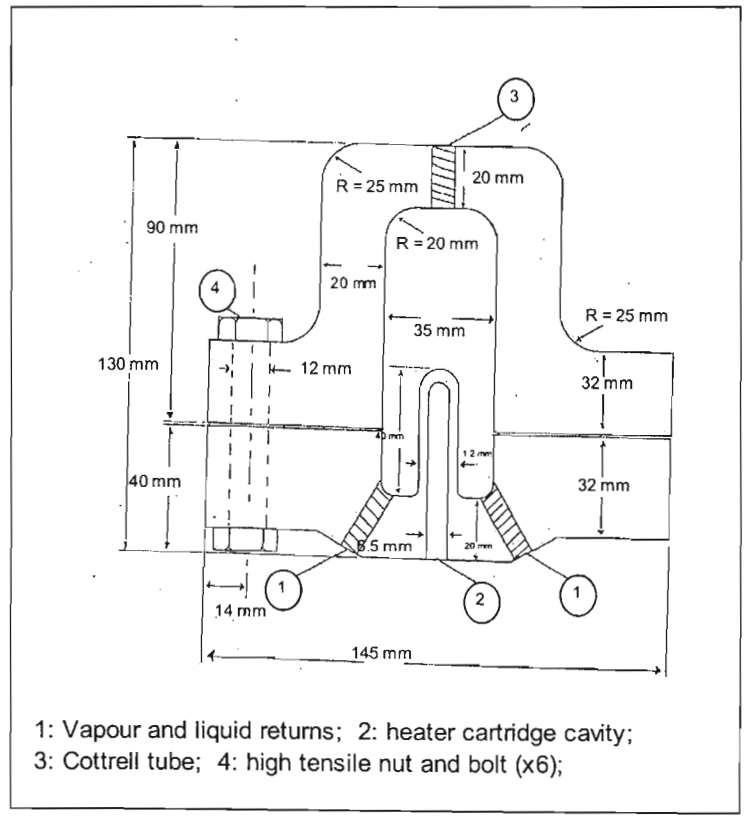

Figure 3-9: The reboiler of Harris et al. (2003b) [Technical diagram].

As mentioned above, the design of the reboiler must ensure that the escaping vapour bubbles exit via the Cottrell tube only. To this purpose the Cottrell tube was placed at the top of the reboiler. Its inlet is large and smooth. Contrary to this the inlets from the vapour and liquid return and the drain valve are at the bottom of the still and are small and constricted. A partial vacuum, to minimize heat transfer from the transported vapour-liquid mixture, thermally insulates the Cottrell tube that is connected to the top of the reboiler. The partial vacuum jacket was achieved by jacketing the Cottrell tube with a larger tube. The larger second concentric tube was welded at one end and then heated up to expel most of the air in the concentric gap and then welded at the other end thus producing a semi-vacuum jacket.

3.4.3 The equilibrium chamber

The design of the equilibrium chamber, like the reboiler, is based on the designs of Raal and Mühlbauer (1998) and Raal and Ramjugernath (1998). The equilibrium chamber must provide a place for the superheated discharge of the Cottrell tube to equilibrate and for the two phases to disengage. The temperature of the equilibrium mixture must be measured accurately and the two separated phases must be returned to the reboiler separately so that they can be sampled. The equilibrium chamber must be designed so that the equilibrium mixture is not disturbed by external fluctuations of temperature. As mentioned above, the Cottrell tube is jacketed and insulated to prevent heat transfer from the superheated mixture. This is not to prevent heat loss but to rather prevent transfer of heat to the equilibrium chamber.

The original concept for the equilibrium chamber is illustrated in Figure 3-10. The equilibrium chamber was designed to contain packing, which would facilitate rapid equilibration of the fluid and disengagement of the phases. The main problem associated with this design was the use of welding to join parts of the vessel. Welds for high-pressure vessels need to be performed by specialists and the welds need to be x-rayed to ensure their safety under pressure. Thus, the process of welding high-pressure vessels is very expensive. Furthermore, thick metal walls enclose the equilibrium chamber. Any system changes would take a long time to manifest, as the walls of the chamber would need to reach the equilibrium temperature before they stopped affecting the fluid.

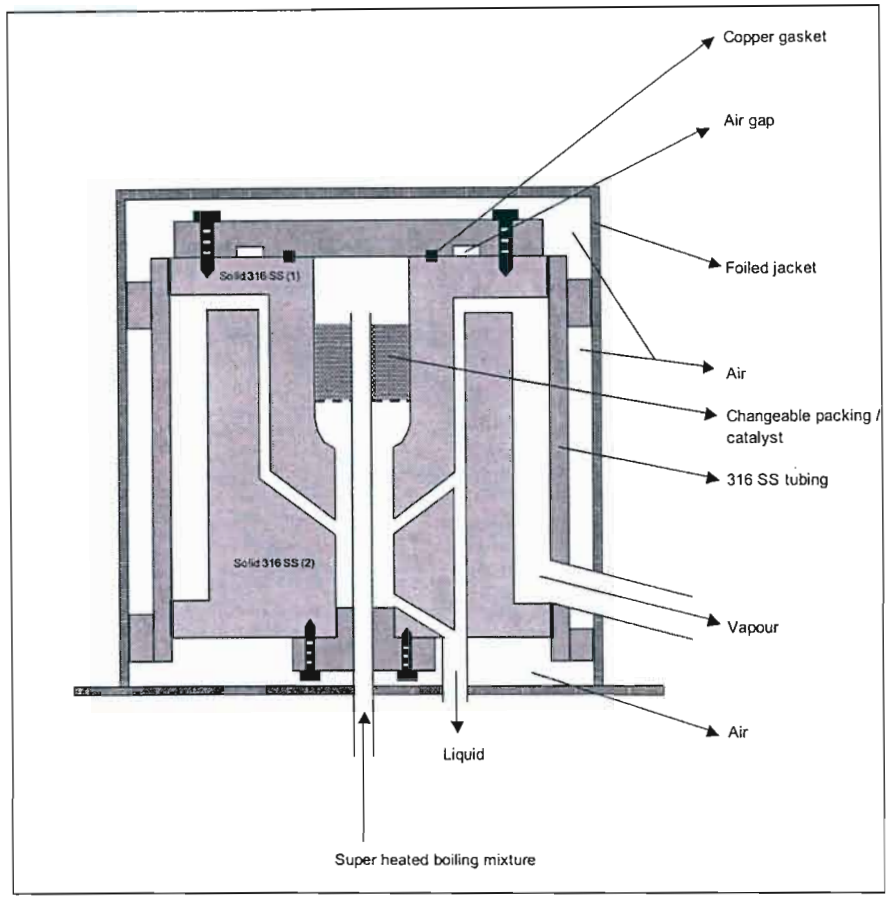

Figure 3-10: Original concept for the equilibrium chamber.

The next design (Figure 3-11) eradicated most of the welding by containing the equilibrium chamber in a flanged cylinder. However, this design had a large amount of steel in the center of the equilibrium chamber as in the above design. It was felt that, unless something could be done about this, equilibrium temperatures would not be stable and it would take a large amount of heat to heat the metal inserts (4 and 7).

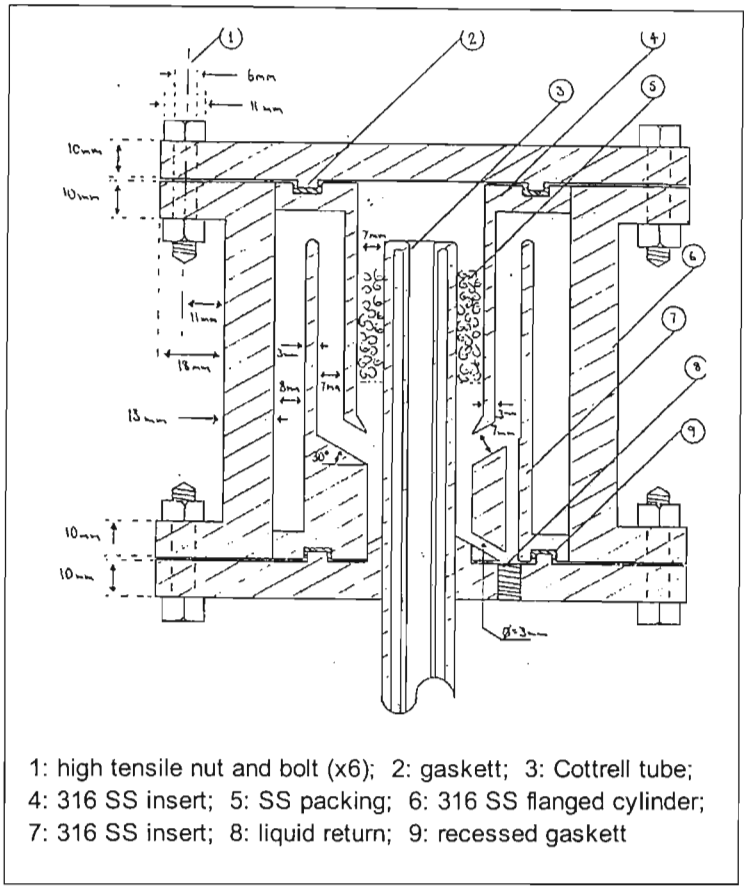

Figure 3-11: Intermediate design of the equilibrium chamber.

The final equilibrium chamber design (Figure 3-12 [Schematic diagram] and Figure 3-13 [Technical diagram]) has many features adopted from the previously described stills (Chapter Two) and previous design concepts (Figures 3-10 and 3-11). As with the reboiler, the equilibrium chamber is machined from 316 SS. The seal between the upper and lower parts of the chamber is with a custom-made Supergraf® gasket. Six 6 mm high tensile bolts hold the two parts together. The thermally insulated Cottrell tube (discussed above) extends approximately 80% into the equilibrium chamber. The jacketed tube is intended to minimize heat transfer from the tube to the contents of the packed chamber. The safety issues discussed in the design of the reboiler, such as wall thickness and structural shape, were also applied in the design of the equilibrium chamber.

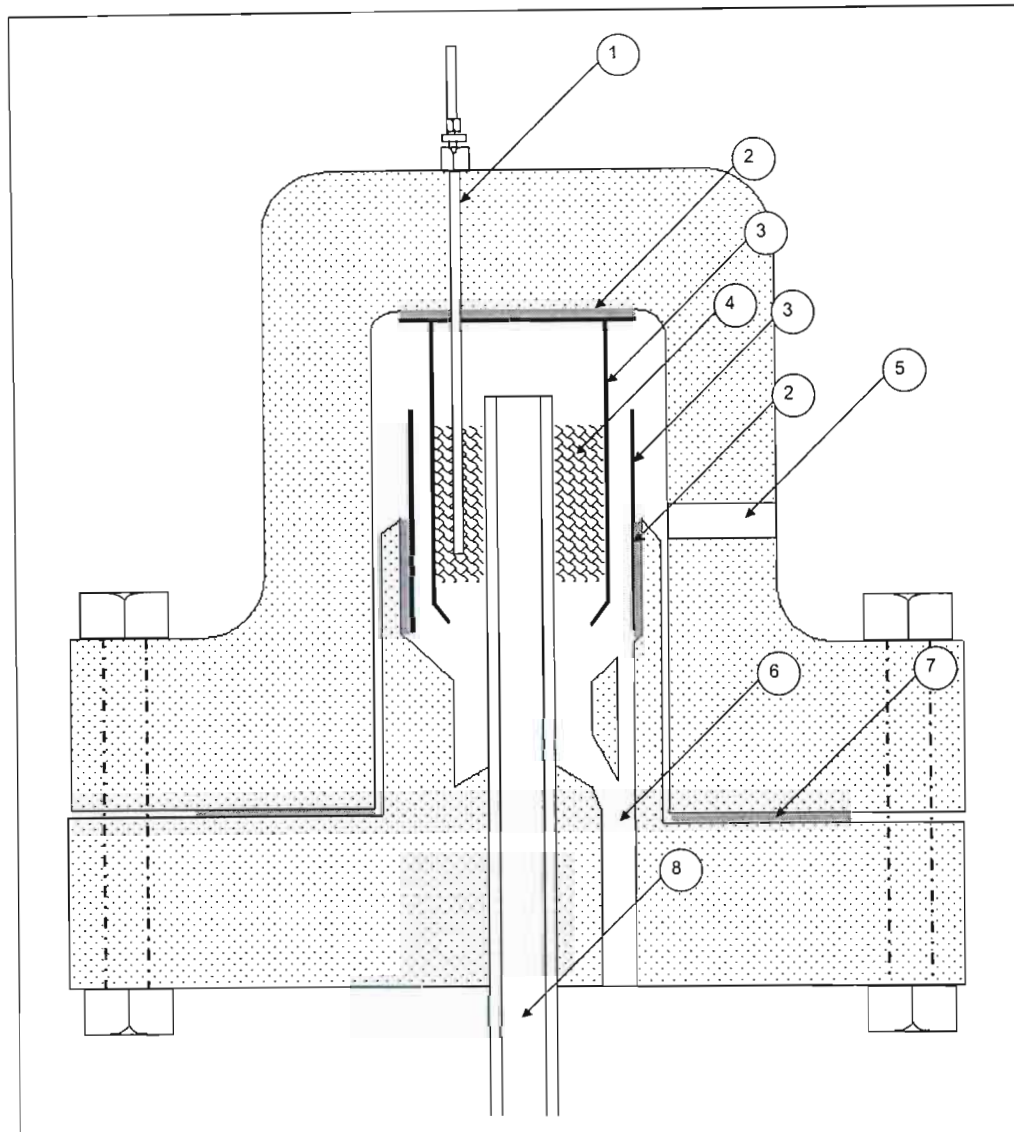

Figure 3-12: Equilibrium chamber of Harris et al. (2003b) [Schematic diagram].

The salient features of the equilibrium chamber design are best described by discussing the intended operation of the chamber. The superheated vapour-liquid mixture from the reboiler is expelled from the top of the Cottrell tube and contacts the top of the chamber. Unlike the previous designs, the top of the chamber is covered by a thin SS plate and insulated from the main block by a thin film of Supergraf® [2]. This insulation retards the effect that the temperature of the main block of the vessel has on the discharged mixture. The discharged

mixture flows over packing (SS mesh 3 mm cylinders [4]) and the two phases are separated. During phase separation the fluid temperature should reach the equilibrium temperature for the mixture. (The semi-vacuum jacket of the Cottrell tube prevents it from affecting the temperature in the packing.) The equilibrium temperature is measured by the temperature probe [1] in the packing. The liquid phase exits through aperture [6] while the vapour phase exits through aperture [5]. There is a siphon break by the liquid exit to prevent bubbles in the return line from restricting the flow. The path of the vapour phase makes two passes before exiting the equilibrium chamber. These two passes are formed by two concentric thin walled SS cylinders [3]. The vapour in the passes is intended to provide thermal buffering of the packed chamber. As opposed to the thick inserts in the two previous designs, the thin-walled cylinders heat up and cool down quickly and are insulated from the main walls of the vessel with Supergraf® material to prevent heat conduction, thus, having a minimal effect on the equilibrium temperature.

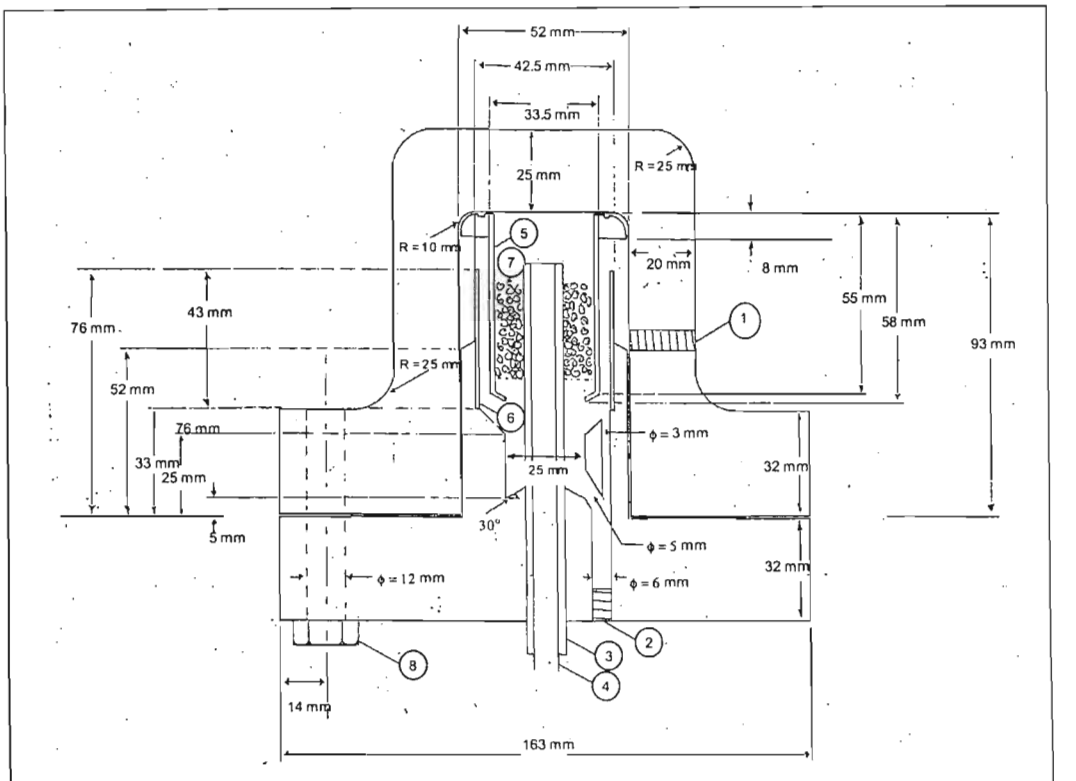

1: Vapour exit; 2: liquid exit; 3: Cottrell tube jacket; 4: Cottrell tube; 5: thin walled SS tubing; 6: thin walled SS tubing; 7: SS packing; 8: high tensile nut and bolt (x6);

Figure 3-13: The equilibrium chamber of Harris et al. (2003b) [Technical diagram].

A custom-made 600 Watt heater is fitted to the exterior of the equilibrium chamber. This heater is only used to heat the main block of the vessel up quickly. The heater should not provide any excess heat to the system once operating at equilibrium. To prevent excess heating of the vessel the heater is switched off during operation once the apparatus has been heated up.

3.4.4 The condenser

The condenser is a heat exchanger designed to cool the vapour exiting the equilibrium chamber to such an extent that it condenses. In the designs discussed in Chapter Two very little mention is made of the condensers used. In our previous work (Harris (2001a,b) and Harris et al. (2002a) we found that a condenser with a cooled jacket and an internal heat exchange coil worked best. However, from our observations (condenser used in these works was glass) it was felt that a relatively long jacketed vessel would suffice.

Thus, originally, the condenser (Figure 3-14) was only a jacketed vessel. The original design was constructed and used in measurements. The main benefit of the design was that only the base of the condenser was machined and that all other parts were standard tubing and fittings readily available. There is no problem with welding the jacket onto the condenser as the jacket is not under pressure. As a cooling fluid a mixture of water (80 %) and glycol (20 %) was used.

With certain systems, however, the single jacket proved to be inadequate as vapour escaped through the top of the condenser. This happened despite the low temperature of the cooling fluid.

Thus, the condenser (Figure 3-15) was modified to a jacketed vessel with an internal heat exchange tube. The single heat exchange tube was added to provide a larger area for vapour to contact the heat exchange surface and to decrease the annular cross-sectional area of the vessel. As with the reboiler and equilibrium chamber, the condenser is machined from 316 SS. Standard (Imperial) sizes have been used for commercially available tubing and fittings wherever possible. By using standard tubing and fittings the temperature and pressure range is assured and the price of construction is substantially decreased.

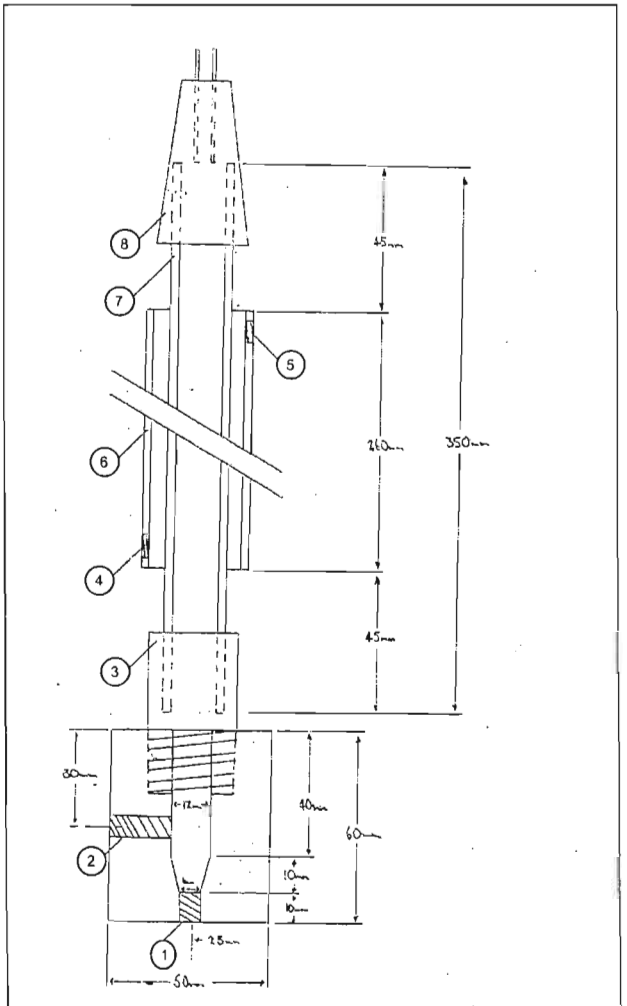

1: Condensed vapour outlet; 2: vapour inlet; 3: 316 SS; 4: cooling fluid in; 5: cooling fluid out; 6: jacket; 7: 3/4" SS tubing; 8: reducer

Figure 3-14: The original condenser design.

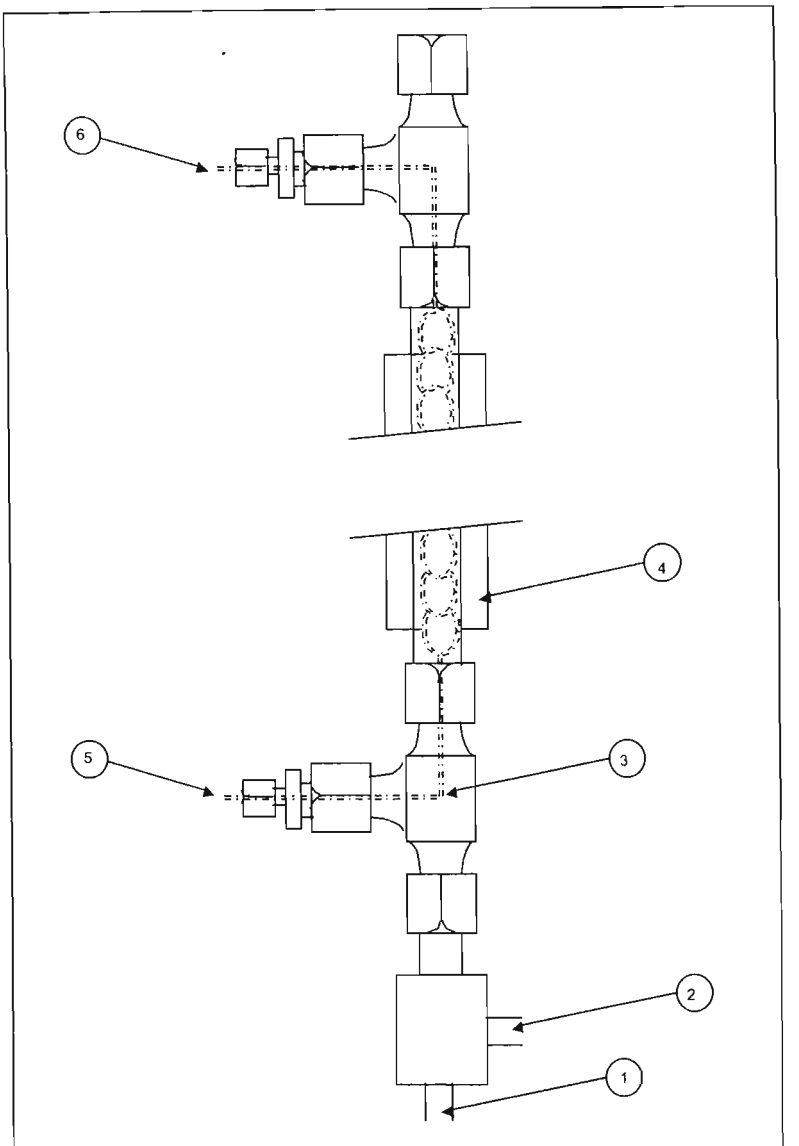

1: Condensed vapour outlet; 2: vapour inlet; 3: internal heat exchanger; 4: jacketted vessel; 5: cooling fluid inlet; 6: cooling fluid outlet

Figure 3-15: Condenser design of Harris et al. (2003b).

3.4.5 Thermal insulation

At elevated temperatures the heat transfer from the still to the surrounding environment is substantial. Originally scant insulation was placed around the reboiler and equilibrium chamber. This proved to be insufficient as it was difficult to reach high temperatures and the temperature

response was somewhat eratic. Furthermore, it was found that mixtures, which solidified when cooled, could not be melted with the three available heaters and thus impeded the operation of the still. To alleviate this problem custom insulation and line heating was added to the still. The insulation made a significant difference to the operation of the still and the line heating made it possible to work with mixtures that solidified without it being a problem. Figure 3-16 illustrates the temperature versus time profile of the still once all heaters have been switched off. The insulation ensures that the heat transfer to the environment is drastically reduced.

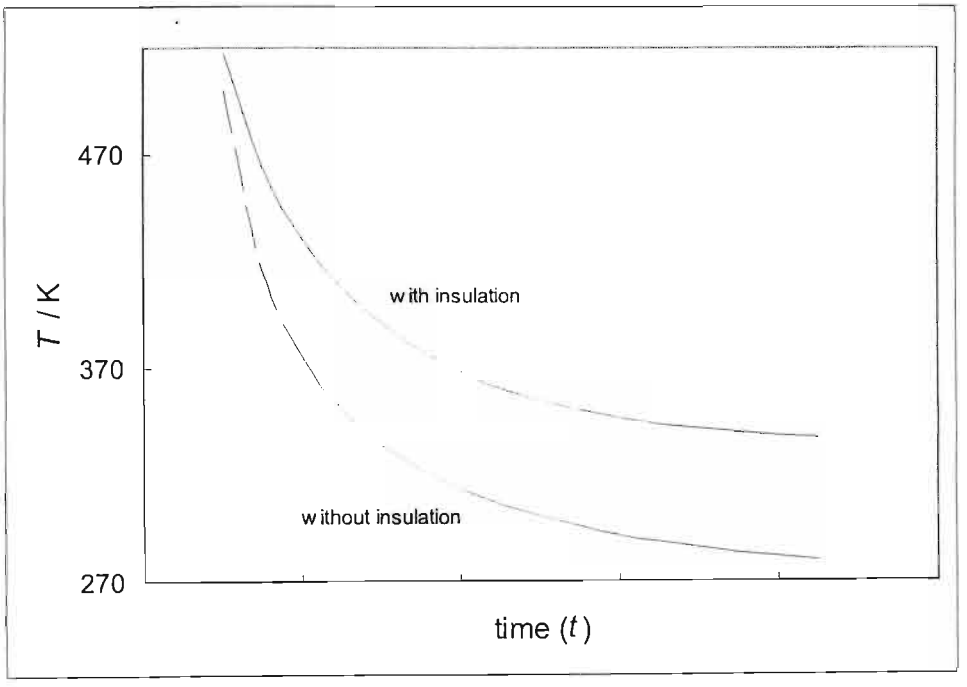

Figure 3-16: Temperature (T) versus time (t) profile for the still before and after insulation was added.

3.4.6 Temperature and pressure measurement

Temperature measurement is of critical importance to VLE measurement. The accuracy of the temperature measurements is dependent on the type of sensor used and the housing of the sensor. The temperature measurement sensor is in a ⅛-in. diameter well which is submersed in the equilibrium chamber packing. The tip of the well where the temperature measurement sensor is housed is located between the Cottrell tube wall and the wall of the thin-walled metal cylinder, approximately 75 % of the way down the packing, as shown in Figure 3-13.

Originally a Pt-100 platinum resistance thermometer was used. The thermometer was encased in a salt packing in the well. The salt provides rapid heat conduction from the equilibrium chamber to the sensor so that the temperature of the chamber can be measured accurately. The calibration curve for this sensor is in Appendix A. Unfortunately this sensor proved to be too fragile at the higher temperatures and was irreparably damaged during measurements at a $T > 400$ K. The suppliers postulated that the high temperature had caused a small air bubble in the solid salt to expand and "pop" (dislodge) the packing of the thermometer during which one of the leads to the thermometer bulb could have been snapped.

For high-temperature measurements a K-type thermocouple thermometer is used. The output from the sensor (mV) is read with an Agilent multimeter (Model 34401A) and fed via a RS 232 port to a Pentium II computer. When using a thermocouple thermometer it is important to note that the mV reading is calibrated as the difference in temperature between the "cold junction[5]" and the "hot junction" (ΔT_{TC}). The "cold junction" is where the leads of the thermo couple thermometer are joined to the leads of the multimeter and the "hot junction" is the join of the two thermo couple metals in the tip of the well. As the calibration curve can only be used to determine ΔT_{TC} accurately, the temperature of the "cold junction" needs to be known so as to determine the equilibrium temperature. The "cold junction" temperature was measured with a Pt. 100 which was encased (with the "cold junction") in a thermally insulated capsule. The calibration curves for the thermo couple and the Pt. 100 are given in Appendix A.

The original Pt-100 was accurate to within 0.1% of the reading. The K-type thermo couple is accurate to within 0.75% of the reading (as stated by the manufacturer). Both devices were calibrated against a NIST traceable thermometer (Cole-Palmer P-68037-05). The calibration graphs are in Appendix A.

The measurement of the pressure in the still is just as important as the temperature measurement. The pressure is measured with a membrane type pressure sensor, which is connected to the pressure ballast. For $P < 200$ kPa a Sensotec Super TJE pressure transducer (Model 1833-02) and DPM display (Model 5004) was used. The output from the display was relayed to the computer

[5] Some voltmeters used with thermo couples have a "cold junction" compensation function which negates the measurement of the "cold junction" temperature. Ours, however, did not.

via a RS 232 port. The device was calibrated against a NIST traceable pressure standard (Cole-Palmer P-68037-05). The calibration curve is in Appendix A.

For $P > 200$ kPa the pressure standard (Cole-Palmer P-68037-05) was connected to the top of the condenser and used directly to determine pressure.

3.4.7 Vapour- and liquid-phase sampling

Phase sampling is crucial to determining the VLE of the system in the case of DRVVs as, unlike the static stills, no accurate measurement is made of the mixture added to the still and thus the respective phase compositions can not be calculated. As both the liquid and vapour returns are liquid (the vapour stream is condensed), the sampling devices are the same. Figure 3-17 is the design of the sampling device for $P < 100$ kPa and Figure 3-18 is the design of the device for $P >$ 100 kPa.

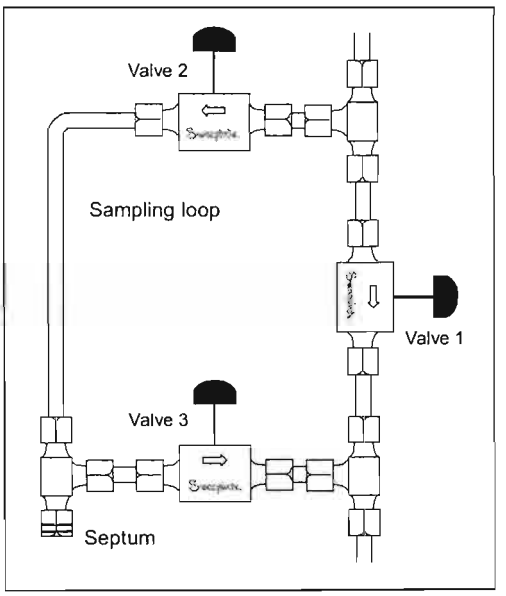

Figure 3-17: Design of the sampling device for $P < 100$ kPa.

The simple device for low-pressure sampling consists of three valves and a sampling loop. Initially valve 1 is open and valves 2 and 3 are closed. Once equilibrium is reached, valve 1 is closed and valves 2 and 3 are opened, thus forcing the returning stream to pass through the sampling loop. The loop is flushed for an acceptable time period and then valves 2 and 3 are

closed thus trapping a small sample of the stream. Valve 1 is opened so as not to affect the operation of the still. The sample is removed by gas-tight syringe through the sampling septum.

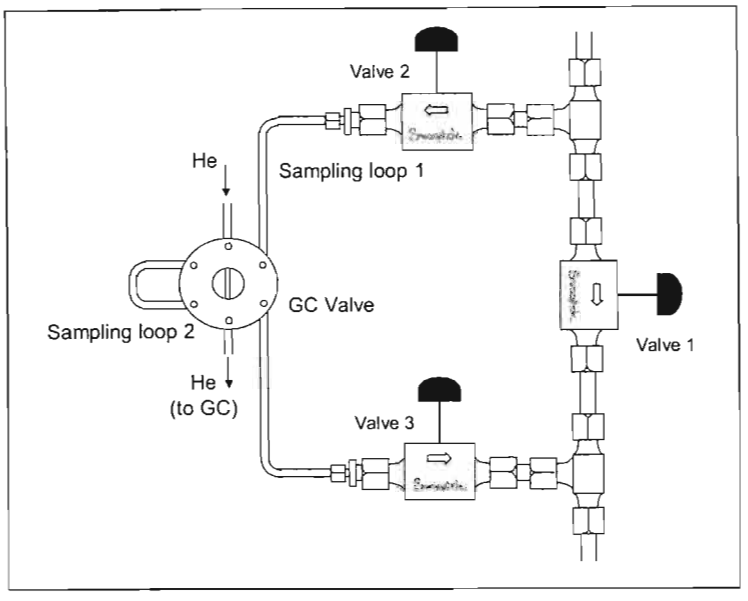

Figure 3-18: Design of the sampling device for $P > 100$ kPa.

The device for high-pressure sampling consists of the same three valves as the low pressure sampling system and a GC valve, two sampling loops and a helium feed. Initially valve 1 is open, valves 2 and 3 are closed and the six-port GC valve is open to sampling loop 2, allowing sampling loop 2 to be flushed with helium without disturbing the operation of the still. Once equilibrium is reached, valve 1 is closed and valves 2 and 3 are opened, thus forcing the returning stream to pass through sampling loop 1. This flushes sampling loop 1. The loop is flushed for an acceptable time period and then the GC valve is switched so that sampling loop 2 is also flushed with sample material. Valves 2 and 3 are then closed thus trapping a small sample of the stream. Valve 1 is opened so as not to affect the operation of the still. The six-port valve is then switched so that a small sample is sent to the GC. The process can repeated depending on the number of samples required.

It is important to note that no change be made during sampling that can change the composition of the phases. The accuracy of VLE is dependent on the stability of the equipment during the sampling period. Furthermore, the samples, which are removed, should not have their temperature or pressure altered so as to affect their composition. If the samples are being

removed as liquid samples then the samples' pressure must not be decreased nor must the samples' temperature be increased. A sudden increase in temperature or decrease in pressure can flash part of the sample and thus cause an incorrect composition measurement. Decreasing the temperature or increasing the pressure will not negatively affect the liquid samples.

One of the initial problems experienced with sampling was the positioning of the sample point. As the equipment is constantly recirculating the phases and returning them to the reboiler, there is constant variation of the liquid level in the return lines. Furthermore, as the return lines are connected to the reboiler, there is some mixing of the returning liquid and the reboiler contents in the return line. Thus, the composition near the bottom of the return line (and in the return line) is not necessarily the composition of that respective phase. For this reason it is imperative that the sample extracted from the sample point comes directly from the equilibrium chamber and is not mixed with the residual fluid in the return line. It was found during early tests that a certain minimum difference in height between the top of the reboiler and the sample point was necessary so as to obtain accurate measurement of the phase compositions. This minimum height was found to be approximately 300 mm.

CHAPTER

FOUR

EXPERIMENTAL PROCEDURE

4.1 INTRODUCTION

Three different types of equipment were used in this study:

iv.) Static apparatus of Rarey and Gmehling (1993),

v.) Static apparatus of Kolbe and Gmehling (1985) as modified by Fischer and Wilken (2001), and,

vi.) Dynamic apparatus of Harris et al. (2003b).

Apparatuses (i) and (ii) were used in the laboratories of Professor Gmehling at the University of Oldenburg while (iii) was designed, constructed and developed in our laboratories at the University of Natal.

Experimental methods for the three apparatus used differed and are thus dealt with independently.

4.2 STATIC SYNTHETIC PROCEDURE

4.2.1 General procedures

For static methods the cell is charged with a chemical mixture and allowed to equilibrate. In the case of the feed composition consisting of liquids, these liquids need to be purified and degassed prior to their introduction to the cell. At equilibrium certain measurements are made by the experimenter so as to determine the equilibrium conditions of the system. These can include the determination of system temperature, pressure and phase compositions.

As discussed in Chapter Two, no samples are taken in the static synthetic method for determining VLE. The accuracy of the final data (x_i-P) is thus dependent on the accurate measurement of the

feed compositions and the system pressure at the equilibrium temperature (z_i-P). The resulting z_i-P data are converted to x_i-P data by following an iterative calculation algorithm. Different variations of this algorithm are discussed by several authors (e.g. Kolbe and Gmehling (1985), Fischer and Wilken (2001) and Raal and Ramjugernath (2001)).

4.2.2 Experimental procedure for the measurement of VLE using the apparatus of Rarey and Gmehling (1993)

Degassing of liquids

The liquids for which VLE were measured were degassed by the method described by Fischer and Gmehling (1994). This method is based on the suggestion of Van Ness and Abbott (1978). The liquids were degassed for several hours by vacuum rectification and the reboiler temperature was kept at approximately 283.15 K. The liberated volatile gases are removed from the vessel through a capillary at the top of the column. The liquids were judged to be degassed when a metallic clicking could be heard in the reboiler. One of the disadvantages of this method of degassing is that less volatile impurities are enriched in the degassed liquid. However, this was deemed negligible in the liquids degassed for this work. Further purification was not deemed necessary.

Cleaning the Equipment

Before each run the equipment is washed and flushed with acetone. The cell is emptied and then rinsed thoroughly with acetone several times. In the case of polar chemicals in the cell, washing is first performed with an alcohol and then with acetone. The washing of the equipment is not restricted to the cell but includes all lines and pumps used during the experimentation procedure. Pumps are washed in a similar fashion to the cell and lines are flushed several times with acetone. Once the washing is complete the cell is sealed and immersed in the water bath. The equipment is then evacuated and kept under vacuum ($P < 1\text{x}10^{-4}$ kPa) for some time to ensure that there are no possible contaminants in the equipment. All residual acetone boils away at these low pressures.

Charging the Cell

Before the cell is charged the piston pumps need to be charged. The degassed liquid components are added to the piston pumps and immediately compressed to prevent their contamination by air. From this point on all manipulations of the apparatus are by computer-control. The components are compressed to about 2 MPa several times (this is repeated when the pumps are partially full) and from the volume-pressure curves a rough estimate can be made of the components' compressibility. The piston pumps are kept at constant temperature and pressure. The valve to the cell is opened and component one is pumped in by the pump's stepping motor. The valve to the cell is closed and the pump is returned to the initial pressure (P_P) and temperature (T_P). The volume of injected component (ΔV_P) can be calculated directly from the number of turns through which the stepper motor has turned. Equation 4-1 shows how the number of moles of injected component is calculated:

$$n_i = \frac{\rho_{i(T_P,P_P)} \cdot \Delta V_P}{M_i} \tag{4-1}$$

where ρ_i is the density for component i for the pump pressure and temperature and is obtained from literature. The cell is allowed to equilibrate and the pure component vapour pressure is measured.

Measuring VLE

To measure VLE for the binary system the composition in the cell is changed by adding small amounts of component two from the second piston pump. The number of moles of component two added is calculated with Equation 4-1 as explained above. Before adding more of component two the cell must first equilibrate. Mechanical stirring of the cell contents speeds up this process. The pressure and temperature of the cell are monitored until the change in both values over ten minutes is insignificant. Figure 4-1 shows a typical relaxation curve after composition change.

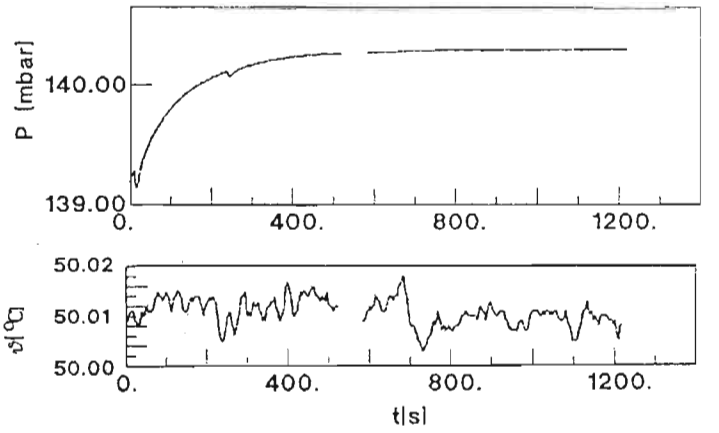

Figure 4-1: Pressure relaxation curve after a composition change for the equipment of Rarey and Gmehling (1993).

This procedure is repeated until the approximate mid point of the VLE curve ($x_1 = x_2 = 0.5$) has been reached. The apparatus is then shut down, cleaned and the process repeated, this time beginning with component two. In this way a complete isotherm is obtained. An important feature of this equipment is its ability to accurately measure data in the dilute regions. This point is demonstrated in the results (Chapter Six) and discussed in Chapter Seven. The accuracy of injected volumes, ΔV_P, is $\pm$ 1x10^{-6} dm^3.

Treatment of raw data

The z_i-P data were converted to x_i-P data by solving the following two equations in an iterative algorithm while taking into account the phase equilibrium:

$$n_i^T = n_i^L + n_i^V \tag{4-2}$$

$$V^T = V^L + V^V \tag{4-3}$$

V and n refer to volume and number of moles respectively. Superscripts T, L, and V refer to Total, Liquid and Vapour phases respectively. Subscript i refers to component i. The total number of moles (n_i^T) of both components and the total cell volume (V^T) are known. (Number of moles of each component are calculated as explained above and the cell volume is known from a previous calibration similar to the one explained in Appendix A.) The phase equilibrium

relationships can be described by either a Gibbs excess (G^E) model or an equation of state (EOS), which are discussed in detail in Chapter Four. Models incorporating the Gibbs-Duhem equation interrelate the concentration dependencies of the activity coefficients but not the absolute values of the coefficients. Thus, it is important to measure a sufficient number of points not only to determine the total pressure over the mixture but also to obtain a precise relationship of pressure as a function of x_i.

An isotherm of approximately 40 points generally takes 3 or 4 days and requires only 3 to 4 hours of manual operation.

4.2.3 Experimental procedure for the measurement of supercritical VLE using the apparatus of Kolbe and Gmehling (1985)

Cleaning the Equipment

As previously discussed, cleaning the equipment is an important part of static synthetic measurement. If the equipment is not cleaned properly, impurities will affect the z_i-P relationship and thus all values for the calculated x_i-P data will be incorrect. As chemicals that are solid at ambient temperature were used in this work cleaning the cell was somewhat troublesome. The solids had to be removed mechanically first. Once most of the solid chemical was removed the cell was washed with acetone and dried in an oven. The process was repeated several times. The lines in the equipment were also flushed. As the pumps contained chemicals that are gases at ambient conditions, they were cleaned by degassing.

Charging the cell

No liquids were used in this work so no degassing of the chemicals was required prior to experimentation. The non-volatile (solid) component (40 g to 50 g) was carefully measured on a mass balance accurate to $m_i \pm 0.0001$ g and added to the cell. The cell was then sealed and evacuated ($P < 1\text{x}10^{-4}$ kPa). This evacuation serves to remove all air (impurities) from the cell and to remove any dissolved gases in the non-volatile chemical. The cell and its contents were then heated until the solid melted. The valve to the vacuum was then opened briefly to remove any further impurities. It is important not to evacuate the cell for long periods at elevated temperatures as the non-volatile chemical can start boiling. If boiling occurs and material is lost,

z_i-P data cannot be determined accurately. Thus, the experimentation procedure has to be terminated and restarted.

Once degassing of the cell and chemical was complete, the cell was connected as shown in Figure 2.8 and heated to the temperature (T) for the isothermal measurement. The solid component melted and was allowed to stabilize giving the pure component vapour pressure.

Measuring VLE

The supercritical component (CO_2) is stored in a thermostatted injection pump at a high pressure to prevent contamination. Unlike the pumps discussed above, this pump is controlled manually. Before adding the CO_2 the volume of gas in the pump is recorded. The CO_2 is added by opening a valve to the equilibrium cell. As in the previous discussion, once a certain amount of the CO_2 is added the valve is closed and the injection pump is returned to the original temperature and pressure. The volume injected (ΔV_P) is calculated and the number of moles of CO_2 injected is calculated as in Equation 4-1. The accuracy of injected volumes, ΔV_P, is $\pm$ $1x10^{-6}$ dm^3. The system is allowed to equilibrate (15 to 60 minutes) and then the process is repeated. Equilibrium is monitored and deemed attained once the pressure of the cell does not change significantly in 10 minutes. The process is repeated until the pressure in the cell is roughly 20 MPa.

Treatment of raw data

Different methods exist for the calculation of x_i-P data from z_i-P data as mentioned above. For this work the specially developed method of Fischer and Wilken (2001) was used. They give detailed accounts of two methods in their publication. For this work the method *"GLEFLASH"* is used. The z_i-P data were converted to x_i-P data by following a similar procedure as that outlined above by solving Equations 4-2 and 4-3 in an iterative algorithm (Figure 4-2):

In this method equations of state (EOS, which are discussed in section 5.3.2) are used to describe the phases. To use the EOS, their mixture parameters need to be calculated from solubility data, which, consequently results in another iterative algorithm (Figure 4-3). In this algorithm the balance equations (Equations 4-2 and 4-3) need to be satisfied as well as the isofugacity criterion:

$$\hat{f}_i^v = \hat{f}_i^l \tag{4-4}$$

Two conditions need to be satisfied before using this method:

i.) The EOS must describe the phase equilibrium and solubility behaviour correctly, and,

ii.) The liquid volume and liquid density must be adequately represented.

Fischer and Wilken (2001) believe that (ii) is poorly obeyed if simple cubic EOS are used but address the problem by using a Péneloux volume translation[5] (Péneloux et al. (1982)).

In brief the algorithm (Figure 4-2) is as follows: the inputs to the main loop are the pure component data, mixing rule starting parameters and the z_i-P and T data. The inputs are used to estimate the Péneloux corrections. An initial flash calculation is performed with the starting values for the mixing rule parameters.

The output from this calculation (values for x_i and y_i) and the z_i-P and T data are then used in an iterative procedure (flash loop [Figure 4-3]) during which the mixing rule parameters are optimised. In this loop the balance equations (Equations 4-2 and 4-3) need to be satisfied as well as the isofugacity criterion (Equation 4-4).

The optimised mixing rules are returned to the main loop where they are used in a final flash calculation to determine the phase equilibrium values. The outputs from the main loop are: x_i-P data, calculated y_i values and calculated liquid and vapour volumes.

Dew Point Measurement

The cell was charged in a similar fashion as explained above. For the measurement of dew points, only a small, known amount of the solid chemical (4 g to 5 g) was added to the cell. The cell was then sealed and connected as explained above. The cell was heated to the equilibrium temperature. CO_2 was then added to the cell until the mixture became a homogenous gas. The amount of CO_2 added to the cell was calculated as explained above and thus the gas composition (y_i) could be calculated. The cell was allowed to reach equilibrium temperature and stabilize.

[5] The Péneloux volume translation is a liquid volume correction to improve volume estimations by the Redlich-Kwong-Soave method that leave the predicted phase equilibrium conditions unchanged.

The homogenous gas was then slowly vented to atmosphere thus lowering the pressure in the cell but keeping the composition constant. This process had to be done slowly and in steps with intervals in between so as to keep the temperature in the cell constant. The pressure was lowered until the first drops of liquid were seen on the view glass. The pressure was recorded as the dew point pressure corresponding to the vapour composition y_i for the temperature, T, of the cell.

Shutting Down the Equipment

To shut the equipment down, the cell is sealed, the heat to the bath is turned off and the equipment is allowed to cool down. Once the equipment is cool, most of the contents of the cell solidify. The cell is depressurised and removed for cleaning.

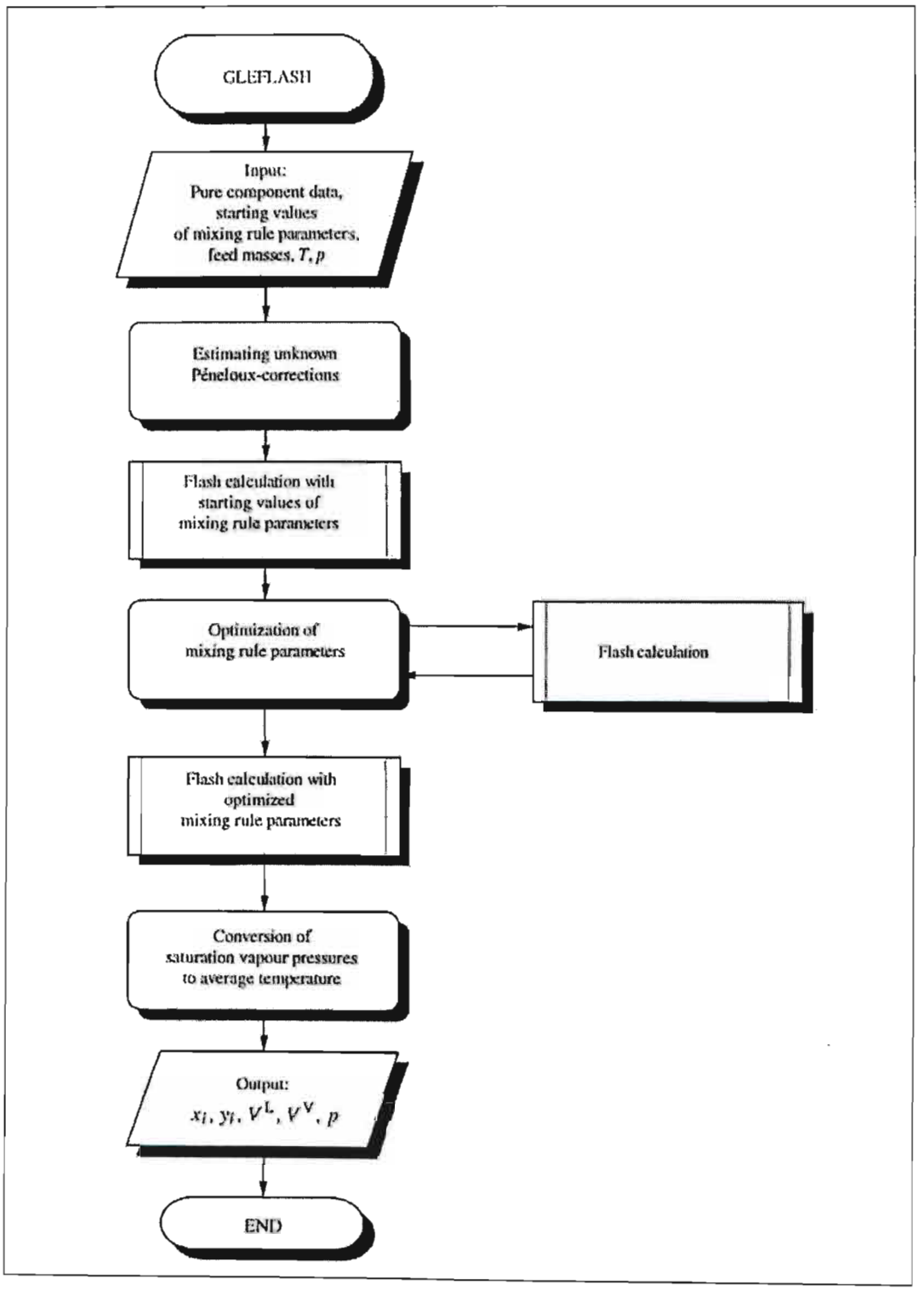

Figure 4-2: Flow diagram for the main loop of the *"GLEFLASH"* procedure.

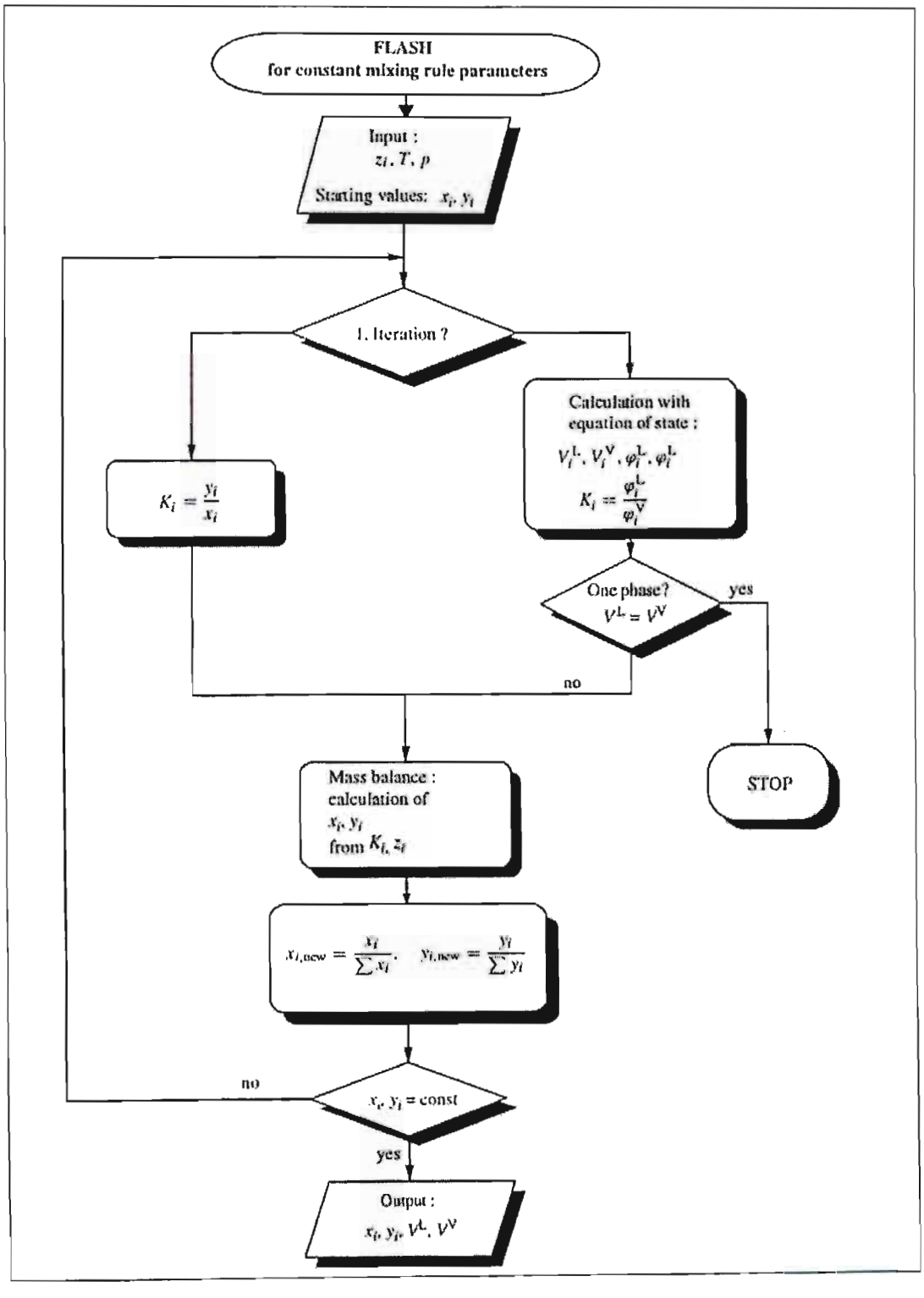

Figure 4-3: Flow diagram of the flash calculation loop.

4.3 PROCEDURE FOR THE DYNAMIC EQUIPMENT OF HARRIS ET AL. (2003B)

4.3.1 General Concepts

The still is charged with a chemical mixture. This chemical mixture is heated in the reboiler until it is boiling (i.e.: it is superheated). The superheated vapour produced propels slugs of liquid up the Cottrell tube into the equilibrium chamber. The transport from the reboiler to the equilibrium chamber dissipates some of the superheat. In the equilibrium chamber the mixture equilibrates over the packing and the liquid and vapour phases disengage. The two phases are separated and return to the reboiler via separate streams. They are sampled en route.

4.3.2 Start-up Procedure

Cleaning the still

Before the still is used it is necessary to clean it so as to remove all traces of previous experimental mixtures. To clean the still it is first flushed with wash grade acetone several times. The still is then charged with acetone and operated for approximately one hour. It is then emptied and the procedure is repeated. With each repetition the effluent is sampled and injected into the GC to test for traces of impurities so as to determine if the procedure needs to be repeated. In some cases the procedure is repeated up to six times. For chemicals that are not totally soluble in acetone several washes are performed with ethanol initially before progressing to the acetone washes. When the still is totally clean it is drained and evacuated to a pressure of $P < 0.3$ kPa for an hour so as to boil off all acetone residues.

Charging the still

The pure component (or chemical mixture) that is to be measured is prepared in a beaker. The optimum working volume for the still is between 125 and 130 ml. It is important to note that liquids expand when heated so if the liquid is prepared at ambient temperature it is necessary to calculate the required volume that will expand to approximately 125ml when at operating temperature. As an alternative, the liquid can be heated prior to being introduced into the cell so as to measure the correct operating volume.

The initial temperature of the still is noted. The vacuum pump is switched on and the control program is initiated to control a vacuum pressure. The mixture is then sucked into the still through the drain valve. It is very important to ensure that the controlled vacuum pressure is greater than the mixture's vapour pressure for the temperature of the still. If the converse is true, the liquid will flash and be lost from the still into the ballast tanks. A worst-case scenario is if the flashing material is sucked into the pump where it can cause damage.

In the case of chemicals that are solid at room temperature, the procedures are considerably more difficult and special consideration is required. Before the still can be charged the entire apparatus must be heated up to a temperature exceeding the melting point of the chemical. All the heaters are turned on including the heating tape which covers all external tubing. Temperature sensors are used to determine when the apparatus has been heated sufficiently. If there are any regions where the temperature of the apparatus is below the melting point of the chemical, blockages will occur which adversely affect the charging procedure and operation of the still. The solid chemical must be melted before the still is charged. As explained above, care must be taken to ensure that the charged component does not flash. In the case of chemicals that are solid at temperatures greater than room temperature extreme care is needed to ensure that the temperature of the still lies between the melting point and the flashing point. Localised hot or cold spots can create problems, which require the entire procedure to be abandoned and repeated once the situation is rectified. These problems can result in large time delays.

It is important to note that the chemicals are not degassed prior to experimentation. Liquids are not degassed as the dynamic nature of operation of these stills degasses the liquids continually *in situ* (Raal and Mühlbauer (1998)).

Heating the still

Once the still is charged, the operating pressure is set and the still is heated up. As there is a large bulk of stainless-steel to heat, this can take several hours. All the heaters as well as the cooling liquid to the condenser are switched on. Initially the heaters can be run at a relatively high wattage so as to heat the metal rapidly. However, as the metal temperature approaches the operating temperature for the system the equilibrium heater is switched off and the other two are turned down so as to prevent superheating of the system.

4.3.3 Operating Procedure

Heat input

Once the still is charged and heated it is important to find the correct energy input to the reboiler so that the system operates in the plateau region. The concept of the plateau region for boiling liquids in an ebulliometer type still is explained and commented on by Kneisl et al. (1989) and Raal and Mühlbauer (1998). The general concept is that, once the mixture is boiling, an increase in the energy input will increase the temperature of the boiling mixture until the plateau region is reached. In the plateau region small increases in energy input have no effect on the temperature. At a certain point the plateau region is exited and any further increases in energy input results in an increase in temperature. Figure 4-4 illustrates the concept of the plateau region.

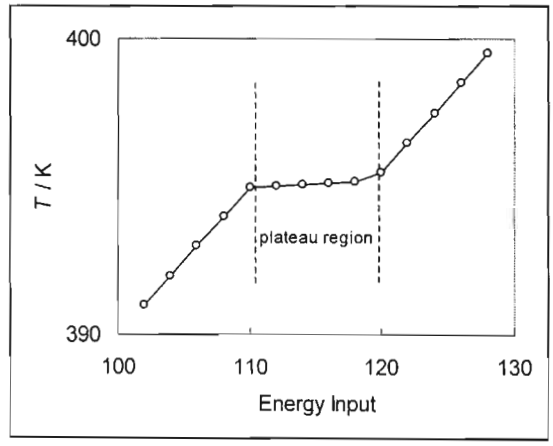

Figure 4-4: The plateau region in the temperature vs. energy input plot for boiling mixtures.

Some chemicals (alkanes) have large, very distinct plateau regions while other chemicals (alcohols) have very small plateau regions, which sometimes appear to be inflection points only. To get accurate boiling point measurements it is important to always operate in the plateau region.

Attaining equilibrium

Before recording measured variables and sampling vapour and liquid samples it is important to ensure that equilibrium has been reached. By logging the pressures and temperatures over time it is easy to assess when physical equilibrium is reached. Phase equilibrium can be determined by

regularly taking chemical samples. Figure 4-5 illustrates the approach to equilibrium for an isobaric measurement.

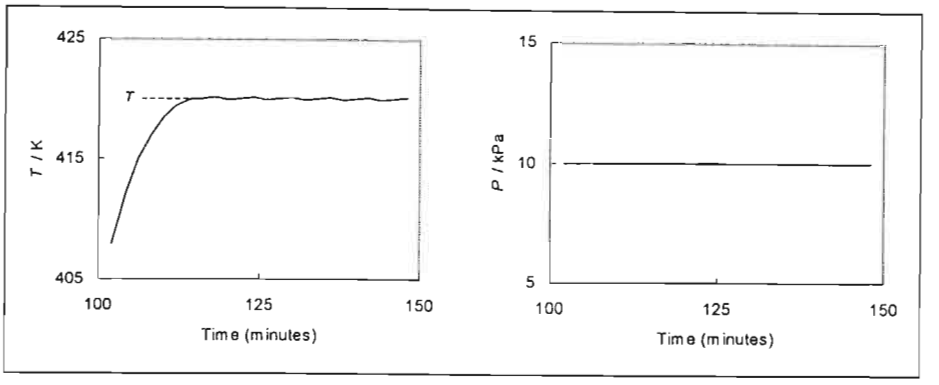

Figure 4-5: Temperature and Pressure curves for logged data illustrating equilibrium.

Isobaric and isothermal operation

For isobaric operation a pressure is set and maintained during operation. The system is allowed to equilibrate and the system variables measured. At sub-atmospheric operation the pressure is controlled by venting to atmosphere if $P_{system} < P_{set}$ and by opening a valve to a vacuum pump if $P_{system} > P_{set}$. The control valves are solenoid valves (Clippard EVO-3) and are controlled by a computer control program. A 25 litre ballast tank stabilises the system and the controller can control to within 0.03 kPa of the set point pressure.

For sub-atmospheric isothermal measurements a similar procedure is used. Initially the pressure is set and controlled isobarically at a point near the assumed equilibrium point. Once the system is boiling the control strategy is changed to isothermal control. The control strategies for isothermal control of Joseph et al. (2000) and Hills (1999) were consulted. Although Hills (1999) used a PI approach this is not suitable for a still in which a large number of different measurements with different chemicals are to be made. The unsuitability is due to the fact that a PI controller needs to be tuned to the system to operate effectively. For each different chemical and measurement the response of the system would be different and thus the PI controller would need to be tuned for each point. This procedure would prove to be too time intensive. The work of Raal and Ramjugernath (2003) gives an exact equation for $\left(\frac{\partial T}{\partial P}\right)_x$ where:

$$\left(\frac{\partial T}{\partial P}\right)_{x_i} = f\left(\gamma_i, P_i^{sat}, \frac{d\ln\gamma_i}{dx_j}, H^E\right) \tag{4-4}$$

This equation would make the tuning of the controller unnecessary. The only problem is that the equation can only be solved provided that the properties (mentioned in Equation 4-4) of the chemicals are known. For systems for which some of these properties are not known the use of Equation 4-4 would be impossible thus requiring the PI controller to be tuned.

The isothermal control used in this work sets a pressure (P_{set}), which it controls as described above. It monitors the temperature over a certain time period and then averages it. If the $T_{system(average)} < T_{set}$ then the P_{set} is increased by a set amount (e.g. 0.03 kPa). This procedure is repeated until $T_{system} = T_{set}$. If the $T_{system} > T_{set}$ then the P_{set} is decreased by a set amount (e.g. 0.03 kPa). This procedure is repeated, as above, until $T_{system} = T_{set}$. The algorithms for isobaric and isothermal control are shown in Figures 4-6 and 4-7 respectively. The isobaric controller worked well for all systems at any pressure setting. The isothermal controller worked well for systems with low boiling temperatures. As the temperatures increased the controller became more and more unstable. The problems associated with isothermal control are directly related to the problems that were experienced at high temperatures with fluctuating temperature readings during isobaric control. The problem of temperature fluctuation is discussed in Chapter Seven. The fluctuating temperature is the direct cause of the failure of the isothermal controller at high temperatures.

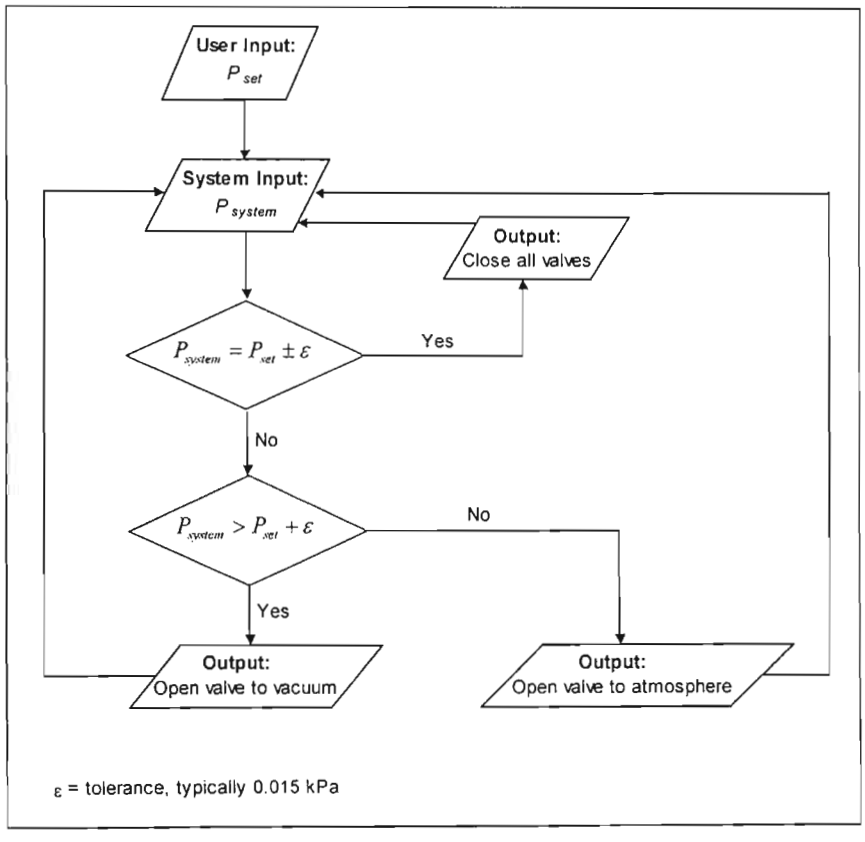

Figure 4-6: The isobaric control flow sheet.

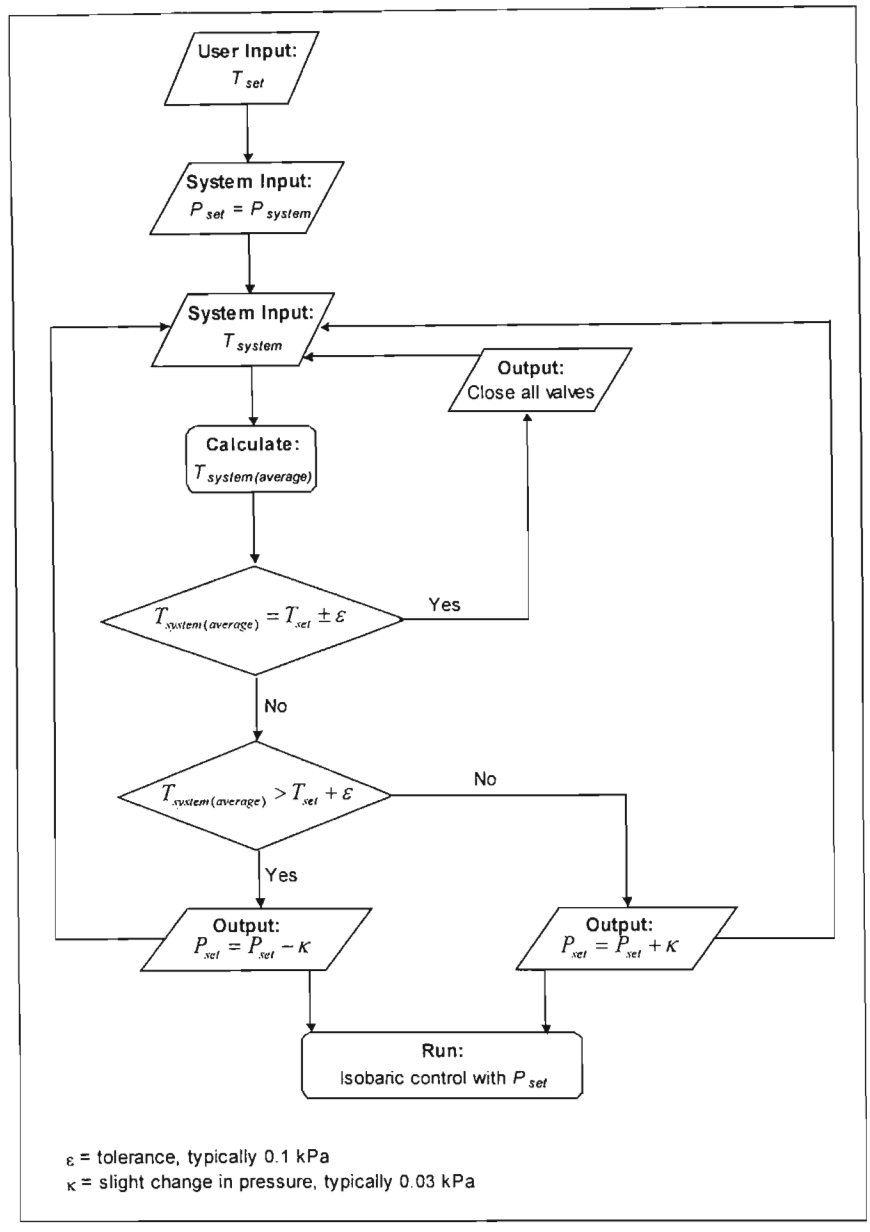

Figure 4-7: The algorithms for isothermal control.

For the high-pressure measurements an inert gas (N_2) was pumped into the system and no ballast was used. The pressure was controlled by having a constant bleed and a regulator connected to the N_2 canister set to the correct pressure. A high-pressure calibration module (Cole-Palmer P-68037-05) was used to accurately measure the pressure. The set-up is illustrated in Figure 4-8.

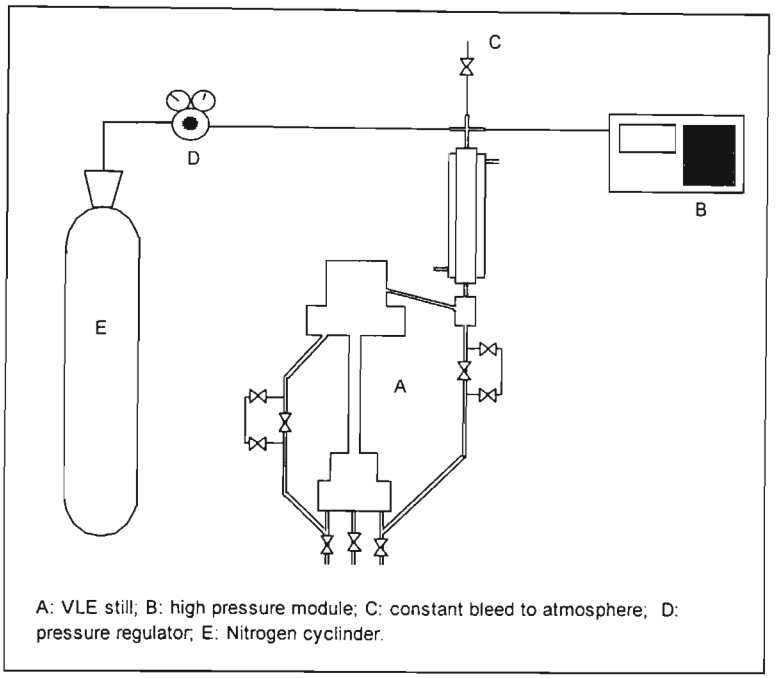

Figure 4-8: High-pressure control set-up.

Experiments utilizing chemicals that have a higher melting point than room temperature

The operating procedure for chemicals that solidify at temperatures greater than room temperature is complicated by the restraint that no part of the equipment can be at a temperature lower than the melting point. To keep the equipment (especially tubing such as the liquid and vapour returns) at a temperature above the melting point the heating tape needs to be on and controlled at all times. Furthermore, the condenser needs to be operated at a temperature above the melting point of the charged component but at a temperature cool enough to ensure total condensation of the liquid phase. An added complication is best described by referring to Figure 4-9 below.

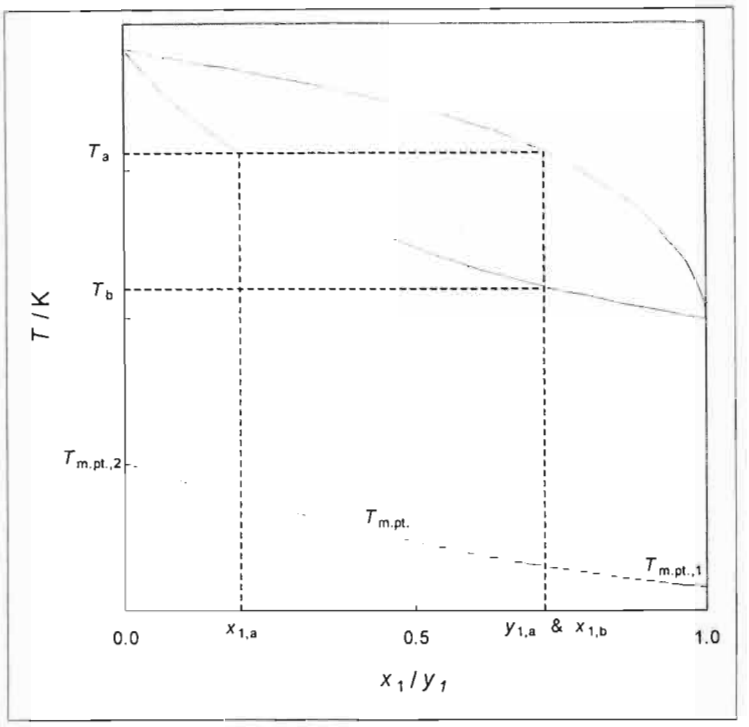

Figure 4-9: Isobaric VLE curve illustrating the complications involved when experimenting with chemicals that are solid at room temperature.

When the mixture is boiling at T_a (regardless of whether it is isobaric or isothermal operation) a liquid phase of composition $x_{1,a}$ is produced and a vapour phase of composition $y_{1,a}$ is produced. When the vapour phase condenses it forms a liquid phase with composition $x_{1,b}$ where $x_{1,b} = y_{1,a}$. The boiling temperature of the condensed liquid phase is, however, less than T_a and is equal to T_b. Thus, while the tubing must always be kept above the melting point ($T_{m.pt.}$) it must never exceed T_b. It is also important to note that $T_{m.pt.}$ is not constant across the composition range and, thus, it is safest to always keep the equipment above $T_{m.pt.,2}$ at all times.

Liquid and vapour sampling

Once equilibrium is attained liquid and vapour samples are extracted from the system as explained in Chapter Two. These samples are analysed in the GC. GC samples are deemed reproducible if they are all within 1% of the averaged value. A minimum of three injections is performed per sample point. Before the GC can be used effectively it needs to be calibrated.

GC Calibration

GC calibration is essential for the measurement of accurate VLE data as integrated mole fractions are often not representative of the true solution mole fractions (Raal and Mühlbauer (1998)). For all systems, the number of moles injected into the GC is proportional to the area recorded by the integrator:

$$n_i = A_i F_i \tag{4-5}$$

where n is the number of moles, A is the peak area and F is the response factor. The response factor is not the same for all chemicals and thus calibration is essential. For a binary mixture it is best to calibrate for area ratios rather than absolute areas as it is easier to reproduce the ratios. The resulting equation for binary area ratios is as follows:

$$\frac{n_1}{n_2} = \left(\frac{A_1}{A_2}\right)\left(\frac{F_1}{F_2}\right) = \frac{x_1}{x_2} \tag{4-6}$$

To calibrate the GC, standard mixtures are prepared gravimetrically and analysed. These mixtures should cover the entire composition spectrum, i.e.: from $x_1 < 0.1$ to $x_1 > 0.9$. The samples are injected, analysed and then $\frac{A_1}{A_2}$ vs. $\frac{x_1}{x_2}$ is plotted up to a maximum value of 1.6 for $\frac{x_1}{x_2}$. Similarly, $\frac{A_2}{A_1}$ vs. $\frac{x_2}{x_1}$ is plotted up to a maximum value of 1.6 for $\frac{x_2}{x_1}$. A linear function is fitted to both plots, passing through the origin, and the slopes ($\frac{F_1}{F_2}$ and $\frac{F_2}{F_1}$ respectively) obtained. The response factor ratio can be assumed to be constant across the entire composition spectrum if $\frac{F_1}{F_2} = 1 \Big/ \left(\frac{F_2}{F_1}\right)$. The GC settings and calibration curves are given in Appendix A.

4.3.4 Shut down

Low pressure shut down

For sub-atmospheric measurements the procedure for shut down is to turn off all the heating elements and to increase the still pressure to atmospheric pressure by shutting down and disconnecting the vacuum pump. As the pressure increases, the boiling ceases as there is no more energy input into the still. Once the boiling has ceased the cooling fluid to the condenser can be shut off and once the still has cooled sufficiently the contents can be drained. In the special case of liquids that solidify at temperatures greater than the ambient temperature, it is necessary to cool the still down to temperatures at which the liquids can be handled safely but that are above the melting point of the liquids. The heaters are then switched on to keep the contents of the still at this new temperature and the contents are then drained.

High pressure shut down

Initially all the heaters are turned off. The pressure in the still is maintained at high pressure as, if the pressure were lowered to atmospheric pressure, the contents of the still would flash. The still is left to cool down. The pressure in the still can only be lowered once the still temperature is such that the vapour pressure of the contents (at that temperature) is less than atmospheric pressure. Once the still pressure has equalized to atmospheric pressure the still contents can be drained.

CHAPTER

FIVE

THERMODYNAMIC ASPECTS OF VLE

5.1 INTRODUCTION

The use of VLE in an industrial context is primarily in the design of separation processes as explained in Chapter One. For industrial processes to operate effectively it is necessary to know the composition of liquid and vapour phases for multi-component systems over a range of temperatures and pressures. The actual data measured in a laboratory are usually restricted to binary systems, which are measured isobarically or isothermally. At best, the data may be for more than one isobar or isotherm. In its raw form the application of the data measured in the laboratory to an industrial situation is very limited. The real use of measured VLE data is to determine the thermodynamic relationships that govern the interaction of the chemicals measured. These relationships can then be used to calculate the properties of mixtures at temperatures and pressures, which were not measured initially. As an example, several isotherms for several binary systems can be used to generate thermodynamic relationships that can be used to calculate the composition of the vapour and liquid phases of a multi-component system at many different temperatures, pressures and compositions.

5.2 PHASE EQUILIBRIA

Almost all chemical thermodynamic texts (e.g. Walas (1985), Prausnitz et al. (1986), Smith and Van Ness (1987), Winnick (1997) and Raal and Mühlbauer (1998)) cover the treatment of phase equilibria in detail. The generalized criterion for phase equilibria is that, if all the phases are at the same temperature and pressure, then they are at equilibrium when the chemical potential (μ) of each species is equal for each phase throughout the system:

$$\mu_i^{\alpha} = \mu_i^{\beta} = \cdots\cdots = \mu_i^{\pi} \qquad i = 1, \ldots\ldots, N \tag{5-1}$$

The use of chemical potential, however, is impractical as it is an abstract concept and is thus not easily related to measurable quantities. A physically more meaningful quantity, the fugacity, was introduced by G.N. Lewis (Smith and Van Ness (1987) and is defined as:

$$d\mu_i = RT\ln \hat{f}_i \tag{5-2}$$

Although fugacity is still an abstract quantity, it is more readily related to measure quantities such as temperature, pressure and volume. Fugacity has the dimension of pressure. Using Equation 5-2, Equation 5-1 can be rewritten as follows:

$$\hat{f}_i^{\alpha} = \hat{f}_i^{\beta} = \cdots\cdots = \hat{f}_i^{\pi} \qquad i = 1, \ldots\ldots, N \tag{5-3}$$

Thus, for a vapour (v) and a liquid (l) in equilibrium, Equation 5-3 can be rewritten as:

$$\hat{f}_i^{v} = \hat{f}_i^{l} \tag{5-4}$$

For an ideal system comprising an ideal gas in equilibrium with an ideal solution, the compositions of the vapour and liquid phase can be related as follows:

$$y_i P = x_i P_i^{sat} \tag{5-5}$$

This ideal situation is commonly defined as Raoult's Law and is dealt with later.

5.3 DATA REDUCTION

5.3.1 Theoretical VLE methods

Many methods, classifications and techniques exist for the computation of phase equilibria. In general, certain procedures have become more common due to their reliability and ease of application. In this work methods that can be used for both high and low pressures have been investigated. To simplify matters only the case of isothermal data is considered. A note on isobaric data reduction is included at the end of the discussion.

Two theoretical methods have been developed for VLE computation. They are:

i.) the combined (γ–ϕ) method, and,

ii.) the direct (ϕ–ϕ)method.

Wichterle (1978a, b) and Raal and Mühlbauer (1998) give excellent reviews on the two theoretical methods mentioned above and describe in detail the procedures of both.

The Combined method

The combined method uses two distinct and separate auxillary functions to describe the non-ideality of both phases. To make practical use of Equation 5-4 the fugacities are related to:

i.) the fugacity coefficient of component *i* in solution ($\hat{\phi}_i$) in the vapour phase, and,

ii.) the activity coefficient of component *i* in solution (γ_i) in the liquid phase.

Thus, in the vapour phase:

$$\hat{f}_i^v = y_i \hat{\phi}_i^v P \tag{5-6}$$

and in the liquid phase:

$$\hat{f}_i^l = x_i \gamma_i f_i \tag{5-7}$$

where the pure component fugacity (f_i) is:

$$f_i = \phi_i^{sat} P_i^{sat} \exp\left[\frac{V_i\left(P - P_i^{sat}\right)}{RT}\right] \tag{5-8}$$

The term $\exp\left[\frac{V_i\left(P - P_i^{sat}\right)}{RT}\right]$ is referred to as the Poynting factor and describes the effect of P on liquid phase fugacity. Equation 5-4 can then be re-written as:

$$y_i \hat{\phi}_i^v P = x_i \gamma_i f_i \tag{5-9}$$

By substituting for the standard state fugacity, f_i^o (see Appendix B for note on standard states),

$$y_i \Phi_i P = x_i \gamma_i P_i^{sat} \tag{5-10}$$

is obtained where

$$\Phi_i = \left(\frac{\hat{\phi}_i}{\phi_i^{sat}} \right) \exp\left[-\frac{V_i \left(P - P_i^{sat} \right)}{RT} \right] \tag{5-11}$$

Gibbs excess (G^E) models (such as those discussed in Section 5.3.3) are used to describe the γ_i parameter and equations of state (EOS) are used to describe the Φ_i parameter. In special cases where Φ_i and γ_i are equal to one, Equation 5-10 simplifies to Raoult's Law (Equation 5-5).

Data reduction for the combined method was first described by Barker (1953) and a similar method was used in this work. The steps are as follows:

1.) A suitable G^E model, such as those discussed in Section 5.3.3, is selected.

2.) The expression for the pressure is given by:

$$P = \frac{x_1 \gamma_1 P_1^{sat}}{\Phi_1} + \frac{x_2 \gamma_2 P_2^{sat}}{\Phi_2} \tag{5-12}$$

The values for γ_i are determined from the G^E models and EOS are used to describe the Φ_i parameter. Equation 5-12 is determined from the sum of the expressions for the vapour phase:

$$\sum y_i P = \sum \frac{x_i \gamma_i P_i^{sat}}{\Phi_i} \tag{5-13}$$

3.) The unknown parameters are then obtained by a regression procedure that produces a best fit for the x_i-P data over the whole composition range. Initially Φ_i is set equal to 1 and the pressure and vapour phase compositions (step 4) are calculated (Equations 5-12 and 5-13 respectively). The new Φ_i value is then calculated using the calculated pressure and vapour phase compositions. This process is repeated until no discernible change in the pressure or Φ_i parameters takes place.

4.) Vapour phase compositions are calculated from Equation 5-13b with the final Φ_i and pressure values.

$$y_i = \frac{x_i \gamma_i P_i^{sat}}{\Phi_i} \tag{5-13b}$$

The Direct method

The direct method offers an alternative to the combined method for data reduction. In this method the vapour and liquid fugacities are expressed as a function of fugacity coefficients.

For the direct method the vapour phase is expressed as:

$$\hat{f}_i^v = y_i \hat{\phi}_i^v P \tag{5-6}$$

and the liquid phase as:

$$\hat{f}_i^l = x_i \hat{\phi}_i^l P \tag{5-7}$$

Substituting 5-12 and 5-13 into Equation 5-5 gives:

$$y_i \hat{\phi}_i^v = x_i \hat{\phi}_i^l \tag{5-14}$$

A suitable EOS can be used to determine $\hat{\phi}_i^v$ and $\hat{\phi}_i^l$. Similar to the above method, a regression procedure is used to find the best fit for the data. EOS are discussed below.

5.3.2 Equations of State

Raal and Mühlbauer (1998) classify equations of state into five main categories. They are as follows:

i.) the statistical mechanical *n*-parameter virial EOS,

ii.) the complex virial-type EOS,

iii.) the traditional thermodynamic cubic EOS,

iv.) the traditional thermodynamic cubic EOS with novel mixing rules, and,

v.) the statistical thermodynamic perturbation theory EOS.

The most commonly used EOSs are virial EOSs and cubic (van der Waals) EOSs. They are the ones used in this work and are discussed in detail. Walas (1985), Sandler (1994) and Raal and Mühlbauer (1998) give excellent reviews on the various EOSs and their application.

The origin of equations of state

EOSs can be traced back to 1662 when Boyle was experimenting with air. Boyle deduced that the pressure of a gas is inversely proportional to its volume at a given temperature. This relationship can be expressed as

$$PV = \text{constant} \tag{5-15}$$

In 1802 Charles and Gay-Lussac, working independently, were able to quantify the effect of temperature on this relationship. Claperyon combined these results and in 1834 produced the first statement of the ideal gas law:

$$PV = R(T + 267) \tag{5-16}$$

With the definition of SI units the ideal gas law was eventually formulated:

$$PV = RT \tag{5-17}$$

or

$$Z = \frac{PV}{RT} = 1 \tag{5-18}$$

where R is the gas constant and Z is the compressibility factor.

However, at low temperatures or high pressures the ideal gas law is usually only an approximation. Real gases have size, shape and structure and as a result the molecules occupy volume and exert either an attractive or repulsive physical or electrical force on each other. A solution was offered by van der Waal in 1873, when he developed an equation to account for these factors. That equation still forms the basis for many currently accepted PVT relationships.

Cubic or van der Waal EOS

The first EOS proposed by van der Waal in 1873 is given as:

$$P = \frac{RT}{(V-b)} - \frac{a}{V^2} \tag{5-19}$$

where the constant b accounts for the molar volume which is not available to a molecule due to the presence of other molecules. The constant a accounts for the intermolecular attraction forces. The contribution of b increases the pressure above that of an ideal gas while a lowers it. These parameters can be obtained by two methods. The first method is to obtain them by regressing them from experimental data. The second method is to use the EOS to fit the parameters to the critical point for the critical point condition: $\left(\frac{\partial P}{\partial V}\right)_T = \left(\frac{\partial^2 P}{\partial V^2}\right)_T = 0$. Thus, from the latter, for the van der Waal's EOS a and b are given as:

$$a = \frac{27R^2T_c^2}{64P_c} \tag{5-20}$$

and

$$b = \frac{RT_c}{8P_c} \tag{5-21}$$

respectively. The subscript c refers to the critical property.

One of the earliest modifications to the van der Waal EOS was that of Redlich and Kwong (1949), who recognized the temperature dependence of the attraction parameter. The modification, although arbitary, did much to improve the applicability of the EOS and is given by Equation 5-22:

$$P = \frac{RT}{(V-b)} - \frac{a}{T^{0.5}V(V+b)} \tag{5-22}$$

The next major modification to the R-K EOS was that of Soave (1972) who modified the temperature-dependent attraction term to include the acentric factor (ω) and the reduced temperature (subscript r):

$$P = \frac{RT}{(V-b)} - \frac{a\alpha}{V(V+b)} \tag{5-23a}$$

where

$$\alpha = \left[1+(0.48+1.57\omega-0.176\omega^2)(1-T_r^{0.5})\right]^2 \tag{5-23b}$$

The S-R-K EOS was able to predict accurate vapour pressures for light hydrocarbons and led to the S-R-K EOS becoming a useful tool in the prediction of vapour pressures for non-polar fluids. However, the S-R-K EOS does not predict liquid densities well, especially near the critical point.

The P-R EOS (Peng and Robinson (1976)) is closely related to the S-R-K EOS and aimed to improve on liquid density predictions and stability near the critical point and is given below:

$$P = \frac{RT}{(V-b)} - \frac{a\alpha}{V(V+b)+b(V-b)} \tag{5-24a}$$

where

$$\alpha = \left[1+(0.37464+1.54226\omega-0.26992\omega^2)(1-T_r^{0.5})\right]^2 \tag{5-24b}$$

The P-R EOS and S-R-K EOS are widely used in industry along with various subsequently developed α functions. There are many other variations on α values, which are detailed in the reviews mentioned. A common one that was used in this work and thus requires mention is that of Stryjek and Vera (1986a, b):

$$\alpha = \left[1+K(1-T_r^{0.5})\right]$$

$$K = K_0 + K_1(1+\sqrt{T_r})(0.7-T_r) \tag{5-25}$$

$$K_0 = 0.378+1.489\omega-0.1171\omega^2+0.019\omega^3$$

where K_1 is a parameter determined from pure component(s) data (such as vapour pressure). To extend these EOS from pure components to mixtures requires mixing rules. Raal and Mühlbauer (1998) describe two distinct methods used to obtain mixture a and b parameters (a_m and b_m respectively). The first method, which is not very common, uses combining rules to determine a mixture's pseudo critical properties (T_{cm}, P_{cm}, ...). These pseudo-mixture properties are then used to determine a_m and b_m as described earlier.

The second, and more commonly used method, uses pure component critical properties (T_{ci}, P_{ci}, ...) to calculate pure component a_i and b_i parameters. Mixing rules are then used to calculate mixture a_m and b_m parameters. For the van der Waals EOS Lorentz-Berthelot mixing rules are used:

$$a_m = \left(\sum y_i (a_i)^{0.5}\right)^2 \tag{5-26}$$

and

$$b_m = \sum y_i b_i \tag{5-27}$$

The R-K EOS uses a cross parameter, $a_{ij} = (a_i a_j)$, in the mixing rules:

$$a_m = \sum y_i y_j a_{ij} \tag{5-28}$$

and

$$b_m = \sum y_i b_i \tag{5-27}$$

Soave introduced a binary interaction parameter, k_{ij}, in a_{ij}:

$$a_m = \sum_i \sum_j x_i x_j \sqrt{a_i a_j}\,(1 - k_{ij}) \tag{5-29}$$

The P-R EOS use Equations 5-29, 5-30 and 5-31 as its basis. This combination of mixing rules is commonly known as the *van der Waals one-fluid-theory classical mixing rules* (or the *classical mixing rules* for short).

Using the P-R EOS and the classical mixing rules, the fugacity coefficiient for component *i* in a mixture can be written as follows (Raal and Mühlbauer (1998)):

$$\ln \hat{\phi}_i = \frac{b_i}{b_m}(Z-1) - \ln(Z-B) - \frac{A}{2\sqrt{2B}}\left[\frac{2}{a_m}\sum y_i a_{ji} - \frac{b_i}{b_m}\right]\ln\left[\frac{Z+2.414B}{Z-0.414B}\right] \tag{5-30}$$

where

$$A = \frac{a_m P}{R^2 T^2} \tag{5-31}$$

and

$$B = \frac{b_m P}{RT} \tag{5-32}$$

The parameters a_m and b_m are calculated using Equations 5-27 – 5-29 with pure component parameters a_i and b_i (derived from the critical point restriction as explained earlier) which are functions of T_{ci}, P_{ci} and R:

$$a_i = 0.45724\left(\frac{R^2 T_{ci}^2}{P_{ci}^2}\right) \tag{5-33}$$

$$b_i = 0.07780\left(\frac{RT_{ci}}{P_{ci}}\right) \tag{5-34}$$

A special mention must be made of mixing rules. This study's scope does not encompass a detailed discussion on mixing rules. However, it is important to note that there is a large field of study devoted to mixing rules and their application. Apart from the classical mixing rules, there are local composition (LCMR), density dependent (DDMR), composition dependent (CDMR) and density independent mixing rules (DIMR) as well as various combinations of the listed rules. Mühlbauer and Raal (1995) give an excellent review of these mixing rules. The mixing rules used in this work are mentioned below and described in more detail in Appendix B.

Huron and Vidal (1979) proposed the first LCMR by relating the excess Gibbs free energy (G^E) to the pure component (ϕ_i) and mixture fugacity coefficients (ϕ):

$$G^E = RT\left[\ln\phi - \sum_{i=1}^{n} x_i \ln\phi_i\right] \tag{5-35}$$

Equation B.4 relates the fugacity coefficients to G^E models, which are discussed in Section 5.3.3. The fugacity coefficients are soley dependent on the EOS used and a_m and b_m are related to the G^E at infinite pressure:

$$G_{\infty}^{E} = -\left[\frac{a_m}{b_m} - \sum x_i \frac{a_i}{b_i}\right]\Delta \tag{5-36}$$

where G^{E}_{∞} is the excess Gibbs free energy in the limit of infinite pressure and Δ is a constant dependant on which EOS is used as explained by Raal and Mühlbauer (1998). In our work $\Delta = \ln 2$.

The b_m parameter is identical to the classical mixing rule term:

$$b_m = \sum y_i b_i \tag{5-27}$$

and thus Equation 5-36 can be rewritten as:

$$a_m = b_m\left[\sum x_i \frac{a_i}{b_i} + \frac{G_{\infty}^{E}}{\Delta}\right] \tag{5-37}$$

Wong and Sandler (1992) proposed a DIMR mixing rule which is valid at both low and high densities without being density dependent. They equate the virial EOS B coefficient with cubic EOS parameters as in Equation 5-38:

$$B = b_m - a_m / RT \tag{5-38}$$

The composition-independent cross second virial coefficient is related to the pure component parameters as shown in Equation 5-39:

$$\left(b - \frac{a}{RT}\right)_{ij} = \frac{\left[\left(b - \frac{a}{RT}\right)_i + \left(b - \frac{a}{RT}\right)_j\right]}{2}(1 - k_{ij}) \tag{5-39}$$

Where k_{ij} is a second virial coefficient binary interaction parameter.

The excess Helmholtz free energy (A^E) can be related to the a_m and b_m parameters by equating the A^E at infinite pressure from an EOS to that of a liquid phase model:

$$A_\infty^E = \left[\frac{a_m}{b_m} - \sum x_i \frac{a_i}{b_i}\right]\Omega \tag{5-40}$$

where Ω is a constant which depends on the EOS used.

Wong et al. (1992a, b) have shown that:

$$G^E(T, P = 1 \text{ bar}, x) = A^E(T, P = 1 \text{ bar}, x) = A^E(T, P = high, x) \tag{5-41}$$

as A^E is essentially pressure-independent.

Combining the equations results in the mixing-rule parameters being defined as follows:

$$\frac{a_m}{RT} = M\frac{N}{1-N} \tag{5-42}$$

and

$$b_m = \frac{M}{1-N} \tag{5-43}$$

where

$$M = \sum\sum x_i x_j \left(b - \frac{a}{RT}\right)_{ij} \tag{5-44}$$

and

$$N = \sum x_i \frac{a_i}{b_i RT} + \frac{G^E(x_i)}{\Omega RT} \tag{5-45}$$

For the P-R EOS $\Omega = \left[\ln\left(\sqrt{2}-1\right)\right]\sqrt{2}$ and the G^E can be modeled using any one of the models discussed in 5.3.3.

The Twu and Coon (1996) DIMR mixing rule is suited for highly non-ideal systems. It is based on the Wong-Sandler mixing rule and incorporates the superb features of the Wong-Sandler mixing rule while not being hindered by the problems associated with it. The mixture parameters are given as follows:

$$b_m = \frac{b_{m,vdw} - a_{m,vdw}}{1 - \left(\frac{a_{m,vdw}}{b_{m,vdw}} + \frac{1}{C}\frac{A_\infty^E}{RT}\right)} \tag{5-46}$$

and

$$a_m = b_m\left(\frac{a_{m,vdw}}{b_{m,vdw}} + \frac{1}{C}\frac{A_\infty^E}{RT}\right) \tag{5-47}$$

where C is dependent on the EOS ($C = \left[\ln\left(\sqrt{2}-1\right)\right]\sqrt{2}$) and A_∞^E is determined as explained above. The $a_{m,vdW}$ and $b_{m,vdW}$ are the mixing parameters derived from the van der Waals (or classical) mixing rules:

$$a_{m,vdw} = \sum_i \sum_j x_i x_j \sqrt{a_i a_j}(1 - k_{ij}) \tag{5-48}$$

and

$$b_{m,vdw} = \sum_i \sum_j x_i x_j \left[\frac{1}{2}(b_i + b_j)\right](1 - l_{ij}) \tag{5-49}$$

Virial EOS

The virial EOS, developed by Thiesen (1885), is an infinite power series in inverse molar volume:

$$Z = \frac{PV}{RT} = 1 + \frac{B}{V} + \frac{C}{V^2} + \frac{D}{V^3} + \ldots\ldots \tag{5-50}$$

and is used to describe the volumetric behaviour of a real fluid as it deviates from the ideal gas equation. The coefficients *B*, *C*, *D*, etc. are known as the virial coefficients. As very little is known about the coefficients from *C* onwards, the equation is usually truncated after *B*, the second virial coefficient, giving:

$$Z = 1 + \left(\frac{BP}{RT}\right) \tag{5-51}$$

The extension of the virial EOS to mixtures is accomplished by introducing mixing rules:

$$B_m = \sum_{i=1}^{n}\sum_{j=1}^{n} y_i y_j B_{ij} \tag{5-52}$$

where n is the number of components. The interaction parameters are based on statistical mechanical theory and the EOS has the advantaged that the virial coefficients of a mixture are related to its composition. For the truncated virial EOS the fugacity coefficient for a two-component mixture can be expressed as:

$$\ln \hat{\phi}_i = \frac{P}{RT}\left(2\sum_{j=1}^{2} y_i B_{ij} - B_m\right) \tag{5-53}$$

There are many correlations available in literature and these are mentioned in the reviews mentioned above (Walas (1985), Sandler (1994) and Raal and Mühlbauer (1998)). By far the most common correlations are those of Tsonopoulos (1974) and Hayden and O'Connell (1975). The general Tsonopoulos correlation is:

$$\frac{BP}{RT} = B^{(0)} + \omega B^{(1)} \tag{5-54}$$

where

$$B^{(0)} = 0.1445 - \frac{0.33}{T_r} - \frac{0.1385}{T_r^2} - \frac{0.0121}{T_r^3} - \frac{0.000607}{T_r^8} \tag{5-55}$$

and

$$B^{(1)} = 0.0637 + \frac{0.331}{T_r} - \frac{0.424}{T_r^2} - \frac{0.008}{T_r^8} \tag{5-56}$$

The Hayden-O'Connell correlation is more complex, containing its own terms for cross second virial coefficients, and is used for predicting pure and cross second virial coefficients for a larger variety of fluids. The correlation requires only the critical temperature and pressure of the component(s), mean radius of gyration, dipole moment and (if necessary) a chemical association parameter. The correlation assumes the virial coefficient to be the sum of two types of interactions:

$$B_{ij} = B_{ij}^F + B_{ij}^D \tag{5-57}$$

Subscript F refers to the relatively "free" molecules (weak physical forces), and D refers to the "bound" or "dimerised" molecules ("chemical" forces).

A full description of the Tsonopoulos correlation (with extensions for polar compounds) and the Hayden and O'Connell correlation is given in Appendix B.

5.3.3 Activity Coefficient or Gibbs Excess (G^E) Models

To obtain some physical explanation for the activity coefficient, the concept of excess properties needs to be introduced (Gess et al. (1991)). The excess properties are a measure of the disparity

between a real liquid's properties and the values that would be exhibited by a hypothetical ideal solution at the same temperature, pressure and composition:

$$M^E = M - M^{id} \tag{5-58}$$

where the *id* superscript denotes an ideal solution property and the E an excess one. Specifically, the G^E energy property is a very useful term for describing the non-ideality of a liquid solution and used for determining phase stability and separation. The excess molar enthalpy (H^E) term, also known as the heat of mixing, can be used to predict isothermal VLE (or, alternatively, can itself be predicted from VLE data). The excess molar volume (V^E) term provides a measure of the change of volume when two or more components are mixed together. The excess properties of a mixture are related as shown in Equation 5-59:

$$d\left[n\left(\frac{G^E}{RT}\right)\right] = \frac{nV^E}{RT}dP - \frac{nH^E}{RT^2}dT + \sum \ln \gamma_i dn_i \tag{5-59}$$

By returning to the chemical potential property, it can be shown that for an ideal solution:

$$\mu_i^{id} = G_i + RT \ln x_i \tag{5-60}$$

while for a non-ideal solution:

$$\mu_i = G_i + RT \ln \gamma_i x_i \tag{5-61}$$

Now, with $\mu_i = \overline{G}$ (where the bar denotes a partial property), by subtracting 5-60 from 5-61 Equation 5-62 can be obtained:

$$\mu_i - \mu_i^{id} = \overline{G}_i - \overline{G}_i^{id} = RT \ln \gamma_i \tag{5-62}$$

By recognizing that the LHS is the excess property, Equation 5-63 can be obtained:

$$\overline{G}_i^E = RT \ln \gamma_i \tag{5-63}$$

and the following derived:

$$\ln \gamma_i = \left[\frac{\partial \left[n\left(G^E / RT \right) \right]}{\partial n_i} \right]_{T,P,n_{j \neq i}} \tag{5-64}$$

In practise, however, the reverse equation is more useful as it allows the calculation of G^E from experimental data:

$$\frac{G^E}{RT} = \sum x_i \ln \gamma_i \tag{5-65}$$

where $x_i = \dfrac{n_i}{\sum_i n_i}$.

By using Equations 5-64 and 5-65 expressions for the activity coefficients in a binary mixture can be derived:

$$\gamma_1 = \exp\left[\left(\frac{G^E}{RT} \right) + x_2 \frac{d\left(G^E / RT \right)}{dx_1} \right] \tag{5-66}$$

$$\gamma_2 = \exp\left[\left(\frac{G^E}{RT} \right) - x_1 \frac{d\left(G^E / RT \right)}{dx_1} \right] \tag{5-67}$$

The γ_i is a function of the measurable properties temperature, pressure and composition.

There are many functional forms for G^E and in general they are purely empirical. The five most common models are listed below and are discussed briefly:

i.) Margules
ii.) Van Laar
iii.) Wilson
iv.) NRTL
v.) UNIQUAC

These models are discussed in detail (as well as some of the others) in Walas (1985), Gess et al. (1991), Malanowski and Anderko (1992), Sandler (1994) and Raal and Mühlbauer (1998).

Margules Equation

Margules first proposed this equation in 1895 and, despite being over a century old, it is still in common use today and gives surprisingly accurate results for some systems. The simplest form of the equation (the two-suffix) can be expressed in terms of the G^E for a binary system as follows;

$$\frac{G^E}{RT} = Ax_1x_2 \tag{5-68}$$

from which the following can be derived using Equation 5-64:

$$\ln \gamma_1 = Ax_2^2 \tag{5-69}$$

$$\ln \gamma_2 = Ax_1^2 \tag{5-70}$$

The use of the two-suffix model is limited due to it's simplicity. It describes a symmetric relationship between x_i and G^E which is not applicable to most real systems, which display asymmetric behaviour. The three-suffix model is more suited to complicated behaviour:

$$\frac{G^E}{RT} = x_1x_2\left[A_{12}x_2 + A_{21}x_1\right] \tag{5-71}$$

with

$$\ln \gamma_1 = \left[A_{12} + 2\left(A_{21} - A_{12}\right) x_1 \right] x_2^2 \tag{5-72}$$

$$\ln \gamma_2 = \left[A_{21} + 2\left(A_{12} - A_{21}\right) x_2 \right] x_1^2 \tag{5-73}$$

The G^E for the four-suffix equation is given by:

$$\frac{G^E}{RT} = x_1 x_2 \left[A_{12} x_2 + A_{21} x_1 - C x_1 x_2 \right] \tag{5-74}$$

with

$$\ln \gamma_1 = \left[A_{12} + 2\left(A_{21} - A_{12} - C\right) x_1 + 3C x_1^2 \right] x_2^2 \tag{5-75}$$

$$\ln \gamma_2 = \left[A_{21} + 2\left(A_{12} - A_{21} - C\right) x_2 + 3C x_2^2 \right] x_1^2 \tag{5-76}$$

Higher order Margules equations can be used for more complicated systems, but with the higher order equations there is the risk that the equation will describe experimental errors giving incorrect curvatures or inflection points. Poor fits for the Margule Equation can be attributed to the fact that the equation does not account for different sized molecules.

van Laar Equation

The van Laar equation was developed in 1910. It accounts for molecules of different sizes and is based on the van der Waals equation. The equation is obtained by expanding the inverse function $\frac{x_1 x_2}{G^E / RT}$ as a polynomial in $(x_1 - x_2)$:

$$\frac{x_1 x_2}{G^E / RT} = B + C(x_1 - x_2) \tag{5-77}$$

which can be expressed as:

$$\frac{G^E}{RT} = \frac{A_{12}A_{21}x_1x_2}{x_1A_{12} + x_2A_{21}} \tag{5-78}$$

This implies:

$$\ln \gamma_1 = A_{12}\left[\frac{A_{21}x_2}{x_1A_{12} + x_2A_{21}}\right]^2 \tag{5-79}$$

$$\ln \gamma_2 = A_{21}\left[\frac{A_{12}x_1}{x_1A_{12} + x_2A_{21}}\right]^2 \tag{5-80}$$

The van Laar equation is best suited to relatively simple, non-polar systems. In general it is found that systems that are well fitted for the van Laar equation give poor results for Margules and vice versa.

The Wilson Equation

Unlike the previous two equations, the equation developed by Wilson (1964) considers local compositions and accounts for molecules of different size and energy interactions between two molecules in a solution. The function for G^E is given as:

$$\frac{G^E}{RT} = -x_1 \ln\left[x_1 + x_2\Lambda_{12}\right] - x_2 \ln\left[x_2 + x_1\Lambda_{21}\right] \tag{5-81}$$

with

$$\ln \gamma_1 = -\ln\left[x_1 + x_2\Lambda_{12}\right] + x_2\left[\frac{\Lambda_{12}}{x_1 + x_2\Lambda_{12}} - \frac{\Lambda_{21}}{x_2 + x_1\Lambda_{21}}\right] \tag{5-82}$$

$$\ln \gamma_2 = -\ln\left[x_2 + x_1\Lambda_{21}\right] - x_1\left[\frac{\Lambda_{12}}{x_1 + x_2\Lambda_{12}} - \frac{\Lambda_{21}}{x_2 + x_1\Lambda_{21}}\right] \tag{5-83}$$

The two adjustable parameters, Λ_{12} and Λ_{21}, are related to the pure component liquid molar volumes (V_i) as follows:

$$\Lambda_{12} = \frac{V_2}{V_1}\exp\left[-\frac{\lambda_{12}-\lambda_{11}}{RT}\right] \tag{5-84}$$

$$\Lambda_{21} = \frac{V_1}{V_2}\exp\left[-\frac{\lambda_{21}-\lambda_{22}}{RT}\right] \tag{5-85}$$

where V_i can be calculated using the Rackett (1970) equation:

$$V_i = V_{ci}Z_{ci}^{(1-T_{ri})^{0.2857}} \tag{5-86}$$

Values for V_{ci}, Z_{ci} (critical compressibility factor of component i) and T_{ri}, can be found for a large number of fluids in Reid et al. (1988).

The (λ_{12}-λ_{11}) and (λ_{21}-λ_{22}) parameters characterise the molecular interactions between the components. The temperature dependence of Λ_{12} and Λ_{21} is shown in Equations 5-84 and 5-85 respectively. It is important to note that the temperature effect is only approximate.

The Wilson equation is generally found to be as good as, if not better than, the three-suffix Margules and van Laar equations. The Wilson equation is able to model systems with molecules of different sizes and systems with large non-ideality. The equation, however, is not able to model systems with liquid immiscibility, nor systems with a maximum or minimum in the ln γ_i vs. x_i curves. The Wilson equation can be extended to multicomponent systems without introducing parameters other than for the constituent binaries.

The NRTL (nonrandom two-liquid) equation

The NRTL equation was developed by Renon and Prausnitz (1968) to overcome the inability of the Wilson equation to model systems with liquid immiscibility. The NRTL equation is a local

composition model that is able to model highly non-ideal and immiscible solutions. The equation for G^E is as follows:

$$\frac{G^E}{RT} = x_1 x_2 \left[\frac{\tau_{21} G_{21}}{x_1 + x_2 G_{21}} + \frac{\tau_{12} G_{12}}{x_2 + x_1 G_{12}} \right] \tag{5-87}$$

with

$$\ln \gamma_1 = x_2^2 \left[\tau_{21} \left(\frac{G_{21}}{x_1 + x_2 G_{21}} \right)^2 + \left(\frac{\tau_{12} G_{12}}{\left(x_2 + x_1 G_{12} \right)^2} \right) \right] \tag{5-88}$$

$$\ln \gamma_2 = x_1^2 \left[\tau_{12} \left(\frac{G_{12}}{x_2 + x_1 G_{12}} \right)^2 + \left(\frac{\tau_{21} G_{21}}{\left(x_1 + x_2 G_{21} \right)^2} \right) \right] \tag{5-89}$$

where

$$\tau_{ji} = \frac{g_{ji} - g_{ii}}{RT} \tag{5-90}$$

$$G_{ji} = \exp\left[-\alpha_{ji} \tau_{ji} \right] \tag{5-91}$$

The NRTL equation has limited explicit temperature dependence that is evident from Equation 5-107. The three adjustable parameters, (g_{12}-g_{22}), (g_{21}-g_{11}) and α_{12} ($\alpha_{12} = \alpha_{21}$), are determined from data reduction. The α_{12} value usually ranges between –1 and 0.5 and is often fixed at 0.3. The NRTL equation is one of the most commonly used and useful equations in describing phase equilibrium. Like the Wilson equation, it can be extended to model multicomponent systems.

The UNIQUAC (universal quasi-chemical theory) Equation

Abrams & Prausnitz [1975] developed the UNIQUAC equation by incorporating the two-liquid model and the concept of local compositions in this equation. The equation has a wide range of applicability (to miscible and immiscible solutions) and incorporates parameter temperature

dependence, however, the equations are more complex than the models discussed previously. The explanation that follows is the modified version of the equation of Anderson and Prausnitz (1978). In the equation, the G^E function is divided into two parts:

$$G^E = G^E(C) + G^E(R) \tag{5-92}$$

In Equation 5-92, the C refers to the combinatorial contribution and the R refers to the residual contribution. For a binary mixture:

$$\frac{G^E(C)}{RT} = x_1 \ln\frac{\Phi_1}{x_1} + x_2 \ln\frac{\Phi_2}{x_2} + \frac{z}{2}\left[q_1 x_1 \ln\frac{\theta_1}{\phi_1} + q_2 x_2 \ln\frac{\theta_2}{\phi_2}\right] \tag{5-93a}$$

$$\frac{G^E(R)}{RT} = -q_1 x_1 \ln\left[\theta_1 + \theta_2 \tau_{21}\right] - q_2 x_2 \ln\left[\theta_2 + \theta_1 \tau_{12}\right] \tag{5-93b}$$

The co-ordination number, z, in Equation 5-93a is set equal to ten, and the segment fractions, Φ_i and area fractions, θ_i are given by:

$$\Phi_i = \frac{x_i r_i}{x_i r_i + x_j r_j} \tag{5-94}$$

$$\theta_i = \frac{x_i q_i}{x_i q_i + x_j q_j} \tag{5-95}$$

The parameters, r_i and q_i (size and surface parameters respectively), are the pure component molecular structure parameters. They are evaluated from molecular structure contributions for various groups and subgroups (r and q). The values for r and q as well as the method of determining r_i and q_i is discussed in Raal & Mühlbauer (1998) and Fredenslund et al. (1977).

The final two parameters, τ_{12} and τ_{21}, in Equation 5-93 are determined by data reduction and are defined by:

$$\tau_{12} = \exp\left[-\frac{(u_{12}-u_{22})}{RT}\right] \tag{5-96a}$$

$$\tau_{21} = \exp\left[-\frac{(u_{21}-u_{11})}{RT}\right] \tag{5-96b}$$

Thus, the activity coefficients for a binary mixture are given by:

$$\ln \gamma_i = \ln \gamma_i^{C} + \ln \gamma_i^{R} \tag{5-97}$$

where

$$\ln \gamma_i^{C} = \ln \frac{\Phi_i}{x_i} + \frac{z}{2} q_i \ln \frac{\theta_i}{\Phi_i} + \Phi_j \left[l_i - \frac{r_i}{r_j} l_j \right] \tag{5-98}$$

$$\ln \gamma_i^{R} = -q_i \ln\left[\theta_i + \theta_j \tau_{ji}\right] + \theta_j q_i \left[\frac{\tau_{ji}}{\theta_i + \theta_j \tau_{ji}} - \frac{\tau_{ij}}{\theta_j + \theta_i \tau_{ij}} \right] \tag{5-99}$$

and where

$$l_i = \frac{z}{2}[r_i - q_i] - [r_i - 1] \tag{5-100}$$

The UNIQUAC equation performs well for a wide variety of liquid mixtures containing polar or non-polar fluids. However, the main drawback of this model is its complexity and the need for group contribution values (r and q), which are not always available in literature. The UNIFAC equations (extension of UNIQUAC) can be used for VLE prediction.

5.4 OTHER THERMODYNAMIC FUNCTIONS

5.4.1 Other Excess Properties

The concept of excess properties was discussed in Section 5.3.3. In Section 5.3.3 the emphasis is on the excess Gibbs energy. However, as is shown by Equation 5-59 (the fundamental excess-property relation), G^E is related to other excess properties:

$$d\left[n\left(\frac{G^E}{RT}\right)\right] = \frac{nV^E}{RT}dP - \frac{nH^E}{RT^2}dT + \sum \ln \gamma_i dn_i \qquad (5\text{-}59)$$

From this equation the following expression for the heat-of-mixing is obtained at constant pressure and composition:

$$H^E = -RT^2\left[\frac{\partial\left(G^E/RT\right)}{\partial T}\right]_{P,\,x_i} \qquad (5\text{-}101)$$

Equation 5-101 is a form of the well-known Gibbs-Helmholtz equation (Raal and Mühlbauer (1998)) relating G^E and H^E. Thus, if a binary system has been measured at two or more temperatures, the isothermal data can be used to determine HE values. (Conversely, VLE can be predicted from experimental HE values as described by Hanks et al. (1971).) First the data are fitted with a GE model as discussed in Section 5.3.3. At selected compositions, a $\frac{G^E}{RT}$ vs. T function is plotted and fitted with a linear equation. The slope of the equation gives the value for $\left[\frac{\partial\left(G^E/RT\right)}{\partial T}\right]$ and thus values for H^E can be determined. The reader is referred to Joseph et al. (2001) for examples of this technique.

The excess entropy (S^E) is calculated using Equation 5-102:

$$G^E = H^E - TS^E \qquad (5\text{-}102)$$

5.4.2 Thermodynamic consistency tests

Thermodynamic consistency tests can only be applied to a full set of VLE data (i.e.: P, T, x_i and y_i) and as most data in this work are P-T-x_i data, these tests could not be applied. However, it is of importance to mention these tests and give an example of one.

Thermodynamic consistency tests are based on the Gibbs-Duhem equation:

$$\sum x_i d\ln\gamma_i = \frac{V^E}{RT}dP - \frac{H^E}{RT^2}dT \tag{5-103}$$

that inter-relates the activity coefficients of all components in a mixture. The Gibbs-Duhem equation can be applied to systems where experimental VLE data are available for all of the activity coefficients. If these data do not satisfy Equation 5-101, they are not correct (Prausnitz et al. (1986)). Only VLE data that satisfy the Gibbs-Duhem equation are thermodynamically consistent.

As an example of thermodynamic consistency tests (TCT) the direct test of van Ness (1995) is used.

Direct test of van Ness (1995)

The TCT of van Ness (1995) requires that the data reduction method minimize the objective function:

$$F = \left(\frac{g^* - g}{g^*}\right)^2 \tag{5-104}$$

where $g = \frac{G^E}{RT}$ and * denotes an experimental value.

For a binary system Equation 5-65 is given by:

$$g^* = x_1 \ln\gamma_1^* + x_2 \ln\gamma_2^* \tag{5-105}$$

and differentiating this equation yields:

$$\frac{dg^*}{dx_1} = \ln\frac{\gamma_1^*}{\gamma_2^*} + \varepsilon + x_1\frac{d\ln\gamma_1^*}{dx_1} + x_2\frac{d\ln\gamma_2^*}{dx_1} - \varepsilon \tag{5-106}$$

where, for isothermal data:

$$\varepsilon = \frac{V^E}{RT}\frac{dP}{dx_1} \tag{5-107}$$

and for isobaric data:

$$\varepsilon = \frac{-H^E}{RT^2}\frac{dT}{dx_1} \tag{5-108}$$

If Equation 5-59 is applied to one mole of a binary liquid, then Equation 5-109 can be derived (written for only isothermal or only isobaric data):

$$\frac{dg}{dx_1} = \ln\frac{\gamma_1}{\gamma_2} + \varepsilon \tag{5-109}$$

By subtracting Equation 5-106 from Equation 5-109, Equation 5-110 is obtained:

$$\frac{dg}{dx_1} - \frac{dg^*}{dx_1} = \ln\frac{\gamma_1}{\gamma_2} - \ln\frac{\gamma_1^*}{\gamma_2^*} - \left[x_1\frac{d\ln\gamma_1^*}{dx_1} + x_2\frac{d\ln\gamma_2^*}{dx_1} - \varepsilon\right] \tag{5-110}$$

and in terms of residuals ($\delta g = g - g^*$), this equation becomes:

$$\frac{d(\delta g)}{dx_1} = \delta\ln\frac{\gamma_1}{\gamma_2} - \left[x_1\frac{d\ln\gamma_1^*}{dx_1} + x_2\frac{d\ln\gamma_2^*}{dx_1} - \varepsilon\right] \tag{5-111}$$

If the data set is regressed with $F = \left(\frac{g^* - g}{g^*} \right)^2$ as the objective function as explained above, then $d(\delta g)/dx_1$ can be said to be effectively zero, and, thus:

$$\delta \ln \frac{\gamma_1}{\gamma_2} = x_1 \frac{d \ln \gamma_1^*}{dx_1} + x_2 \frac{d \ln \gamma_2^*}{dx_1} - \varepsilon \tag{5-112}$$

At constant T and P the Gibbs-Duhem equation reduces to Equation 5-113:

$$\sum x_i d \ln \gamma_i = 0 \tag{5-113}$$

Using this reduced form, the right-hand side of Equation 5-112 should be zero for consistent data. Thus the residual on the left is a direct measure of the system's deviation from the Gibbs-Duhem equation. The data's departure from thermodynamic consistency is measured by the extent to which values of this residual fail to scatter about zero.

Van Ness (1995) developed a consistency index (Table 5-1) which can be used to evaluate the level of consistency of the data. The index uses the root-mean square (RMS) value of $\delta \ln(\gamma_1/\gamma_2)$ as reference points. Thus to use the test the data must first be regressed and then the RMS value of the $\delta \ln(\gamma_1/\gamma_2)$ calculated and compared to Table 5-1 to assess the consistency of the data.

Table 5-1 Consistency index based on RMS values $\delta \ln(\gamma_1/\gamma_2)$ (van Ness (1995))

Index	RMS $\delta \ln(\gamma_1/\gamma_2)$		Comments
1	>0	< 0.025	excellent
2	>0.025	< 0.050	very good
3	>0.050	< 0.075	good
4	>0.075	< 0.100	satisfactory
5	>0.100	< 0.125	poor
6	>0.125	< 0.150	very poor
7	>0.150	< 0.175	
8	>0.175	< 0.200	
9	>0.200	< 0.225	
10	>0.225		

5.4.3 Infinite dilution activity coefficients (IDACs)

As $x_i \rightarrow 0$ so $\gamma_i \rightarrow \gamma_i^{\infty}$. This value, γ_i^{∞}, is defined as the IDAC. IDACs are extremely important for the design and operation of separation processes especially those concerned with extracting very high purity chemicals from solutions. There are many experimental procedures as well as specialized equipment setups to determine IDACs. These are not discussed here but are discussed in detail by Raal and Mühlbauer (1998). IDACs can be deterermined from VLE data by either extrapolating the data in the dilute region (including special deviation pressure techniques) or directly from the fitted G^E models. The latter is the less satisfactory method.

IDACs calculated directly from G^E *models*

Most G^E models can be reduced to give an expression for the IDACs. Below are the equations used which are directly linked to the G^E models:

- Margules two-suffix

$$\ln \gamma_i^{\infty} = A \tag{5-114}$$

- Margules three- and four-suffix

$$\ln \gamma_i^{\infty} = A_{ij} \tag{5-115}$$

- Van Laar

$$\ln \gamma_i = A_{ij} \tag{5-116}$$

- Wilson

$$\ln \gamma_i^{\infty} = -\ln \Lambda_{ij} + 1 - \Lambda_{ji} \tag{5-117}$$

- NRTL

$$\ln \gamma_i^{\infty} = \tau_{ij} \exp(-\alpha_{ij}\tau_{ij}) + \tau_{ji} \tag{5-118}$$

where $\alpha_{ij} = \alpha_{ji}$.

- UNIQUAC

$$\ln \gamma_i^{\infty} = m + q_i - q_i\left(\tau_{ij} + \ln \tau_{ji}\right) \tag{5-119}$$

where

$$m = \ln\left(\frac{r_i}{r_j}\right) + \frac{z}{2} q_i \ln\left(\frac{q_i r_j}{q_j r_i}\right) + l_i - \left(\frac{r_i}{r_j}\right) l_j \tag{5-120}$$

The accuracy of determining IDACs directly from the fitted G^E model depends on the dispersal of the data and the fit of the model.

IDACs calculated by extrapolating VLE data

Simply extrapolating the γ_i curve to the end point where $x_i = 0$ usually does not give good values for γ_i^∞ (Hartwick & Howat (1995)). A better technique for obtaining γ_i^∞ values from isothermal data is the method of Ellis & Jonah (1962), as modified by Maher & Smith (1979) which was used in this work.

The equations of Gautreaux and Coates (1955) relate the IDAC to the partial derivative of pressure with respect to liquid composition. They are complex and difficult to use but can be simplified at low P and moderate T (Pividal et al. (1992)) to give:

$$\gamma_1^\infty = \varepsilon_1^\infty \left(P_2^{sat} / P_1^{sat} \right) \left\{ 1 + \beta_2 \left(1 / P_2^{sat} \right) \left(\partial P / \partial x_1 \right)_T^{x_1=0} \right\} \tag{5-121}$$

where

$$\varepsilon_1^\infty = \exp\left[\frac{\left(B_{11} - V_1\right)\left(P_2^{sat} - P_1^{sat}\right) + \delta_{12} P_2^{sat}}{RT} \right] \tag{5-122}$$

$$\beta_2 = 1 + P_2^{sat} \left(\frac{B_{22} - V_2}{RT} \right) \tag{5-123}$$

$$\delta_{12} = 2B_{12} - B_{11} - B_{22} \tag{5-124}$$

where B is the second virial coefficient and V is the liquid molar volume. The final accuracy of the γ_1^∞ value is dependent on the evaluation of the partial derivative, $\left(\partial P / \partial x_1 \right)_T^{x_1=0}$. Maher and Smith (1979) proposed converting the P vs. x_1 data to deviation pressure, P_D, vs. x_1 values using:

$$P_D = P - \left[P_2^{sat} + \left(P_1^{sat} - P_2^{sat} \right) x_1 \right] \tag{5-125}$$

By differentiating Equation 5-125 and taking the limit as $x_1 \rightarrow 0$, Equation 5-126 is obtained:

$$\left(P_D / x_1 x_2 \right)_{x_1=0} = \left(\partial P / \partial x_1 \right)_{x_1=0} - P_1^{sat} + P_2^{sat} \tag{5-126}$$

where $\left(P_D / x_1 x_2 \right)_{x_1=0}$ is determined by extrapolating a linear plot of $\left(P_D / x_1 x_2 \right)$ vs. x_1 to $x_1 = 0$. If the slope of $\left(P_D / x_1 x_2 \right)$ vs. x_1 is not linear, it is suggested that $\left(x_1 x_2 / P_D \right)$ vs. x_1 be used. A similar procedure is used to determine γ_2^{∞}.

5.4.4 Henry's Constant

Henry's constant (H_i) is defined as:

$$\hat{f}_i^{id} = x_i H_i \tag{5-127}$$

for dilute solutions and is used to describe the solubility of the gas in the solvent. It is usually only applicable to situations where the partial pressure of the gas is below 500 to 1000 kPa (Prausnitz et al. (1986)). Dispensing with the term fugacity we can equate:

$$y_i \hat{\phi}_i^v P = H_i x_i \tag{5-128}$$

CHAPTER

SIX

RESULTS

6.1 INTRODUCTION

Vapour pressures and VLE data were measured on three pieces of equipment:

vii.) Static apparatus of Rarey and Gmehling (1993),

viii.) Static apparatus of Kolbe and Gmehling (1985) as modified by Fischer and Wilken (2001), and,

ix.) Dynamic apparatus of Harris et al. (2003b).

Fourteen sets of VLE data and eight vapour pressure data sets were measured. Temperatures ranged from 308.33 K to 583.90 K and pressures from 1.00 kPa to 20 877.80 kPa (20.88 Mpa). Twelve of the fourteen sets of VLE data measured are new data sets. Six of the VLE data sets are high-pressure measurements, four are moderate-pressure measurements and four are low-pressure measurements. All the vapour pressure measurements, except one, were at low pressures. In total 370 data points were measured.

6.2 SYSTEMS MEASURED

6.2.1 Chemicals Used

Table 6-1 lists the chemicals used in the experimental work. The chemical suppliers, stated purities and GC analyses are also listed.

Table 6-1 List of chemicals and their respective purities

Chemical	Supplier	Stated Purity	GC Purity
Carbon dioxide	N/A	>99.999%	N/A
n-Hexane	MERCK	99%	N/A
n-Heptane	Lab-Scan	99%	>99%
n-Decane	Sigma	>99%	>99%
n-Dodecane	Sigma	99%	>99%
n-Hexadecane	Aldrich	>99%	>99%
1-Octadecene	MERCK	92%	98.6%
Cyclohexane	Riedel de Haen	99.50%	>99.5%
Benzene	MERCK	99%	N/A
Napthalene	MERCK	99%	N/A
Ethanol	Saarchem	99.50%	>99.5%
1-Hexadecanol	Fluka	99%	>99%
Benzoic acid	MERCK	99%	N/A
Chlorobenzene	MERCK	99%	N/A
Acetonitrile	MERCK	99%	N/A
n-Methyl formamide	MERCK	99%	N/A
d,l Menthol	UNILAB	99%	>99%
(+)-isoMenthol	Fluka	99%	>99%

6.2.2 Static Equipment Systems

As explained in Chapter Three, two pieces of static apparatus were used. Table 6-2 lists the measurements conducted on the apparatus of Gmehling and Rarey (1993). These measurements were conducted at low to moderate pressures. The measurements were performed in the laboratories of Professor Jurgen Gmehling in Oldenburg, Germany as part of a collaboration between the Thermodynamics Research Unit (University of Natal) and the Department of Industrial Chemistry (University of Oldenburg) and are published in Harris et al. (2003a) and Harris et al. (2003d). The work of Ms. S. Laue is gratefully acknowledged.

Table 6-2 Systems measured on the static apparatus of Rarey and Gmehling (1993)

System	T / K	P_{min} / kPa	P_{max} / kPa
n-Hexane (1) + N-Methylformamide (2)	363.15	2.01	189.20
Benzene (1) + N-Methylformamide (2)	363.15	1.95	137.28
Chlorobenzene (1) + N-Methylformamide (2)	363.15	2.10	28.33
Acetonitrile (1) + N-Methylformamide (2)	363.15	2.13	131.21

Table 6-3 lists the measurements conducted on the apparatus of Kolbe and Gmehling (1985) (as modified by Fischer and Wilken (2001)). The measurements are for high pressure VLE and several dew points. These measurements were performed in the laboratories of Professor Jurgen Gmehling in Oldenburg, Germany as part of a collaboration between a collaboration between the Thermodynamics Research Unit (University of Natal) and the Department of Industrial Chemistry (University of Oldenburg) and are published in Harris et al. (2002b) and Harris et al. (2003a). The help and collaboration of Mr. M. Wilken is gratefully acknowledged.

Table 6-3 Systems measured on the apparatus of Kolbe and Gmehling (1985) (as modified by Fischer and Wilken (2001))

System	T / K	P_{min} / kPa	P_{max} / kPa
Carbon dioxide (1) + Napthalene (2)	372.45	23.80	19413.80
Carbon dioxide (1) + Napthalene (2)	403.85	23.80	20877.80
Carbon dioxide (1) + Napthalene (2)	430.65	30.80	20559.80
Carbon dioxide (1) + Benzoic acid (2)	403.28	37.80	19923.80
Carbon dioxide (1) + Benzoic acid (2)	432.62	13.80	20711.80
Carbon dioxide (1) + Benzoic acid (2)	458.37	28.80	20507.80

All these measurements were of the static synthetic type except for the dew point measurements.

6.2.3 Dynamic Equipment Systems

Low Pressure – High Temperature Test Systems

Several test systems were measured to encompass the large temperature range for which the equipment was designed. Table 6-4 lists the vapour pressure measurement ranges for the test systems.

Table 6-4 Vapour pressures measured as test systems

System	T_{min} / K	T_{max} / K	P_{min} / kPa	P_{max} / kPa
n-Heptane	308.33	363.82	10.01	80.01
n-Decane	373.95	412.15	9.99	40.01
n-Dodecane	369.79	469.01	1.50	70.05
n-Hexadecane	473.45	529.84	10.07	50.02
1-Octadecene	466.04	543.85	3.02	40.03
1-Hexadecanol	480.78	583.90	3.50	80.00
d,l Menthol	362.23	481.39	1.00	89.93

Table 6-5 lists the isobaric VLE test systems that were measured.

Table 6-5 Isobaric VLE test systems

System	P / kPa	T_{min} / K	T_{max} / K
Cyclohexane (1) + Ethanol (2)	40.00	314.56	329.55
n-Dodecane (1) + 1-Octadecene (2)	26.66	439.51	527.44

Low Pressure – High Temperature Systems

Two new systems were measured in the low pressure – high temperature regime. These systems are listed in Table 6-6.

Table 6-8 VLE Data for the System Hexane (1) + N-Methylformamide (2) at 363.15 K

x_1	P /kPa	x_1	P /kPa	x_1	P /kPa
0.000	2.01	0.126	189.05	0.675	188.86
0.002	13.51	0.152	189.06	0.736	188.88
0.004	22.47	0.182	189.08	0.789	188.86
0.007	33.12	0.214	189.12	0.837	188.86
0.010	44.93	0.248	189.14	0.879	188.85
0.012	56.36	0.274	188.96	0.913	188.84
0.019	83.32	0.283	189.20	0.941	188.84
0.026	105.96	0.309	188.93	0.959	188.82
0.034	129.69	0.349	188.90	0.971	188.82
0.043	153.13	0.394	188.89	0.981	188.81
0.053	175.07	0.443	188.88	0.988	188.74
0.065	188.98	0.497	188.88	0.994	188.44
0.081	189.04	0.554	188.86	0.997	188.38
0.102	189.05	0.614	188.86	1.000	188.05

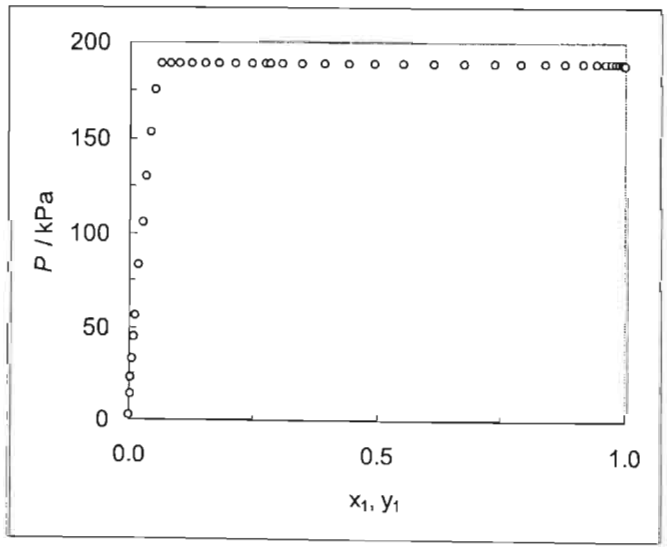

Figure 6-1: Experimental P–x_1 data for the system n-Hexane (1) + N-Methylformamide (2) at 363.15 K.

Table 6-6 Isothermal systems measured with the equipment of Harris et al. (2003b)

System	T_{min} / K	T_{max} / K	P_{min} / kPa	P_{max} / kPa
d,l Menthol (1) + d iso-Menthol (2)	448.15	constant	28.70	33.00
n-Dodecane (1) + 1-Octadecene (2)	387.05	463.53	3.00	constant

High Pressure Systems

Table 6-7 gives the details of the vapour pressures measured as the high-pressure test system.

Table 6-7 Vapour pressures measured as test systems

System	T_{min} / K	T_{max} / K	P_{min} / kPa	P_{max} / kPa
Acetone	327.82	414.12	98.50	995.60

6.3 RESULTS

6.3.1 Static Equipment Systems

Systems measured on the equipment of Rarey and Gmehling (1993)

Measurements were conducted as explained in Chapter Three. Tables 6-8 to 6-11 list the experimental data for the four binary VLE systems, hexane (1) + N-methylformamide (2), benzene (1) + N-methylformamide (2), chlorobenzene (1) + N-methylformamide (2) and acetonitrile (1) + N-methylformamide (2), measured at 363.15 K. The P-x_1 data are plotted in Figures 6-1 to 6-4.

Table 6-9 VLE Data for the System Benzene (1) + N-Methylformamide (2) at 363.15 K

x_1	P /kPa	x_1	P /kPa	x_1	P /kPa
0.000	1.95	0.221	82.85	0.807	129.39
0.002	3.15	0.258	90.36	0.849	130.44
0.004	4.46	0.297	96.99	0.886	131.41
0.007	5.92	0.337	102.82	0.917	132.38
0.010	7.40	0.359	105.32	0.942	133.30
0.012	8.74	0.378	107.84	0.961	134.26
0.021	13.43	0.400	109.72	0.974	135.04
0.032	19.06	0.418	111.99	0.982	135.66
0.046	25.55	0.444	113.66	0.989	136.18
0.061	32.63	0.492	117.17	0.993	136.55
0.080	40.30	0.543	120.18	0.997	136.94
0.101	48.47	0.596	122.75	0.999	137.15
0.125	56.77	0.650	124.87	1.000	137.28
0.154	65.78	0.704	126.62		
0.186	74.56	0.757	128.09		

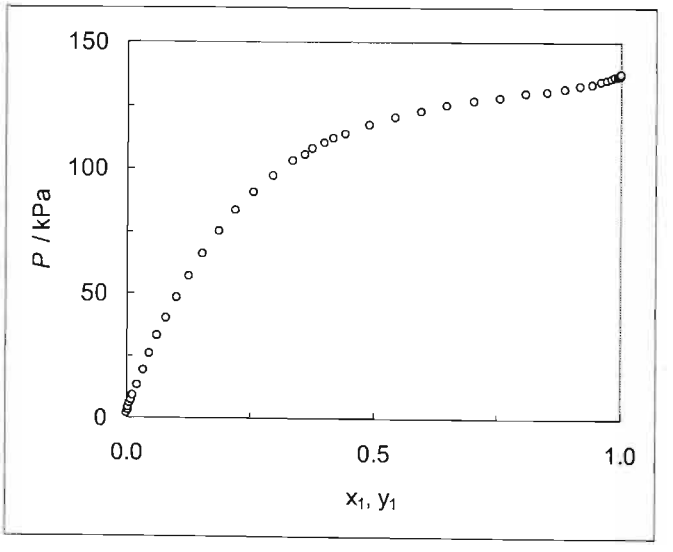

Figure 6-2: Experimental P–x_1 data for the system Benzene (1) + N-Methylformamide (2) at 363.15 K.

Table 6-10 VLE Data for the System Chlorobenzene (1) + N-Methylformamide (2) at 363.15 K

x_1	P /kPa	x_1	P /kPa	x_1	P /kPa
0.000	2.10	0.189	17.86	0.732	27.17
0.002	2.34	0.223	19.39	0.786	27.44
0.003	2.52	0.260	20.73	0.831	27.65
0.005	2.76	0.299	21.91	0.871	27.85
0.008	3.18	0.330	22.77	0.906	28.03
0.012	3.67	0.338	22.91	0.933	28.18
0.017	4.32	0.369	23.60	0.955	28.30
0.024	5.20	0.378	23.73	0.970	28.36
0.034	6.36	0.413	24.36	0.979	28.39
0.047	7.69	0.417	24.43	0.986	28.39
0.062	9.15	0.460	25.03	0.991	28.38
0.080	10.80	0.511	25.61	0.996	28.36
0.101	12.53	0.564	26.10	0.999	28.34
0.127	14.37	0.620	26.52	1.000	28.33
0.156	16.16	0.676	26.87		

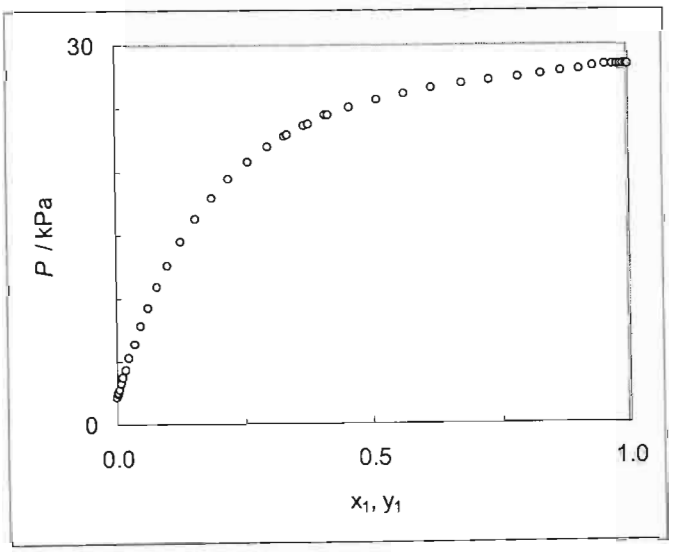

Figure 6-3: Experimental $P - x_1$ data for the system Chlorobenzene (1) + N-Methylformamide (2) at 363.15 K.

Table 6-11 VLE Data for the System Acetonitrile (1) + N-Methylformamide (2) at 363.15 K

x_1	P /kPa	x_1	P /kPa	x_1	P /kPa
0.000	2.13	0.286	52.47	0.841	113.04
0.005	3.14	0.331	58.76	0.876	116.67
0.008	3.93	0.377	64.74	0.905	119.69
0.013	5.03	0.423	70.38	0.929	122.37
0.018	6.05	0.469	75.64	0.949	124.67
0.026	7.70	0.513	80.51	0.964	126.56
0.041	10.82	0.554	84.93	0.976	128.04
0.058	14.20	0.576	87.31	0.984	129.02
0.080	18.46	0.594	88.97	0.989	129.68
0.105	23.09	0.622	91.93	0.992	130.17
0.133	28.22	0.668	96.46	0.995	130.55
0.165	33.78	0.714	100.85	0.998	130.85
0.200	39.59	0.759	105.10	0.999	131.01
0.242	46.05	0.802	109.19	1.000	131.21

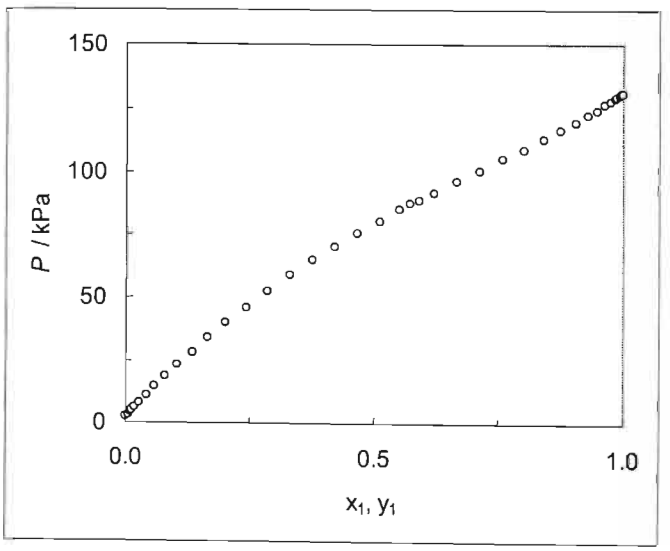

Figure 6-4: Experimental $P - x_1$ data for the system Acetonitrile (1) + N-Methylformamide (2) at 363.15 K.

Systems measured on the equipment of Kolbe and Gmehling (1985)

Measurements were conducted as explained in Chapter Three. Table 6-12 lists the experimental P-x_1 data for the three binary VLE systems CO_2 (1) + Napthalene (2) measured at T = 372.45 K, 403.85 K and 430.65 K. Table 6-13 lists the experimental dew points measured at T = 372.45 K, 403.85 K and 430.65 K for the system CO_2 (1) + Napthalene (2). The P-x_1 data and dew points are plotted in Figure 6-5.

Table 6-14 lists the experimental P-x_1 data for the three binary VLE systems CO_2 (1) + Benzoic acid (2) measured at T = 403.28 K, 432.62 K and 458.37 K. The P-x_1 data are plotted in Figure 6-5.

Table 6-12 P-x_1 Data for the System CO_2 (1) + Napthalene (2)

T / K	372.45	403.85		430.65	
x_1	P / MPa	x_1	P / MPa	x_1	P / MPa
0.000	0.024	0.000	0.024	0.000	0.031
0.003	0.103	0.004	0.164	0.002	0.115
0.032	0.981	0.024	0.835	0.021	0.850
0.106	3.293	0.079	2.767	0.070	2.782
0.133	4.116	0.136	4.818	0.123	4.863
0.191	5.901	0.195	6.914	0.173	6.858
0.261	8.012	0.246	8.788	0.231	9.191
0.325	9.977	0.304	10.910	0.275	10.938
0.393	12.014	0.358	12.956	0.322	12.818
0.458	13.987	0.412	14.991	0.370	14.732
0.521	15.873	0.466	17.037	0.415	16.530
0.580	17.609	0.523	19.168	0.469	18.658
0.644	19.414	0.569	20.878	0.518	20.560

Table 6-13 Dew points for the system CO_2 (1) + naphthalene (2)

T / K	372.45	403.85		430.65	
y_1	P / MPa	y_1	P / MPa	y_1	P / MPa
0.980	18.798	0.980	19.825	0.970	23.404
0.980	18.523	0.980	19.755	0.980	20.933
				0.980	20.769

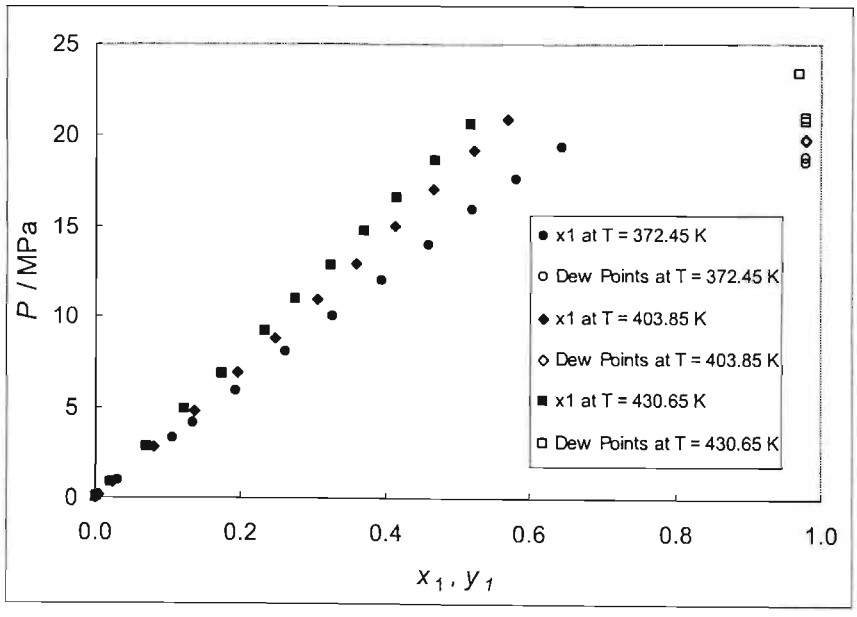

Figure 6-5: Experimental P-x_1 and dew points for the system CO_2 (1) + Napthalene (2).

Table 6-14 P-x_1 Data for the System CO_2 (1) + Benzoic Acid (2)

T / K	403.28		432.62		458.37	
x_1	P / MPa	x_1	P / MPa	x_1	P / MPa
0.000	0.038	0.000	0.014	0.000	0.029
0.011	0.499	0.003	0.149	0.002	0.141
0.020	0.935	0.018	0.825	0.015	0.860
0.066	3.102	0.059	2.756	0.049	2.697
0.107	5.040	0.101	4.724	0.089	4.814
0.147	6.943	0.147	6.870	0.133	7.095
0.194	9.198	0.189	8.920	0.170	9.038
0.233	11.128	0.227	10.797	0.209	11.007
0.274	13.192	0.268	12.856	0.245	12.815
0.317	15.382	0.307	14.822	0.286	14.875
0.350	17.089	0.346	16.862	0.321	16.637
0.385	18.960	0.385	18.921	0.365	18.839
0.403	19.924	0.418	20.712	0.399	20.508

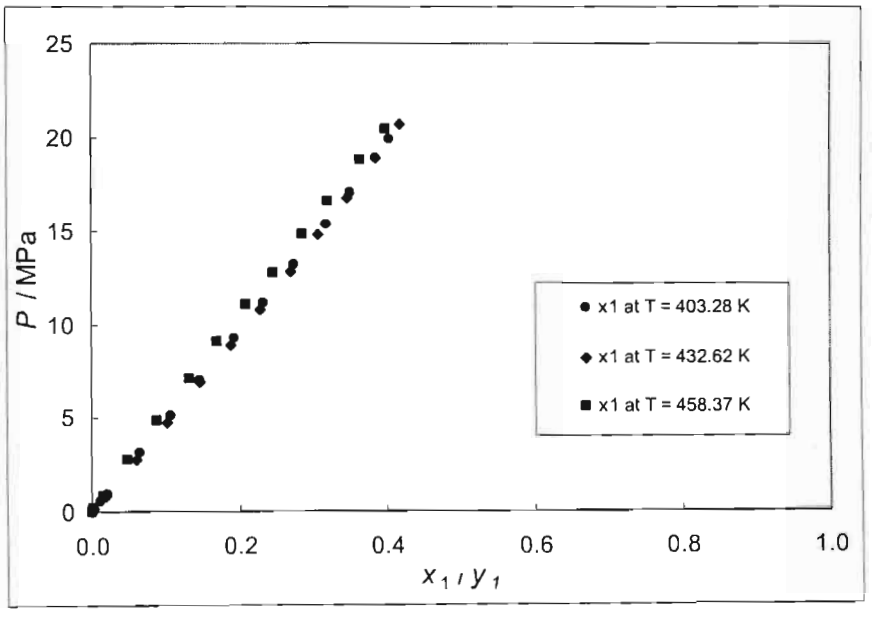

Figure 6-6: Experimental P-x_1 and dew points for the system CO_2 (1) + Benzoic Acid (2).

6.3.2 Dynamic Equipment Measurements

Low Pressure – High Temperature Test Systems

Several test systems were measured as explained in Chapter Three with the equipment of Harris et al (2003b). Table 6-15 lists the vapour pressure data measured for the test systems n-heptane, n-decane, n-dodecane, n-hexadecane, 1-octadecene, 1-hexadecanol and d,l-menthol. Figures 6-7 to 6-19 (odd numbers) compare the measured data to literature and the fitted Antoine Equation. Figures 6-8 to 6-20 (even numbers) show the deviation (ΔT) between the measured and the literature temperature. The Antoine Equation (Equation 6-1)

$$\ln P / kPa = A - \frac{B}{T / K + C} \tag{6-1}$$

was fitted to all the measured data. The Antoine coefficients are listed in Table 6-16. Unless otherwise stated, all literature data are from DECHEMA (1999).

Table 6-15 Measured Vapour Pressures

n-heptane		n-decane		n-dodecane		n-hexadecane	
T/K	*P*/kPa	*T*/K	*P*/kPa	*T*/K	*P*/kPa	*T*/K	*P*/kPa
308.33	10.01	373.95	9.99	369.79	1.50	473.45	10.07
317.43	15.02	378.85	12.01	384.61	2.97	479.58	12.07
326.91	22.01	392.55	20.02	396.99	5.07	484.41	14.07
334.79	30.02	404.85	29.99	413.41	10.07	486.38	15.00
342.64	40.00	412.15	40.01	424.66	15.02	489.08	16.06
349.36	50.03			431.99	20.03	492.65	18.06
354.53	60.01			441.82	30.05	529.84	50.02
358.75	70.00			450.98	40.06		
363.82	80.01			460.47	50.10		
				465.47	60.01		
				469.01	70.05		

Table 6-15 Continued...

1-octadecene		1-hexadecanol		d/l - menthol	
T/K	*P*/kPa	*T*/K	*P*/kPa	*T*/K	*P*/kPa
466.04	3.02	480.78	3.50	362.23	1.00
480.04	5.02	489.58	5.04	381.23	2.55
490.81	7.60	506.50	10.04	396.96	5.04
497.05	10.10	530.70	20.09	413.87	9.99
505.13	14.05	546.30	30.00	425.30	15.00
517.19	20.07	557.55	45.00	433.09	20.01
524.13	25.05	575.04	60.00	445.14	30.01
530.65	30.03	583.90	80.00	453.95	39.96
537.10	35.04			461.97	50.01
543.85	40.03			467.86	59.95
				473.31	69.95
				477.72	79.97
				481.39	89.93

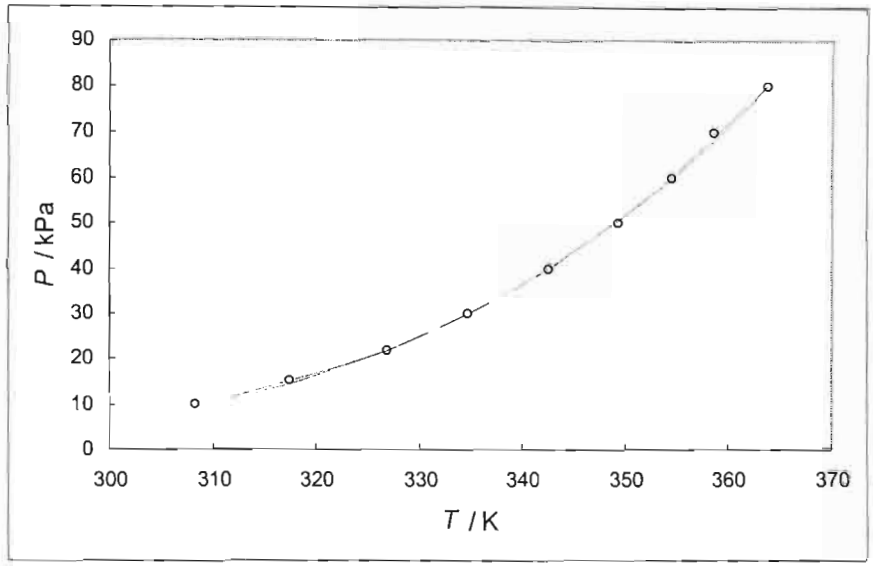

Figure 6-7: Measured vapour pressure compared to literature for n-heptane: Measured data = o, Literature data = —— and Fitted Antoine Equation = ----.

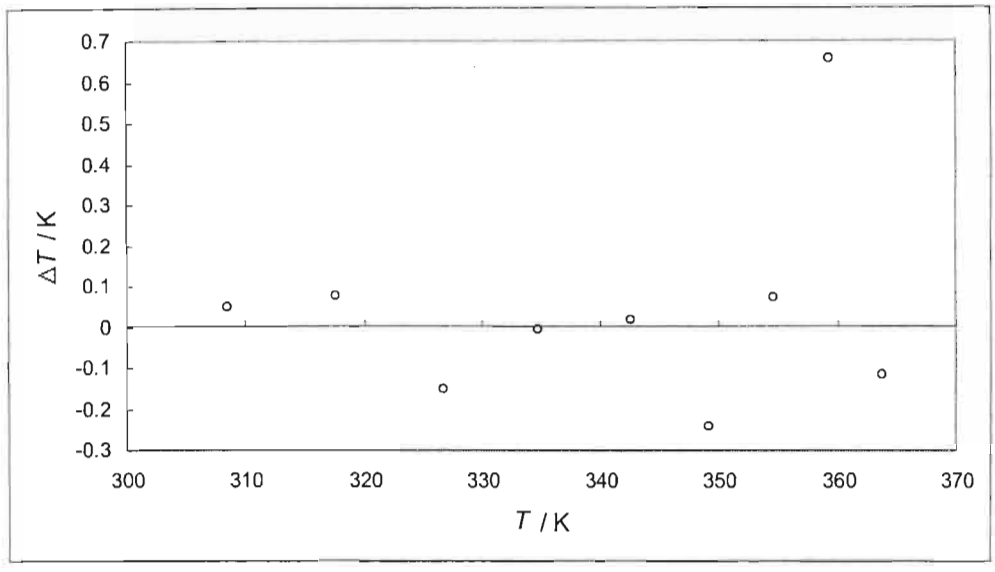

Figure 6-8: Deviation (ΔT) between the measured and the literature temperatures for the vapour pressure of n-heptane.

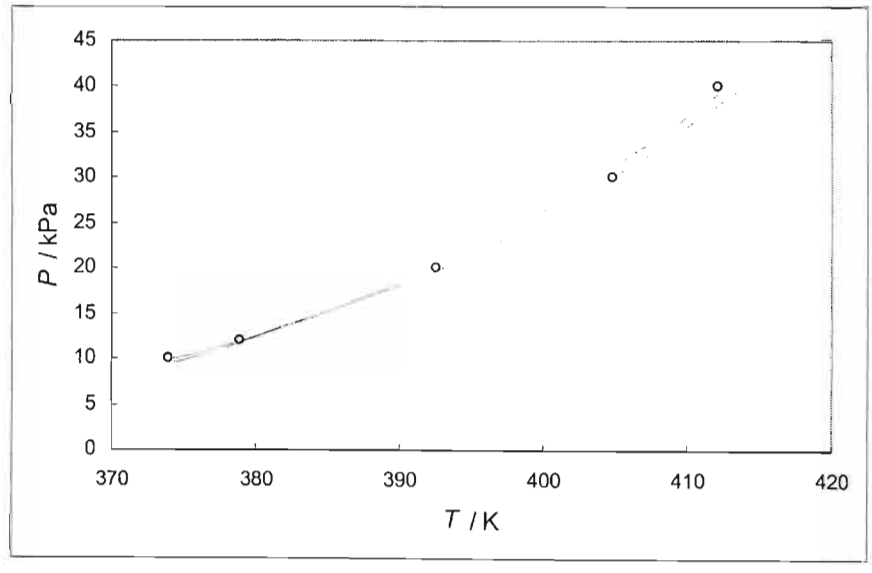

Figure 6-9: Measured vapour pressure compared to literature for n-decane: Measured data = o, Literature data = —— and Fitted Antoine Equation = ----.

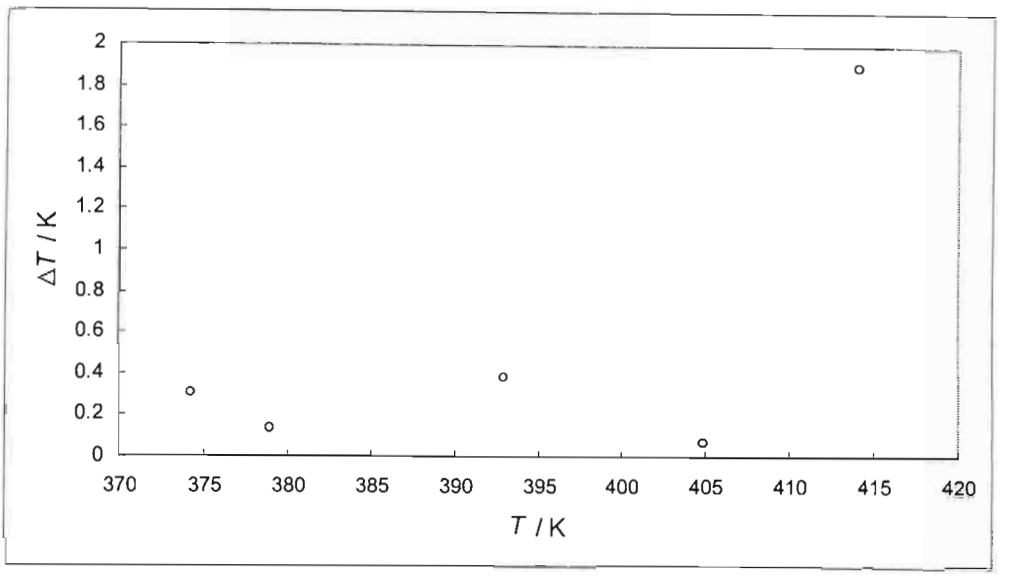

Figure 6-10: Deviation (ΔT) between the measured and the literature temperatures for the vapour pressure of n-decane.

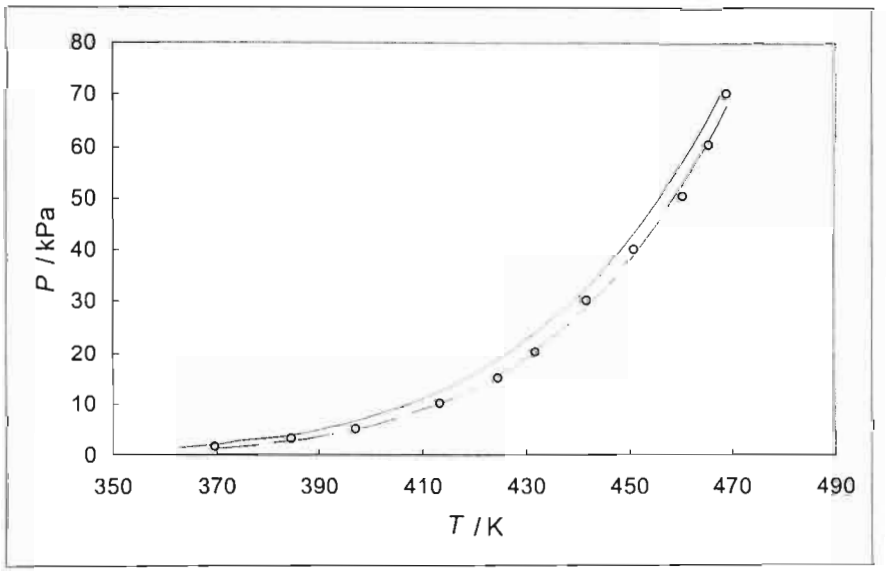

Figure 6-11: Measured vapour pressure compared to literature for n-dodecane: Measured data = o, Literature data = —— and Fitted Antoine Equation = ----.

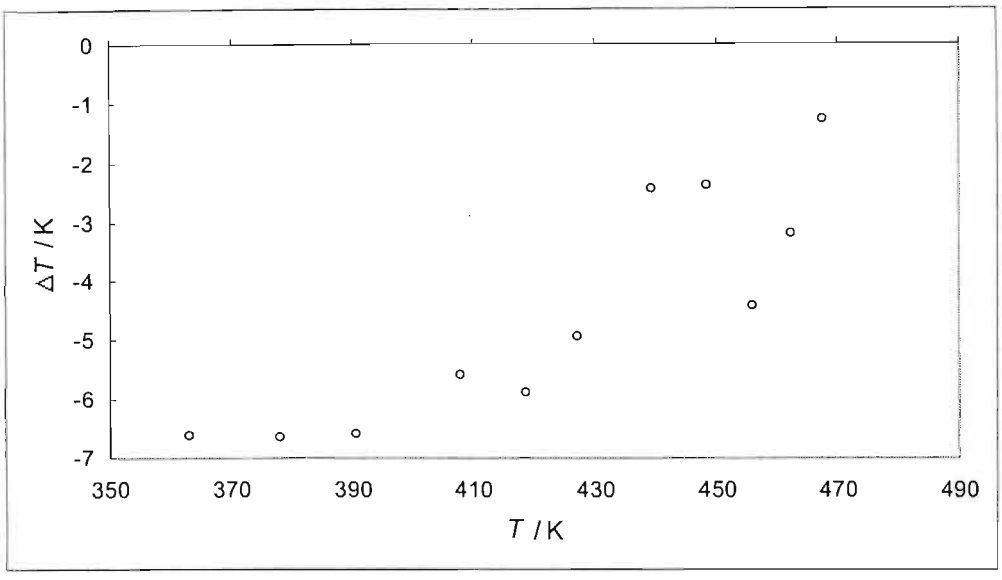

Figure 6-12: Deviation (ΔT) between the measured and the literature temperatures for the vapour pressure of n-dodecane.

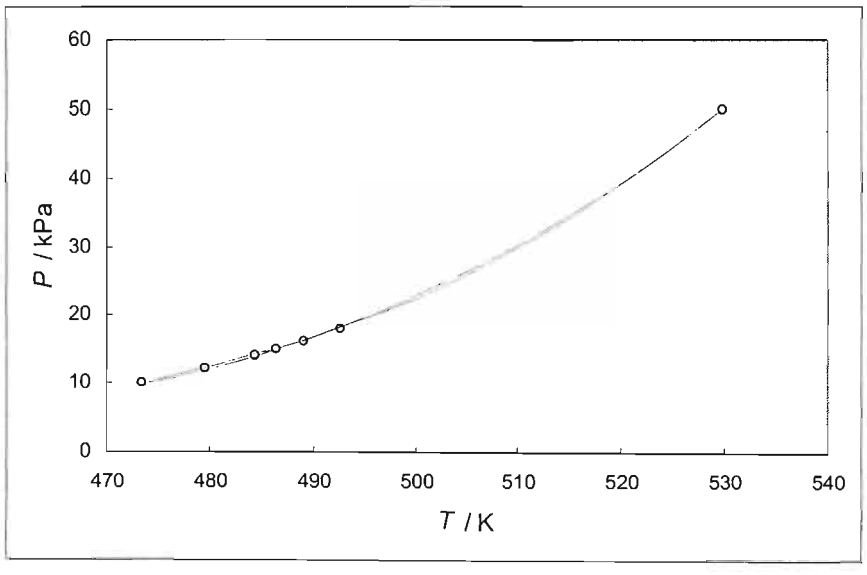

Figure 6-13: Measured vapour pressure compared to literature for n-hexadecane: Measured data = o, Literature data = —— and Fitted Antoine Equation = ----.

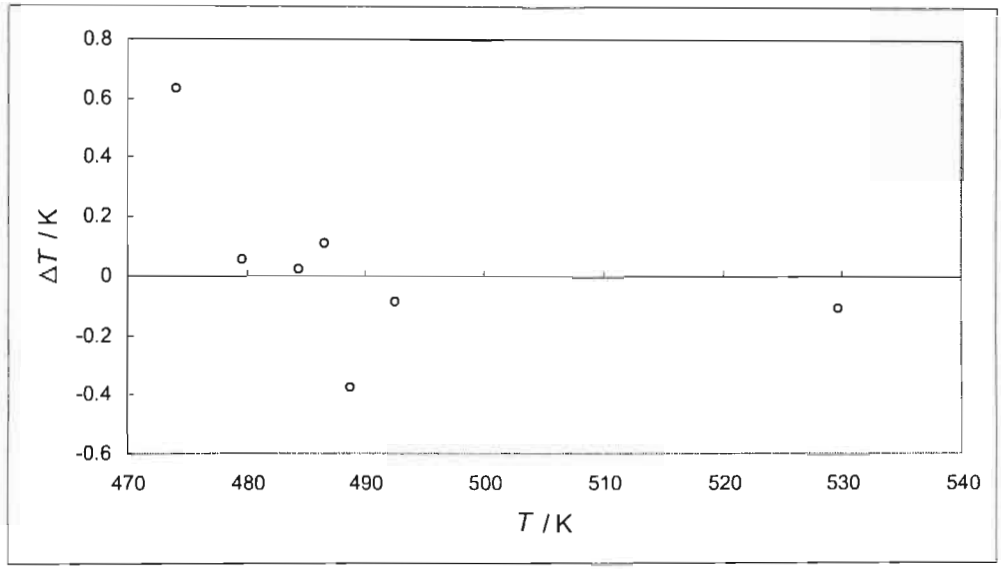

Figure 6-14: Deviation (ΔT) between the measured and the literature temperatures for the vapour pressure of n-hexadecane.

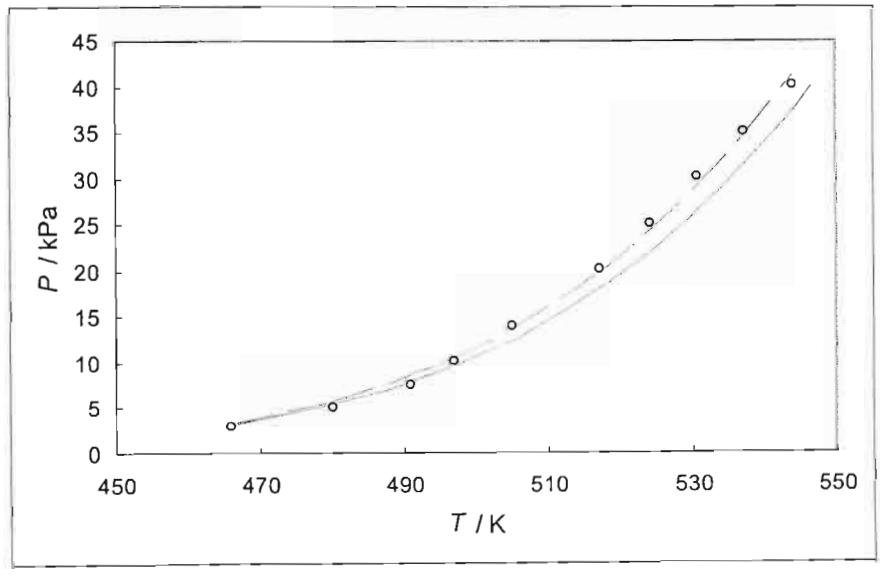

Figure 6-15: Measured vapour pressure compared to literature for 1-octadecene: Measured data = o, Literature data = —— and Fitted Antoine Equation = ----.

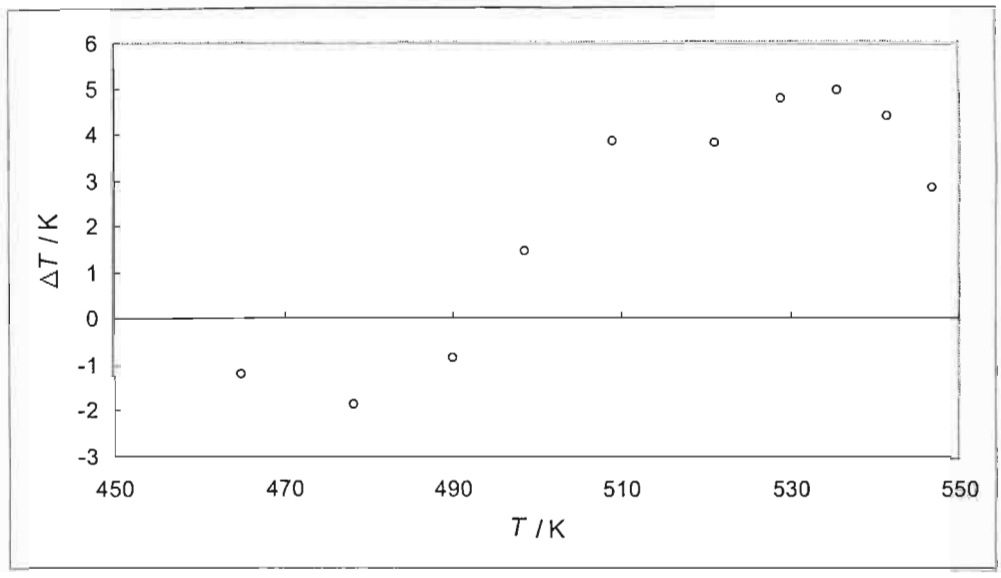

Figure 6-16: Deviation (ΔT) between the measured and the literature temperatures for the vapour pressure of 1-octadecene.

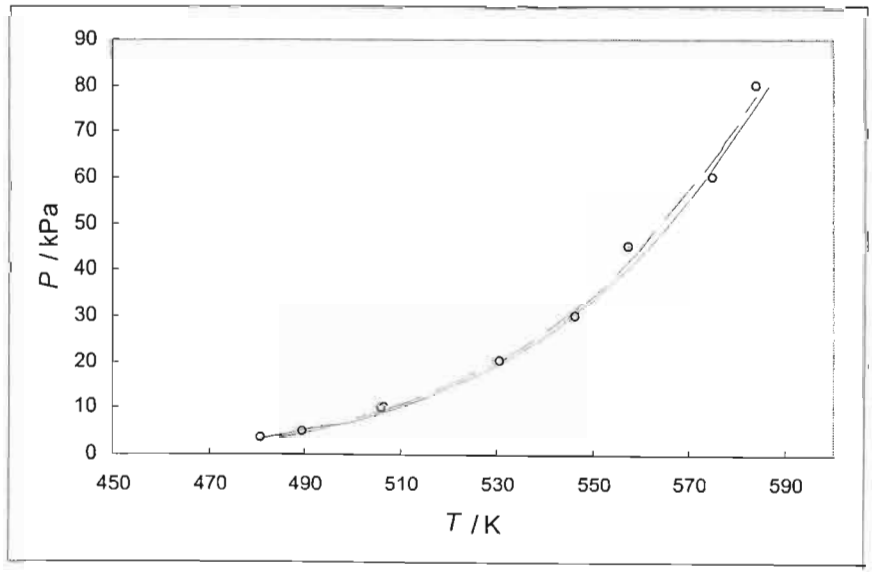

Figure 6-17: Measured vapour pressure compared to literature for 1-hexadecanol: Measured data = o, Literature data = —— and Fitted Antoine Equation = ----.

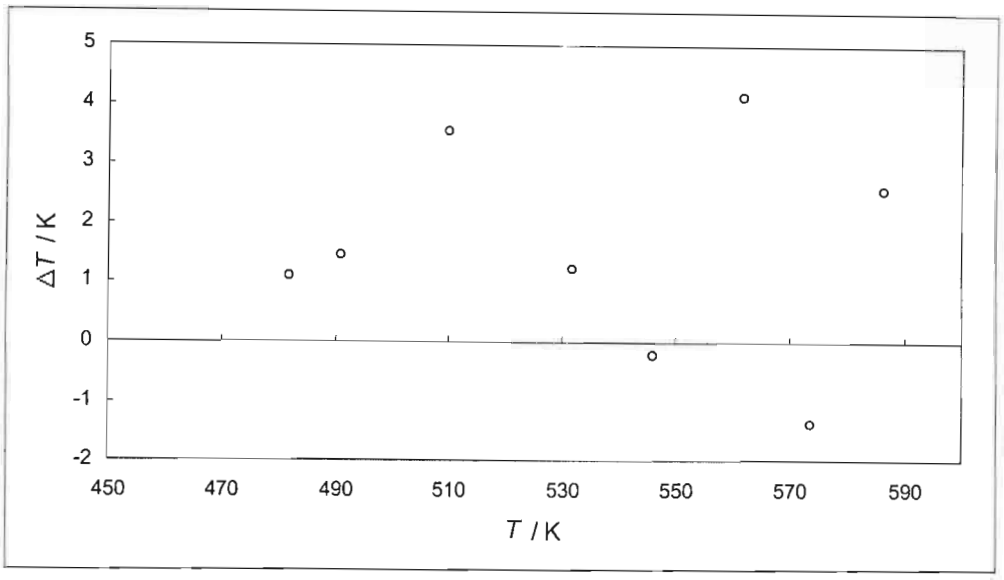

Figure 6-18: Deviation (ΔT) between the measured and the literature temperatures for the vapour pressure of 1-hexadecanol.

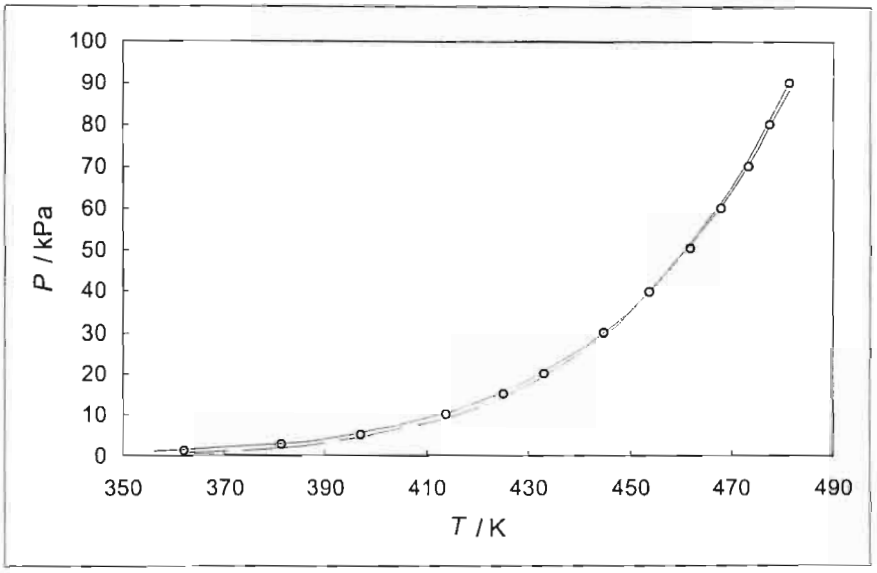

Figure 6-19: Measured vapour pressure compared to literature for d,l-menthol: Measured data = o, Literature data = —— and Fitted Antoine Equation = ----.

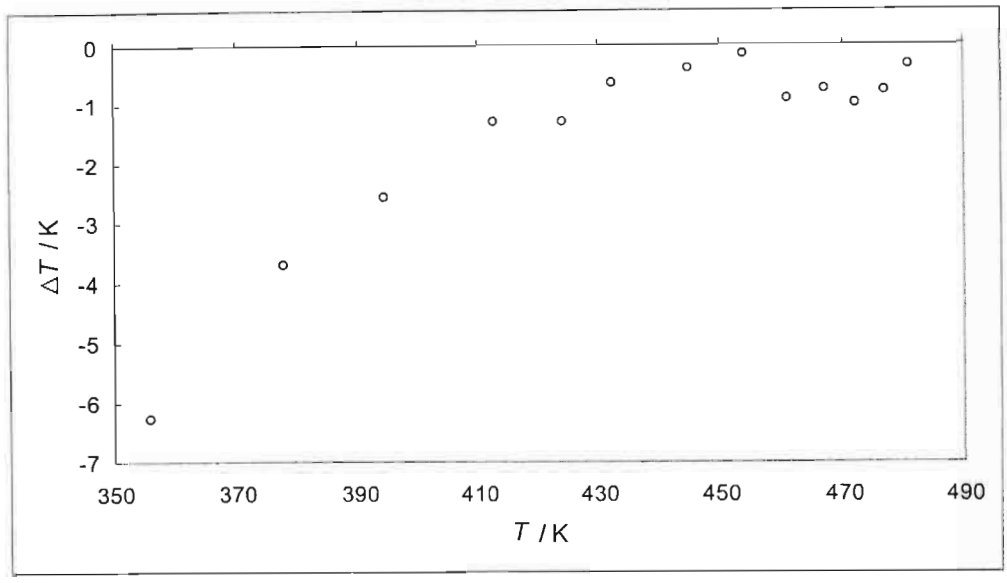

Figure 6-20: Deviation (ΔT) between the measured and the literature temperatures for the vapour pressure of d,l-menthol.

Table 6-16 Fitted Antoine Coefficients

System	*A*	*B*	*C*	T_{min} / K	T_{max} / K
n-Heptane	11.7405	1815.32	-116.995	308.33	363.82
n-Decane	11.2034	1819.66	-170.591	373.95	412.15
n-Dodecane	14.1911	3430.79	-125.010	369.79	469.01
n-Hexadecane	11.2801	2280.13	-220.406	473.45	529.84
1-Octadecene	13.0762	3432.83	-176.926	466.04	543.85
1-Hexadecanol	13.0396	3433.42	-188.697	480.78	583.90
d,l Menthol	14.0927	3430.77	-124.380	362.23	481.39
(+)-isoMenthol					

Two isobaric VLE test systems were measured. Table 6-17 lists the measured T-x_1-y_1 data for the test system cyclohexane (1) + ethanol (2) measured at 40 kPa. Figure 6-21 compares the measured T-x_1-y_1 data to that of Joseph et al. (2001) and Figure 6-22 compares the x_1-y_1 data to the literature.

Table 6-17 Measured T-x_1-y_1 data for cyclohexane (1) + ethanol (2) at 40 kPa

x_1	y_1	T / K
0.000	0.000	329.55
0.018	0.134	326.00
0.039	0.229	324.15
0.064	0.357	320.85
0.185	0.479	316.85
0.520	0.616	314.87
0.657	0.625	314.56
0.911	0.661	315.23
0.972	0.732	317.32
1.000	1.000	325.55

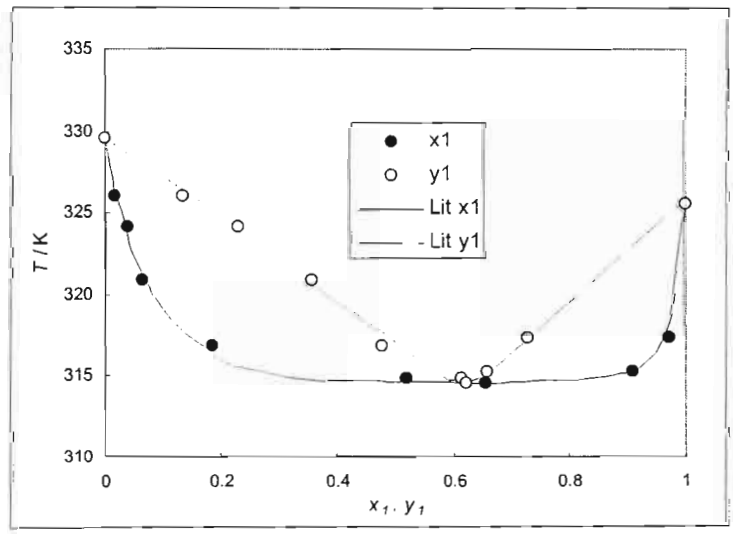

Figure 6-21: Measured T-x_1-y_1 data compared to literature (Joseph et al. (2001)) for the system cyclohexane (1) + ethanol (2) at 40 kPa.

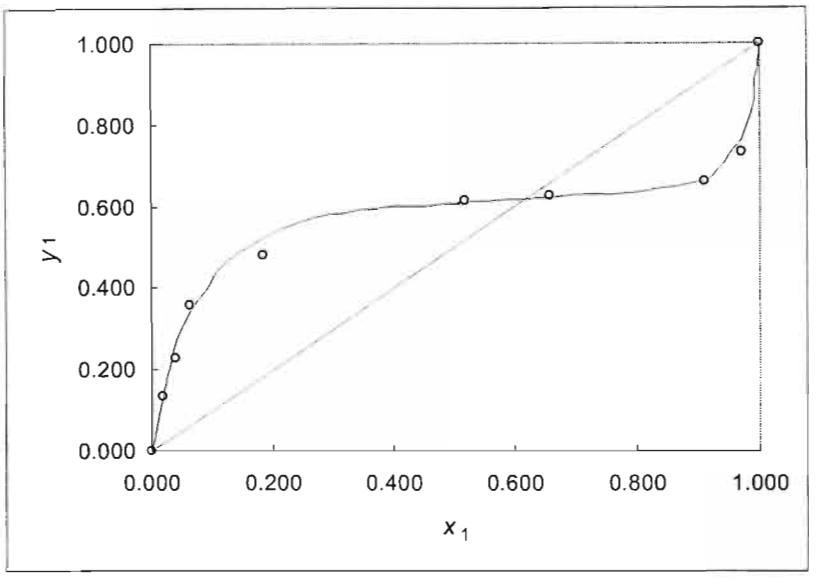

Figure 6-22: Measured x_1-y_1 data compared to literature (Joseph et al. (2001)) for the system cyclohexane (1) + ethanol (2) at $P = 40$ kPa.

Table 6-18 lists the measured T-x_1 data for the test system n-dodecane (1) + 1-octadecene (2) at 26.66 kPa. Figure 6-23 compares the measured T-x_1 data to that of Jordan and van Winkle (1951) and Figure 6-24 shows the disparity (ΔT) between the measured and literature temperatures.

Table 6-18 Measured T-x_1 data for n-dodecane (1) + 1-octadecene (2) at 26.66 kPa

x_1	T / K	x_1	T / K
0.000	527.44	0.884	445.49
0.021	524.47	0.927	444.53
0.074	509.65	0.971	441.79
0.140	497.26	1.000	439.51
0.257	483.74		
0.360	471.79		
0.554	459.35		
0.626	453.49		
0.696	451.78		
0.793	449.31		

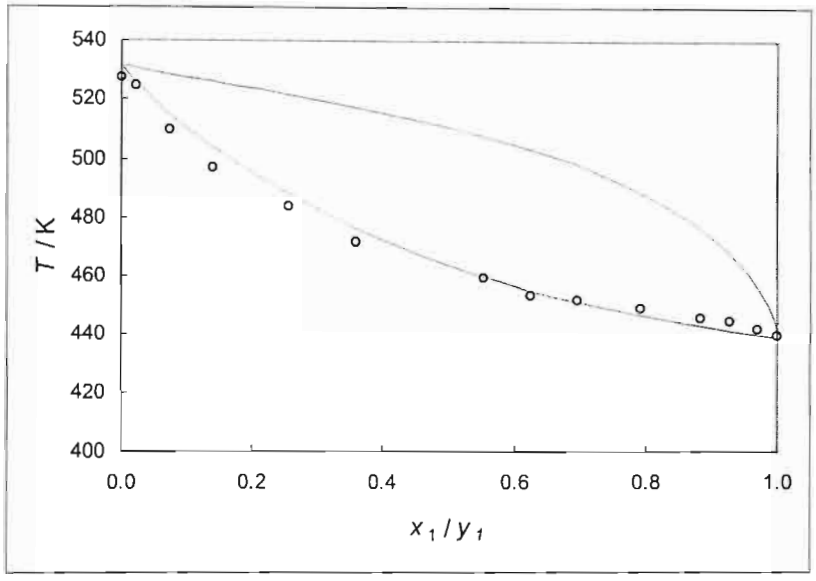

Figure 6-23: Measured T-x_1 data compared to literature (Jordan and van Winkle (1951)) for the system n-dodecane (1) + 1-octadecene (2) at 26.66 kPa: o, Measured x_1 data; —, Literature data.

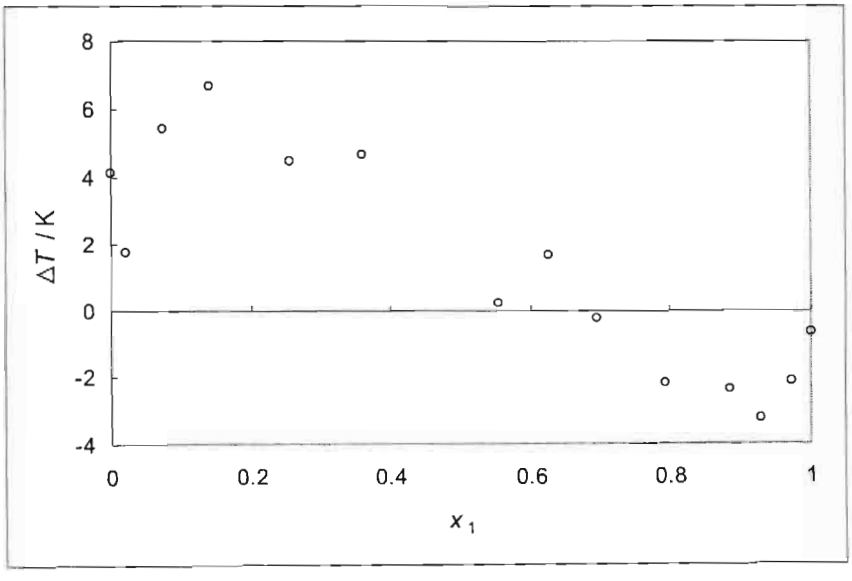

Figure 6-24: Disparity (ΔT) between the measured and literature (Jordan and van Winkle (1951)) temperatures for n-dodecane (1) + 1-octadecene (2) at P = 26.66 kPa.

Low Pressure – High Temperature Systems

One new isothermal system and one new isobaric system were measured in the low pressure – high temperature regime. Table 6-19 lists the measured P-x_1-y_1 data for the system d,l-menthol (1) + l-isomenthol (2) at $T = 448.15$ K. The P-x_1-y_1 data and the x_1-y_1 data are plotted in Figures 6-25 and 6-26 respectively.

Table 6-19 Measured P-x_1-y_1 data for d,l-menthol (1) + l-isomenthol (2) at $T = 448.15$ K

x_1	y_1	P / kPa	x_1	y_1	P / kPa
0.000	0.000	28.7	0.661	0.676	30.7
0.184	0.187	29.8	0.770	0.782	31.1
0.206	0.209	30.1	0.872	0.877	31.2
0.272	0.280	30.0	0.929	0.935	31.6
0.491	0.507	30.0	1.000	1.000	33.0
0.570	0.585	30.3			

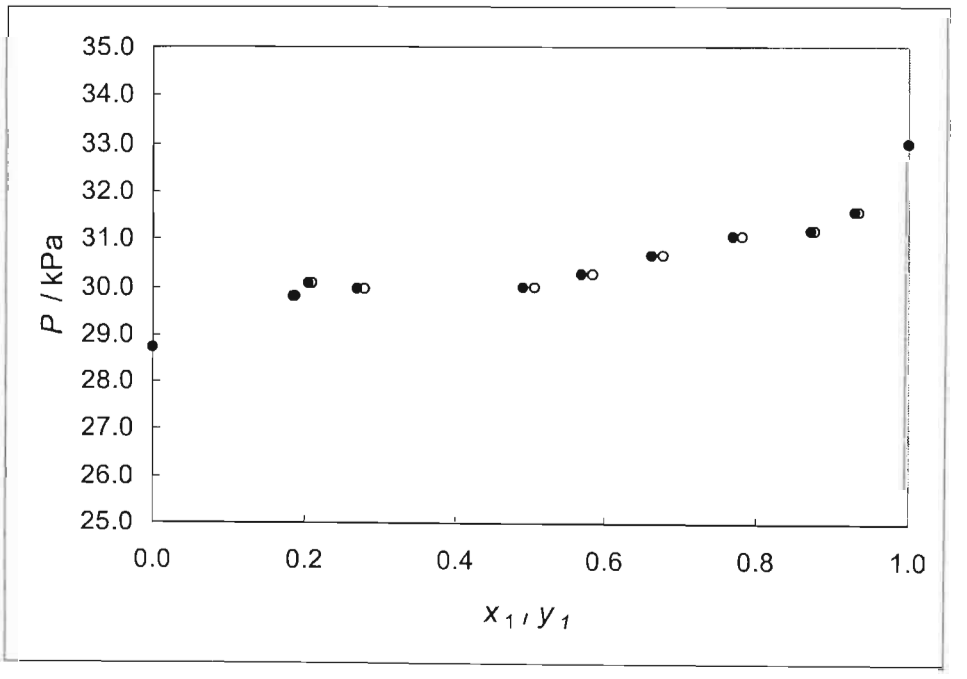

Figure 6-25: P-x_1-y_1 data for d,l-menthol (1) + l-isomenthol (2) at $T = 448.15$ K: ●, Experimental x_1-P data; o, Experimental y_1-P data.

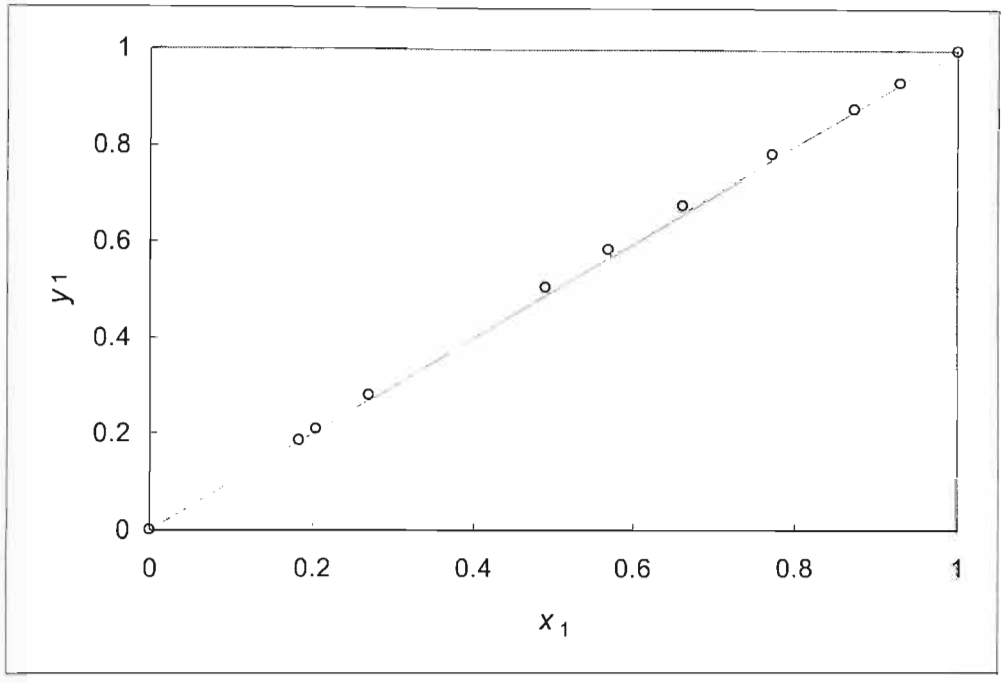

Figure 6-26: x_1-y_1 data for d,l-menthol (1) + l-isomenthol (2) at $T = 448.15$ K.

Table 6-20 lists the measured T-x_1 data for the system n-dodecane (1) + 1-octadecene (2) at $P = 3.0$ kPa. The T-x_1 data are plotted in Figure 6-27.

Table 6-20 Measured T-x_1 data for n-dodecane (1) + 1-octadecene (2) at $P = 3.0$ kPa

x_1	T/K	x_1	T/K
0.000	463.53	0.692	401.63
0.089	458.29	0.762	400.03
0.095	456.49	0.792	399.32
0.318	420.86	0.813	398.35
0.402	419.04	0.887	397.91
0.496	410.60	0.920	391.61
0.582	407.68	1.000	387.05
0.643	404.42		

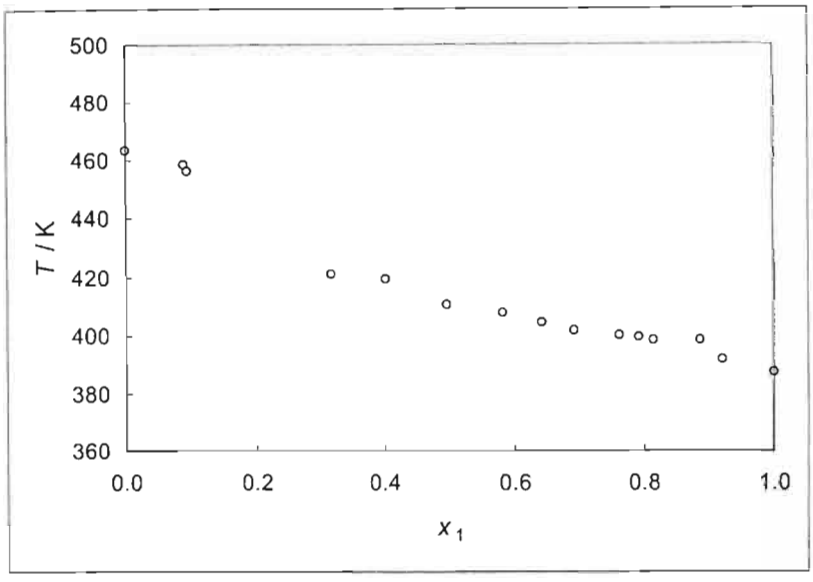

Figure 6-27: T-x_1 data for n-dodecane (1) + 1-octadecene (2) at P = 3.0 kPa.

High Pressure Systems

Table 6-21 lists the vapour pressure data for acetone measured at high pressures. Figure 6-28 compares the measured data to literature and the fitted Antoine Equation. Figure 6-29 shows the deviation (ΔT) between the measured and the literature temperature. The Antoine Equation, (Equation 6-1), was fitted to all the measured data. The Antoine coefficients are listed in Table 6-22. Literature data are from DECHEMA (1999).

Table 6-21 Vapour pressures measured for Acetone

T / K	*P* / kPa
327.82	98.5
334.05	120.0
340.65	149.7
356.56	230.6
364.79	299.6
381.50	456.6
390.10	546.6
414.12	995.6

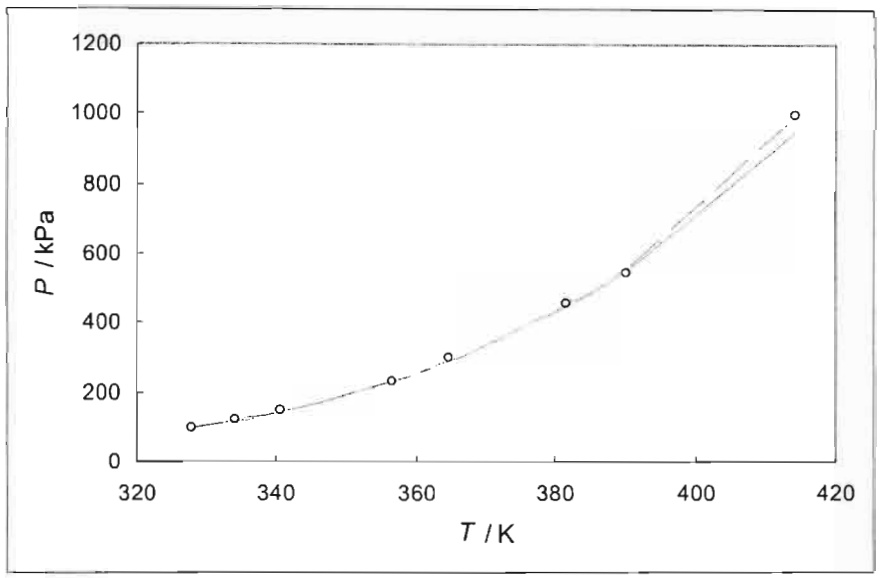

Figure 6-28: Measured vapour pressure compared to literature for Acetone: Measured data = o, Literature data = —— and Fitted Antoine Equation = ----.

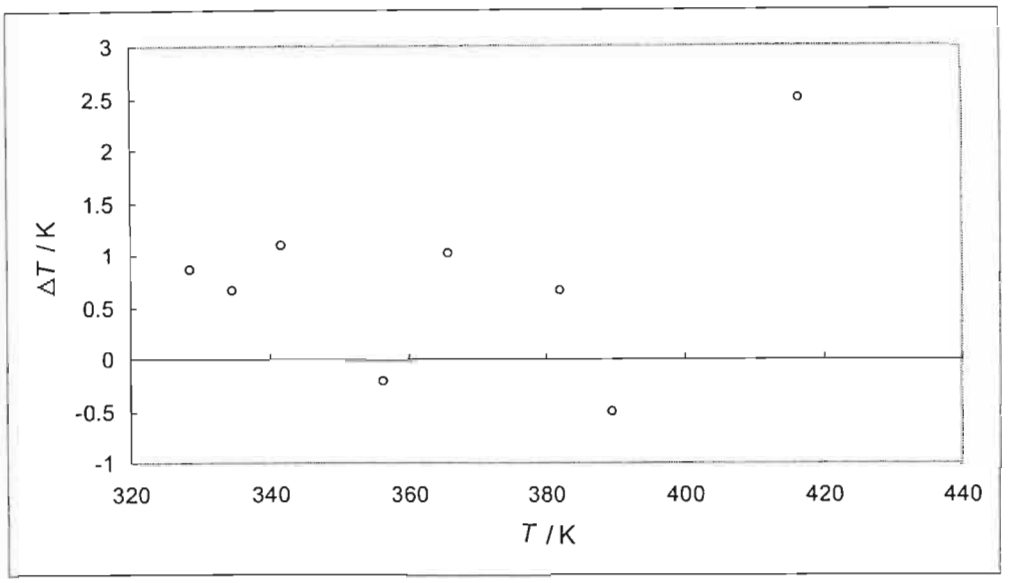

Figure 6-29: Deviation (ΔT) between the measured and the literature temperatures for the vapour pressure of Acetone.

Table 6-22 Fitted Antoine Coefficients for Acetone at High Pressure

System	*A*	*B*	*C*	T_{min} / K	T_{max} / K
Acetone	18.2964	5810.21	95.614	327.82	414.12

CHAPTER

SEVEN

DISCUSSION

7.1 INTERPRETATION OF EXPERIMENTAL RESULTS

Although the determination of experimental values is an important task, these values need to be refined by fitting thermodynamic models to them to gain the most use from the data. Fitting thermodynamic models to raw data is extremely important for many reasons:

- it allows accurate interpolation of the data as well as a limited amount of extrapolation[7],
- it allows one to test the thermodynamic consistency of certain data,
- it allows one to extend binary data to predict multicomponent data,
- it can be used to create and refine VLE predictive methods,
- it makes it possible to determine other thermodynamic properties, and,
- it allows large amounts of data to be summarized very comprehensively and compactly.

The interpolation of VLE data is very important. In the case of isothermal[8] data, the data cannot be used directly to design distillation columns, as these do not themselves operate isothermally but rather isobarically[9]. However, if several (at least two but preferably three) isothermal data sets exist then these can be modelled. From the model a limited temperature dependence for the

[7] Certain models, such as the Wong-Sandler mixing rule, make accurate extrapolation of data over a large temperature range possible.

[8] Abbott (1986) and Van Ness (1995) discuss the benefits of isothermal data over isobaric data. In essence isothermal data are more useful for modeling purposes and the determination of other thermodynamic properties such as H^E is all but impossible from isobaric data. Furthermore, the temperature dependence of the limiting activity coefficient is very important for the design of separation equipment. This dependence can only be determined from isothermal data sets and not from isobaric data. The pressure dependence of limiting activity coefficients is almost non-existent.

[9] Technically, distillation columns do not operate purely isobarically as there is a small pressure change along the height of the column due to the packing / trays.

model parameters can be determined. From the fitted parameters the data can be interpolated to accurately design distillation columns.

The use of models, to extend binary data to multicomponent data, is very useful. Multicomponent VLE data are very time-consuming to measure and thus usually only binary data are measured. However, in most industrial separation processes it is multicomponent streams that need to be separated. Fortunately there are several techniques for extending the constituent components' binary VLE data to multicomponent data. (Seader and Henley (1998)).

The importance of developing VLE predictive methods cannot be underestimated. The number of commercially available chemicals increases every year and thus the number of possible mixtures and combinations increases too, far beyond the capabilities of laboratories to accurately measure. Thus, predictive methods are essential for the construction of future processes and accurate, modelled VLE data are required to create and refine these predictive techniques (Prausnitz (1986), Raal and Mühlbauer (1998) and Fischer and Gmehling (1994) among others).

Although VLE modelling is not the focus of this study, it is a necessary tool to complete the work presented here and to add meaning to some of the VLE measurements. In this discussion the results presented in Chapter Six are modelled and some of the values obtained from these models are analysed and discussed.

7.2 DISCUSSION OF RESULTS FOR MEASUREMENTS UNDERTAKEN ON THE EQUIPMENT OF RAREY AND GMEHLING (1993)

7.2.1 VLE Data Reduction

In this work experimental VLE data were measured for N-methylformamide + hexane, N-methylformamide + benzene, N-methylformamide + chlorobenzene and N-methylformamide + acetonitrile at 363.15 K. The measured data are shown in Chapter Six. The data measured are x_i-P data, thus it was necessary to compute the corresponding vapour phase compositions (as discussed in Chapter Five). For these data a G^E model was used and the vapour phase was corrected using an EOS. G^E models and EOS are discussed in Chapter Five. For this work the data were reduced by optimising the objective function

$$F = \left(\frac{P_{expt} - P_{calc}}{P_{expt}} \right)^2 \qquad (7\text{-}1)$$

There are many different objective functions (Appendix B), however, most objective functions are for x_i-y_i-P data and as the data are x_i-P data the above-mentioned objective function is the best suited. The importance of modelling the data is discussed above.

For this work the best results were obtained using the NRTL G^E model with a virial EOS and Hayden and O'Connell mixing rules. For the NRTL equation all three parameters (Δg_{12}, Δg_{21} and α_{12}) were obtained by regression.

The fitted data and their respective ΔP, where

$$\Delta P = P_{expt} - P_{calc} \qquad (7\text{-}2)$$

are shown in the following Figures:

- Hexane (1) + N-methylformamide (2) at 363.15 K [Figure 7-1],
- Benzene (1) + N-methylformamide (2) at 363.15 K [Figure 7-2 and 7-3],
- Chlorobenzene (1) + N-methylformamide (2) at 363.15 K [Figure 7-4 and 7-5], and,
- Acetonitrile + N-methylformamide (2) at 363.15 K [Figure 7-6 and 7-7].

The model did not fit the hexane (1) + N-methylformamide (2) well as this system exhibits two liquid phases. However, of the models used the NRTL fitted the data best.

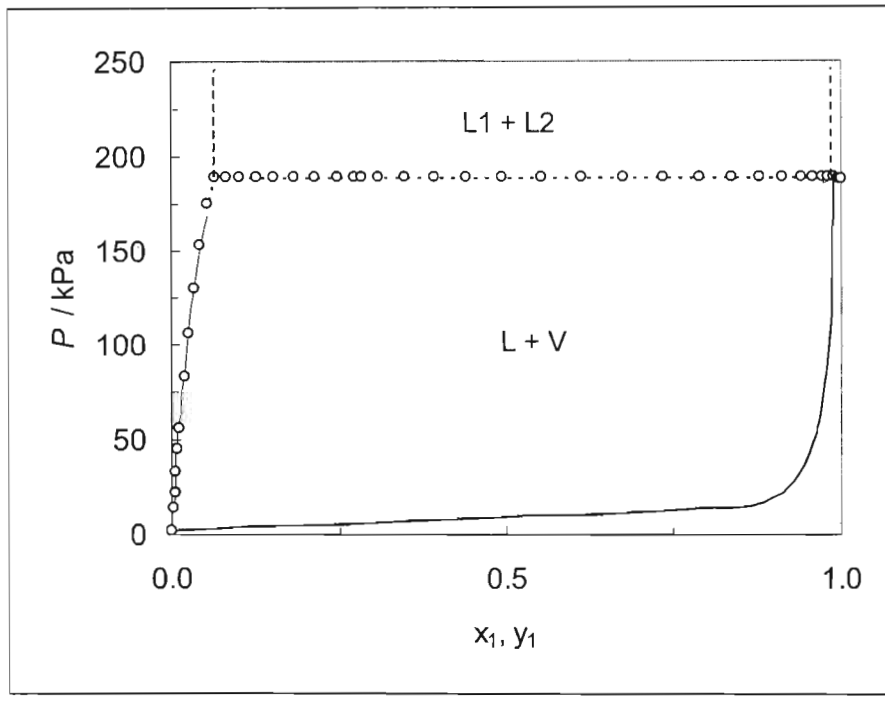

Figure 7-1: Experimental and calculated P - x (y) data for the system Hexane (1) + N-methylformamide (2) at 363.15 K: o, experimental data; ——, NRTL.

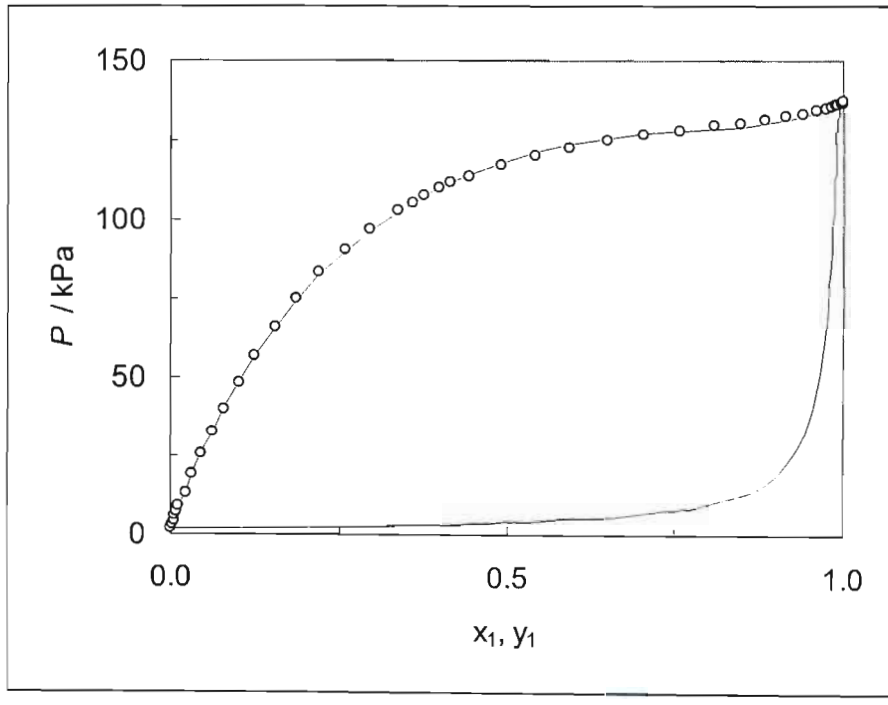

Figure 7-2: Experimental and calculated P - x (y) data for the system Benzene (1) + N-methylformamide (2) at 363.15 K: o, experimental data; ——, NRTL.

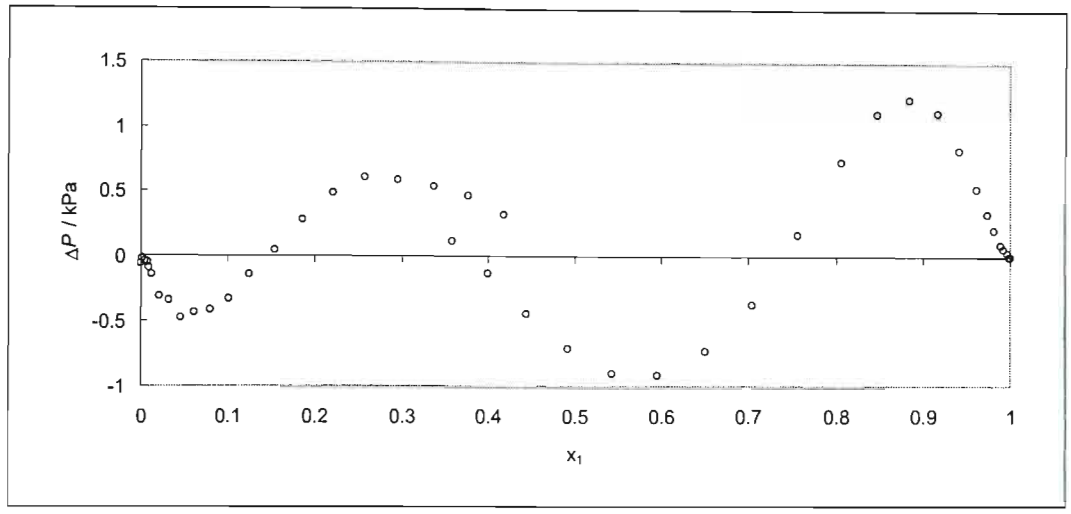

Figure 7-3: Pressure difference (ΔP) between actual pressures and NRTL model pressures for benzene (1) + N-methylformamide (2) at 363.15 K.

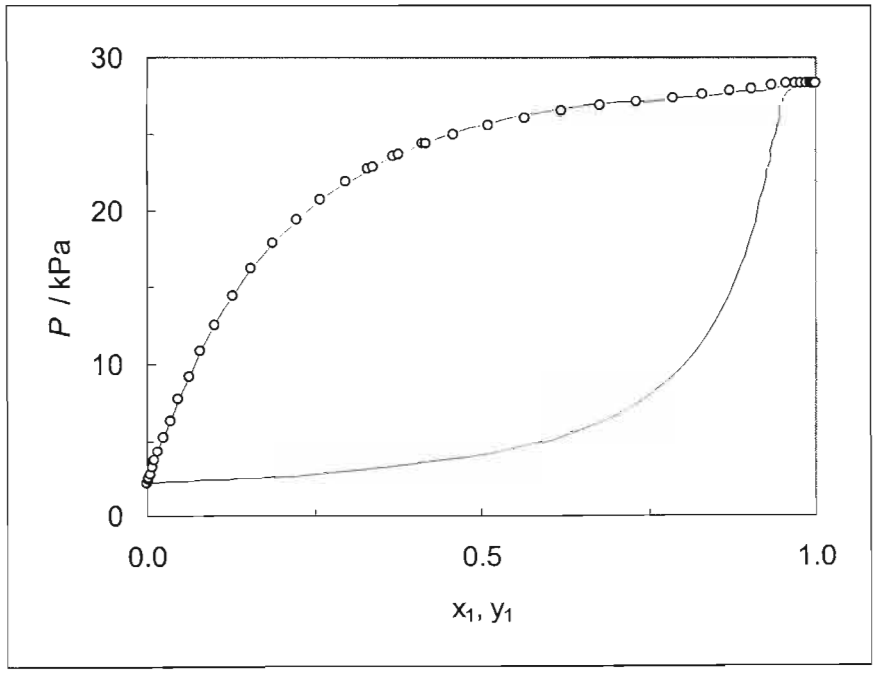

Figure 7-4: Experimental and calculated *P* - *x* (*y*) data for the system Chlorobenzene (1) + N-methylformamide (2) at 363.15 K: o, experimental data; ——, NRTL.

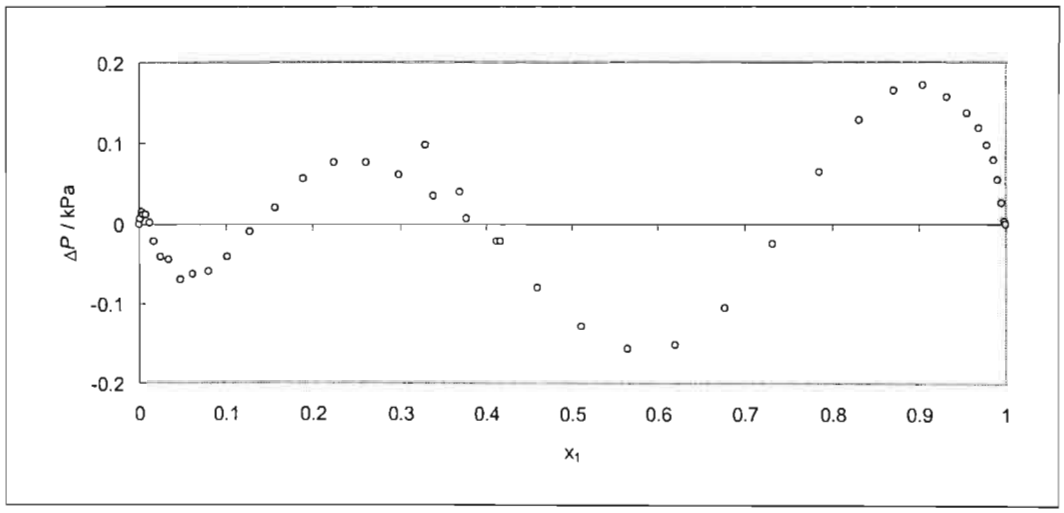

Figure 7-5: Pressure difference (ΔP) between actual pressures and NRTL model pressures for chlorobenzene (1) + N-methylformamide (2) at 363.15 K.

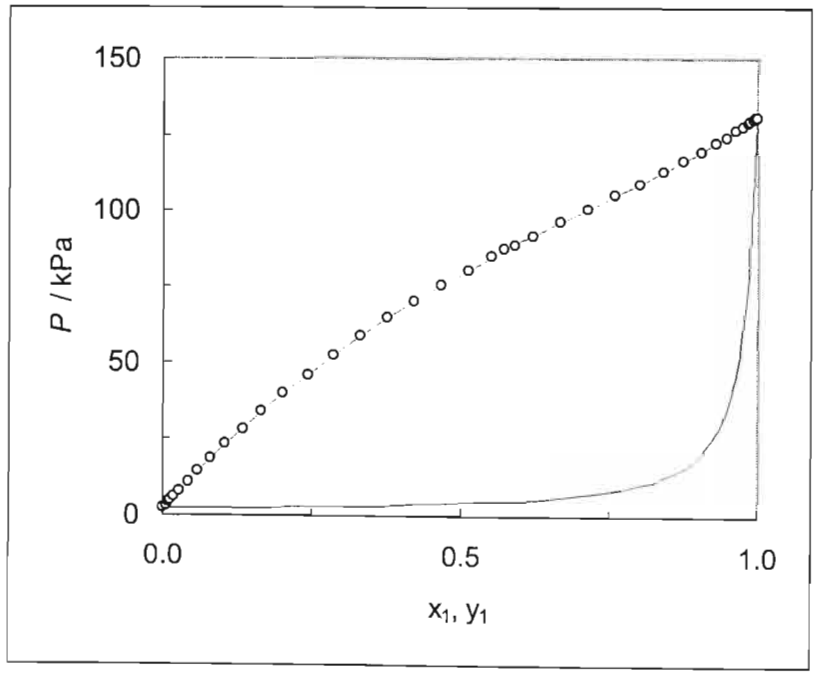

Figure 7-6: Experimental and calculated P - x (y) data for the system Acetonitrile (1) + N-methylformamide (2) at 363.15 K: o, experimental data; ——, NRTL.

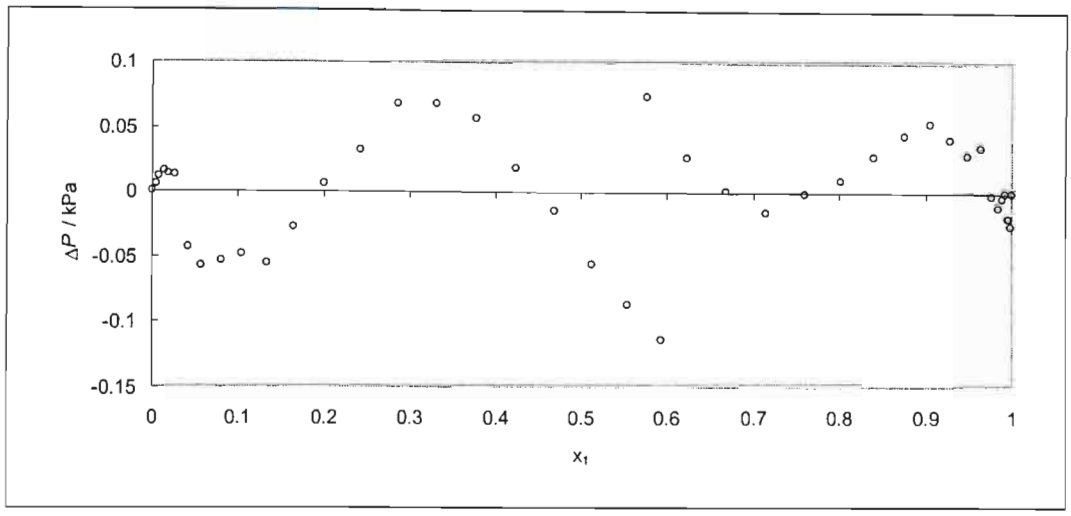

Figure 7-7: Pressure difference (ΔP) between actual pressures and NRTL model pressures for acetonitrile (1) + N-methylformamide (2) at 363.15 K.

The regressed NRTL ($\Delta g_{12}, \Delta g_{21}$ and α_{12}) and Wilson ($\Lambda_{12}$and Λ_{21}) parameters are given in Table 7-1.

Table 7-1 Regressed parameters for the experimental VLE data at 363.15 K

System [NRTL]	Δg_{12} / J.mol^{-1}	Δg_{21} / J.mol^{-1}	α_{12}	$\lvert\Delta P\rvert_{ave.}$
Hexane (1) + N-methylformamide (2)	8108	7378	0.373	2.29
Benzene (1) + N-methylformamide (2)	6641	2306	0.497	0.39
Chlorobenzene (1) + N-methylformamide (2)	6220	2689	0.503	0.06
Acetonitrile (1) + N-methylformamide (2)	2212	794.7	0.989	0.03

System [Wilson]	$\Delta\lambda_{12}$ / J.mol^{-1}	$\Delta\lambda_{21}$ / J.mol^{-1}	$\lvert\Delta P\rvert_{ave.}$
Hexane (1) + N-methylformamide (2)	9111	15337	3.14
Benzene (1) + N-methylformamide (2)	3915	6017	0.47
Chlorobenzene (1) + N-methylformamide (2)	3785	5265	0.11
Acetonitrile (1) + N-methylformamide (2)	3955	-1352	0.05

It is important to note that the measured x_i-P data sets are extremely smooth and this makes accurate modelling of the systems possible. As can be seen from the model-fitting plots, the NRTL model fits the data superbly with the modelled pressure and measured pressure being in very good agreement across the entire composition range. Only a single isotherm was measured for these four systems so it is not possible to determine values such as H^E from the data, however, as the data are new for these systems, they provide valuable information for the understanding of these chemical combinations.

7.2.2 Infinite Dilution Activity Coefficients

An important aspect of the data is not just the number of points measured for each data set but the number of points measured in the dilute regions. Of the more than forty data points measured per VLE set, more than half of the measured points fall in the composition range $x_1 < 0.1$ or $x_1 > 0.9$. This concentration of data in the dilute regions is important for the design of separation equipment. From this data we can determine infinite dilution activity coefficients with a high degree of confidence.

Infinite dilution activity coefficients (γ^{∞}) were determined from the Wilson and NRTL parameters and also from the preferred deviation pressure method, all of which are discussed in Chapter Five. Determination of the limiting values, $(P_D/x_i x_j)^{\infty}$, according to the method of Maher and Smith (1979) is demonstrated for the chlorobenzene (1) + N-methylformamide (2) system in Figure 7-8, as was discussed in Chapter 5. The excellent linearity in the dilute regions may be noted and was also found for the other systems. These plots for the other systems can be found in Appendix C.

As discussed by Fischer and Gmehling (1996), derivation of γ^{∞} values from P - x data are difficult for high boiling substances (such as N-methylformamide) in low boiling components, thus only γ^{∞} values with component 2 (the less volatile component) as the solvent are considered in their work. Table 7-2 compares the γ^{∞} values calculated by these methods for the four binary systems studied. The reasoning behind this is described in Raal and Ramjugernath (2001).

If we consider the function $\left(\frac{\partial T}{\partial P}\right)_{x_1}$ or rather its inverse $\left(\frac{\partial P}{\partial T}\right)_{x_1}$ it is evident that as $x_1 \rightarrow 0$ the function $\left(\frac{\partial P}{\partial T}\right)_{x_1}$ represents the relation of the vapour pressure of the less volatile component (2) to temperature and as $x_1 \rightarrow 1$ the function $\left(\frac{\partial P}{\partial T}\right)_{x_1}$ represents the relation of the vapour pressure of the more volatile component (1) to temperature. Now, although the water bath in which the cell is submersed is kept at a constant temperature, there will always be small fluctuations in temperature. In the case of $\left(\frac{\partial P}{\partial T}\right)_{x_1=0}$ these small temperature fluctuations have very little affect on the pressure and thus very little effect on the $(P_D/x_i x_j)$ values. Consequently it is usually possible to obtain very linear functions for $(P_D/x_i x_j)$ vs. x_1 as $x_1 \rightarrow 0$. For this reason the γ_1^∞ values determined by the method of Maher and Smith (1979) are usually very reliable.

In the case of $\left(\frac{\partial P}{\partial T}\right)_{x_1=1}$ these small temperature fluctuations, however, have a larger effect on the pressure and thus a larger effect on the $(P_D/x_i x_j)$ values. Thus the $(P_D/x_i x_j)$ vs. x_1 function as $x_1 \rightarrow 1$ is not always very linear and thus the γ_2^∞ values determined by the method of Maher and Smith (1979) are usually not as reliable as the γ_1^∞ values.

The $(P_D/x_i x_j)$ vs. x_1 functions as $x_1 \rightarrow 1$ in this work, however, were very linear (Figure 7-8 and Appendix C) and thus values for both γ_1^∞ and γ_2^∞ were determined and are presented in Table 7-2. As mentioned earlier, more than half of the VLE points measured in this work were in the dilute regions. Due to these concentrations of data in the dilute regions, excellent linear functions were determined for all the systems at both composition extremes and the IDACs determined can be reported with a high degree of confidence.

The comparison of the deviation pressure (P_D) to the model IDACs show that for γ_1^∞ there is good agreement (less than 10 % difference) between the P_D method and the Wilson equation for the chlorobenzene and acetonitrile systems and for the NRTL equation for all four systems. For

γ_2^∞ there is good agreement (less than 10 % difference) between the P_D method and the Wilson equation for the acetonitrile system only and for the NRTL equation for the benzene system only.

The model IDAC values are usually not accurate for both composition extremes as the model does not fit the entire curve with the same accuracy. The model usually fits some regions better than others.

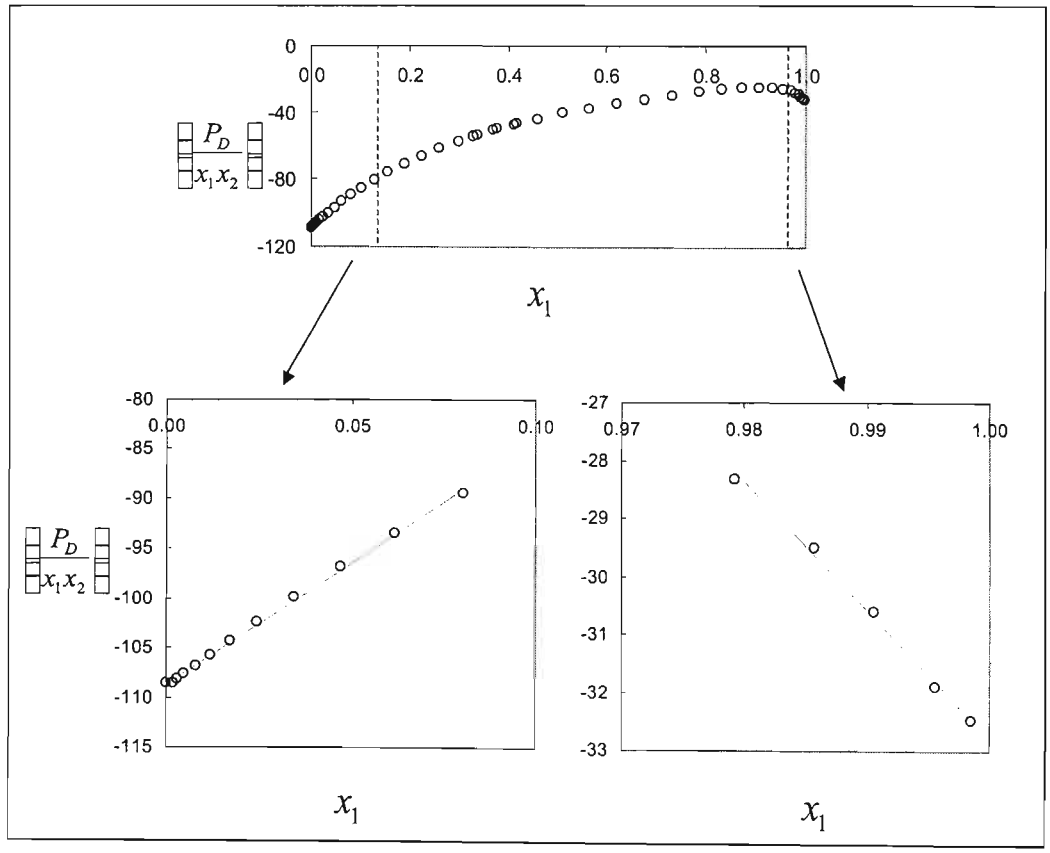

Figure 7-8: Determination of the limiting values, $(P_D/x_i x_j)^\infty$, according to the method of Maher and Smith (1979) for the Chlorobenzene (1) + N-methylformamide (2) system.

Table 7-2 γ^{∞} values for the four binary systems determined from VLE data at 363.15 K

System	γ_1^{∞} (a)	γ_1^{∞} (b)	γ_1^{∞} (c)
Hexane (1) + N-methylformamide (2)	43.6	30.9	33.6
Benzene (1) + N-methylformamide (2)	4.8	4.5	4.2
Chlorobenzene (1) + N-methylformamide (2)	5.1	5.1	4.9
Acetonitrile (1) + N-methylformamide (2)	1.8	1.9	1.7
System	γ_2^{∞} (a)	γ_2^{∞} (b)	γ_2^{∞} (c)
Hexane (1) + N-methylformamide (2)	523.0	96.9	48.8
Benzene (1) + N-methylformamide (2)	22.6	17.6	18.1
Chlorobenzene (1) + N-methylformamide (2)	16.2	13.8	16.7
Acetonitrile (1) + N-methylformamide (2)	2.4	2.3	7.1

a) Calculated using Wilson parameters

b) Calculated using NRTL parameters

c) Calculated using pressure deviation method of Maher and Smith (1979)

7.3 DISCUSSION OF RESULTS FOR THE MEASUREMENTS UNDERTAKEN ON THE EQUIPMENT OF KOLBE AND GMEHLING (1985)

7.3.1 VLE Data Reduction

In Chapter Six experimental isothermal *P-x* data and dew points are presented for naphthalene + CO_2 at 372.45 K, 403.85 K and 430.65 K and experimental *P-x* data are presented for benzoic acid + CO_2 at 403.28 K, 432.62 K and 458.37 K. Most of the isotherms measured are new data and improve the understanding of these systems. Several sets of data exist in literature for the naphthalene + CO_2 system (Barrick et al. (1987), Jan and Tsai (1991) and Yanagiuchi et al. (1991)), however, the data are not extensive; especially at high pressures. Two data sets for naphthalene + CO_2 at 373.15 K are reported in the literature (Barrick et al. (1987) and Jan and Tsai (1991)) and are compared to our work at 372.45 K in Figure 7-9. There is very good agreement between the literature and our work.

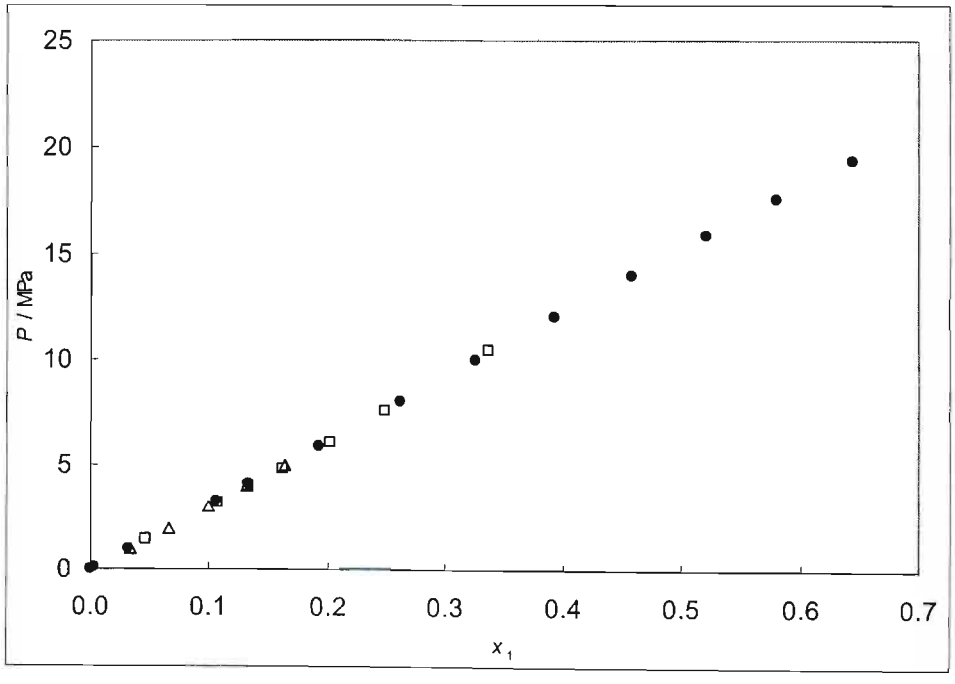

Figure 7-9: x_1-P data for Naphthalene + CO_2 at 373.15 K: our work compared to the literature: ●, this work; □, Barrick et al. (1987); Δ, Jan and Tsai (1991).

For modelling purposes data were regressed using the direct method with the Peng-Robinson cubic EOS with Stryjek-Vera modification as explained in Chapter Five. Both the Huron-Vidal and the Wong-Sandler mixing rules were used in association with the NRTL G^E model. For the NRTL model an alpha value of 0.5 (Huron-Vidal) and 0.4 (Wong-Sandler) was used, respectively, as this fitted the data better than the conventional value of 0.3. (The alpha value was varied in increments of 0.1 from –1.0 to 0.5 to find the best value.)

The fitted data (fitted using objective function 7-1) and their respective ΔP are shown in the following figures (for the P-x (y) data only the best fit model is plotted):

- CO_2 (1) + Naphthalene (2) at 372.45 K [Figure 7-10 and 7-11],
- CO_2 (1) + Naphthalene (2) at 403.85 K [Figure 7-12 and 7-13],
- CO_2 (1) + Naphthalene (2) at 430.65 K [Figure 7-14 and 7-15],
- CO_2 (1) + Benzoic acid (2) at 403.28 K [Figure 7-16 and 7-17],
- CO_2 (1) + Benzoic acid (2) at 432.62 K [Figure 7-18 and 7-19], and,
- CO_2 (1) + Benzoic acid (2) at 458.37 K [Figure 7-20 and 7-21].

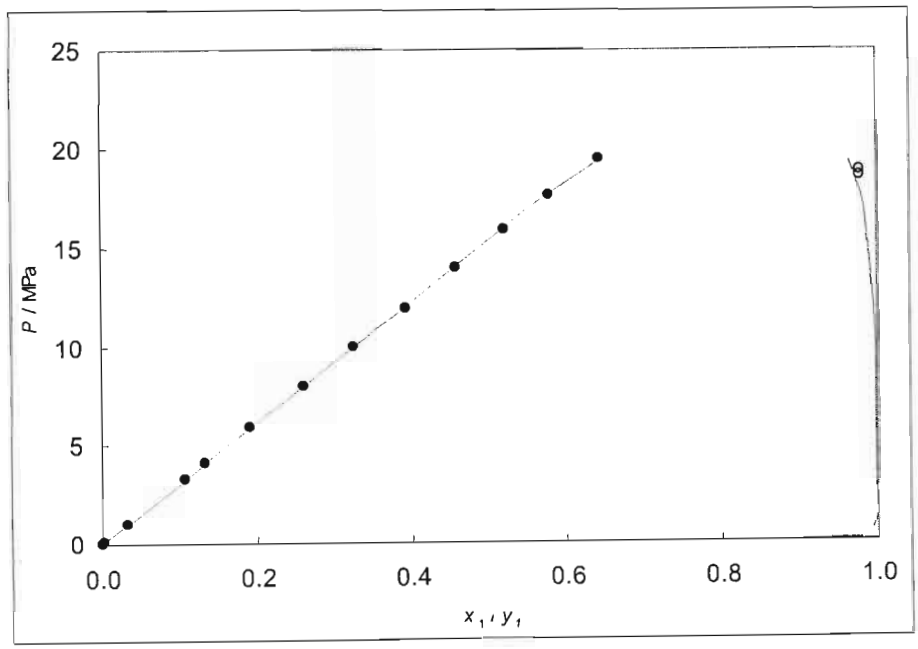

Figure 7-10: Experimental and calculated P - x (y) data for the system CO_2 (1) + Naphthalene (2) at 372.45 K: •, experimental x_1 data; o, experimental dew point data; ——, modelled data (Wong-Sandler mixing rule).

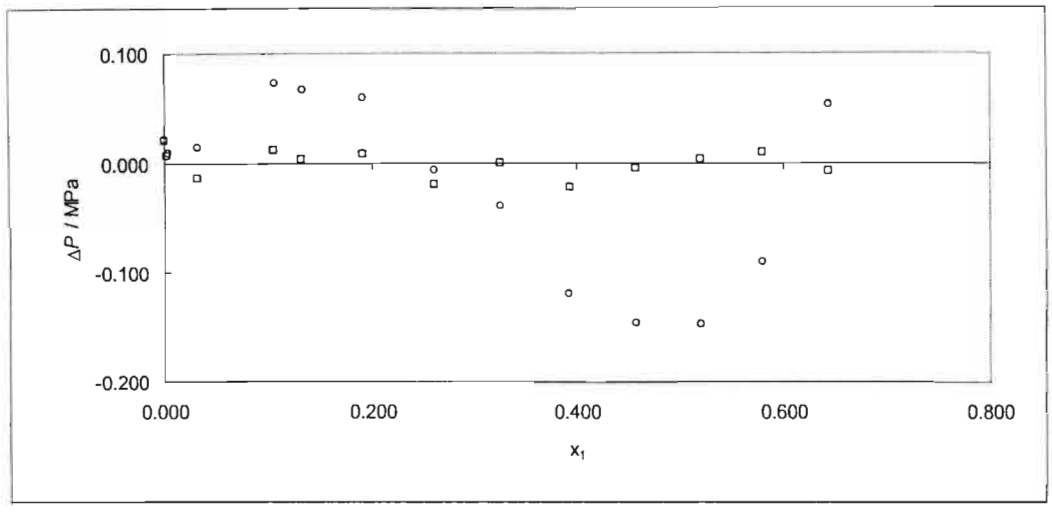

Figure 7-11: Pressure difference (ΔP) between actual pressures and model pressures for CO_2 (1) + Naphthalene (2) at 372.45 K: o, Huron-Vidal mixing rule; □, Wong-Sandler mixing rule.

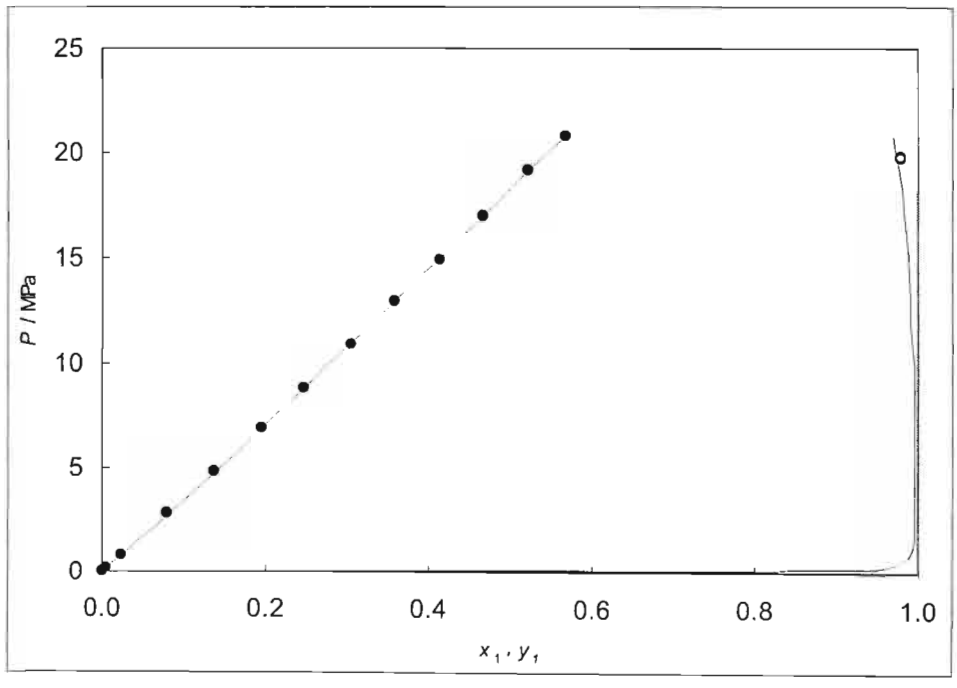

Figure 7-12: Experimental and calculated P - x (y) data for the system CO_2 (1) + Naphthalene (2) at 403.85 K: •, experimental x_1 data; o, experimental dew point data; ——, modelled data (Huron-Vidal mixing rule).

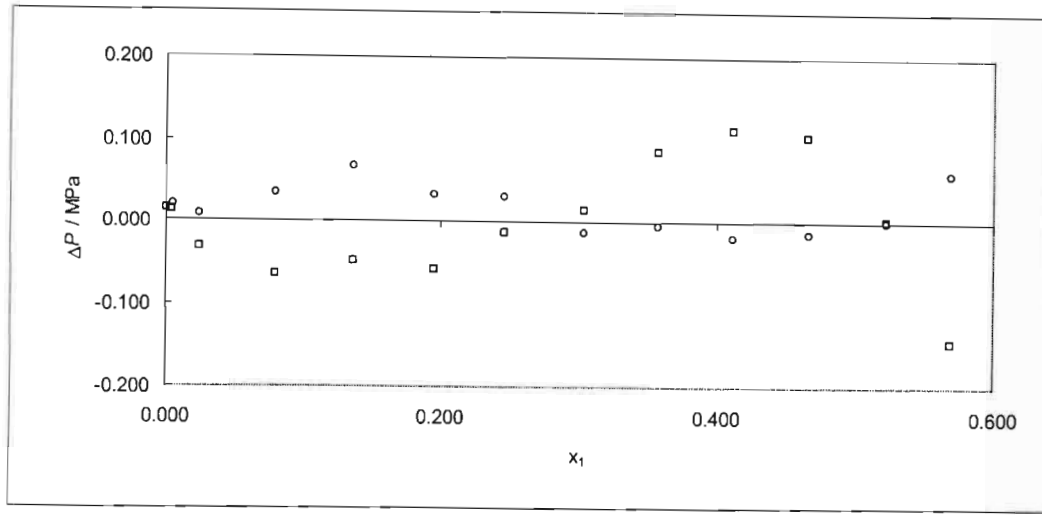

Figure 7-13: Pressure difference (ΔP) between actual pressures and model pressures for CO_2 (1) + Naphthalene (2) at 403.85 K: o, Huron-Vidal mixing rule; □, Wong-Sandler mixing rule.

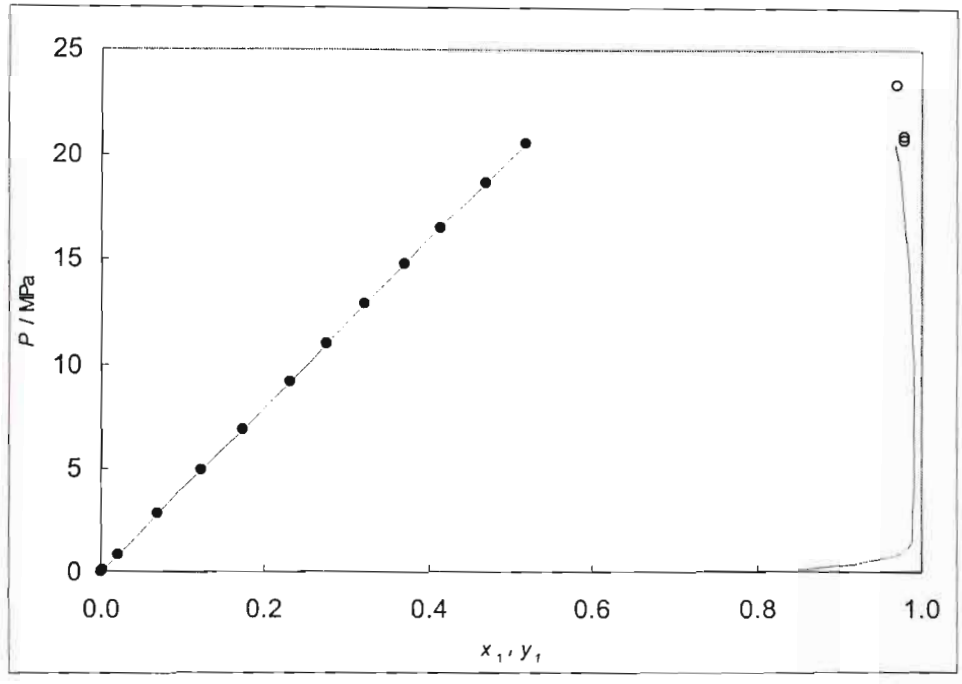

Figure 7-14: Experimental and calculated P - x (y) data for the system CO_2 (1) + Naphthalene (2) at 430.65 K: •, experimental x_1 data; o, experimental dew point data; ——, modelled data (Huron-Vidal mixing rule).

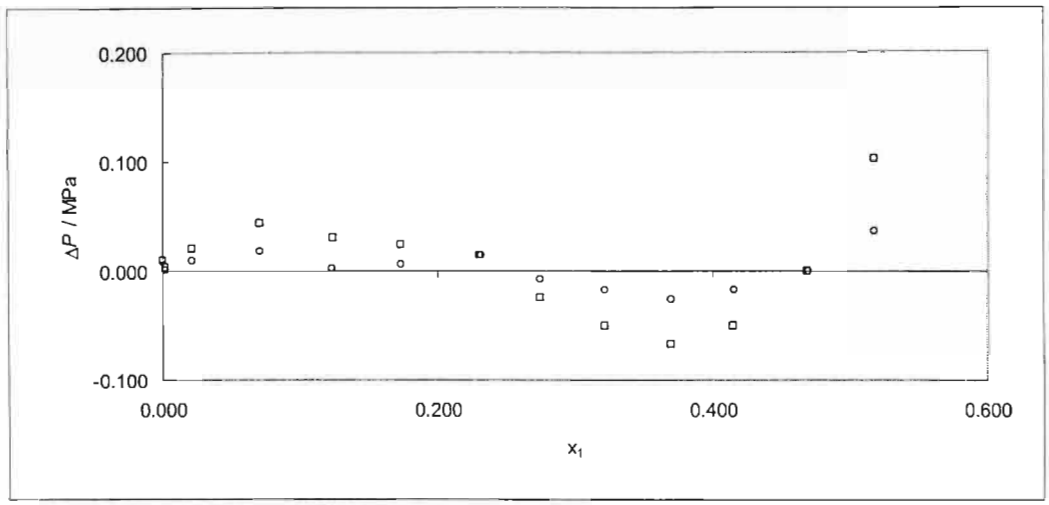

Figure 7-15: Pressure difference (ΔP) between actual pressures and model pressures for CO_2 (1) + Naphthalene (2) at 430.65 K: o, Huron-Vidal mixing rule; □, Wong-Sandler mixing rule.

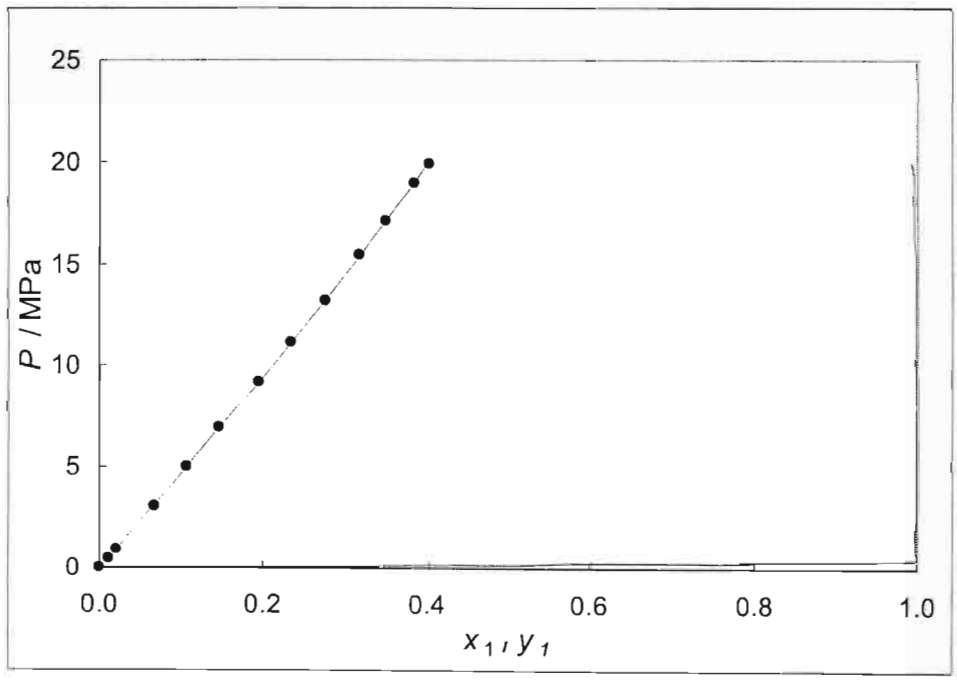

Figure 7-16: Experimental and calculated P - x (y) data for the system CO_2 (1) + Benzoic acid (2) at 403.28 K: •, experimental x_1 data; ——, modelled data (Huron-Vidal mixing rule).

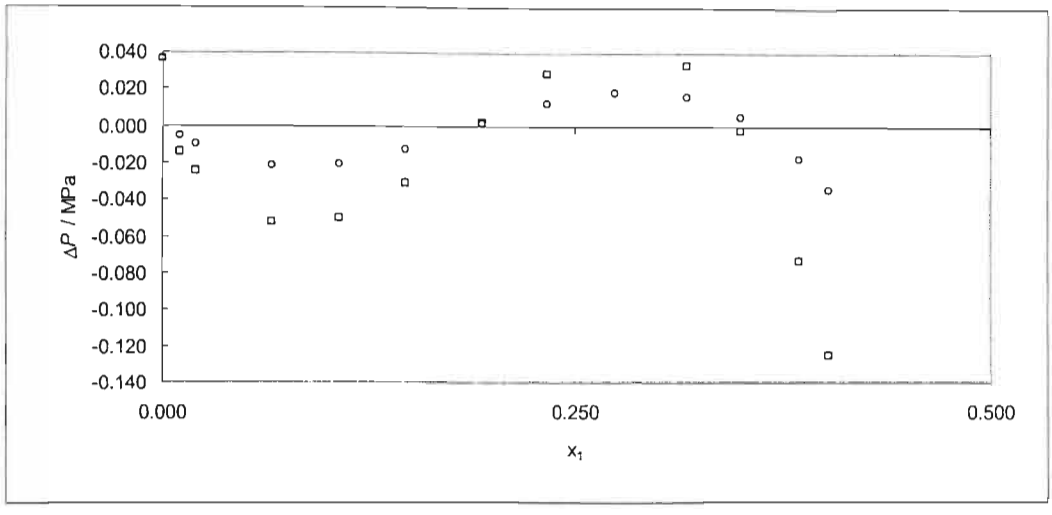

Figure 7-17: Pressure difference (ΔP) between actual pressures and model pressures for CO_2 (1) + Benzoic acid (2) at 403.28 K: o, Huron-Vidal mixing rule; □, Wong-Sandler mixing rule.

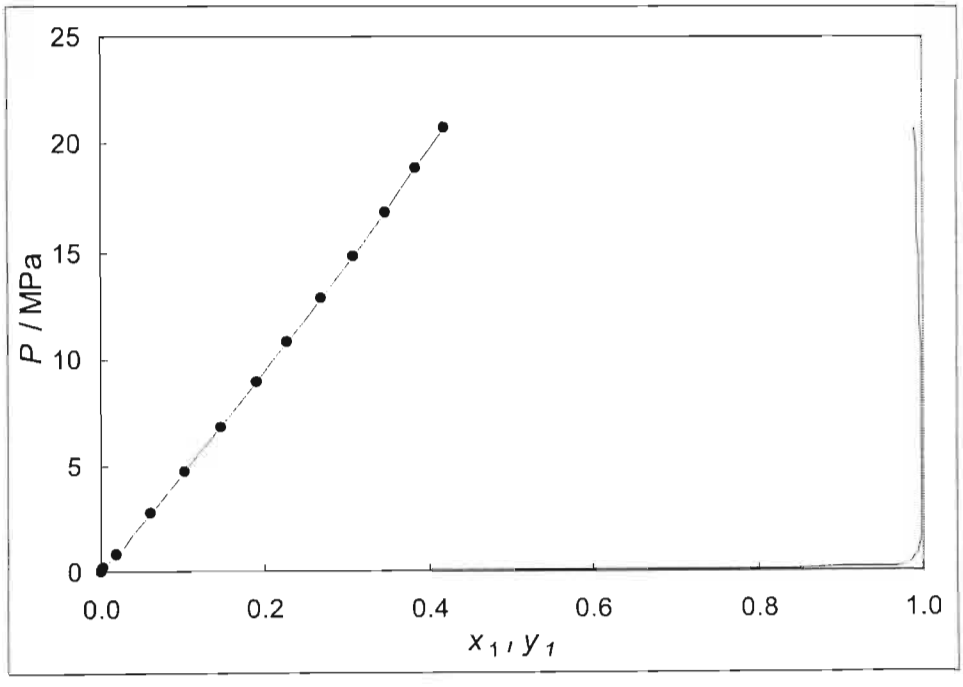

Figure 7-18: Experimental and calculated P - x (y) data for the system CO_2 (1) + Benzoic acid (2) at 432.62 K: •, experimental x_1 data; ——, modelled data (Huron-Vidal mixing rule).

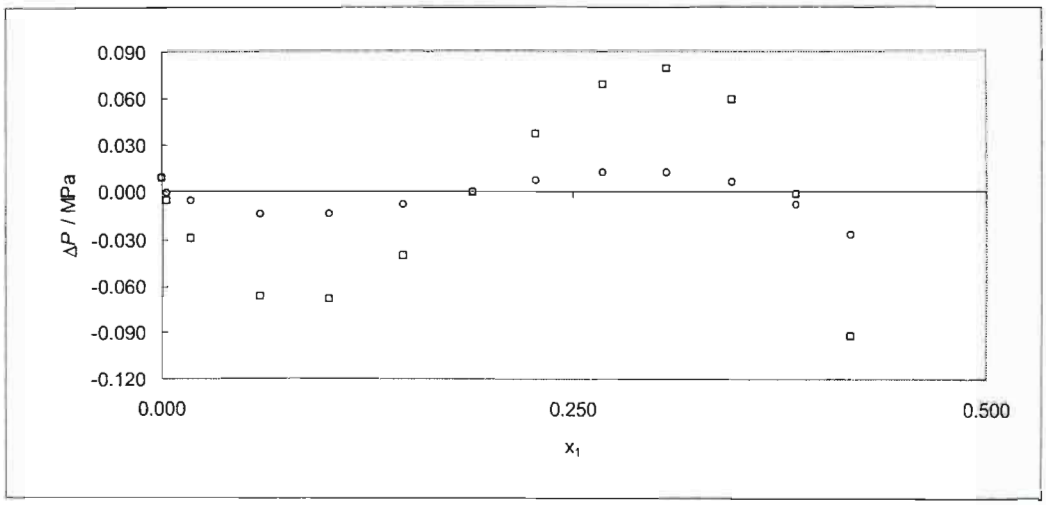

Figure 7-19: Pressure difference (ΔP) between actual pressures and model pressures for CO_2 (1) + Benzoic acid (2) at 432.62 K: o, Huron-Vidal mixing rule; □, Wong-Sandler mixing rule.

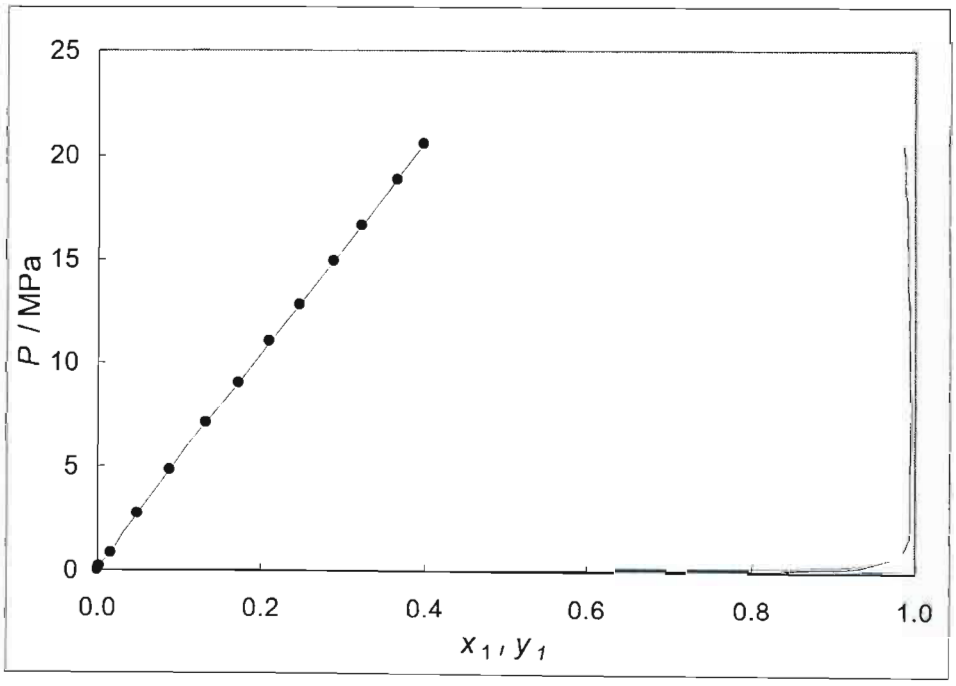

Figure 7-20: Experimental and calculated P - x (y) data for the system CO_2 (1) + Benzoic acid (2) at 458.37 K: •, experimental x_1 data; ——, modelled data (Huron-Vidal mixing rule).

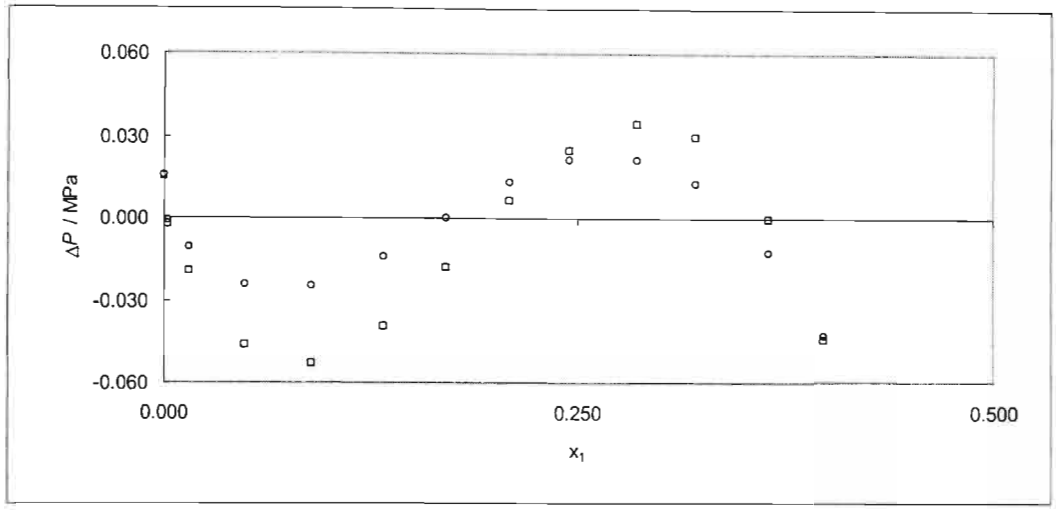

Figure 7-21: Pressure difference (ΔP) between actual pressures and model pressures for CO_2 (1) + Benzoic acid (2) at 458.37 K: o, Huron-Vidal mixing rule; □, Wong-Sandler mixing rule.

The regressed NRTL parameters ($\Delta g_{12}, \Delta g_{21}$ and α_{12}) used in the Huron-Vidal and Wong-Sandler mixing rules are given in Table 7-3 (including the fitted k_{12} parameter for the Wong-Sandler mixing rule). The average $|\Delta P|$ values are also listed. Apart from the system CO_2 (1) + Naphthalene (2) at 372.45, the Huron-Vidal mixing rule provided the best fit for the measured data. The direct method models the supercritical VLE system well and the ΔP vs. x_1 plots show that both the models provide very good fits for the measured data. There is very little scatter for the ΔP values and it is important to note that the measured data are very smooth. Both models predict very similar y_1 values. The regressed parameters vs. T are plotted in the following figures[10]:

- CO_2 (1) + Naphthalene (2) (Huron-Vidal mixing rule) [Figure 7-22],
- CO_2 (1) + Naphthalene (2) (Wong-Sandler mixing rule) [Figure 7-23],
- CO_2 (1) + Benzoic acid (2) (Huron-Vidal mixing rule) [Figure 7-24], and,
- CO_2 (1) + Benzoic acid (2) (Wong-Sandler mixing rule) [Figure 7-25].

Measurements do not extend for the entire composition range as the equipment was not designed to measure pressures greater than 20 MPa.

[10] Wong and Sandler (1992) suggest that the reduced parameters should be constant but this was not found to be true for our work.

Table 7-3 Regressed parameters for the experimental VLE data for CO_2 (1) + Naphthalene (2) and CO_2 (1) + Benzoic acid (2)

Model Parameters	CO2 (1) + Naphthalene (2)		
	T = 372.45 K	T = 403.85 K	T = 430.65 K
Huron-Vidal			
α_{12}	0.5	0.5	0.5
Δg_{12} / J.mol^{-1}	4041.6	4165.4	3734.4
Δg_{21} / J.mol^{-1}	637.6	249.5	335.5
$\lvert\Delta P\rvert_{average}$ / MPa	0.78	0.63	0.29
Wong-Sandler			
α_{12}	0.4	0.4	0.4
Δg_{12} / J.mol^{-1}	4039.1	2885.2	4772.7
Δg_{21} / J.mol^{-1}	467.3	570.1	-57.3
k_{12}	0.662	0.704	0.650
$\lvert\Delta P\rvert_{average}$ / MPa	0.76	0.63	0.33
Model Parameters	**CO2 (1) + Benzoic Acid (2)**		
	T = 403.28 K	T = 432.62 K	T = 458.37 K
Huron-Vidal			
α_{12}	0.5	0.5	0.5
Δg_{12} / J.mol^{-1}	1735.8	1355.6	886.3
Δg_{21} / J.mol^{-1}	1028.0	386.8	2165.7
$\lvert\Delta P\rvert_{average}$ / MPa	0.78	0.52	0.45
Wong-Sandler			
α_{12}	0.4	0.4	0.4
Δg_{12} / J.mol^{-1}	787.3	-171.2	-207.7
Δg_{21} / J.mol^{-1}	1851.8	2262.0	2918.0
k_{12}	0.690	0.692	0.670
$\lvert\Delta P\rvert_{average}$ / MPa	0.82	0.59	0.45

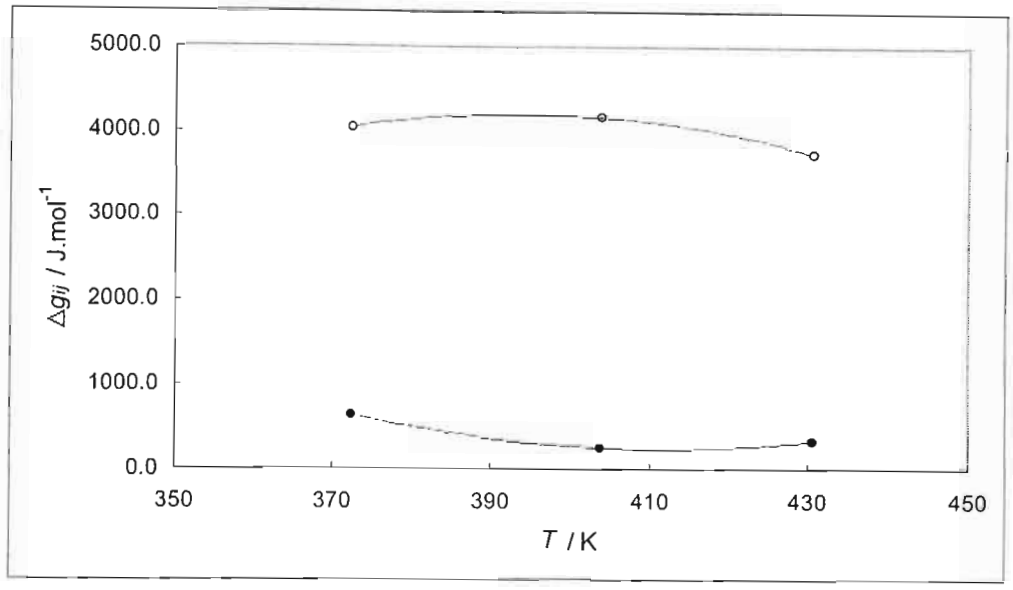

Figure 7-22: Regressed parameters for the Huron-Vidal mixing rule for CO_2 (1) + Naphthalene (2): o, Δg_{12}; •, Δg_{21}.

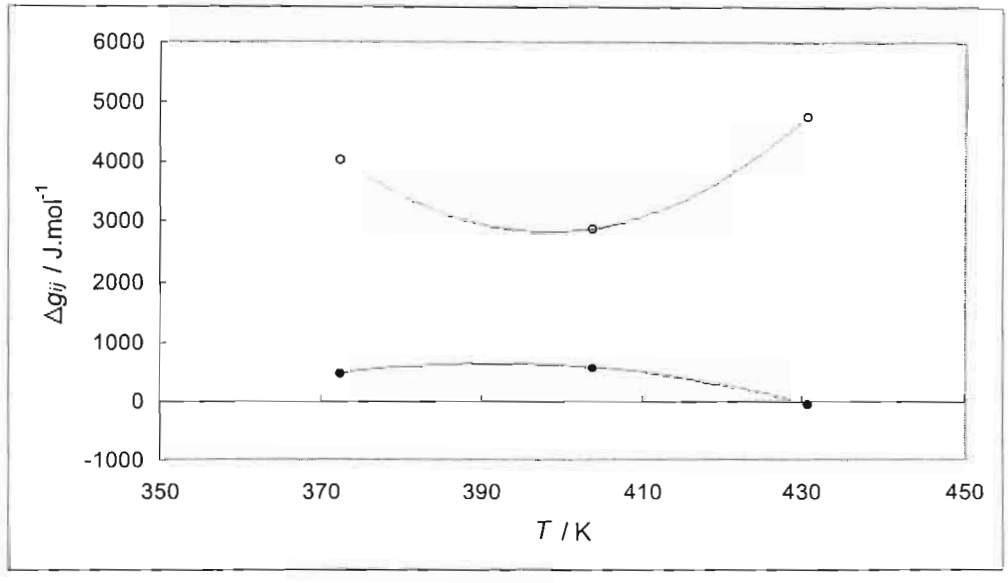

Figure 7-23: Regressed parameters for the Wong-Sandler mixing rule for CO_2 (1) + Naphthalene (2): o, Δg_{12}; •, Δg_{21}.

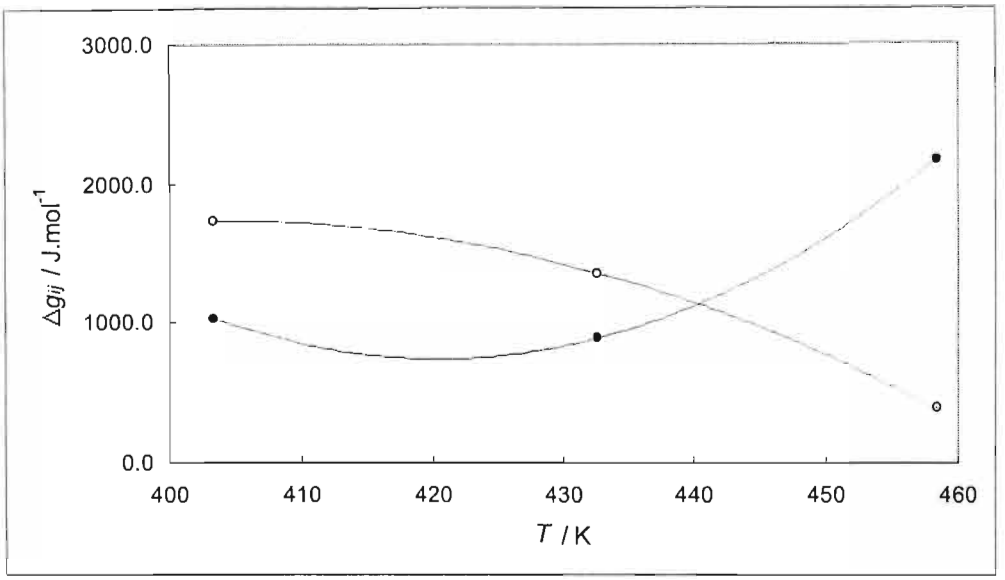

Figure 7-24: Regressed parameters for the Huron-Vidal mixing rule for CO_2 (1) + Benzoic acid (2): o, Δg_{12}; •, Δg_{21}.

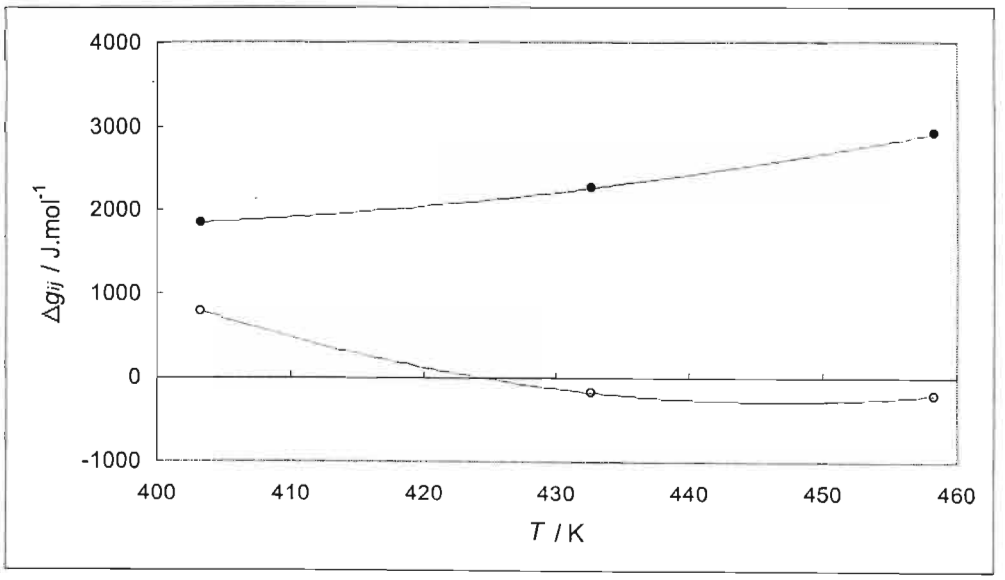

Figure 7-25: Regressed parameters for the Wong-Sandler mixing rule for CO_2 (1) + Benzoic acid (2): o, Δg_{12}; •, Δg_{21}.

The plots of the regressed parameters are useful in several ways. They illustrate that the parameters change with temperature (temperature dependence), from the plots it is evident that this dependence is not linear, and, from the plots it is also possible to interpolate values for the parameters at other temperatures. It is important to note that if only two isotherms had been measured per point, the resulting temperature dependence would have been represented by a linear function. If this had been the case, the discrepancy between interpolated parameters would have been quite large, thus the necessity for at least three isotherms is confirmed for any interpolation of temperature dependence of the parameters.

7.3.2 Excess Properties

Excess properties were determined as explained in Chapter Five. The best fitting model parameters were used in the calculations. Figure 7-26 illustrates the $\frac{G^E}{RT}$ vs. T relationship for CO_2 (1) + Naphthalene (2), which is used to determine $\left[\frac{\partial\left(G^E/RT\right)}{\partial T}\right]$. Only a few points are included so as to prevent confusion. The complete set of points and data for these calculations are given in Appendix C. It is important to note that the temperature dependence displayed in Figure 7-26 is linear. In some of the other $\frac{G^E}{RT}$ vs. T plots shown in Appendix C, the linearity is not so precise. The problem then arises that a small error in the determination of the slope of $\frac{G^E}{RT}$ can give a large error in the calculated value for H^E. It is difficult to assess the accuracy of these values (calculated from the VLE data) but it is important to note that they should only ever be used as an indication of the H^E values. In practice, good results can be obtained when predicting VLE data from experimental H^E values (Hanks et al. (1971)).

The predicted H^E values for CO_2 (1) + Naphthalene (2) and CO_2 (1) + Benzoic acid (2) are given in Tables 7-4 and 7-5 respectively. H^E values are useful in industrial practice in designing distillation columns. They are used in the enthalpy balances and to calculate the required duty of the reboiler. TS^E properties were also calculated. They are of academic interest only and are not useful for any industrial design purpose. The excess properties are not predicted for compositions greater than the composition range measured in the VLE experiments.

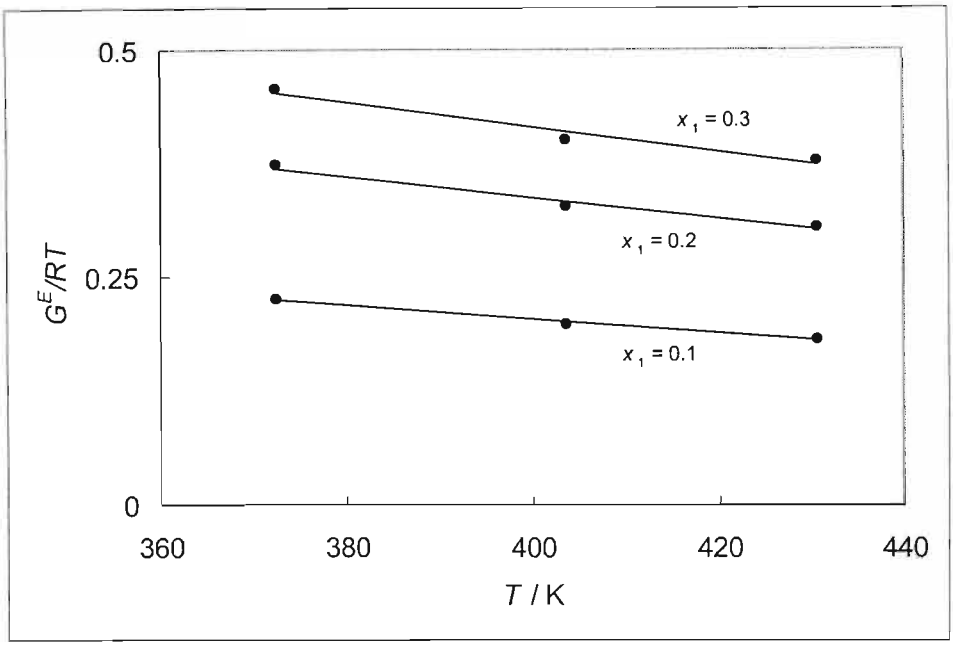

Figure 7-26: $\frac{G^E}{RT}$ vs. T relationship for CO_2 (1) + Naphthalene (2).

Table 7-4 Calculated H^E values for CO_2 (1) + Naphthalene (2)

x_1	H^E/ J.mol^{-1}		
	372.45 K	**403.85 K**	**430.65 K**
0.0	0.0	0.0	0.0
0.1	858.1	1008.8	1147.2
0.2	1348.2	1585.1	1802.5
0.3	1581.2	1859.0	2114.0
0.4	1630.8	1917.3	2180.3
0.5	1545.4	1817.0	2066.2
0.6	1360.9	1600.0	1819.5

Table 7-5 Calculated H^E values for CO_2 (1) + Benzoic acid (2)

x_1	H^E / J.mol^{-1}		
	403.28 K	432.62 K	458.37 K
0.0	0.0	0.0	0.0
0.1	615.2	708.0	794.8
0.2	985.7	1134.4	1273.4
0.3	1150.7	1324.2	1486.5
0.4	1153.4	1327.3	1490.0
0.5	1034.4	1190.4	1336.3

The predicted excess properties (G^E, H^E and TS^E) are plotted in the following figures:

- CO_2 (1) + Naphthalene (2) [Figure 7-27, 7-28 and 7-29], and,
- CO_2 (1) + Benzoic acid (2) [Figure 7-30, 7-31 and 7-32].

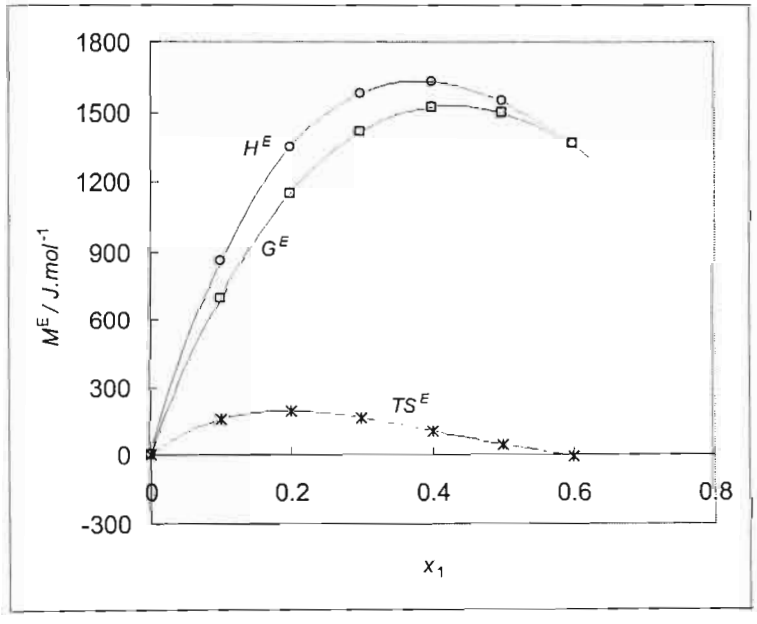

Figure 7-27: Predicted excess properties (G^E, H^E and TS^E) for CO_2 (1) + Naphthalene (2) at 372.45 K: □, G^E; o, H^E and *, TS^E.

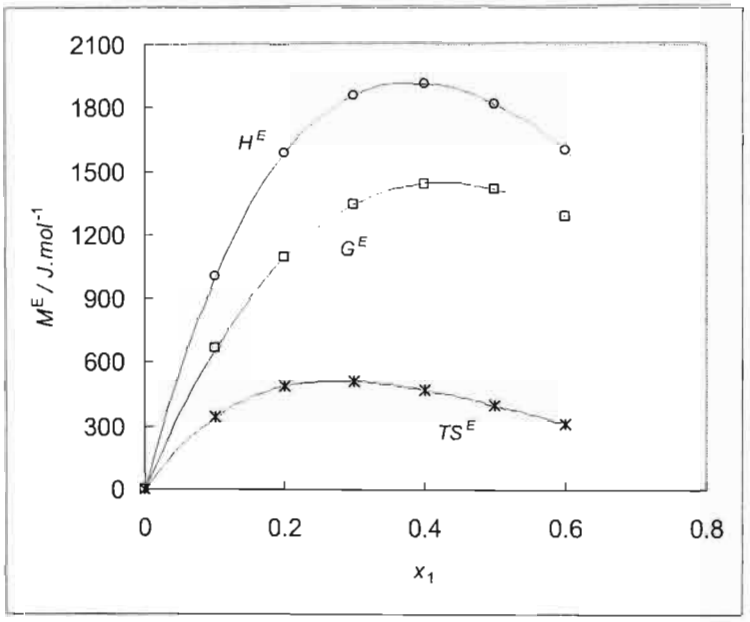

Figure 7-28: Predicted excess properties (G^E, H^E and TS^E) for CO_2 (1) + Naphthalene (2) at 403.85 K: □, G^E; o, H^E and *, TS^E.

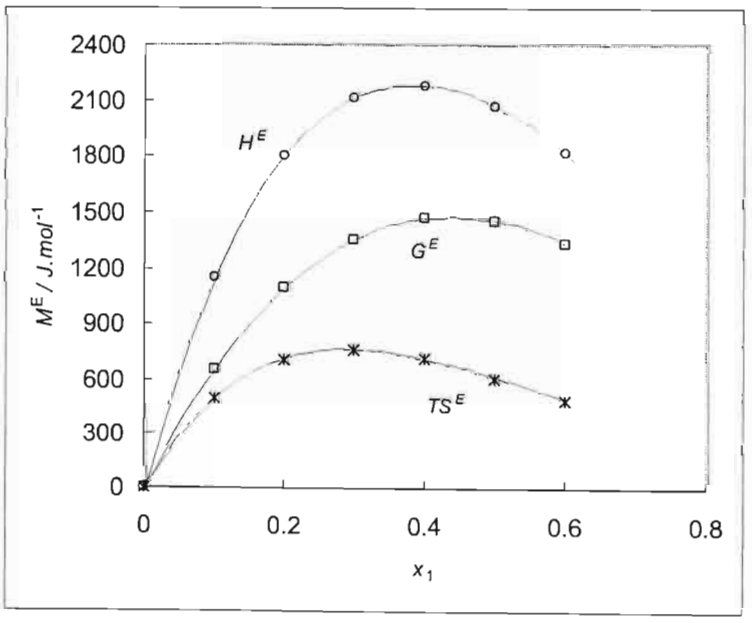

Figure 7-29: Predicted excess properties (G^E, H^E and TS^E) for CO_2 (1) + Naphthalene (2) at 430.65 K: □, G^E; o, H^E and *, TS^E.

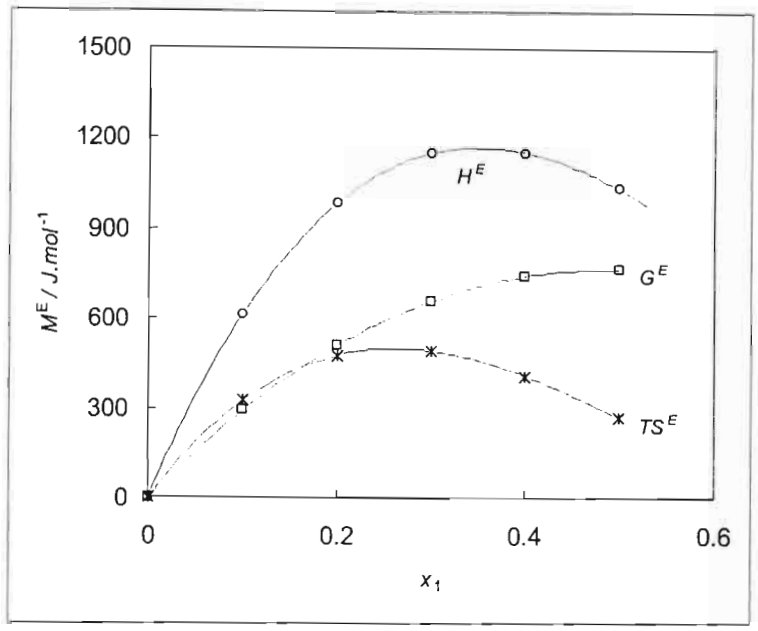

Figure 7-30: Predicted excess properties (G^E, H^E and TS^E) for CO_2 (1) + Benzoic acid (2) at 403.28 K: □, G^E; o, H^E and *, TS^E.

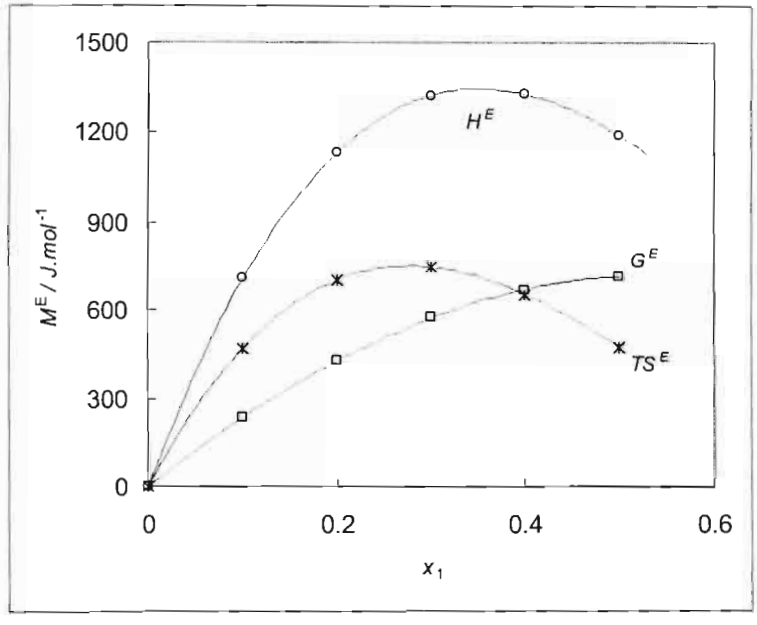

Figure 7-31: Predicted excess properties (G^E, H^E and TS^E) for CO_2 (1) + Benzoic acid (2) at 432.62 K: □, G^E; o, H^E and *, TS^E.

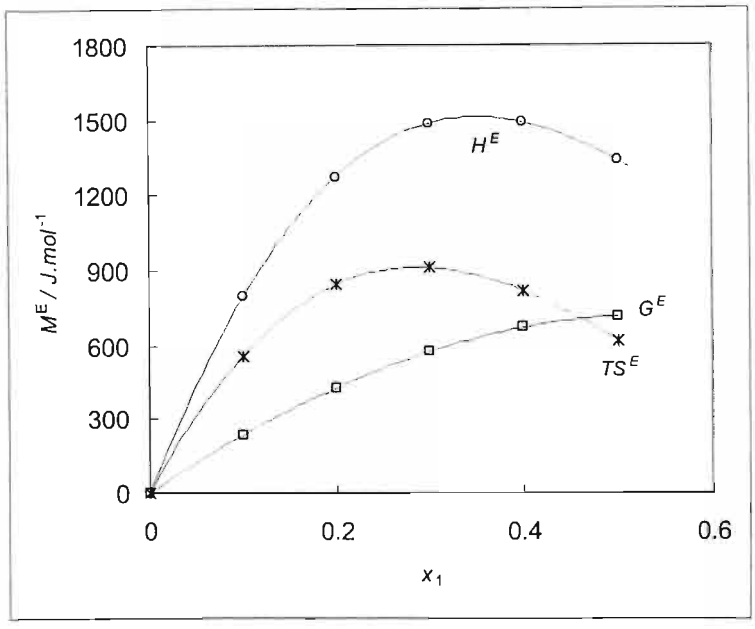

Figure 7-32: Predicted excess properties (G^E, H^E and TS^E) for CO_2 (1) + Benzoic acid (2) at 458.37 K: □, G^E; o, H^E and *, TS^E.

7.2.3 Henry's Constants

Henry's constants (H_i) were calculated as discussed in Chapter Five. As explained previously, the Henry's constant can be used to describe the phase equilibria in the CO_2 dilute region ($P < 0.5$ to 1 MPa). The Henry's constant is useful as it is simple to use and for low CO_2 concentrations it is sufficiently accurate. The Henry's coefficients (H_1) for CO_2 (1) + Naphthalene (2) and CO_2 (1) + Benzoic acid (2) are given in Tables 7-6 and 7-7 respectively. The relationship H_1 vs. T for CO_2 (1) + Naphthalene (2) and CO_2 (1) + Benzoic acid (2) is plotted in Figures 7-33 and 7-34 respectively.

Table 7-6 Henry's Constants (H_1) for CO_2 (1) + Naphthalene (2)

T / K	H_1 / MPa
372.45	31.08
403.85	34.69
430.65	39.24

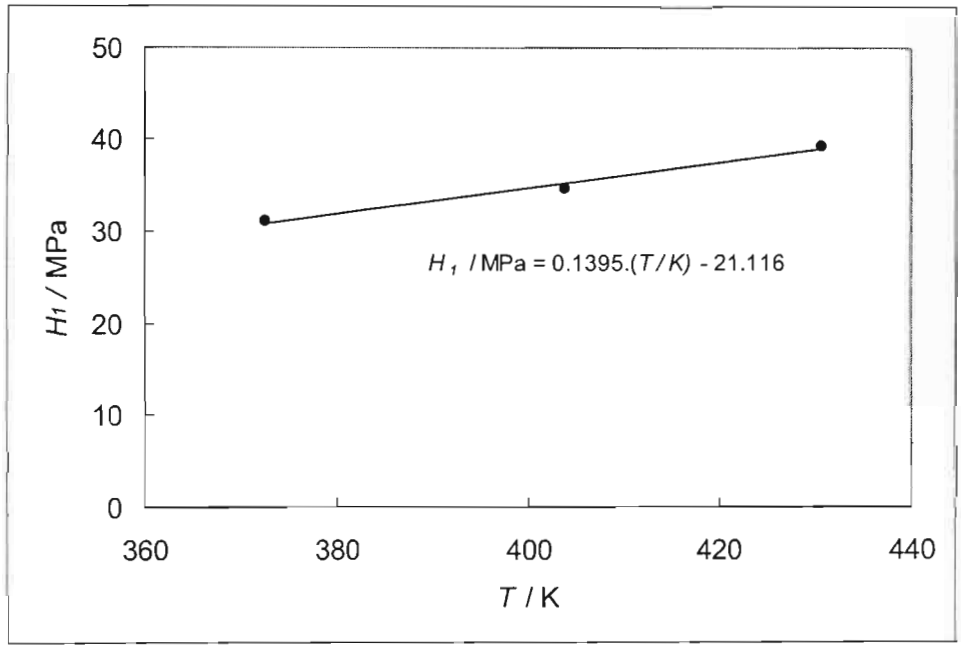

Figure 7-33: H_1 vs. T for CO_2 (1) + Naphthalene (2).

Table 7-7 Henry's Constants (H_1) for CO_2 (1) + Benzoic acid (2)

T / K	H_1 / MPa
403.28	46.92
432.62	45.93
458.37	55.02

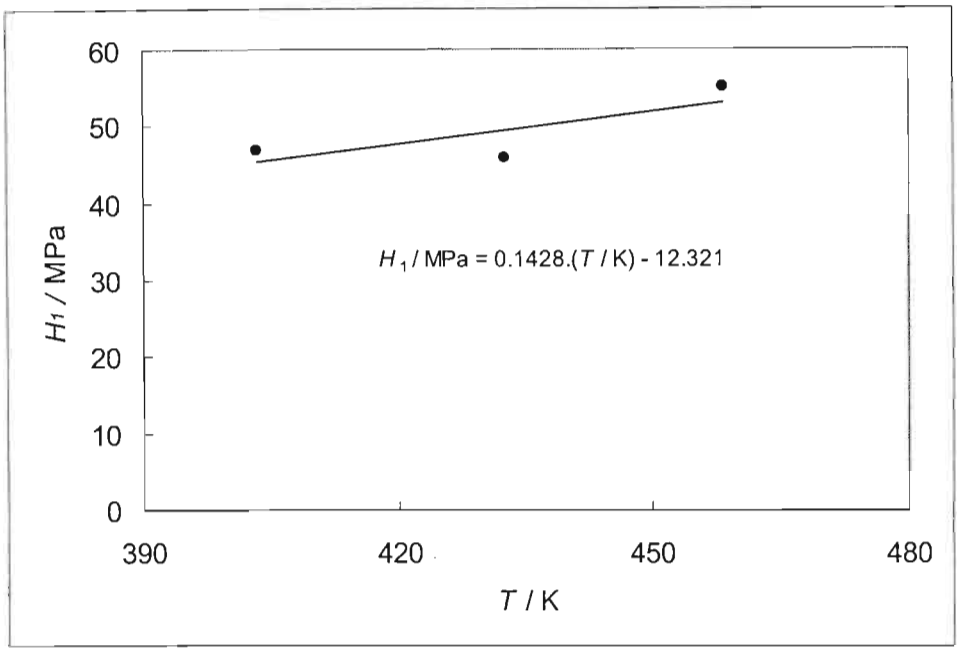

Figure 7-34: H_1 vs. T for CO_2 (1) + Benzoic acid (2).

From the linear approximations for both H_1 vs. T functions we can see that H_1 increases with an increase in temperature. This trend indicates that the solubility of the CO_2 in both Naphthalene and Benzoic acid decreases with increasing temperature. From Figure 7-33 it is seen that the linear approximation for the H_1 vs. T relationship for CO_2 (1) + Naphthalene (2) gives a reasonably good fit. Thus interpolation and even some extrapolation for the Henry's constant can be performed with confidence. The linear approximation for the H_1 vs. T relationship for CO_2 (1) + Benzoic acid (2) is a poor fit. For interpolative purposes a quadratic function would be more accurate.

7.4 DISCUSSION OF RESULTS FOR THE MEASUREMENTS UNDERTAKEN ON THE EQUIPMENT OF HARRIS ET AL. (2003B)

As this equipment was new and its development of a pioneering kind, most of the data measured with it was not new but rather systems found in literature, which were used as test systems. A large number of vapour pressure measurements were conducted to assess the operation and performance of the equipment over a large range of temperatures. Some VLE data was measured and compared to literature data to assess the performance of the equilibrium cell in separating the phases and two new VLE systems were measured.

7.4.1 Vapour Pressures

Low-Pressure High-Temperature VP

Vapour pressures for seven systems were measured in the low-pressure region. The vapour pressures are compared to literature data in Chapter Six. These vapour pressure measurements were across a large range of temperatures and were used to determine:

- an operating procedure for the general use of the equipment,
- an operating procedure for troublesome chemicals such as those which solidify at ambient temperature,
- the effect that different charge volumes have on the measured properties, and,
- the accuracy and precision of the measurements performed with the new still.

The lowest pressure measured was 1.00 kPa and the temperatures ranged from 308.33 K to 583.90 K (Table 6-4). By comparing the measured vapour pressures to literature data it is possible to assess the accuracy of the measured data. It is important to note the accuracy over the entire range of chemicals measured so as to determine the capabilities of the still. Most of the measured vapour pressures compared well to literature. Table 7-8 shows the average temperature deviations for the chemicals measured.

From Table 7-8 it can be seen that there is good agreement for n-heptane, n-decane and n-hexadecane. There is reasonable agreement for 1-hexadecanol and d,l-menthol and poor agreement for n-dodecane and 1-octadecene. A possible explanation is that there are fewer literature data available (and thus less confidence in the literature) for the chemicals that were not fitted well. Most important to note from the results, which fitted well, is that the comparison to

literature is good across the entire temperature range. From this we can conclude that the equipment measurements across a large temperature range have reasonable accuracy.

Table 7-8 Average temperature deviation from literature (DECHEMA (1999)) for measured vapour pressures

System	$\lvert\Delta T\rvert_{average}$ / K
n-Heptane	0.15
n-Decane	0.56
n-Dodecane	4.55
n-Hexadecane	0.20
1-Octadecene	2.99
1-Hexadecanol	1.95
d,l Menthol	1.55

In Chapter Six Antoine equations were fitted to the measured data. The scatter in these fits can be used to determine the precision with which the new equipment is able to measure data. The difference between the accuracy of the equipment and its precision is important for measurement of new data as it allows us to determine the degree of confidence for the measurements. Figure 7-35 compares the measured data to the fitted Antoine equations across the entire temperature range. This plot is then divided into three sections (for added clarity) and plotted separately as follows:

- $T < 373.15$ K [Figure 7-36],
- $373.15\ \text{K} \leq T < 473.15$ K [Figure 7-37], and,
- $T \geq 473.15$ K [Figure 7-38].

The average temperature deviations for these three divisions are given in Table 7-9.

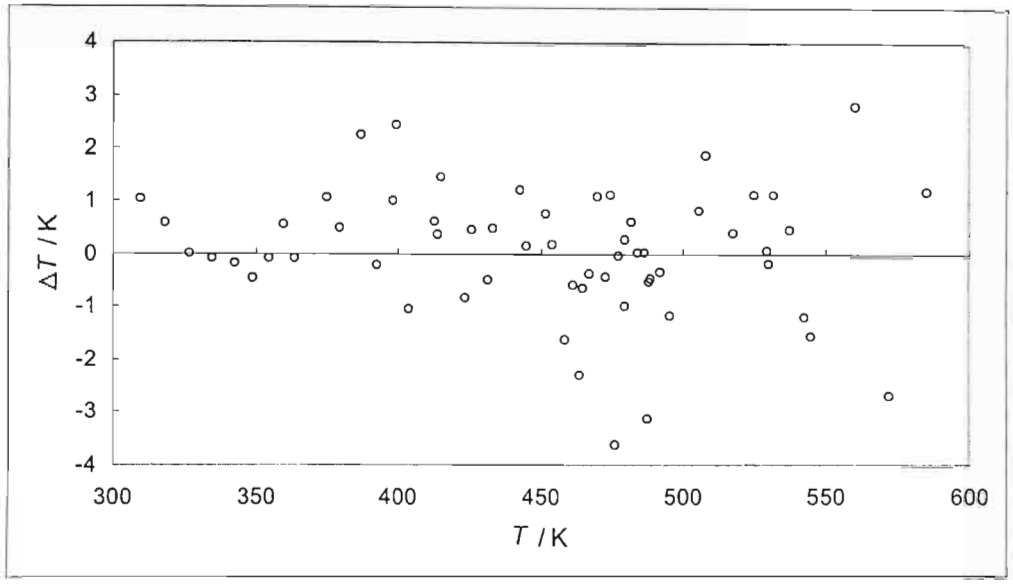

Figure 7-35: Deviation (ΔT) between the measured and the fitted Antoine equations for the entire temperature range.

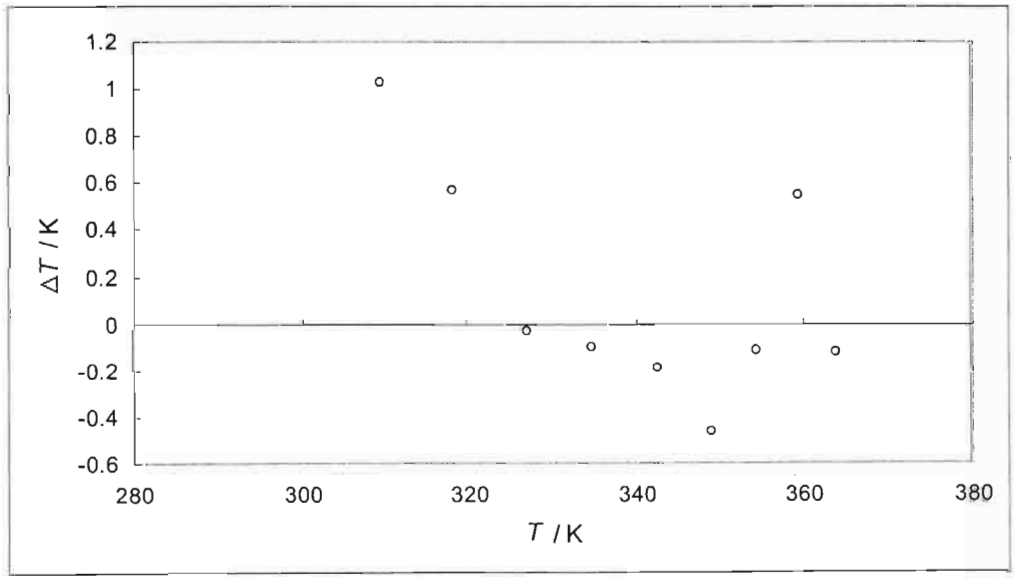

Figure 7-36: Deviation (ΔT) between the measured and the fitted Antoine equations for $T < 373.15$ K.

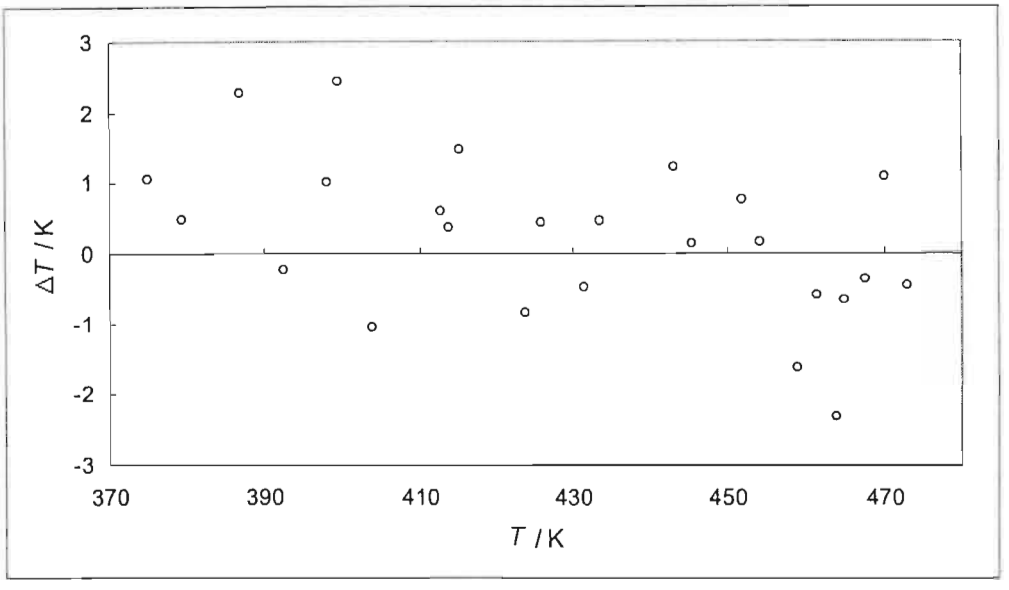

Figure 7-37: Deviation (ΔT) between the measured and the fitted Antoine equations for 373.15 K $\leq T <$ 473.15 K.

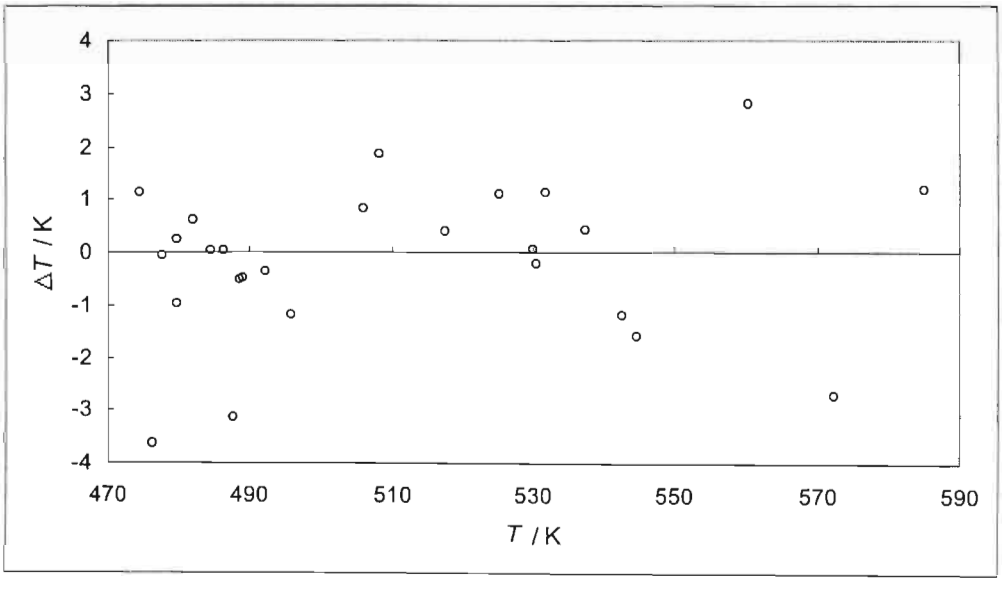

Figure 7-38: Deviation (ΔT) between the measured and the fitted Antoine equations for $T \geq$ 473.15 K.

Table 7-9 Average temperature deviation from fitted Antoine equation for vapour pressures

Division	$\lvert\Delta T\rvert_{average}$ / K
T < 373.15 K	0.38
373.15 K < T < 473.15 K	0.90
T > 473.15 K	1.07

From Table 7-9 it can be seen that as the temperature increases, the scatter increases. The scatter for temperatures over 473.15 K is just over one Kelvin which is less than 0.25% of the measured value (in Kelvin). The effect that this scatter has on the data is best visualized by inspecting the term $\left(\frac{\partial P}{\partial T}\right)_{x_1=1}$ again. For large $\left(\frac{\partial P}{\partial T}\right)_{x_1=1}$ values a 1 K scatter can have a large effect on the measured pressure, whereas for small $\left(\frac{\partial P}{\partial T}\right)_{x_1=1}$ values the effect may be negligible.

High-Pressure VP

Acetone's vapour pressure was measured at pressures up to 1 MPa and compared to literature in Chapter Six. The measurement of the vapour pressures for acetone was to determine the capabilities of the still at high pressures. Although the still was designed for much higher pressures than 1 MPa it was not possible to approach these pressures. The equipment exhibited certain problems with temperature measurement, which are discussed later. These problems made it difficult to extend the vapour pressure measurement for acetone to higher pressures. The problem with designing the equipment for pressures larger than practically necessary is discussed later. The comparison of the measured data to the literature data (Chapter Six) is satisfactory.

The scatter of the measured data around the fitted Antoine equation for the acetone system is shown in Figure 7-39. The values are within the above-mentioned averages. From this result it can be seen that the still works as well at elevated pressures as at the lower pressures.

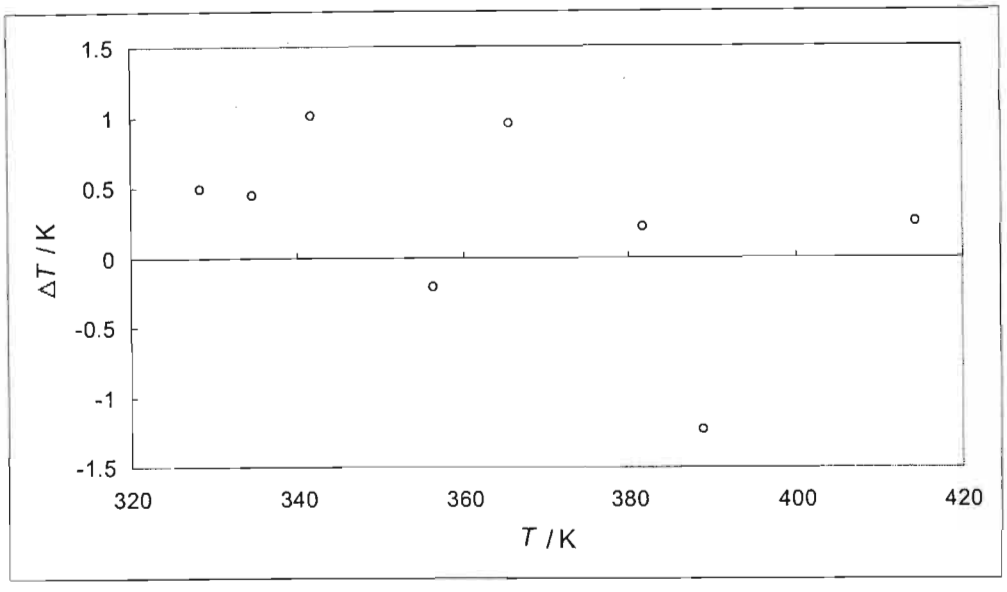

Figure 7-39: Deviation (ΔT) between the measured and the fitted Antoine equation for Acetone at pressures up to 1 MPa.

7.4.2 VLE Data Reduction

Test Systems

The data for the test systems are presented in Chapter Six. The first test system measured was cyclohexane (1) + ethanol (2) at 40.0 kPa. This system has been used many times as a test system in our laboratory (Joseph (2001), Sewnarain (2001), Harris (2001a)) as it exhibits non-ideal behaviour and high relative volatilities near the limits (i.e.: as $x_1 \rightarrow 0$ and as $x_1 \rightarrow 1$). The system boils at low temperatures and was used to test the basic functioning of the still and the equilibrium chamber's ability to separate the vapour and liquid phases. The data were regressed with the combined method using G^E models and a virial equation of state with Hayden and O'Connell correlation as discussed in Chapter Five. The two best models are plotted as follows:

- T-x_1-y_1 for cyclohexane (1) + ethanol (2) at 40.0 kPa [Figure 7-40],
- x_1-y_1 for cyclohexane (1) + ethanol (2) at 40.0 kPa [Figure 7-41], and,
- ΔT for the models and measured data for cyclohexane (1) + ethanol (2) at 40.0 kPa [Figure 7-42].

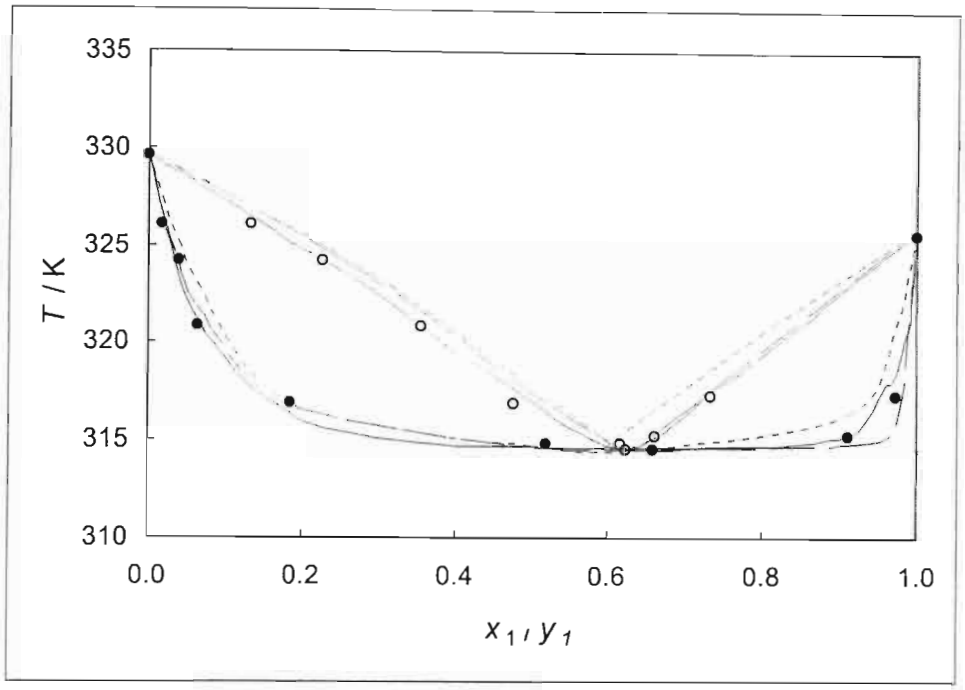

Figure 7-40: T-x_1-y_1 for cyclohexane (1) + ethanol (2) at 40.0 kPa: o, Experimental values; ——, Literature (Joseph et al. (2001)); - - -, Wilson; · · ·, NRTL.

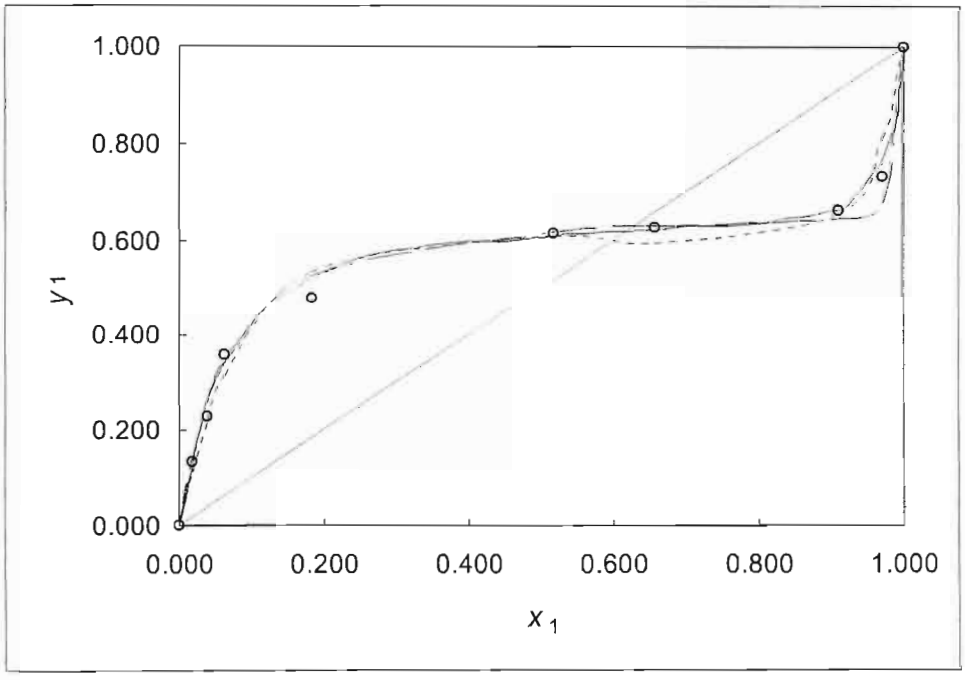

Figure 7-41: T-x_1-y_1 for cyclohexane (1) + ethanol (2) at 40.0 kPa: o, Experimental values; ——, Literature (Joseph et al. (2001)); - - -, Wilson; · · ·, NRTL.

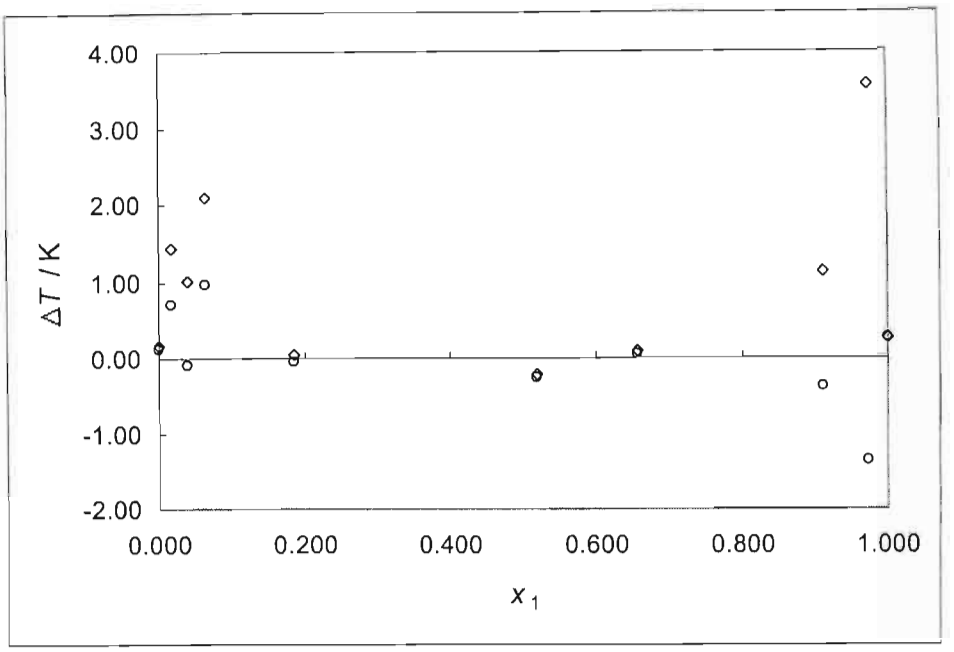

Figure 7-42: ΔT for the models and measured data for cyclohexane (1) + ethanol (2) at 40.0 kPa: o, Wilson and ◊, NRTL.

The fitted parameters are given in Table 7-10.

Table 7-10 Regressed parameters for the experimental VLE data at 40 kPa

System [NRTL]	Δg_{12} / J.mol^{-1}	Δg_{21} / J.mol^{-1}	α_{12}	$\lvert\Delta T\rvert_{ave.}$ / K
Cyclohexane (1) + Ethanol (2)	-4195	8830	0.063	1.00
System [Wilson]	**$\Delta\lambda_{12}$ / J.mol-1**	**$\Delta\lambda_{21}$ / J.mol-1**		**$\lvert\Delta T\rvert_{ave.}$ / K**
Cyclohexane (1) + Ethanol (2)	1396	11265		0.42

From the table it is evident that the Wilson model provides the best fit for the data. The measured data compares well with the literature data of Joseph et al. (2001). Furthermore, the models provide good fits for the measured data. From these results it is possible to conclude that the equipment works well at these conditions (low-temperature and low-pressure). During the experiment various variables were assessed:

- the effect charge volume has on VLE measurement,
- the effect the heaters have on the still operation,
- the operating procedure,
- the condenser temperature and its effects, and,
- the sampling procedure.

From this experiment it was found that operation and measured variables were not drastically affected for still charge volumes between 100 to 140 ml. The heaters are very sensitive and it was found that if the external heater is set too high it could cause the entire contents of the reboiler to vaporize thus destroying the experiment. Setting of the heaters requires careful adjustment and some knowledge of prior operating conditions. The condenser temperature did not affect the operation of the still provided that the condenser was kept at least 15 to 20 K colder than the equilibrium temperature. However, when comparing the amount of material drained from the still to the amount added in the beginning, it was found that small amounts of material were lost over long operation periods. Hence, the interior heat exchange coil discussed in Chapter Four was added to the interior of the condenser. From the sampling procedure the vital conclusion was reached that a minimum height difference between sampling point and the top of the reboiler (as discussed in Chapter Four) was needed. The vapour sampling point had to be heightened to conform with this finding and only after the modification could accurate vapour phase compositions be measured.

The data for the high temperature test system n-dodecane (1) + 1-octadecene (2) at 26.66 kPa are recorded in Chapter Six. There were severe difficulties in measuring the vapour phase composition. Despite several attempts to remedy the situation, it was not possible to obtain vapour composition values. This problem occupied a large amount of time during experimentation and is discussed in detail later in this Chapter. For the present discussion it is important to note that only x_i-P data was measured and that models fitted to this data were used to calculate the vapour phase compositions as explained I Chapter Five.

The data were regressed by:

i.) the direct method using the P-R EOS with Twu and Coon mixing rules, and,

ii.) the combined method using G^E models with a Virial EOS,

as explained in Chapter Three. The regressed data are presented as follows:

- T-x_1-y_1 data for n-dodecane (1) + 1-octadecene (2) at 26.66 kPa fitted with P-R EOS [Figure 7-43],
- x_1-y_1 data for n-dodecane (1) + 1-octadecene (2) at 26.66 kPa fitted with P-R EOS [Figure 7-44],
- Regressed parameters for the EOS [Table 7-11],
- T-x_1-y_1 data for n-dodecane (1) + 1-octadecene (2) at 26.66 kPa fitted with G^E models [Figure 7-45],
- x_1-y_1 data for n-dodecane (1) + 1-octadecene (2) at 26.66 kPa fitted with G^E models [Figure 7-46],
- Regressed parameters for the G^E models [Table 7-12],
- Deviation (ΔT) for the regressed data and measured data for n-dodecane (1) + 1-octadecene (2) at 26.66 kPa [Figure 7-47], and,
- Deviation (Δy_1) for the regressed data and literature data for n-dodecane (1) + 1-octadecene (2) at 26.66 kPa [Figure 7-48].

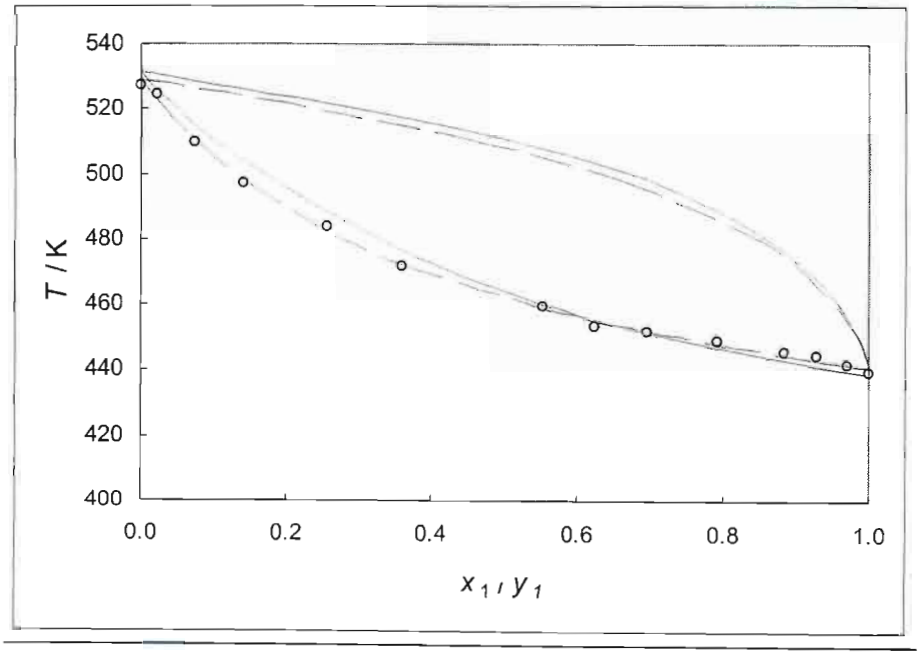

Figure 7-43: T-x_1-y_1 data for n-dodecane (1) + 1-octadecene (2) at 26.66 kPa fitted with P-R EOS: o, Experimental values; ——, Literature (Jordan and van Winkle (1951)); - - -, P-R EOS.

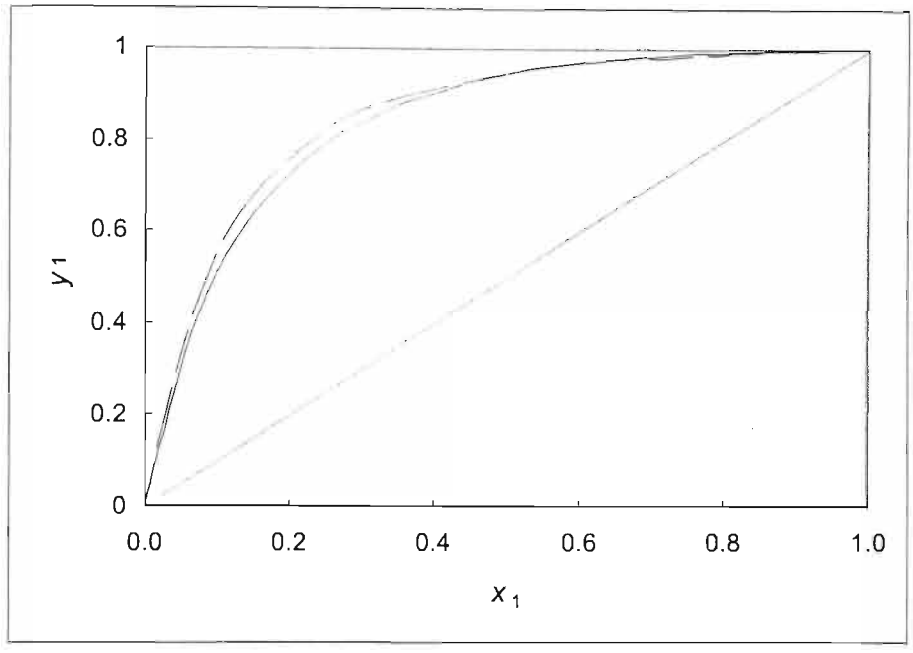

Figure 7-44: x_1-y_1 data for n-dodecane (1) + 1-octadecene (2) at 26.66 kPa fitted with P-R EOS: ——, Literature (Jordan and van Winkle (1951)); - - -, P-R EOS.

Table 7-11 Regressed parameters for the P-R EOS with Twu and Coon mixing rules for n-dodecane (1) + 1-octadecene (2) at 26.66 kPa

Model Parameters	n-dodecane (1) + 1-octadecene (2)
	P = 26.66 kPa
NRTL parameters	
α_{12}	0.31
Δg_{12} / J.mol^{-1}	14047
Δg_{21} / J.mol^{-1}	995.5
EOS parameters	
l_{ij}	-0.012
k_{ij}	-0.035
$\lvert\Delta T\rvert_{average}$ / K	1.00

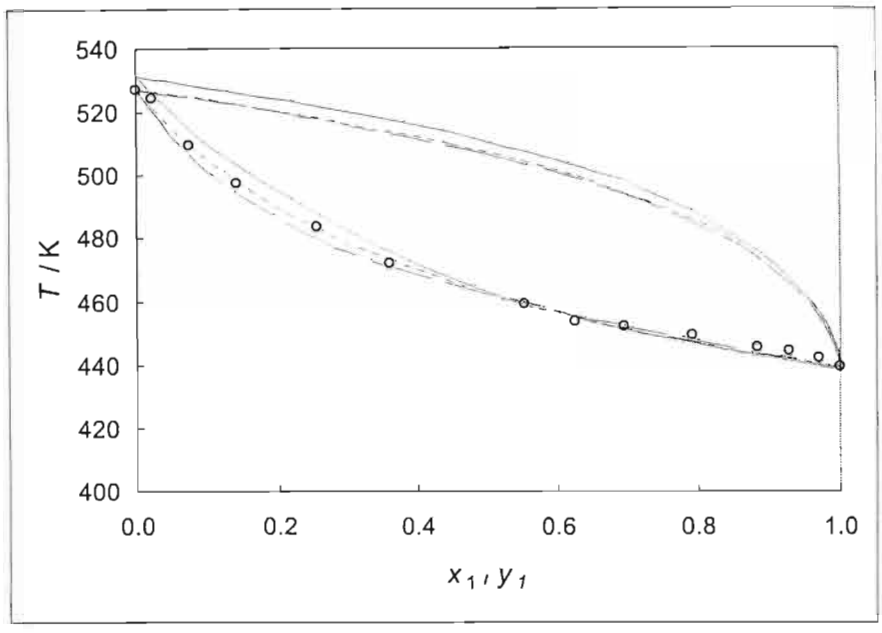

Figure 7-45: T-x_1-y_1 data for n-dodecane (1) + 1-octadecene (2) at 26.66 kPa fitted with G^E models: o, Experimental values; ——, Literature (Jordan and van Winkle (1951)); - - -, Wilson; · · ·, NRTL.

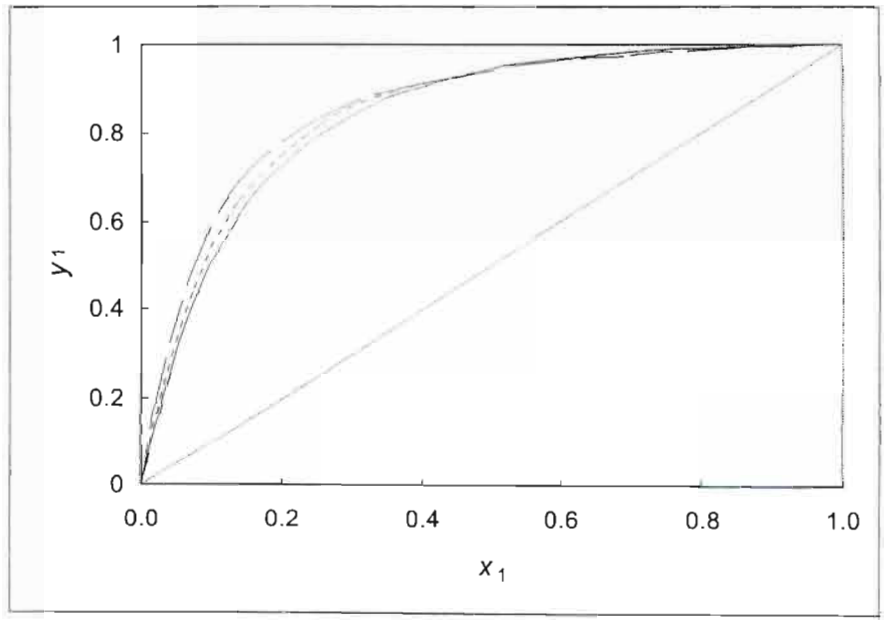

Figure 7-46: x_1-y_1 data for n-dodecane (1) + 1-octadecene (2) at 26.66 kPa fitted with G^E models: ——, Literature (Jordan and van Winkle (1951)); - - -, Wilson; · · ·, NRTL.

Table 7-12 Regressed parameters for the experimental VLE data for n-dodecane (1) + 1-octadecene (2) at 26.66 kPa

System [NRTL]	Δg_{12} / J.mol^{-1}	Δg_{21} / J.mol^{-1}	α_{12}	$\lvert\Delta T\rvert_{ave.}$ / K	$\lvert\Delta y_1\rvert_{ave.}$
n-dodecane (1) + 1-octadecene (2)	-10352	5020	0.300	1.73	0.021
System [Wilson]	$\Delta\lambda_{12}$ / J.mol-1	$\Delta\lambda_{21}$ / J.mol-1		$\lvert\Delta T\rvert_{ave.}$ / K	$\lvert\Delta y_1\rvert_{ave.}$
n-dodecane (1) + 1-octadecene (2)	-3190	3367		1.20	0.009

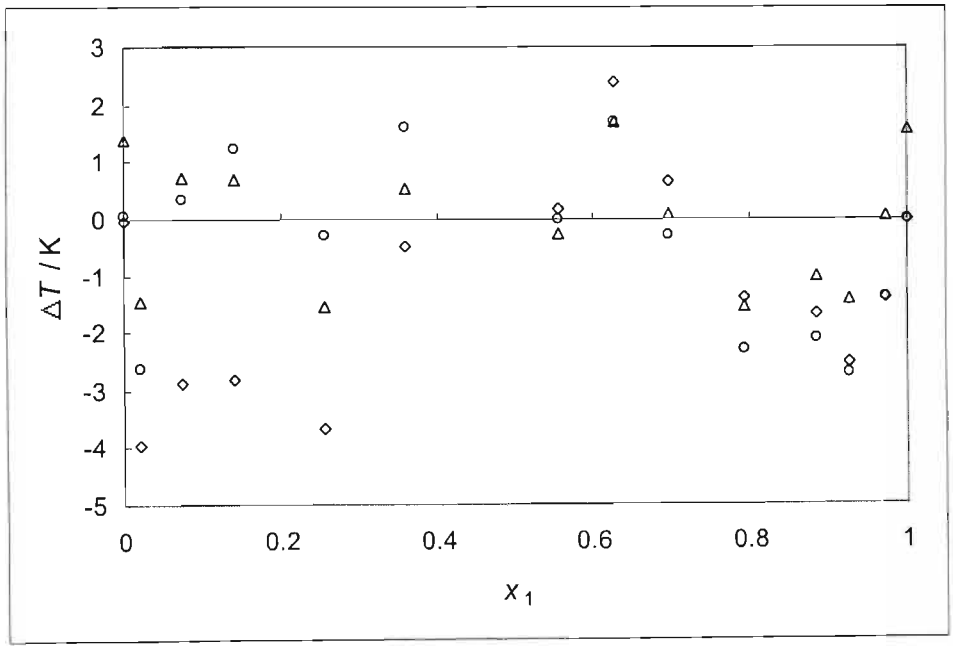

Figure 7-47: Deviation (ΔT) for the regressed data and measured data for n-dodecane (1) + 1-octadecene (2) at 26.66 kPa: Δ, P-R EOS; o, Wilson and ◊, NRTL.

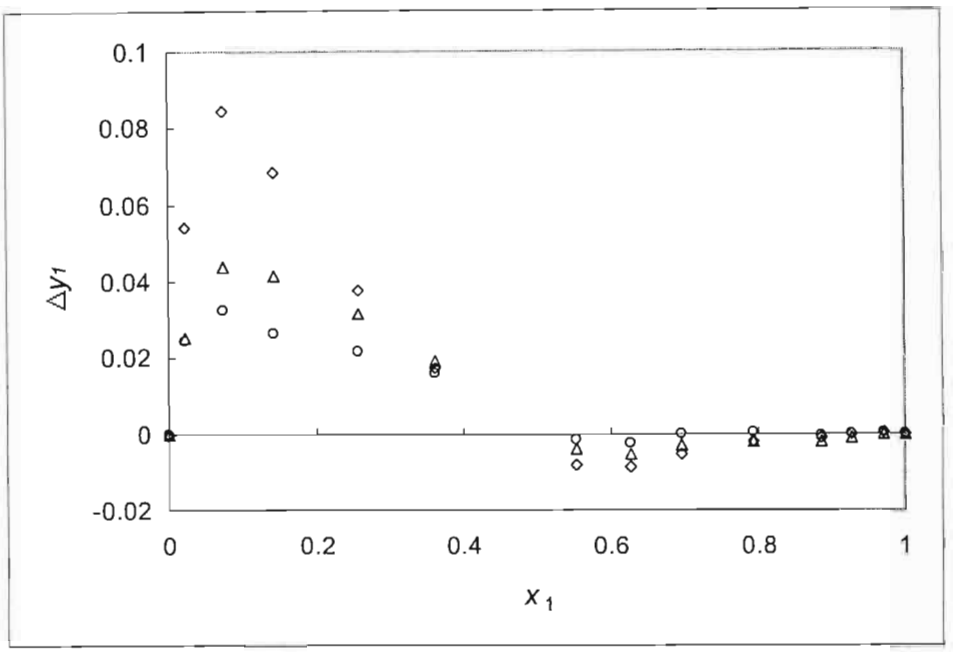

Figure 7-48: Deviation (Δy_1) for the regressed data and literature data (Jordan and van Winkle (1951)) for n-dodecane (1) + 1-octadecene (2) at 26.66 kPa: Δ, P-R EOS; o, Wilson and ◊, NRTL.

From the fitted data it can be seen that the P-R EOS provides the best fit for the T-x_1 data while the Wilson G^E model provides the best prediction for the vapour phase composition compared to literature. From the measured data we can see that the equipment measures the VLE data with a reasonable degree of accuracy when compared to the literature. However, the scatter of the data when compared to the fitted models is quite large (in excess of 3 K at some points) but on average it is within the values observed for temperature measurement deviation for the vapour pressure measurements.

Low-Pressure – High-Temperature Systems

Two high temperature systems were measured with the new equipment:

i.) n-dodecane (1) + 1-octadecene (2) at 3.00 kPa, and,

ii.) d,l-menthol (1) + l-isomenthol (2) at 448.15 K.

The data for the high temperature system n-dodecane (1) + 1-octadecene (2) at 3.00 kPa are recorded in Chapter Six. Originally only isothermal data was supposed to be measured but the temperature problems, which are discussed in detail later, made this impossible and thus a single isobar was measured instead.

These are new data, which have not been measured previously. As mentioned earlier, problems were encountered in measuring the vapour phase composition, which will be discussed later. Thus the data measured are x_1-P data. The regressed model fits were used to predict vapour phase compositions.

The data were regressed by:

i.) the direct method using the P-R EOS with Twu and Coon mixing rules, and,

ii.) the combined method using G^E models with a Virial EOS,

as explained in Chapter Three.

The regressed data are presented as follows:

- T-x_1-y_1 data for n-dodecane (1) + 1-octadecene (2) at 3.00 kPa fitted with P-R EOS [Figure 7-49],
- x_1-y_1 data for n-dodecane (1) + 1-octadecene (2) at 3.00 kPa fitted with P-R EOS [Figure 7-50],
- Regressed parameters for the EOS [Table 7-13],
- T-x_1-y_1 data for n-dodecane (1) + 1-octadecene (2) at 3.00 kPa fitted with G^E models [Figure 7-51],
- x_1-y_1 data for n-dodecane (1) + 1-octadecene (2) at 3.00 kPa fitted with G^E models [Figure 7-52],
- Regressed parameters for the G^E models [Table 7-14],
- Deviation (ΔT) for the regressed data and measured data for n-dodecane (1) + 1-octadecene (2) at 3.00 kPa [Figure 7-53], and,

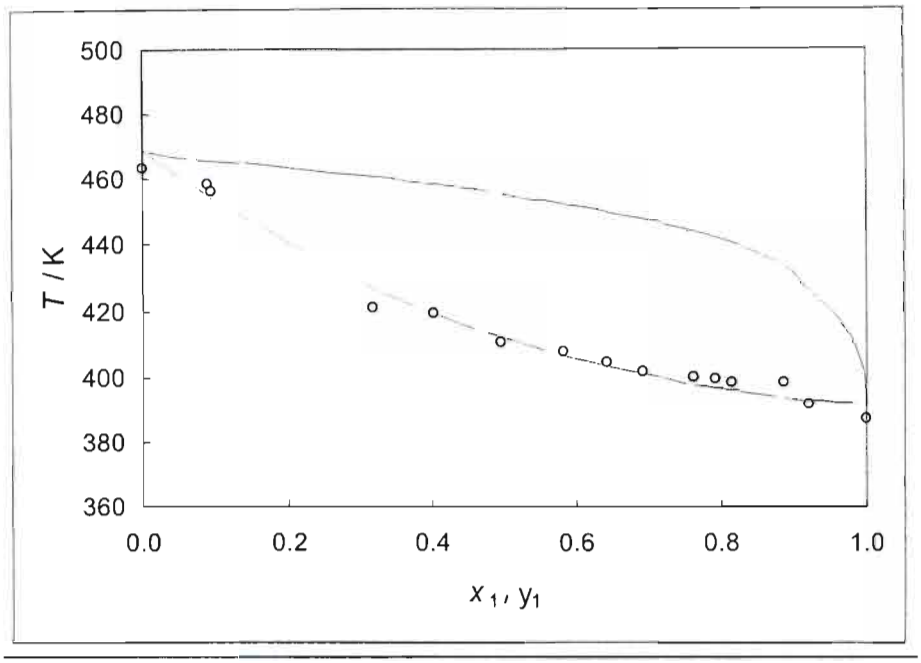

Figure 7-49: T-x_1-y_1 data for n-dodecane (1) + 1-octadecene (2) at 3.00 kPa fitted with P-R EOS: o, Experimental values; - - -, P-R EOS.

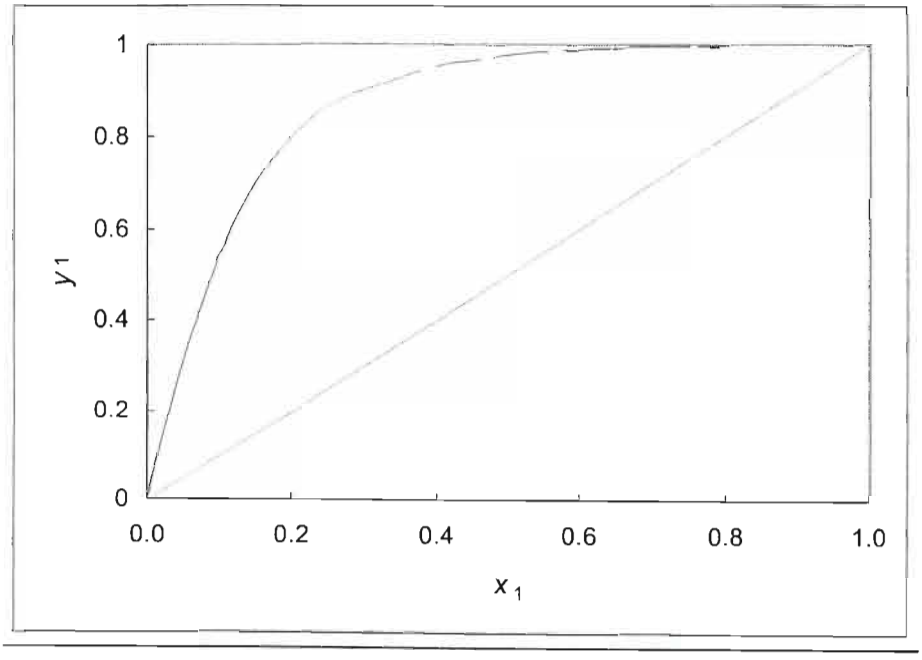

Figure 7-50: x_1-y_1 data for n-dodecane (1) + 1-octadecene (2) at 3.00 kPa fitted with P-R EOS: - - -, P-R EOS.

Table 7-13 Regressed parameters for the P-R EOS with Twu and Coon mixing rules for n-dodecane (1) + 1-octadecene (2) at 3.00 kPa

Model Parameters	n-dodecane (1) + 1-octadecene (2)
	P = 3.00 kPa
NRTL parameters	
α_{12}	-0.11
Δg_{12} / J.mol^{-1}	-20307
Δg_{21} / J.mol^{-1}	-7590
EOS parameters	
l_{ij}	-0.030
k_{ij}	-0.062
$\lvert\Delta T\rvert_{average}$ / K	2.70

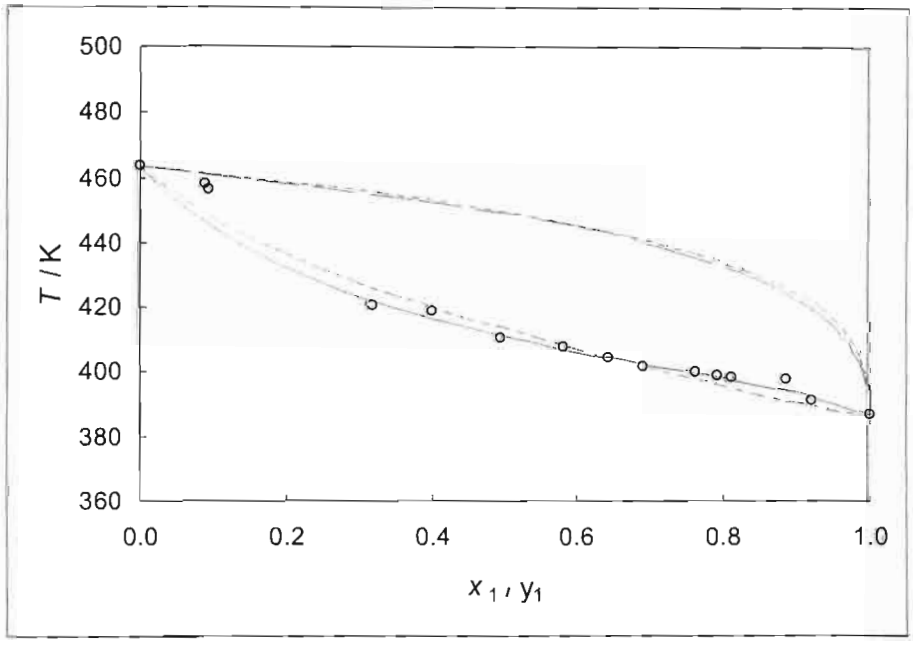

Figure 7-51: T-x_1-y_1 data for n-dodecane (1) + 1-octadecene (2) at 3.00 kPa fitted with G^E models: o, Experimental values; - - -, Wilson; · · ·, NRTL.

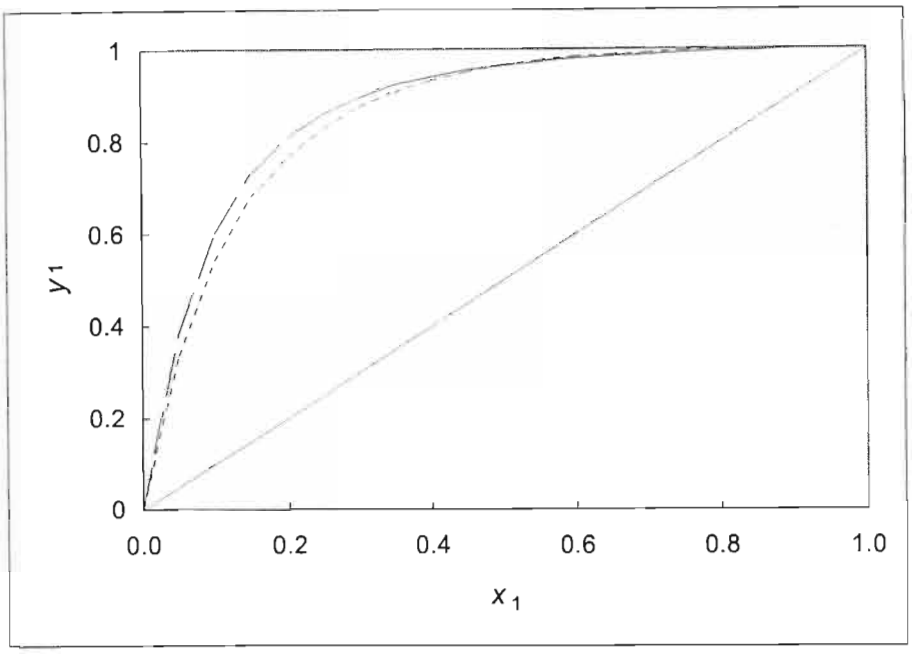

Figure 7-52: x_1-y_1 data for n-dodecane (1) + 1-octadecene (2) at 3.00 kPa fitted with G^E models: - - -, Wilson; · · ·, NRTL.

Table 7-14 Regressed parameters for the experimental VLE data for n-dodecane (1) + 1-octadecene (2) at 3.00 kPa

System [NRTL]	Δg_{12} / J.mol^{-1}	Δg_{21} / J.mol^{-1}	α_{12}	$\lvert\Delta T\rvert_{ave.}$ / K
n-dodecane (1) + 1-octadecene (2)	-34646	-153.9	0.298	2.27
System [Wilson]	$\Delta\lambda_{12}$ / J.mol-1	$\Delta\lambda_{21}$ / J.mol-1		$\lvert\Delta T\rvert_{ave.}$ / K
n-dodecane (1) + 1-octadecene (2)	-6100	6468		2.92

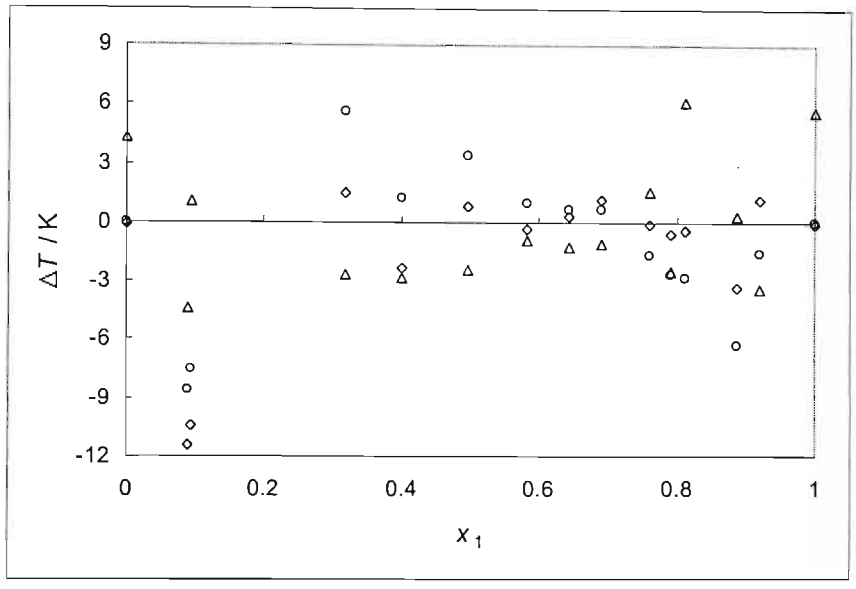

Figure 7-53: Deviation (ΔT) for the regressed data and measured data for n-dodecane (1) + 1-octadecene (2) at 3.00 kPa: Δ, P-R EOS; o, Wilson and ◊, NRTL.

From the regressed data it can be seen that the NRTL G^E model provides the best fit for the T-x_1 data. From the results obtained for the isobar at 26.66 kPa it is safe to assume that the predicted vapour phase compositions are reasonably accurate. Cause for concern, however, is the large scatter in the measured temperatures (almost three times larger than in previous measurements) when compared to the fitted models. As the models were able to fit this same binary system at a different pressure, it is unlikely that the problem lies with the models. The only suggestion is that the $\left(\frac{\partial T}{\partial P}\right)_{x_1}$ values at this lower pressure are much higher than at the higher pressure and thus the temperature could exhibit greater scatter.

The data for the high temperature system d,l-menthol (1) + l-isomenthol (2) at 448.15 K are recorded in Chapter Six. It was possible to measure vapour composition values for this data and thus the x_i-y_i-P data are presented.

The data were regressed by the combined method using G^E models with a Virial EOS as explained in Chapter Three. The regressed data are presented as follows:

- P-x_1-y_1 data for d,l-menthol (1) + l-isomenthol (2) at 448.15 K fitted with G^E models [Figure 7-54],
- x_1-y_1 data for d,l-menthol (1) + l-isomenthol (2) at 448.15 K fitted with G^E models [Figure 7-55],
- Deviation (ΔP) for the regressed data and measured data for d,l-menthol (1) + l-isomenthol (2) at 448.15 K [Figure 7-56],
- Deviation (Δy_1) for the regressed data and measured data for d,l-menthol (1) + l-isomenthol (2) at 448.15 K [Figure 7-57], and,
- Regressed parameters for the G^E models [Table 7-15].

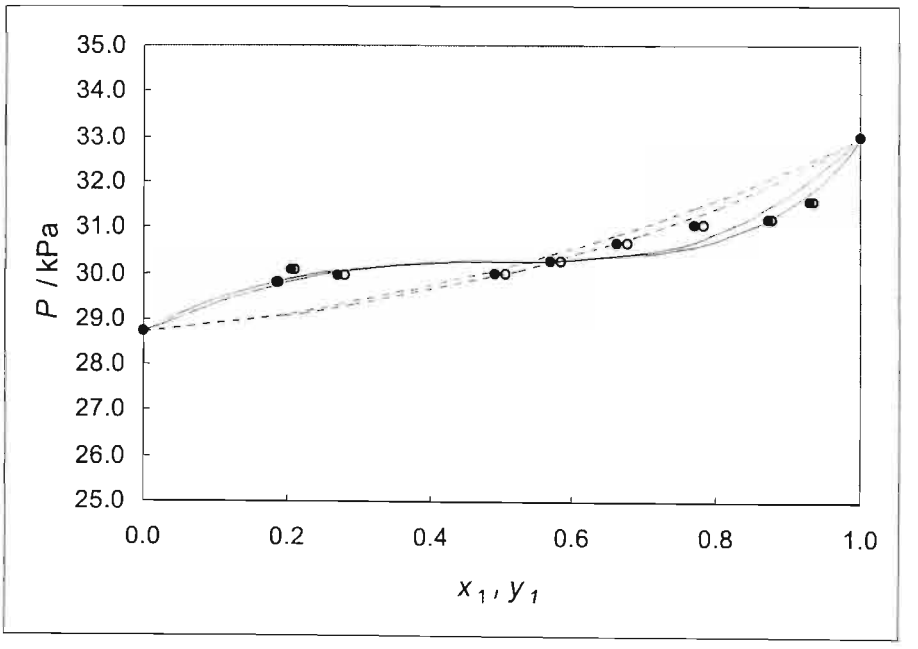

Figure 7-54: P-x_1-y_1 data for d,l-menthol (1) + l-isomenthol (2) at 448.15 K fitted with G^E models: •, Experimental x_1 values; o, Experimental y_1 values; - - -, Wilson; · · ·, NRTL.

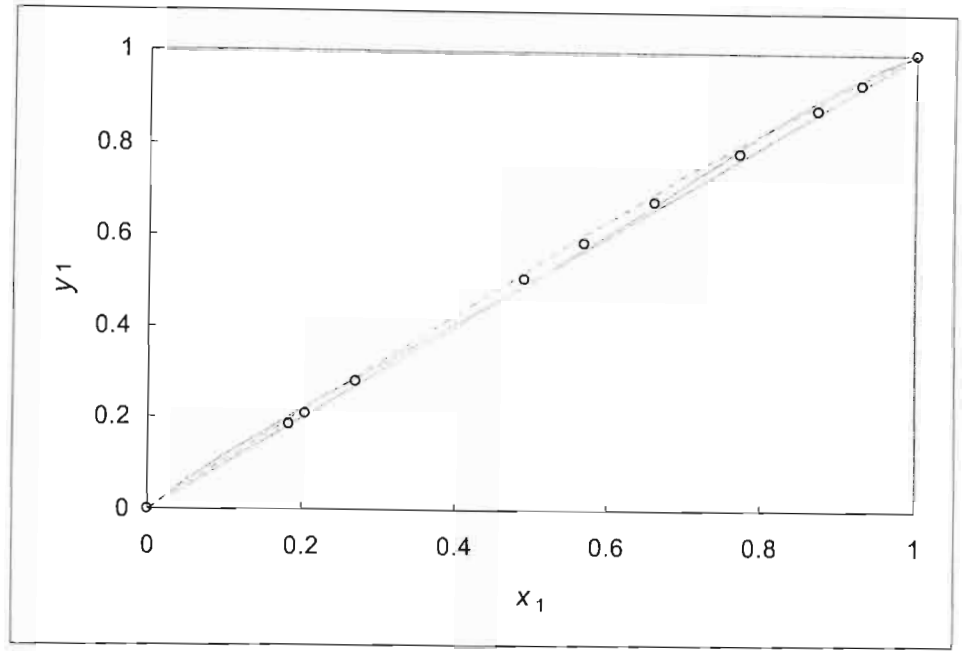

Figure 7-55: x_1-y_1 data for d,l-menthol (1) + l-isomenthol (2) at 448.15 K fitted with G^E models: o, Experimental values; - - -, Wilson; · · ·, NRTL.

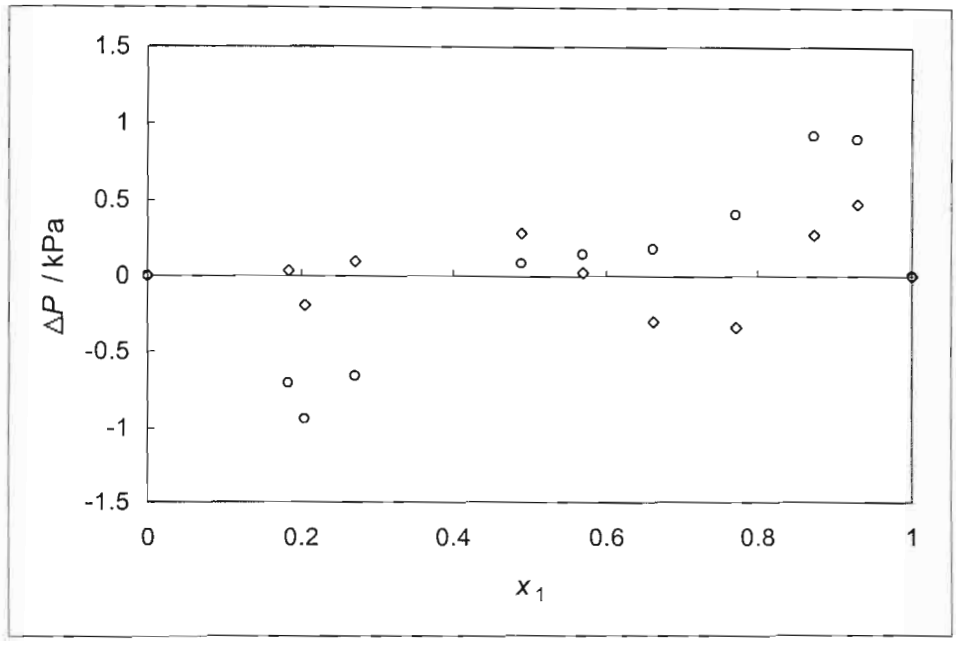

Figure 7-56: Deviation (ΔT) for the regressed data and measured data for d,l-menthol (1) + l-isomenthol (2) at 448.15 K: o, Wilson and ◊, NRTL.

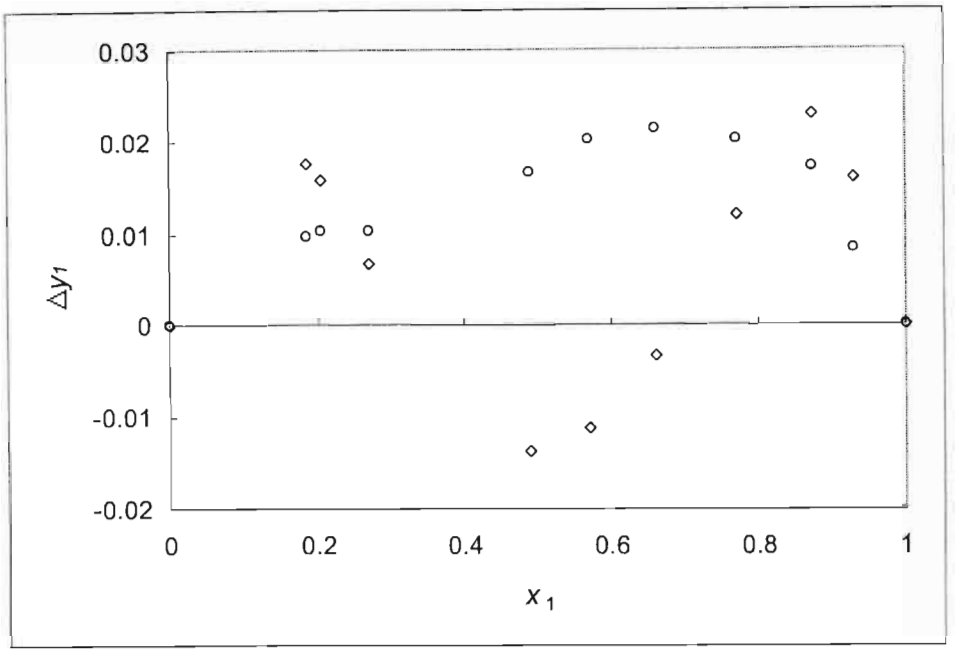

Figure 7-57: Deviation (Δy_1) for the regressed data and measured data for d,l-menthol (1) + l-isomenthol (2) at 448.15 K: o, Wilson and ◊, NRTL.

Table 7-15 Regressed parameters for the experimental VLE data for d,l-menthol (1) + l-isomenthol (2) at 448.15 K

System [NRTL]	Δg_{12} / J.mol^{-1}	Δg_{21} / J.mol^{-1}	α_{12}	$\lvert\Delta P\rvert_{ave.}$ / kPa	$\lvert\Delta y_1\rvert_{ave.}$
n-dodecane (1) + 1-octadecene (2)	-28631	21403	0.041	0.20	0.012
System [Wilson]	$\Delta\lambda_{12}$ / J.mol-1	$\Delta\lambda_{21}$ / J.mol-1		$\lvert\Delta P\rvert_{ave.}$ / kPa	$\lvert\Delta y_1\rvert_{ave.}$
n-dodecane (1) + 1-octadecene (2)	-1651	1651		0.49	0.013

From the table it is evident that the NRTL model provides the best fit for the data. This system, however, is a good example of the sort of problems that data scatter can cause. As the system is comprised of two isomers, it is expected that the system should be almost ideal in behaviour and exhibit a very small relative volatility. It is quite possible that the data are *accurate* within a certain degree of error. The problem, however, is that this system exhibits a very small pressure range. The system pressure range and degree of error are of the same magnitude. Furthermore, the *precision* of the measurements in the previous systems have been shown to have some scatter,

which is also of the same degree of magnitude of the system pressure range. Thus, in all likelihood, the shape of the measured VLE curve is completely wrong. This assumption is given further weight by comparing the different shapes of the model fits. Although the NRTL provides a better fit, the model exhibits a deflection in the middle of the x_i-y_i plot, which is not correct. From this result it is concluded that the equipment is not precise enough to measure data over such a small pressure range for systems with such a small relative volatility.

7.4.3 Problems Associated with the Equipment

Although VLE measurements were possible, there were two persistent problems which could not be remedied:

i.) Temperature fluctuations, and,

ii.) Vapour phase composition measurement problems.

Temperature Fluctuations

From the outset the equipment displayed a tendency towards temperature fluctuations. That is, at equilibrium, the temperature was not steady. (It is important to note that the fluctuations were much larger than the stated 0.75% accuracy of the device.) Although the temperature fluctuated, the average temperature taken over a time period at equilibrium was relatively steady. The temperature fluctuations increase as the equilibrium temperature increases:

- At $T < 373.15$ K, $\Delta T \approx 0.2$ K (where $T = T \pm \Delta T$),
- At $373.15 \text{ K} \leq T < 473.15$ K, $\Delta T \approx$ up to 1.0 K, and,
- At $T \geq 473.15$ K, $\Delta T \approx$ up to 2.5 K.

The fluctuations are regular and sinusoidal in shape. This phenomenon decreases the accuracy of the measurements. Several possible causes and solutions were investigated:

Possible Cause	Possible Solution
• Volume of material in the reboiler is insufficient – the reboiler is not operating properly.	• Several charge volumes were tried ranging from 90 ml to 200ml – their effect was negligible.
• The cool condensed vapour return is disrupting reboiler operation.	• The vapour return line was insulated and heated – the effect was positive but very small.
• Too much heat is being lost from the system.	• The entire equipment was insulated with thick cladding. There was a marked improvement but the fluctuation was still evident.

As the problem still persists it is assumed that the large bulk of the equipment (approximately 50 kg of Stainless Steel[11]) is causing the temperature fluctuation. The only solution is to redesign the equipment with much thinner walls and thus decrease the maximum pressure capacity.

Vapour Phase Composition Measurement Problems

The vapour phase composition determination was very accurate for the low temperature test system (cyclohexane (1) + ethanol (2)), however, for the high temperature test system (n-dodecane (1) + 1-octadecene (2)) it was impossible to measure accurate vapour compositions. The longer the equipment was left to equilibrate, the more the vapour composition tended to be equivalent to the liquid phase composition ($y_1 \rightarrow x_1$) despite the high relative volatility of the test system. The problem was not evident for the d,l-menthol (1) + l-isomenthol (2) which has a very low relative volatility ($\alpha_{12} < 1.15$) and which was measured over a shorter time span. Possible causes and solutions are listed below:

[11] This large mass of metal has a large heat capacity (mC_p); it requires a large amount of energy to heat it up and a large amount of energy is given off when it cools down. The heat capacity of the equipment is most probably more than 500 times larger than that of the contents and thus if it is too hot or too cold it has a large effect on the operation of the still. This large heat capacity is the likely cause of the large T fluctuations observed with large temporal delay.

Possible Cause	Possible Solution
• Volume of material in the reboiler is insufficient – the reboiler is not operating properly.	• Several charge volumes were tried ranging from 90 ml to 200ml – their effect was negligible.
• The reboiler charge is boiling material *up* the vapour return line.	• A non-return valve was added to the juncture of the reboiler and the vapour return line. The non-return valve had no effect on the problem.
• The superheat from the Cottrell tube is being conducted into the base of the equilibrium chamber. This heats the metal above the equilibrium temperature and thus the liquid returning is being flashed off (Figure 7-58).	• A vent was drilled through the cladding and cool compressed air was used as a cooling fluid to try and cool the base of the equilibrium chamber (Figure 7-58). The effect was negligible.
• The insulation is retaining too much heat even with the cooling vent.	• Two VLE points were measured for the acetone (1) + methanol (2) system. The points were very accurate when compared to the literature. However, this system is at a low temperature and was measured in a short space of time.

As the problem persists it is assumed that the base of the equilibrium chamber is heated by conduction not just from the superheat of the fluid travelling up the Cottrell tube but also from excess heat from the external reboiler heater. The cooling effect of the compressed air is not sufficient to cool the base and thus returning liquid is being flashed and contaminating the vapour phase composition. The longer the equipment is used without a break the worse the heat build up is. For the acetone (1) + methanol (2) system and the cyclohexane (1) + ethanol (2) test system the heat build up was minimal as these systems were measured over a short space of time and at low temperatures and, thus, the vapour phase composition was not affected. For high-boiling mixtures the still was run with a shut-down between each point. This, however, did not solve the problem as the base of the equilibrium chamber heats up too much before equilibrium is reached and thus the problem mentioned above persists.

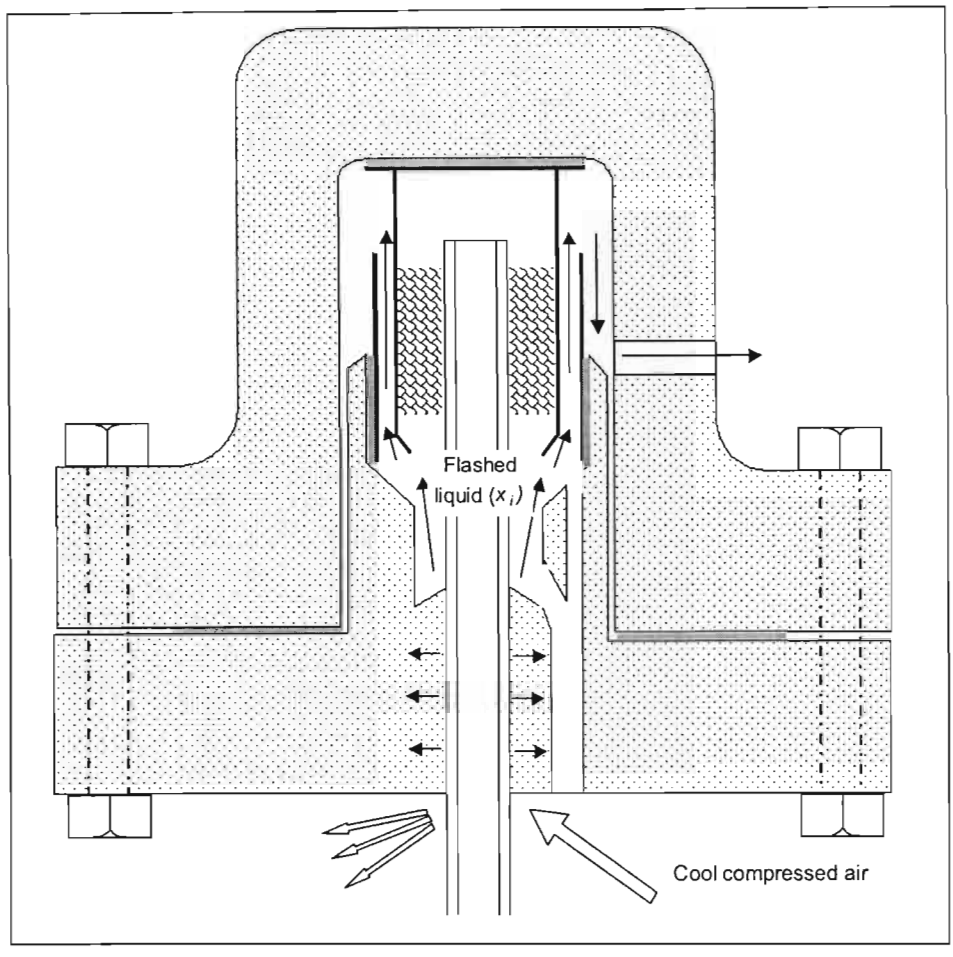

Figure 7-58: Superheating of the equilibrium chamber.

The smoothness of the measured VLE data is poor for this equipment when compared to the very smooth VLE curves determined with the apparatus of Rarey and Gmehling (1993). In general, the results show that the equipment can measure VLE within a certain degree of accuracy. However, the precision of the data is not sufficient to be able to use measured VLE data to determine other thermodynamic quantities as was done with the data measured with the equipment of Rarey and Gmehling (1993) and the modified equipment of Kolbe and Gmehling (1985).

CHAPTER

EIGHT

CONCLUSIONS

8.1 INTRODUCTION

VLE measurements were performed on three different pieces of equipment. The measurements ranged from 1.00 kPa to 20.8 MPa and from 308.33 K to 583.90 K. In total nine vapour pressures and fourteen sets of VLE data were measured. Eleven of the fourteen sets of VLE data represented previously unmeasured data. All of the VLE data was modelled using thermodynamic relationships discussed in Chapter Five.

8.2 EQUIPMENT OF RAREY AND GMEHLING (1993)

P-x_1 data were measured for the four binary VLE systems, hexane (1) + N-methylformamide (2), benzene (1) + N-methylformamide (2), chlorobenzene (1) + N-methylformamide (2) and acetonitrile (1) + N-methylformamide (2), at 363.15 K. All four VLE systems represent new data. The systems were modelled very successfully and the best fit was with the NRTL equation using the virial equation with the Hayden and O'Connell correlation to describe the vapour phase. The NRTL model provides the best fit for the data within 1.5 kPa (for pressure) for systems N-Methylformamide + benzene, + chlorobenzene and + acetonitrile as shown in Chapter Seven. The model does not fit the N-Methylformamide + hexane system well, however, out of the models assessed it gave the best fit. The N-Methylformamide + hexane system forms two liquid phases as is indicated in Figure 7-1.

Most significantly, more than forty VLE data points were measured per system. Furthermore, more than half of these points were in the dilute regions ($x_1 < 0.1$ and $x_1 > 0.9$). This concentration of data in these regions provides a very accurate description of phase behaviour in the dilute regions and is essential for the design of efficient separation processes. From the VLE

data γ^{∞} values were calculated for all four systems, both from the fitted G^E models (Wilson and NRTL equations) and from the generally more reliable method of Maher and Smith (1979). The different methods give better comparisons for the γ_1^{∞} values and only give comparable values for N-methylformamide + benzene and N-methylformamide + chlorobenzene for the γ_2^{∞} values.

This work was published in the *Journal of Chemical Engineering Data* (Harris et al. (2003a)) and presented at the ICCT conference in Rostock, Germany (Harris et al. (2002b)).

8.3 EQUIPMENT OF KOLBE AND GMEHLING (1985)

P-x_1 data were measured for the two binary VLE systems, CO_2 (1) + Naphthalene (2) at T = 372.45 K, 403.85 K and 430.65 K and CO_2 (1) + Benzoic acid (2) at T = 403.28 K, 432.62 K and 458.37 K. Experimental dew points were measured at T = 372.45 K, 403.85 K and 430.65 K for the system CO_2 (1) + Naphthalene (2). Apart from CO_2 (1) + Naphthalene (2) at T = 372.45 K, these isotherms measured are new data and improve the understanding of these systems. The systems were modelled and fitted with the Stryjek-Vera modification of the P-R EOS using Huron-Vidal mixing rules and Wong-Sandler mixing rules incorporating the NRTL equation.

The data are especially useful for determining thermodynamic properties as:

- The data are smooth and well-fitted by the EOS used for the data regression.
- The data covers a large range of pressures from $P < 0.05$ MPa to $P > 20$ MPa. When compared to the literature for naphthalene + CO_2 at 373.15 K (Barrick et al. (1987) and Jan and Tsai (1991)) it is seen that our data have double the pressure range of the literature data.
- Three isotherms were measured for each binary system. This makes it possible to determine the temperature-dependence of properties such as the mixing rule parameters and the excess thermodynamic properties.

From the VLE data, Henry's constants were determined and H^E, G^E and TS^E values were predicted for CO_2 (1) + naphthalene (2) at 372.45 K, 403.85 K and 430.65 K and for CO_2 (1) + benzoic acid (2) at 403.28 K, 432.62 K and 458.37 K.

This work is in the process of being published (Harris et al. (2003d)) and was presented at Venice, Italy (Harris et al. (2002d)).

8.4 EQUIPMENT OF HARRIS ET AL. (2003B)

Vapour pressures and VLE systems were measured on the new equipment of Harris et al. (2003b). Vapour pressures were measured for n-heptane, n-decane, n-dodecane, n-hexadecane, 1-octadecene, 1-hexadecanol, d,l-menthol and l-isomenthol at low pressures and acetone at high pressures. These vapour pressure measurements were used as test systems and ranged from 1.00 kPa to 1 000 kPa and from 308.33 K to 583.90 K. In conclusion, although most of the vapour pressure systems show good agreement with literature, it is important to note that the equilibrium temperature at high temperatures was not stable and fluctuated in a sinusoidal pattern.

Two isobaric VLE test systems were measured. The measured T-x_1-y_1 data for the test system cyclohexane (1) + ethanol (2) at 40 kPa compares very well with that of Joseph et al. (2001) and from this it can be seen that the equipment measures highly non-ideal low-pressure, low-temperature systems well.

The measured T-x_1 data for the test system n-dodecane (1) + 1-octadecene (2) at 26.66 kPa was compared to the literature data of Jordan and van Winkle (1951). The measured temperatures do not compare very well with the literature. The measured vapour pressures for the two components showed marked disparity with literature while the VLE data shows a disparity of up to 7 K with the literature. From these measurements the following could be concluded:

- that the equipment could not measure the vapour phase accurately for systems with a relative volatility greater than 1.15 at temperatures exceeding 400 K.
- Accurate temperature measurement is difficult at high temperatures as the measured temperature fluctuates.
- The T-x_1 data are modelled and the vapour phase compositions are predicted; these predictions agree well with the literature values.

P-x_1-y_1 data for the system d,l-menthol (1) + l-isomenthol (2) were measured at $T = 448.15$ K. This is new data. T-x_1 data were measured for the system n-dodecane (1) + 1-octadecene (2) at $P = 3.0$ kPa. It was not possible to accurately measure the vapour phase compositions. Similar problems to those detailed above were experienced and thus it is possible to conclude that these problems are not system specific.

Some of this work was presented at ICCT Rostock, Germany (Harris et al. (2002c)), Pisa, Italy (Harris et al. (2003c)) and at Natmeet Sun City, South Africa (Harris et al. (2003b)).

Initially, the equipment was designed to measure data ranging from zero to 35 MPa and from 300 K to 650 K. The DRVS design was used as it allows for rapid equilibration of the system and, as it disengages the liquid and vapour phases, easy phase composition measurement. Due to the high pressure rating the equipment was made from 316 SS. Large billets were used to machine the thick-walled reboiler and equilibrium chamber. The still weighs approximately 50 kg. As discussed in Chapter Seven, the large weight of the still causes the temperature to fluctuate and makes the determination of vapour phase composition for most systems at temperatures greater than 400 K impossible.

The conclusion of this work is that a DRVS with very large pressure and temperature ranges such as those aimed for is impractical. Recommendations are given in Chapter Nine for a suitable DRVS with practical applications. From the work performed the following points can be concluded:

- A DRVS type still is not practical for high temperature – high pressure measurements as the mass of the still required to make it safe has a very large heat capacity. This makes accurate and precise temperature measurements all but impossible. In its present form the still could be used for measurements such as those conducted on the apparatus of Rarey and Gmehling (1993) in this work.
- Chemicals, which have high vapour pressures at low temperatures, are usually gases at ambient temperatures (e.g.: CO_2). These chemicals cannot be used in the DRVS type still as measurement of the vapour phase composition requires complete condensation of the stream (Chapter Three).
- A stainless steel DRSV type still would best be suited to measurements of systems at pressures up to 3 MPa.

- The still worked extremely well for chemicals that temperature. The insulation and heating of the still made possible difficult task of measuring vapour pressures and VLE for chemicals which are solid at room temperature. Unlike the glass stills, solidification of the still contents or heating of the still to maintain the chemicals as liquids did not damage the stainless steel still. It must, however, be noted that, while the stainless-steel still can be used to measure these chemicals with greater ease than the glass still, the equipment of Kolbe and Gmehling (1985), with modifications, was also used to measure such chemicals (that are solid at ambient temperature) and exhibited no problems with these measurements.
- The interior insulation of the equilibrium chamber with a graphite composite was a useful innovation that should be incorporated in a lower-pressure version of the still.

CHAPTER

NINE

RECOMENDATIONS

9.1 INTRODUCTION

Chapters Seven and Eight discuss some of the problems associated with the still. In Chapter Seven some of the solutions and possible solutions, which, were tried, are discussed. However, in Chapter Eight it is concluded that the still is not suitable to high-temperature measurements in its present form. Below are some recommendations for major modifications, which would improve the operation of the equipment.

9.2 REBOILER AND EQUILIBRIUM CHAMBER MODIFICATIONS

As is mentioned in Chapter Seven and eight it is the large mass of steel used in the construction of the reboiler and equilibrium chamber which cause temperature fluctuations and the errors in vapour phase composition measurements. As mentioned previously it is reasoned that that the metal heats up to temperatures greater than the equilibrium temperature. This causes erratic behaviour in the equilibrium chamber and prevents accurate measurement of the equilibrium temperature and vapour phase composition. The most obvious solution is to reduce the metal mass by re-designing these two components with thinner walls. The flanges can be dispensed with by incorporating two halves that screw into each other. With these modifications the pressure rating would be drastically reduced. However, a piece of equipment, which could handle high temperatures and moderate pressures and could produce rapid equilibration, would be very useful. As a guideline, the equipment could be constructed from 316 SS with a wall thickness of 5 mm. By having two pieces that screw into each other (Figure 9-1) it is possible to greatly reduce the amount of metal needed as the flanges constitute a large part of the bulk of the equipment. Thus one is able to reduce the heat capacity of the equipment as a whole and this should make the heating up and cooling down of the equipment less problematic.

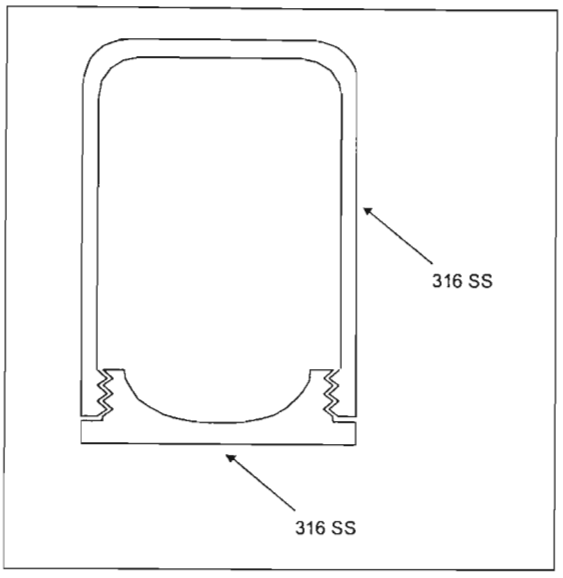

Figure 9-1: Suggested modification to eradicate the flanges in the reboiler and equilibrium chamber.

Another modification that would limit the conduction of superheat from the Cottrell tube to the base of the equilibrium chamber is to bring the inlet of the Cottrell pump in through the side of the equilibrium chamber as in the equipment of Wiśniewska et al (1993) which is discussed in Chapter Two.

A useful modification would be to incorporate a view glass (possibly a sapphire view glass) in the equilibrium chamber. This, however, provides added complications such as:

- it makes sealing of the chamber difficult;
- it adds bulk to the chamber as the glass needs to be relatively thick, and,
- it creates structural complications.

None of these modifications were undertaken in this work as equipment construction is performed in-house and requires a large amount of time.

9.3 SAMPLING

For high-temperature measurements the sampling equipment and technique discussed in Chapter Three is used. This requires the use of a septum. At high temperatures and with repeated sampling the septum breaks down which affects the control of the equipment and the reproducibility of the samples. It is recommended that the high-pressure sampling device be used as the default for all measurements.

As mentioned above, the addition of a view glass to the equilibrium chamber is difficult. An easier option is to include glass inserts in the vapour and liquid return lines. These inserts would make it possible to approximate the flow rates in these lines and monitor any changes in the fluid's appearance during experimentation.

9.4 PRESSURE CONTROL

Presently, twenty-five litres of ballast are used to maintain a stable pressure for the low-pressure measurements. For the high-pressure measurements no ballast was used and a nitrogen cylinder was connected directly to the still. It is recommended that a stainless-steel ballast tank be constructed for the high-pressure measurements. This will need to be outsourced, as such construction needs to be x-rayed for safety reasons.

CHAPTER

TEN

PUBLICATIONS AND CONFERENCE PROCEEDINGS RESULTING FROM THIS WORK

The work detailed in this thesis resulted in several publications and conference proceedings. These are listed below:

Harris, R.A., Wittig, R., Letcher, T.M., Ramjugernath, D., and Raal, J.D., **2002b**, "Vapour-Liquid Equilibria for Four Binary Systems at 363.15 K: N-Methylformamide + a) Hexane, b) Benzene, c) Chlorobenzene and d) Acetonitrile", *17th IUPAC Conference*, Rostock, Germany.

Harris, R.A., Ramjugernath, D., Raal, J.D. and Letcher, T.M., **2002c**, "Design and Construction of Equipment to determine Vapour - Liquid Equilibrium at Extreme Conditions", *17th IUPAC Conference*, Rostock, Germany.

Harris, R.A., Wilken, M., Fischer, K., Gmehling, J., Letcher, T.M., Raal, J.D. and Ramjugernath, D., **2002d**, "High Pressure Vle Measurements Of Naphthalene + CO_2 And Benzoic Acid + CO_2 Binary Systems Using A Static Synthetic Apparatus", *ICheaP 5 – The Fifth Italian Conferrence on Chemical and Process Engineering*, Venice, Italy.

Harris, R.A., Wittig, R., Letcher, T.M., Ramjugernath, D., and Raal, J.D., **2003a**, "Vapour-Liquid Equilibria for Four Binary Systems at 363.15 K: N-Methylformamide + a) Hexane, b) Benzene, c) Chlorobenzene and d) Acetonitrile", *Journal of Chemical Engineering Data*, **48**, 341-343.

Harris, R.A., Ramjugernath, D., Raal, J.D. and Letcher, T.M., **2003b**, "Robust Equipment for the Measurement of Vapour-Liquid Equilibrium at High Temperatures and Pressures", *SAIChE 2003 – South African Chemical Engineering Congress*, Sun City.

Harris, R.A., Ramjugernath, D., Raal, J.D. and Letcher, T.M., **2003c**, "Robust Equipment for the Measurement of Vapour-Liquid Equilibrium at High Temperatures and Pressures", *ICheaP 6 – The Sixth Italian Conferrence on Chemical and Process Engineering*, Pisa, Italy.

Harris, R.A., Wilken, M., Fischer, K., Gmehling, J., Letcher, T.M., Raal, J.D. and Ramjugernath, D., **2003d**, "High Pressure Vle Measurements Of Naphthalene + CO_2 And Benzoic Acid + CO_2 Binary Systems Using A Static Synthetic Apparatus", submitted to *Journal of Chemical Engineering Data, 2003*.

McKnight, T.J., Harris, R.A., Ramjugernath, D., Raal, J.D. and M Starzak, **2003a**, "Molecular simulation and experimental measurement: A comparison", *ICheaP 6 – The Sixth Italian Conferrence on Chemical and Process Engineering*, Pisa, Italy.

McKnight, T.J., Harris, R.A., Ramjugernath, D., Raal, J.D. and M Starzak, **2003b**, "Comparing The Experimental And Simulation Approaches For The Prediction Of Vapour-Liquid Phase Equilibrium", *SAIChE 2003 – South African Chemical Engineering Congress*, Sun City.

CHAPTER

ELEVEN

REFERENCES

Abbott, M., **1986**, "Low-Pressure Phase Equilibria: Measurement of VLE", *Fluid Phase Equilibria*, **29**, 193-207.

Adams, W.R., Zollweg, J.A.., Street, W. and Rizvi, S.S.H., **1988**, "New Apparatus for Measurement of Supercritical Fluid-Liquid Equilibria.", *AIChE J.*, **34**, 1387-1391.

Anderson, T.F. and Prausnitz, J.M., **1978**, "Application of the UNIQUAC Equation to Calculation of Muticomponent Phase Equilibria. 1: Vapor-Liquid Equilibria; 2: Liquid-Liquid Equilibria", *Industrial and Engineering Chemistry. Process Design and Development*, **17**, 552-567.

Barrick, M.W., McRay Anderson, J., Robinson, R.L., Jr., **1987**, "Solubilities of carbon dioxide in naphthalene, phenanthrene, and pyrene at pressures to 10.6 MPa and temperatures from 373 to 433 K.", *Journal of Chemical Engineering Data*, **32**, 372-374.

Behrens, P.K. and Sandler, S.I., **1983**, "Vapor-Liquid Equilibria for the Carbon Dioxide-1-Butene System at 37.7 and 45.0 °C.", *Journal of Chemical Engineering Data*, **28**, 52-56.

Brown, I., **1952**, "Liquid-Vapour Equilibria. III. The Systems Benzene–n-Heptane, n-Hexane – Chlorobenzene and Cyclohexane–Nitrobenzene", *Australian Journal of Scientific Research*, **5**, 530-540.

DECHEMA Database, **1999**, "Pure Component Properties and Vapour-Liquid Data", Compact Disc Version, Frankfurt.

D'Souza, R., Patrick, J.R. and Teja, A.S., **1988**, "High Pressure Phase Equilibria in the Carbon Dioxide – n-Hexadecane and Carbon Dioxide Water Systems.", *The Canadian Journal of Chemical Engineering*, **66**, 319-323.

D'Souza, R. and Teja, A.S., **1988**, "High Pressure Phase Equilibria in the System Glucose + Fructose + Water + Ethanol + Carbon Dioxide", *Fluid Phase Equilibria*, **39**, 211-224.

Ellis, S.R.M. and Jonah, D.A., **1962**, "Prediction of activity coefficients at infinite dilution", *Chemical Engineering Science*, **17**, 971-976.

Fischer, K. and Gmehling, J., **1994**, "P-x and γ^{∞} Data for the Different Binary Butanol-Water Systems at 50 °C.", *Journal of Chemical Engineering Data*, **39**, 309-315.

Fischer, K. and Gmehling, J., **1996**, "Vapor-liquid equilibria, activity coefficients at infinite dilution and heats of mixing for mixtures of N-methyl pyrrolidone-2 with C5 or C6 hydrocarbons and for hydrocarbon mixtures", *Fluid Phase Equilibria*, **119**, 113-130.

Fischer, K. and Wilken, M., **2001**, "Experimental determination of oxygen and nitrogen solubility in organic solvents up to 10 MPa at temperatures between 298 K and 398 K", *J. Chem. Thermodynamics*, **33**, 1285-1308.

Fontalba, F., Richon, D. and Renon, H., **1984**, "Simultaneous determination of vapor-liquid equilibria and saturated densities up to 45 MPa and 433 K.", *Rev. Sc. Instrum.*, **55**, 944-951.

Fontana, M.G., **1986**, "Corrosion Engineering: 3rd Edition", McGraw-Hill, Inc.

Gaube, **1988**, *Private communication between Gaube and* Rarey, As reported by Rarey and Gmehling (1993).

Gautreaux, M.F. and Coates, J., **1955**, "Activity Coefficients at Infinite Dilution", *American Institute of Chemical Engineers. Journal*, **1**, 496-500.

Gess, M.A., Danner, R.P. and Nagvekar, M., **1991**, "Thermodynamic Analysis of Vapor-Liquid Equilibria: Recommended Models and a Standard Data Base", Design Institute for Physical Property Data, American Institute of Chemical Engineers.

Gibbs, R.E. and Van Ness, H.C., **1972,** "Vapor-Liquid Equilibria from Total-Pressure Measurements. A New Apparatus", *Ind. Eng. Chem. Fundam.*, **11**, 3, 410-413.

Gillespie, D.T.C., **1946**, "Vapor-Liquid Equilibrium Still for Miscible Liquids", *Industrial and Engineering Chemistry, Analytical Edition*, **18**, 575-577.

Hála, E., Pick, J., Fried, V. and Vilím, O., **1967**, *Vapour-Liquid Equilibrium*, 2nd ed., Pergamon Press, Oxford.

Hanks, R.W., Gupta, A.C., and Christensen, J.J., **1971**, "Calculation of Isothermal Vapor-Liquid Equilibrium Data for Binary Mixtures from Heats of Mixing", *Ind. Eng. Chem. Fundam.* **10**, 504-509.

Harris, R.A., **2001a**, "Monoethanolamine: Suitability as an Extractive Solvent", *M.Sc. Thesis*, University of Natal, Durban.

Harris, R.A., **2001b**, Personal correspondence to Prof. D. Ramjugernath, *Contract work for Datachem - Confidential.*

Harris, R.A., Ramjugernath, D., Raal, J.D., and Letcher, T.M., **2002a**, "Monoethanolamine as an extractive solvent for the n-hexane + benzene, cyclohexane + ethanol and acetone + methanol binary systems", *Journal of Chemical Engineering Data*, **47**, 781-787.

Harris, R.A., Wittig, R., Letcher, T.M., Ramjugernath, D., and Raal, J.D., **2002b**, "Vapour-Liquid Equilibria for Four Binary Systems at 363.15 K: N-Methylformamide + a) Hexane, b) Benzene, c) Chlorobenzene and d) Acetonitrile", *17th IUPAC Conference*, Rostock, Germany.

Harris, R.A., Ramjugernath, D., Raal, J.D. and Letcher, T.M., **2002c**, "Design and Construction of Equipment to determine Vapour - Liquid Equilibrium at Extreme Conditions", *17th IUPAC Conference*, Rostock, Germany.

Harris, R.A., Wilken, M., Fischer, K., Gmehling, J., Letcher, T.M., Raal, J.D. and Ramjugernath, D., **2002d**, "High Pressure Vle Measurements Of Naphthalene + Co_2 And Benzoic Acid + Co_2 Binary Systems Using A Static Synthetic Apparatus", *ICheaP 5 – The Fifth Italian Conferrence on Chemical and Process Engineering*, Venice, Italy.

Harris, R.A., Wittig, R., Letcher, T.M., Ramjugernath, D., and Raal, J.D., **2003a**, "Vapour-Liquid Equilibria for Four Binary Systems at 363.15 K: N-Methylformamide + a) Hexane, b) Benzene, c) Chlorobenzene and d) Acetonitrile", *Journal of Chemical Engineering Data*, **48**, 341-343.

Harris, R.A., Ramjugernath, D., Raal, J.D. and Letcher, T.M., **2003b**, "Robust Equipment for the Measurement of Vapour-Liquid Equilibrium at High Temperatures and Pressures", *SAIChE 2003 – South African Chemical Engineering Congress*, Sun City.

Harris, R.A., Ramjugernath, D., Raal, J.D. and Letcher, T.M., **2003c**, "Robust Equipment for the Measurement of Vapour-Liquid Equilibrium at High Temperatures and Pressures", *ICheaP 6 – The Sixth Italian Conferrence on Chemical and Process Engineering*, Pisa, Italy.

Harris, R.A., Wilken, M., Fischer, K., Gmehling, J., Letcher, T.M., Raal, J.D. and Ramjugernath, D., **2003d**, "High Pressure Vle Measurements Of Naphthalene + CO_2 And Benzoic Acid + CO_2 Binary Systems Using A Static Synthetic Apparatus", submitted to *Journal of Chemical Engineering Data, 2003.*

Hartwick, R.P. and Howat, C.S., **1995**, "Infinite Dilution Activity Coefficients of Acetone in Water. A New Experimental Method and Verification", *Journal of Chemical and Engineering Data*, **40**, 738-745.

Hayden, J.G. and O'Connel, J.P., **1975**, "A Generalized Method for Predicting Second Virial Coefficients", *Industrial and Engineering Chemistry. Process Design and Development*, **14**, 209-216.

Heertjies, P.M., **1960**, "Determination of Vapour-Liquid Equilibria of Binary Mixtures", *Chemical and Process Engineering*, **41**, 385-386.

Hiaki, T., Kazutaka, Y., Miyazawa, H. and Kojima, K., **1994**, "Computer-aided Measurement of Vapor-Liquid Equilibrium in a Still", *The Canadian Journal of Chemical Engineering*, **72**, 142-147.

Hills, P., **1999**, Personal correspondence to M. Joseph, *e-mail correspondence.*

Hsu, J.J-C., Nagarajan, N. and Robinson, J.R.L., **1985**, "Equilibrium Phase Compositions, Phase Densities and Interfacial Tensions for CO_2 + Hydrocarbon Systems. 1. CO_2 + n-Butane." *Journal of Chemical Engineering Data*, **30**, 485-491.

Huron, M.J. and Vidal, J., **1979**, "New Mixing Rules in Simple Equations of State for Representing Vapour-Liquid Equilibria in Strongly Non-Ideal Mixtures", *Fluid Phase Equilibria*, **3**, 255-271.

Inomata, H., Arai, K. and Saito, S., **1986**, "Measurement of Vapor-Liquid Equilibria at Elevated Temperatures and Pressures using a Flow Type Apparatus.", *Fluid Phase Equilibria*, **29**, 225-232.

Jan, D-S. and Tsai, F-N., 1991, "Modelling Phase Behavior of Carbon Dioxide with Aromatic Solvents.", *Ind. Eng. Chem. Res.*, **30**, 1965-1970.

Jenings, D.W. and Teja, A.S., **1989**, "Vapor-Liquid Equilibria in the Carbon Dioxide – 1-Hexene and Carbon Dioxide – 1-Hexyne Systems.", *Journal of Chemical Engineering Data*, **34**, 305-309.

Jordan, B.T. and van Winkle, M., **1951**, "Vapor-Liquid Equilibrium at Subatmospheric Pressures. Dodecane-Octadecene System.", *Industrial and Engineering Chemistry*, **43**, 12, 2908-2912.

Joseph, M.A., Raal, J.D. and Ramjugernath, D., **2001**, "Phase Equilibrium Properties of Binary Systems with Diacetyl from a Computer Controlled Vapour-Liquid Equilibrium Still", *Fluid Phase Equilibria*, **182**, 157-176.

Joseph, M.A., Raal, J.D. and Ramjugernath, D., **2002**, "Computer-aided Measurement of Vapour-Liquid Equilibria in a Dynamic Still at Sub-Atmospheric Pressures", *Developments in Chemical Engineering Mineral Processes*, **10**, 615-637.

Kim, C.H., Clark, A.B., Vimalchand, P. and Donohue, M.D., **1989**, "High-Pressure Binary Phase Equilibria of Aromatic Hydrocarbons with CO_2 and C_2H_6.", *Journal of Chemical Engineering Data*, **34**, 391-395.

King, M., Alderson, D., Fallah, F., Kassim, K., Sheldon, J. and Mahmud,R., **1983**, As reported in: Paulitis, M., Penninger, J., Gray, R. and Davidson, P. (Editors), "Chemical Engineering at Supercritical Fluid Conditions", The Butterworth Group, Ann Arbor, MI.

Kneisl, P., Zondlo, J.W. and Wallace, B.W., **1989**, "The Effect of Fluid Properties on Ebulliometer Operation", *Fluid Phase Equilibria*, **46**, 85-94.

Kneisl, P., Zondlo, J.W. and Whiting, W.B., **1988**, "An Apparatus for Measurement of Multi-Phase Equilibria at elevated Pressures.", *Ind. Eng. Chem. Res.*, **27**, 1541-1543.

Kohn, J.P., **1961**, "Hetrogenous Phase and Volumetric Behavior of the Methane n-Heptane System at Low Temperatures.", *AIChE Journal*, **7**, 514-518.

Kolbe, B. and Gmehling, J., **1985**, "Thermodynamic Properties of Ethanol + water. I. Vapour – Liquid Equilibria Measurements from 90 to 150°C by the Static Method.", *Fluid Phase Equilibria*, **23**, 213-226.

Konrad, R., Swaid, I. and Schneider, G.M., **1983**, "High-Pressure Phase studies on Fluid Mixtures of Low-Volatile Organic Substances with Supercritical Carbon Dioxide.", *Fluid Phase Equilibria*, **10**, 307-314.

Kubota, H., Inatome, H., Tanaka, Y. and Makita, T., **1983**, "Vapor-Liquid Equilibria of the Ethylene-Propylene System Under High Pressure.", *Journal of Chemical Engineering of Japan*, **16**, 99-103.

Kuk and Montagna **1983** *Chemical Engineering at Supercritical Fluid Condition.*

Laugier, S., Richon, D. and Renon, H., **1990**, "Simultaneous Determination of Vapor-Liquid Equilibria and Volumetric Properties of Ternary Systems with a New Experimental Apparatus." *Fluid Phase Equilibria*, **54**, 19-34.

Lee, S.C., **1931**, "Partial Pressure Isotherms", *Journal of Physical Chemistry*, **35**, 3558-3582.

Ljunglin, J.J. and Van Ness, H.C., **1962**, "Calculation of vapour-liquid equilibria from vapour pressure data", *Chem. Eng. Sci.*, **17**, 531-539.

Maher, P.J. and Smith, B.D., **1979**, "Infinite Dilution Activity Coefficient Values from Total Pressure VLE data. Effect of equation of state used", *Industrial and Engineering Chemistry Fundamentals*, **18**, 354-357.

Malinowski, S., **1982a**, "Experimental Methods for Vapor-Liquid Equilibria. Part I. Circulation Methods", *Fluid Phase Equilibria*, **8**, 197-219.

Malinowski, S., **1982b**, "Experimental Methods for Vapor-Liquid Equilibria. Part II. Dew- and Bubble Point Method", *Fluid Phase Equilibria*, **9**, 311-317.

Malinowski, S. and Anderko, A., **1992**, "Modelling Phase Equilibria: Thermodynamic Background and Practical Tools", John Wiley and Sons, Inc., New York, USA.

Marsh, K., **1989**, "New Methods for Vapor-Liquid-Equilibria Measurements", *Fluid Phase Equilibria*, **52**, 169-184.

McKnight, T.J., Harris, R.A., Ramjugernath, D., Raal, J.D. and M Starzak, **2003a**, "Molecular simulation and experimental measurement: A comparison", *ICheaP 6 – The Sixth Italian Conferrence on Chemical and Process Engineering*, Pisa, Italy.

McKnight, T.J., Harris, R.A., Ramjugernath, D., Raal, J.D. and M Starzak, **2003b**, "Comparing The Experimental And Simulation Approaches For The Prediction Of Vapour-Liquid Phase Equilibrium", *SAIChE 2003 – South African Chemical Engineering Congress*, Sun City.

Meskel-Lesavre, M., Richon, D. and Renon, H., **1981**, "New Variable Volume Cell for Determining Vapor-Liquid Equilibria and Saturated Liquid Molar Volumes by the Static Method.", *Ind. Eng. Chem. Fund.*, **20**, 284-289.

Moodley, K., **2003**, *Ph.D. Thesis*, University of Natal, Durban, South Africa.

Morris, W.O. and Donohue, M.D., **1985**, "Vapor-Liquid Equilibria in Mixtures Containing Carbon Dioxide, Toluene and 1-Methylnaphthalene.", *Journal of Chemical Engineering Data*, **30**, 259-263.

Moser, B. and Kistenmacher, H., **1987**, "An analysis of the industrial use of phase equilibria prediction model based on thermodynamic perturbation theory", *Fluid Phase Equilibria*, **34**, 189-201.

Mühlbauer, A.L. and Raal, J.D., **1995**, "Computation and thermodynamic interpretation of high-pressure vapour-liquid equilibria – a review." *The Chemical Engineering Journal*, **60**, 1-29.

Muirbrook, N.K. and Prausnitz, J.M., **1965**, "Multicomponent Vapor-Liquid Equilibria at High Pressures: Part 1. Experimental Study of the Nitrogen-Oxygen-Carbon Dioxide System at 0 °C.", *AIChE J.*, **11**, 1092-1096.

Occhiogrosso, R.N., Igel, J.T. and McHugh, M.A., **1986**, "Phase Behavior of Carbon Dioxide – Aromatic Hydrocarbon Mixtures.", *Fluid Phase Equilibria*, **26**, 165-179.

Othmer, D.F., **1928**, "Composition of Vapors from Boiling Binary solutions. Improved equilibrium still", *Industrial and Engineering Chemistry*, **20**, 743-766.

Péneloux, A., Rauzy, E. and Fréze, R., **1982**, "A consistent correction for Redlich-Kwong-Soave volumes", *Fluid Phase Equilibria*, **8**, 7-23.

Peng, D.Y. and Robinson, D.B., **1976**, "A new two-constant equation of state.", *Ind. Eng. Chem. Fund.*, **15**, 59-64.

Pillay, B., **2001**, Personal correspondence to Prof. D. Ramjugernath and Mr. R.A.Harris, *Contract work for SASOL Ltd. - Confidential.*

Pividal, K.A., Britigh, A. and Sandler, S.I., **1992**, "Infinite Dilution Activity Coefficients for Oxygenate Systems Determined Using a Differential Static Cell", *Journal of Chemical and Engineering Data*, **37**, 484-487.

Prausnitz, J.M., Lichtenthaler, R.N., Gomes de Azevedo, E., **1986**, "Molecular Thermodynamics of Fluid Phase Equilibria", Prentice-Hall, Englewood Cliffs, NJ.

Raal, J.D. and Mühlbauer, A.L., **1994**, "The Measurement of High-Pressure Vapour-Liquid Equilibria", *Developments in Chemical Engineering and Mineral Processing*, **2**, 69-104.

Raal, J.D. and Mühlbauer, A.L., **1998**, "Phase Equilibria: Measurement and Computation", Taylor and Francis, Bristol PA.

Raal, J.D. and Ramjugernath, D., **1998**, PVDF still designed as contract work for AEC, personal correspondence.

Raal, J.D. and Ramjugernath, D., **2001**, "Rigorous characterization of static and dynamic apparatus for measuring limiting activity coefficients" *Fluid Phase Equilibria*, **187-188**, 473-487.

Raal, J.D. and Ramjugernath, D., **2003**, "Experimental Discussion", Vol. 7", Chapter 2a and Chapter5, Elsevier, In Press.

Rackett, H.G., **1970**, "Equation of State for Saturated Liquids", *Journal of Chemical and Engineering Data*, **15**, 514-517.

Radosz, M., **1984**, "Variable-Volume Circulation Apparatus for Measuring High-Pressure Fluid-Phase Equilibria." *Phys. Chem.*, **88**, 859-862.

Ramjugernath, D., **2000**, "High Pressure Phase Equilibrium Studies", *Ph.D. Thesis*, University of Natal, Durban, South Africa.

Rarey, J.R., **1991**, *Ph.D. Thesis*, University of Dortmund, Federal Republic of Germany.

Rarey, J.R. and Gmehling, J., **1993**, "Computer-Operated Differential Static Apparatus for the Measurement of Vapour-Liquid Equilibrium Data", *Fluid Phase Equilibria*, **83**, 279-287.

Rarey, J.R., Horstmann, S. and Gmehling, J., **1999**, "Vapor-Liquid Equilibria and Vapor Pressure Data for the Systems Ethyl tert-Butyl Ether + Ethanol and Ethyl tert-Butyl Ether +Water", *Journal of Chemical Engineering Data*, **44**, 532-538.

Renon, H. and Prausnitz, J.M., **1968**, "Local Compositions in Thermodynamic Excess Functions for Liquid Mixtures", *American Institute of Chemical Engineers. Journal*, **14**, 135-144.

Rogalski, M. and Malanowski, S., **1980**, "Ebulliometers Modified for the Accurate Determination of Vapour-Liquid Equilibrium", *Fluid Phase Equilibria*, **5**, 97-112.

Rose, A. and Williams, E.T., **1955**, "Vapor Liquid Equilibrium Self-Lagging Stills. Design and Evaluation", *Industrial Engineering Chemistry*, **47**, 1528-1533.

Rousseaux, P., Richon, D. and Renon, H., **1983**, "A Static Method for Determination of Vapor-Liquid Equilibria and Saturated Liquid Molar Volumes at High Pressures and Temperatures using a New Variable-Volume Cell.", *Fluid Phase Equilibria*, **11**, 153-168.

Redlich, O. and Kwong, J.N.S., **1949**, "On Thermodynamics of Solutions V: An equation of State. Fugacities of gaseous solutions." *Chem. Rev.*, **44**, 233-244.

Sandler, I., **1994**, "Models for Thermodynamic and Phase Equilibria Calculations", New York, Marcel and Decker, Inc.

Seader, J.D. and Henley, E.J., **1998**, "Separation Process Principles", John Wiley & Sons, Inc.

Sewnarain, R., **2001**, "Multipurpose Separation and Purification Facility", *M.Sc. Thesis*, University of Natal, Durban, South Africa.

Sewnarain, R., Raal, J.D., and Ramjugernath, D., **2002**, "Isobaric Vapour-Liquid Equilibria for the Systems Propionic Acid + Butyric Acid, Isobutyric Acid + Butyric Acid, Butyric Acid + Isovaleric Acid, and Butyric Acid + Hexanoic Acid at 14 kPa", *Journal of Chemical Engineering Data*, **47**, 603-607.

Shibata, S.K. and Sandler, S.I., **1989**, "High-Pressure Vapor-Liquid Equilibria Involving Mixtures of Nitrogen, Carbon Dioxide and n-Butane.", *Journal of Chemical Engineering Data*, **34**, 291-298.

Sinnott, R.K., **1998**, "Coulson and Richardson's Chemical Engineering. Volume Six: Chemical Engineering Design: Rev. 2nd Ed.", Butterworth-Heinemann, Oxford.

Smith, J.M. and Van Ness, H.C., **1987**, "Introduction to Chemical Engineering Thermodynamics", 4th ed., McGraw-Hill, Singapore.

Soave, G., **1972**, "Equilibrium constants from a modified Redlich-Kwong equation of state.", *Chem. Eng. Science*, **27**, 1197-1203.

Stryjek, R. and Vera, J.H., **1986a**, "PRSV: An Improved Peng-Robinson Equation of State for Pure Compounds and Mixtures.", *The Canadian Journal of Chemical Engineering*, **64**, 323-333.

Stryjek, R. and Vera, J.H., **1986b**, "PRSV2: A Cubic equation of state for accurate vapour-liquid equilibrium calculations.", *The Canadian Journal of Chemical Engineering*, **64**, 820-826.

Suzuki, K., Sue, H., Itou, M., Smith, R.L., Inomata, H., Arai, K. and Saito, S., **1990**, "Isothermal Vapor-Liquid Equilibrium Data for Binary Systems at High Pressure: Carbon Dioxide – Methanol, Carbon Dioxide – Ethanol, Carbon Dioxide – 1-Propanol, Methane – Ethanol, Methane – 1-Propanol, Ethane – Ethanol and Ethane – 1-Propanol Systems.", *Journal of Chemical Engineering Data*, **35**, 63-66.

Takashima, S., Saiki, K., Arai, K. and Saito, S., **1986**, "Phase Equilibrium for CO_2 - C_2H_5OH - H_2O System.", *Journal of Chemical Engineering of Japan*, **19**, 48-56.

Thiesen, M., **1885**, "Untersuchengen über die zustandsgleichung", *Ann. Phys. Chem.*, **24**, 467-492.

Tsonopolous, C., **1974**, "An empirical correlation of second virial coefficients", *AIChE J.*, **20**, 263-272.

Twu, C.H. and Coon, J.E., **1996**, "CEOS/A^E Mixing Rules Constrained by vdW Mixing Rule and Second Virial Coefficient", *American Institute of Chemical Engineers Journal*, **42**, 3212-3222.

Van Ness, H.C., **1995**, "Thermodynamics in the Treatment of Vapor/Liquid Equilibrium (VLE) Data", *Pure and Applied Chemistry*, **67**, 859-872.

Van Ness, H.C. and Abbott, M.M., **1978**, "A Procedure for Rapid Degassing of Liquids",*Ind. Eng. Chem. Fundam.*, **17**, 66-67.

Van Ness, H.C. and Abbott, M.M., **1982**, "Classical Thermodynamics of Nonelectrolyte Solutions: With Applications to Phase Equilibria", McGraw-Hill, New York.

Van Ness, H.C., Soczek, C.A., Kochar, N.K., **1967a**, "Thermodynamic excess properties for ethanol-n-heptane", *Journal of Chemical Engineering Data*, **12**, 346-351.

Van Ness, H.C., Soczek, C.A., Peloquin, G.L., Machado, R.L., **1967b**, "Thermodynamic excess properties of three alcohol-hydrocarbon systems", *Journal of Chemical Engineering Data*, **12**, 217-224.

Walas, S.M., **1985**, "Phase Equilibrium in Chemical Engineering", Butterworth, Boston.

Wichterle, I., **1987a**, "High-Pressure Vapour-Liquid Equilibrium. IV." *Fluid Phase Equilibria*, **2**, 59-78.

Wichterle, I., **1987a**, "High-Pressure Vapour-Liquid Equilibrium. V." *Fluid Phase Equilibria*, **2**, 143-159.

Wilson, G.M., **1964**, "Vapor-Liquid Equilibrium. XI: A New Expression for the Excess Free Energy of Mixing", *Journal of the American Chemical Society*, **86**, 127-130.

Winnick, J., **1997**, "Chemical Engineering Thermodynamics: An Introduction to Thermodynamics for Undergraduate Engineering Students" John Wiley and Sons, Inc.

Wiśniewska, B., Gregorowicz, J. and Malanowski, S., **1993**, "Development of a Vapour-Liquid Equilibrium Apparatus to Work at Pressures up to 3 MPa", **86**, 173-186.

Wong, D.S.H. and Sandler, S.I., **1992**, "A Theoretically Correct Mixing Rule for Cubic Equations of State", *American Institute of Chemical Engineers Journal*, **38**, 671-680.

Yanagiuchi, M., Ueda, T., Matsubara, K., Inomata, H., Arai, K., and Saito, S., 1991, "Fundamental Investigation on Supercritical Extraction of Coal-Derived Aromatic Compounds", *J. Supercritical Fluids*, **4**, 145-151.

Yerazunis, S., Plowright, J.D. and Smola, F.M., **1964**, "Vapor-Liquid Equilibrium Determination by a New Apparatus", *American Institute of Chemical Engineers. Journal*, **10**, 660-665.

Yorizane, M., Yoshimura, S., Masuoka, H., Mitano, Y. and Kakimoto, Y., **1985**, "New Procedure for Vapor-Liquid Equilibria. Nitrogen + Carbon Dioxide, Methane + Freon 22 and Methane + Freon 12.", *Journal of Chemical Engineering Data*, **30**, 174-176.

APPENDIX

A

CALLIBRATIONS

A.1 CALIBRATIONS FOR THE EQUIPMENT OF KOLBE AND GMEHLING (1986)

A.1.1 Pressure Calibration

Accurate pressure measurement is vital for the VLE measurements performed on this equipment. Not only is it necessary to know the pressure in the cell accurately but it is also important to know the pressure in the CO_2 pump very accurately. The pressure in the pump is used to calculate the amount of CO_2 injected into the system. The calibration curves for the cell and pump pressure transducers are given in Figure A-1 and A-2 respectively.

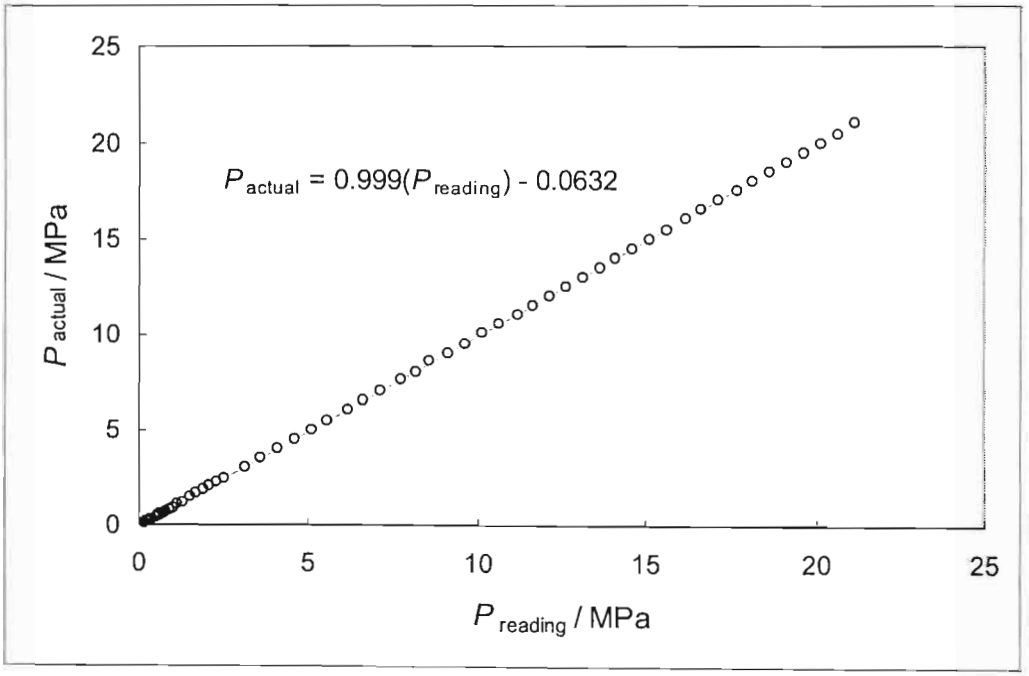

Figure A-1: Calibration curve for the cell pressure transducer.

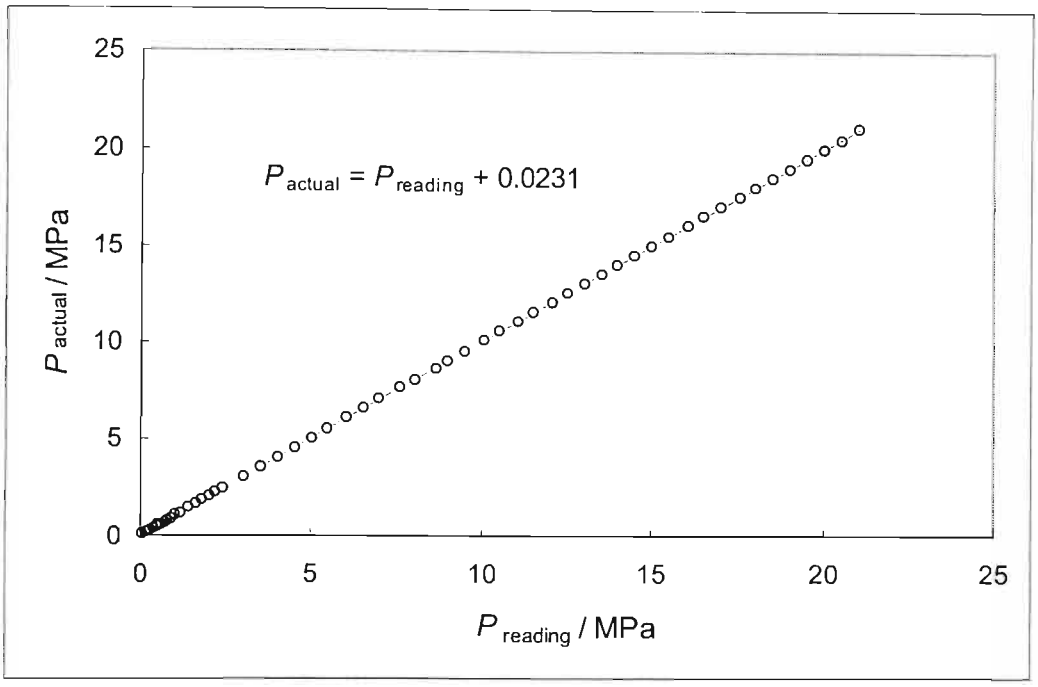

Figure A-2: Calibration curve for the CO_2 pump pressure transducer.

A.1.2 Cell Volume Calibration

The cell volume was calibrated by injecting distilled water into the evacuated cell. The water was injected into the cell using a pump kept at constant temperature. The cell was kept at a constant temperature and water was injected until the pressure in the cell was 2 MPa. The volume of water injected into the cell was calculated from the volume indicator on the pump. From the *PVT* data for pure water the amount of water injected into the cell can be calculated and from the temperature and the pressure in the cell the cell volume can be calculated.

Cell volume = 112.82 ml.

A.2CALIBRATIONS FOR THE EQUIPMENT OF HARRIS ET AL. (2003B)

A.2.1 Pressure Calibration

As mentioned above, pressure calibration is essential for accurate VLE measurements. The pressure transducer for this equipment was calibrated using a Cole-Palmer (model P-68037-05) pressure module which is NIST traceable. The pressure calibration curve is given below in Figure A-3.

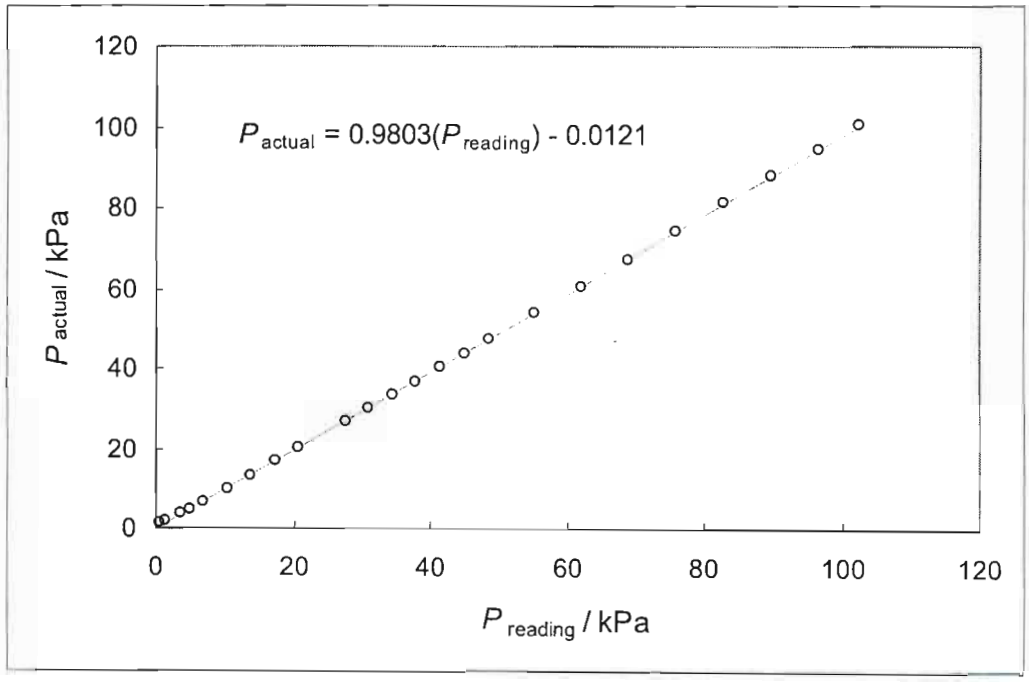

Figure A-3: Calibration curve for the still pressure transducer.

A.2.2 Temperature Calibrations

As with pressure it is important to calibrate the temperature probe. The original temperature probe used in the equipment was a Pt-100. Figure A-4 shows the plot of actual temperature versus the resistance of the Pt-100. The Pt-100 probe proved to be too fragile for the equipment and thus had to be replaced with a thermocouple. To measure the temperature with a thermocouple it is important to measure the temperature at the junction of the thermocouple and

the volt meter. The thermocouple voltage can be equated to the temperature difference (ΔT_{TC}) between the measured temperature (T) and the junction temperature (T_J). Thus the temperature is expressed as:

$$T = T_J + \Delta T_{TC} \tag{A-1}$$

The junction temperature was measured with a Pt-100. Figure A-5 shows the relationship of ΔT_{TC} to the voltage of the thermocouple and Figure A-6 is the temperature calibration of the Pt-100.

Thermocouples were used to measure the temperature at various points on the equipment. They were calibrated very roughly (Figure A-7).

All temperature probes were calibrated using a Cole-Palmer (model P-68037-05) temperature module which is NIST traceable.

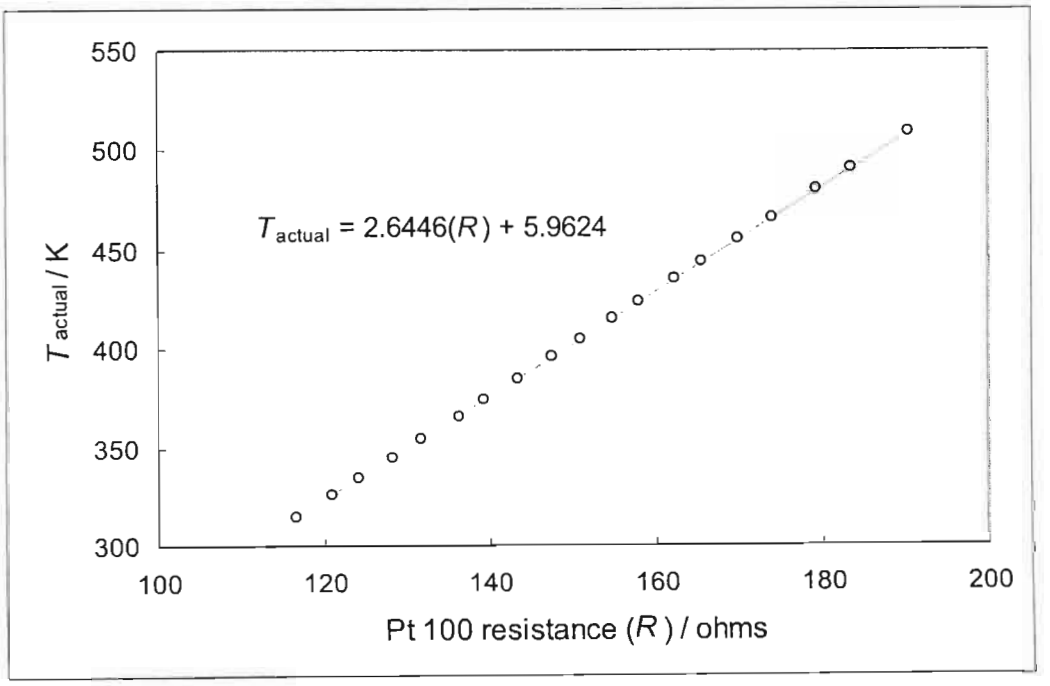

Figure A-4: Temperature calibration for Pt-100 temperature probe.

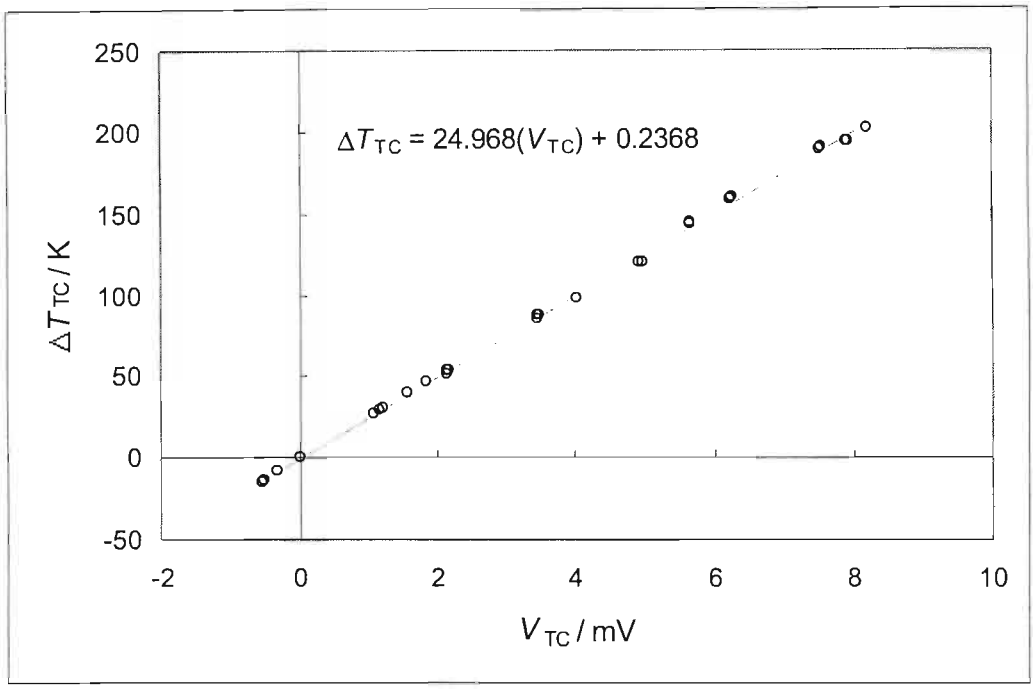

Figure A-5: Temperature calibration for thermocouple temperature probe.

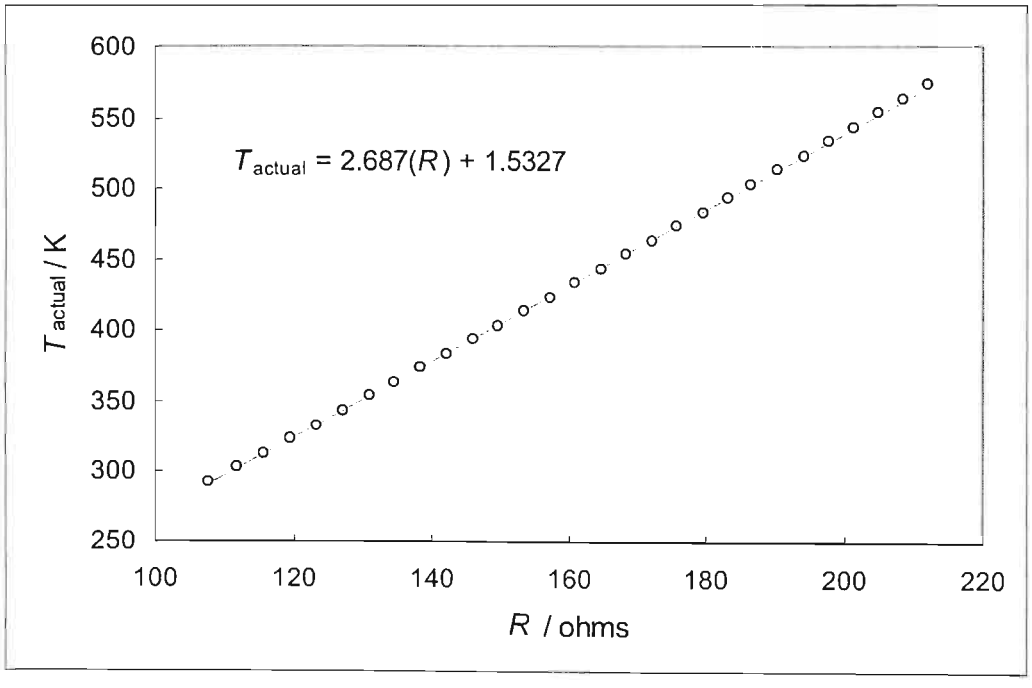

Figure A-6: Temperature calibration for Pt-100 at thermocouple junction.

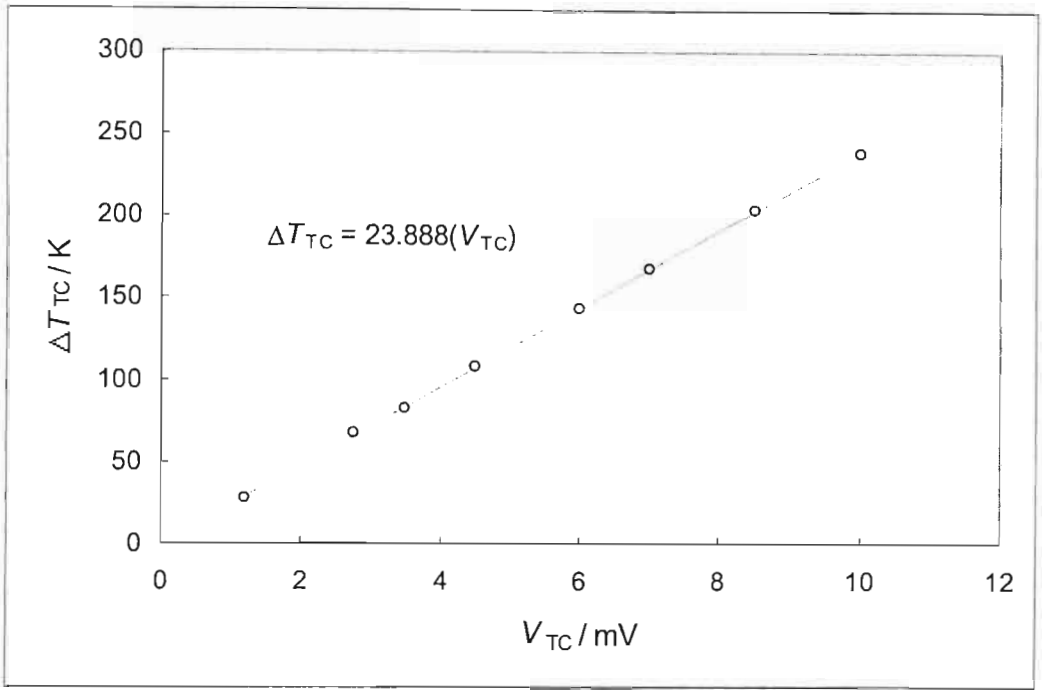

Figure A-7: Temperature calibration for thermocouples used on the equipment.

A.2.3 GC Calibration

GC Calibration is discussed in Chapter Four. The GC calibrations require a pair of plots and a table detailing the GC settings and are given for the systems as follows:

- Cyclohexane (1) + ethanol (2) [Table A-1, Figure A-8 and A-9],
- n-Dodecane (1) + 1-octadecene (2) [Table A-2, Figure A-10 and A-11], and,
- d,l-Menthol (1) + l-isomenthol (2) [Table A-3, Figure A-12 and A-13].

Table A-4 summarises the GC calibration results for the systems. If the difference between $\frac{F_1}{F_2}$ and $\frac{1}{(F_2/F_1)}$ is less than 1%, then the GC Calibration can be assumed to be linear across the entire mole fraction range.

Table A-1 GC Specifications and setup for cyclohexane (1) + ethanol (2)

Hardware	
GC	Shimadzu GC 17A
Bus	Shimadzu CBM 101 Connection Bus Module
Integrater	Shimadzu Software - *Pro Line* 486
GC Column	Ohio Valley Capillary Column 30m x 0.53mm 1.0 Micron Film BONDED
GC Program / Settngs	
Control Mode	Split
Detector	FID
Column Pressure	122 kPa
Column Flow	4.42ml/min
Linear Velocity	30.41 cm/sec
Total Flow	128 ml/min
Split Ratio	1:28
Injection Port Temperature	473.15 K
Column Oven Temperature	313.15 K
Detector Temperature	523.15 K
Detector Range	N/A
Detector Attenuation	N/A

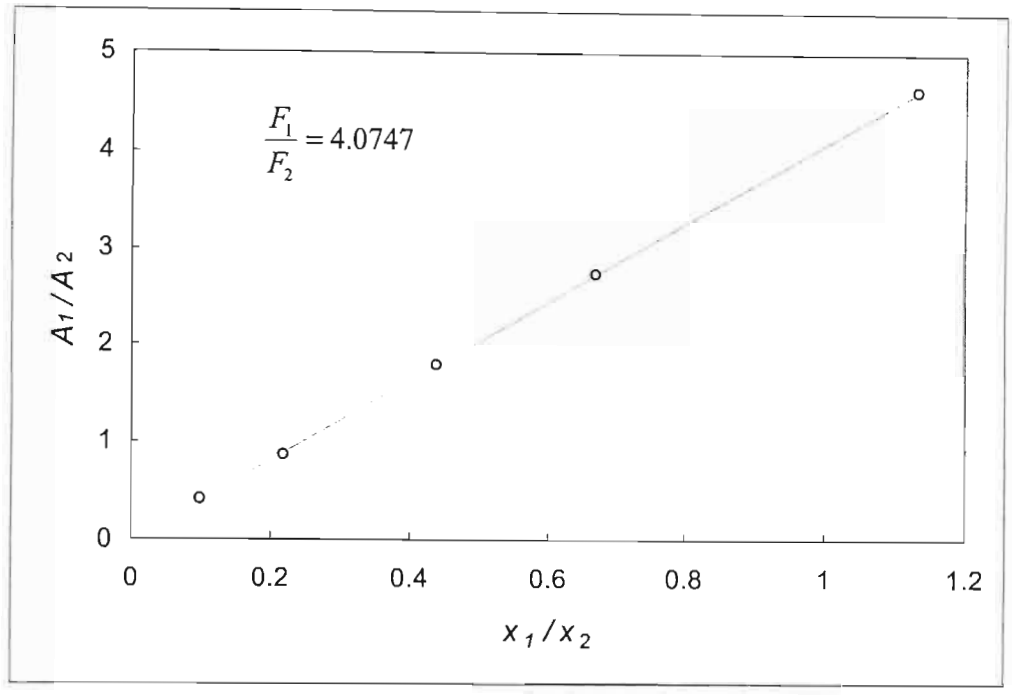

Figure A-8: A_1/A_2 vs. x_1/x_2 for cyclohexane (1) + ethanol (2).

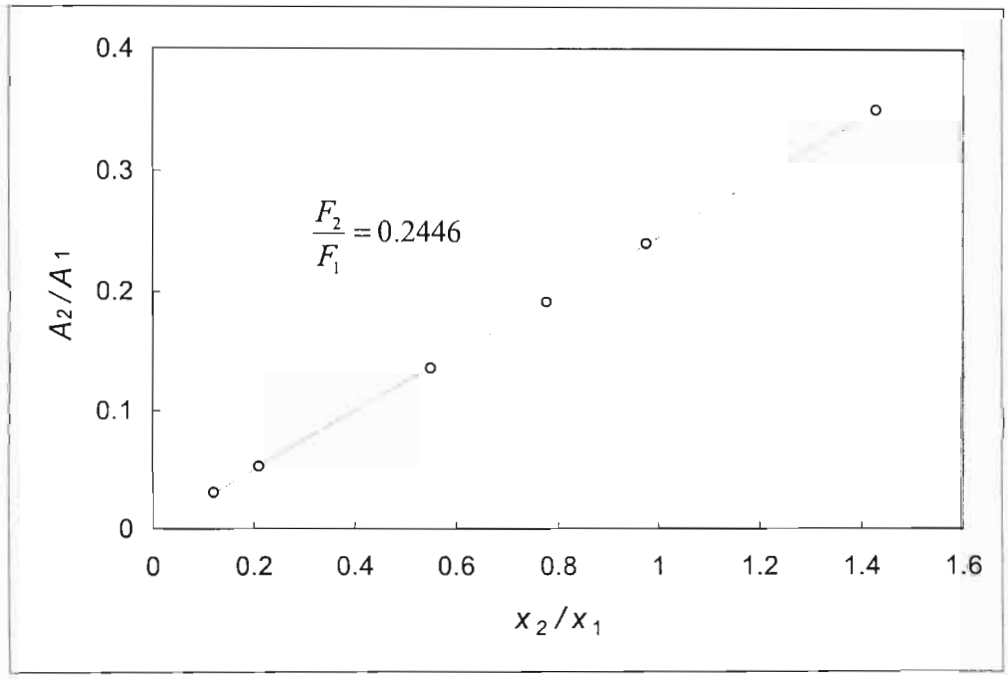

Figure A-9: A_2/A_1 vs. x_2/x_1 for cyclohexane (1) + ethanol (2).

Table A-2 GC Specifications and setup for n-dodecane (1) + 1-octadecene (2)

Hardware	
GC	Varian 3000
Bus	N/A
Integrater	Pentium II PC
GC Column	30 m Megabore Capillary column with 007-FFAP on fused silica
GC Program / Settngs	
Control Mode	Split
Detector	FID
Column Pressure	133 kPa
Column Flow	4 ml/min
Linear Velocity	N/A
Total Flow	40 ml/min
Split Ratio	1:10
Injection Port Temperature	473.15 K
Column Oven Temperature	423.15 K
Detector Temperature	483.15 K
Detector Range	9
Detector S	16

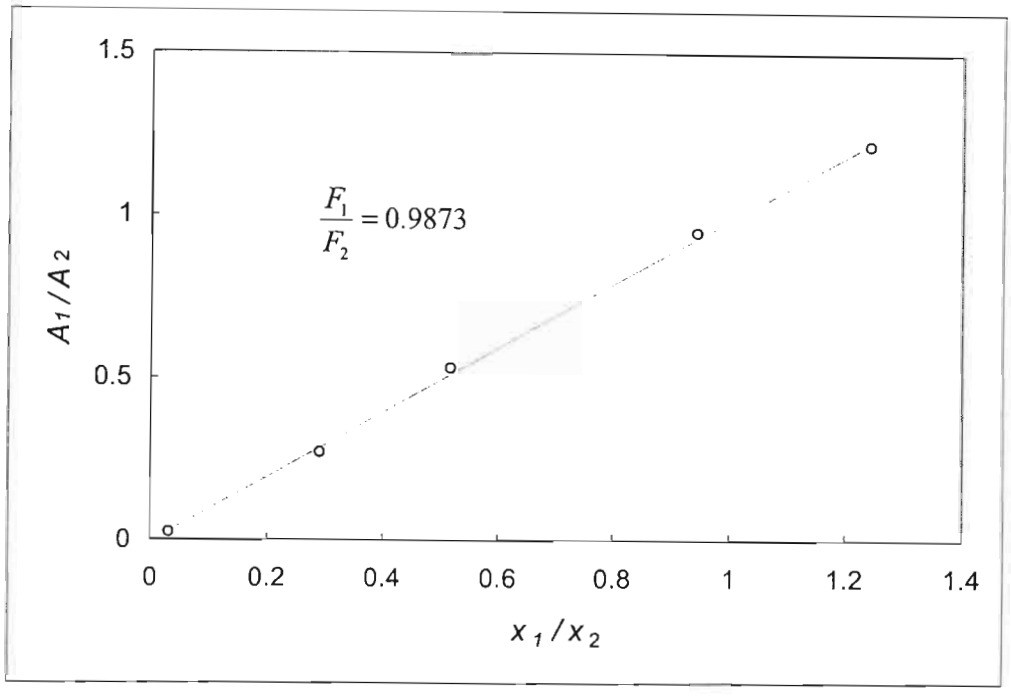

Figure A-10: A_1/A_2 vs. x_1/x_2 for n-dodecane (1) + 1-octadecene (2).

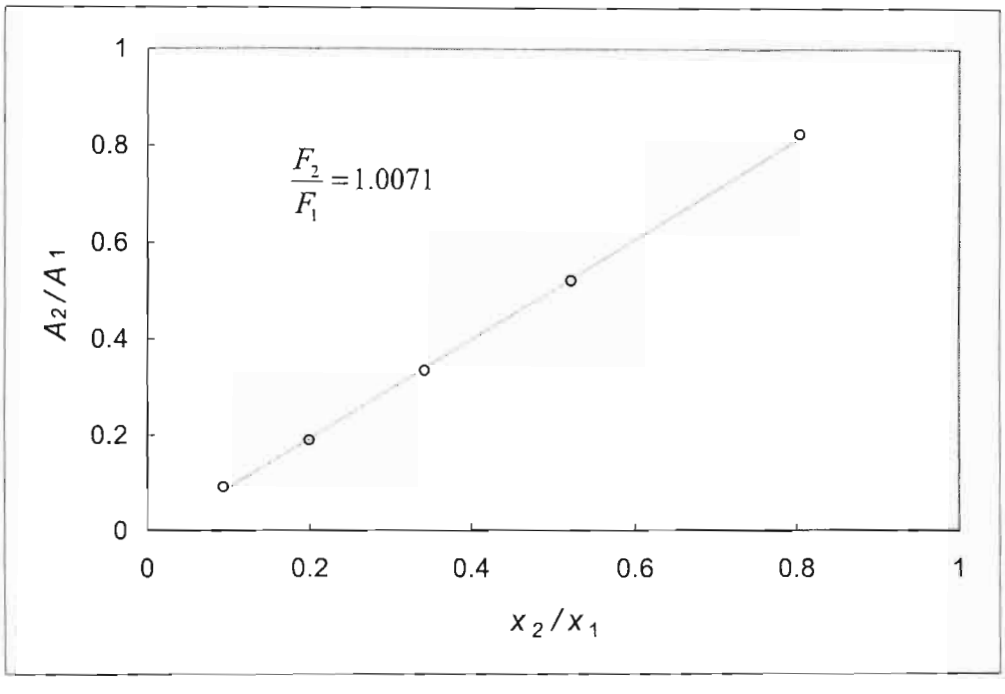

Figure A-11: A_2/A_1 vs. x_2/x_1 for n-dodecane (1) + 1-octadecene (2).

Table A-3 GC Specifications and setup for d,l-menthol (1) + l-isomenthol (2)

Integrater	Shimadzu Software - *Pro Line* 486
GC Column	Ohio Valley Capillary Column 30m x 0.53mm 1.0 Micron Film BONDED

GC Program / Settngs	
Control Mode	Split
Detector	FID
Column Pressure	122 kPa
Column Flow	4.42ml/min
Linear Velocity	30.41 cm/sec
Total Flow	128 ml/min
Split Ratio	1:28
Injection Port Temperature	473.15 K
Column Oven Temperature	453.15 K
Detector Temperature	523.15 K
Detector Range	N/A
Detector S	N/A

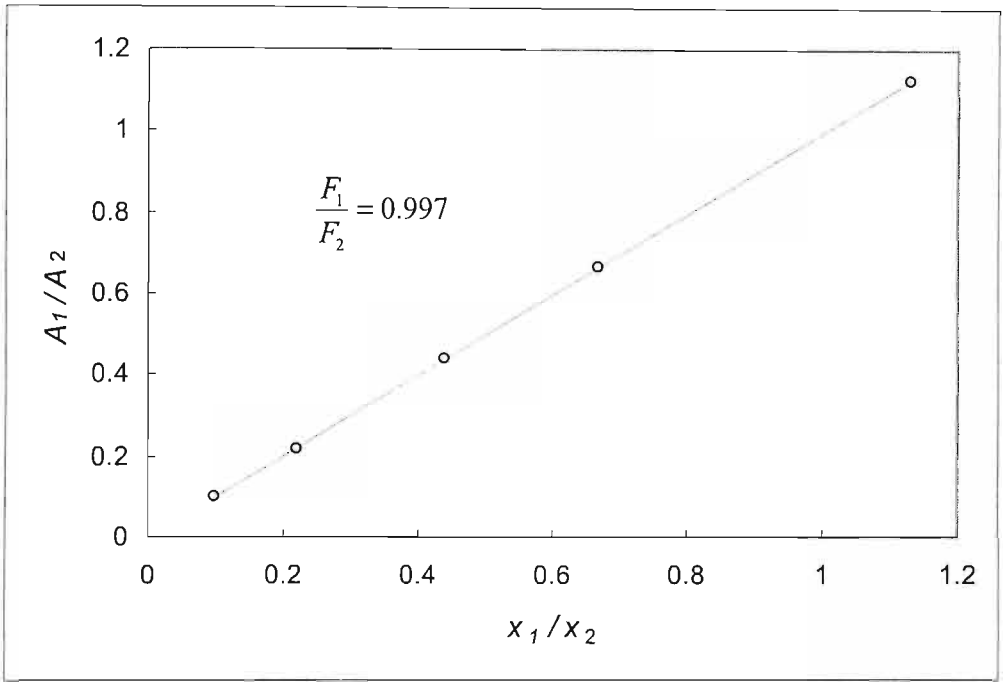

Figure A-12: A_1/A_2 vs. x_1/x_2 for d,l-menthol (1) + l-isomenthol (2).

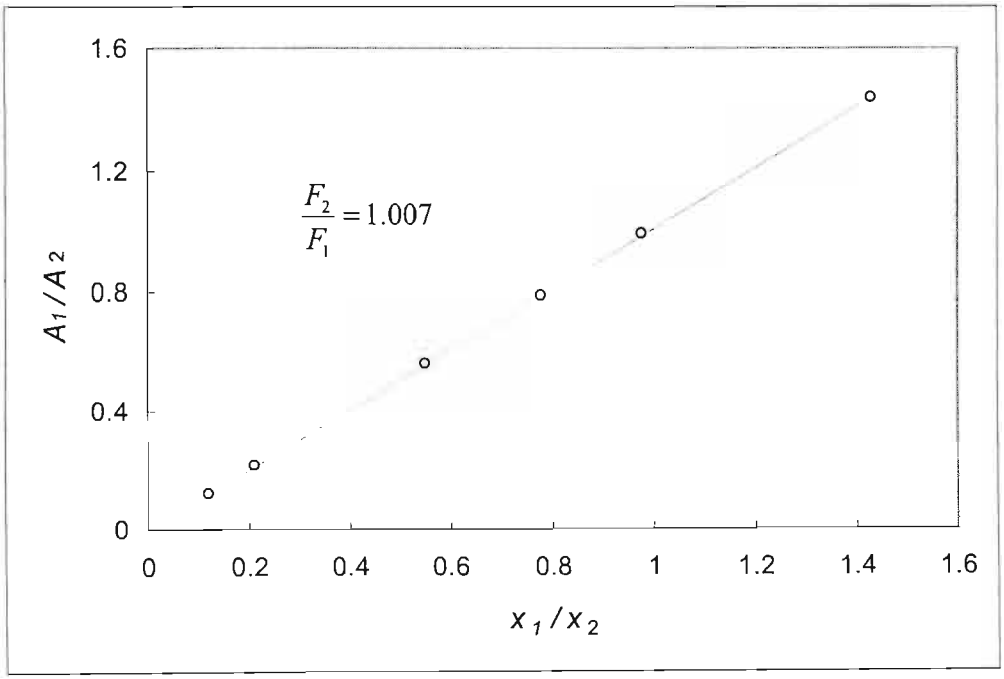

Figure A-13: A_2/A_1 vs. x_2/x_1 for d,l-menthol (1) + l-isomenthol (2).

Table A-4 GC calibrations summary

System	F_1 / F_2	F_2 / F_1	$1/(F_1 / F_2)$	% Diff.	Comment
Cyclohexane (1) + Ethanol (2)	4.0747	0.2446	4.0883	0.33	Linear
n-Dodecane (1) + 1-Octadecene (2)	0.9873	1.0071	0.9930	0.57	Linear
d,l-Menthol (1) + l-isoMenthol (2)	0.9970	1.0070	0.9930	0.40	Linear

APPENDIX

B

THEORY

B.1 STANDARD STATE FUGACITY

The standard state fugacity, f_i^o is used in Chapter Five to simplify the relationship between the vapour phase and liquid phase compositions:

$$y_i \hat{\phi}_i^v P = x_i \gamma_i f_i \tag{5-9}$$

By substituting for the standard state fugacity, f_i^o

$$y_i \Phi_i P = x_i \gamma_i P_i^{sat} \tag{5-10}$$

If $T_{system} < T_{ci}$ the activity coefficient is normalized as in Equation B-1:

$$\lim_{x_i \to 1} \gamma_i = 1 \tag{B-1}$$

Thus as the composition tends towards that of the pure component $\hat{f}_i^l \to x_i f_i^o$. This convention is referred to as symmetric normalization.

For noncondensable components, i.e.: $T_{system} > T_{ci}$ the normalization is given in Equation B-2:

$$\lim_{x_i \to 0} \gamma_i^* = 1 \tag{B-2}$$

Thus $\hat{f}_i^I \rightarrow x_i f_i^o$ as the component mole fraction becomes infinitesimally small. This convention is referred to as unsymmetric. This concentration region can be defined by Henry's Law:

$$H_i = \lim_{x_i \rightarrow 0} \frac{\hat{f}_i}{x_i} = f_i^o \tag{B-3}$$

where H_i is Henry's constant.

The standard states are thus dependent on the system temperature as well as the component properties. For binary systems containing both a condensable and non-condensable component both Equation B-1 and B-2 are used. Since normalization is not the same for both components they are said to follow the unsymmetric convention.

B.2 MIXING RULES

Mixing rules are used to determine the a_m and b_m parameters used in the cubic EOS as discussed in Chapter Five. The classical mixing rules are given in Chapter Five. Apart from the classical mixing rules, there are local composition (LCMR), density dependent (DDMR), composition dependent (CDMR) and density independent mixing rules (DIMR) as well as various combinations of the listed rules. The following mixing rules were used in this work and are discussed here:

- Huron and Vidal (1979) [LCMR],
- Wong and Sandler (1992) [DIMR], and,
- Twu and Coon (1996) [DIMR].

B.2.1 Huron-Vidal Mixing Rules

Special mention must be made of the LCMR developed by Huron and Vidal (1979) as it was used in this study. Huron and Vidal (1979) proposed the first LCMR by relating the excess Gibbs free energy (G^E) to the pure component (ϕ_i) and mixture fugacity coefficients (ϕ):

$$G^E = RT\left[\ln\phi - \sum_{i=1}^{n} x_i \ln\phi_i\right] \tag{5-35}$$

Equation B-4 relates the fugacity coefficients to G^E models which are discussed in Section 5.3.3. The fugacity coefficients are soley dependent on the EOS used and a_m and b_m are related to the G^E at infinite pressure:

$$G^E_\infty = -\left[\frac{a_m}{b_m} - \sum x_i \frac{a_i}{b_i}\right]\Delta \tag{5-36}$$

where G^E_∞ is the excess Gibbs free energy in the limit of infinite pressure and Δ is a constant dependant on which EOS is used as explained by Raal and Mühlbauer (1998). In our work $\Delta = \ln 2$.

The b_m parameter is identical to the classical mixing rule term:

$$b_m = \sum y_i b_i \tag{5-27}$$

and thus Equation 5-36 can be rewritten as:

$$a_m = b_m\left[\sum x_i \frac{a_i}{b_i} + \frac{G^E_\infty}{\Delta}\right] \tag{5-37}$$

B.2.2 Wong-Sandler Mixing Rule

Wong and Sandler (1992) proposed a mixing rule, which is valid at both low and high densities without being density dependent. They equate the virial EOS B coefficient with cubic EOS parameters as in Equation 5-38:

$$B = b_m - a_m / RT \tag{5-38}$$

where

$$a_m = \sum\sum x_i x_j \sqrt{a_i a_j}(1-k_{ij}) \tag{B-4}$$

$$b_m = \sum\sum x_i x_j 0.5(b_i + b_j) \tag{B-5}$$

The composition dependence for the second virial coefficient is quadratic thus:

$$b_m = \frac{\sum\sum x_i x_j \left(b - \frac{a}{RT}\right)_{ij}}{1 - \frac{a_m}{b_m RT}} \tag{B-6}$$

where $(b\text{-}a/RT)_{ij}$ is the composition-independent cross second virial coefficient which is related to the pure component parameters as shown in Equation 5-39:

$$\left(b - \frac{a}{RT}\right)_{ij} = \frac{\left[\left(b - \frac{a}{RT}\right)_i + \left(b - \frac{a}{RT}\right)_j\right]}{2}(1-k_{ij}) \tag{5-39}$$

Where k_{ij} is a second virial coefficient binary interaction parameter.

The excess Helmholtz free energy (A^E) can be related to the a_m and b_m parameters by equating the A^E at infinite pressure from an EOS to that of a liquid phase model:

$$A^E_\infty = \left[\frac{a_m}{b_m} - \sum x_i \frac{a_i}{b_i}\right]\Omega \tag{5-40}$$

where Ω is a constant which depends on the EOS used.

Wong et al. (1992a, b) have shown that:

$$G^E(T, P = 1 \text{ bar}, x) = A^E(T, P = 1 \text{ bar}, x) = A^E(T, P = high, x) \tag{5-41}$$

as A^E is essentially pressure-independent.

Combining Equations B-6, 5-40 and 5-41 results in the mixing-rule parameters being defined as follows:

$$\frac{a_m}{RT} = M\frac{N}{1-N} \tag{5-42}$$

and

$$b_m = \frac{M}{1-N} \tag{5-43}$$

where

$$M = \sum\sum x_i x_j \left(b - \frac{a}{RT}\right)_{ij} \tag{5-44}$$

and

$$N = \sum x_i \frac{a_i}{b_i RT} + \frac{G^E(x_i)}{\Omega RT} \tag{5-45}$$

For the P-R EOS $\Omega = \left[\ln\left(\sqrt{2}-1\right)\right]\sqrt{2}$ and the G^E can be modeled using any one of the models discussed in 5.3.3.

B.2.3 Twu and Coon Mixing Rule

Twu and Coon also based their mixing rules on the Helmholtz free energy relationship as was discussed above. They developed the following equations for a_m and b_m:

$$b_m = \frac{b_{m,vdw} - a_{m,vdw}}{1 - \left(\frac{a_{m,vdw}}{b_{m,vdw}} + \frac{1}{C} \frac{A_\infty^E}{RT} \right)} \tag{5-46}$$

and

$$a_m = b_m \left(\frac{a_{m,vdw}}{b_{m,vdw}} + \frac{1}{C} \frac{A_\infty^E}{RT} \right) \tag{5-47}$$

where C is dependent on the EOS ($C = \left[\ln\left(\sqrt{2} - 1\right)\right]\sqrt{2}$) and A_∞^E is determined as explained above. The $a_{m,vdW}$ and $b_{m,vdW}$ are the mixing parameters derived from the van der Waals (or classical) mixing rules:

$$a_{m,vdw} = \sum_i \sum_j x_i x_j \sqrt{a_i a_j} (1 - k_{ij}) \tag{5-48}$$

and

$$b_{m,vdw} = \sum_i \sum_j x_i x_j \left[\frac{1}{2} (b_i + b_j) \right] (1 - l_{ij}) \tag{5-49}$$

B.3 VIRIAL EOS CORRELATIONS

Two virial EOS correlations were used in this work. They are:

- The Common Tsonopolous correlation, and,
- The more complex Hayden and O'Connell correlation.

B.3.1 Tsonopolous Correlation

The general Tsonopoulos (1974) correlation is:

$$\frac{BP}{RT} = B^{(0)} + \omega B^{(1)} \tag{5-54}$$

where

$$B^{(0)} = 0.1445 - \frac{0.33}{T_r} - \frac{0.1385}{T_r^2} - \frac{0.0121}{T_r^3} - \frac{0.000607}{T_r^8} \tag{5-55}$$

and

$$B^{(1)} = 0.0637 + \frac{0.331}{T_r} - \frac{0.424}{T_r^2} - \frac{0.008}{T_r^8} \tag{5-56}$$

B.3.2 Hayden and O'Connell Correlation

The Hayden and O'Connell (1975) correlation is more complex, containing its own terms for cross second virial coefficients, and is used for predicting pure and cross second virial coefficients for a larger variety of fluids. The correlation requires only the critical temperature and pressure of the component(s), mean radius of gyration, dipole moment and (if necessary) a chemical association parameter. The correlation assumes the virial coefficient to be the sum of two types of interactions:

$$B_{ij} = B_{ij}^{F} + B_{ij}^{D} \tag{5-57}$$

where

$$B_{ij}^{F} = \left(B_{nonpolar}^{F}\right)_{ij} + \left(B_{polar}^{F}\right)_{ij} \tag{B-7}$$

and

$$B_{ij}^{D} = \left(B_{metastable}\right)_{ij} + \left(B_{bond}\right)_{ij} + \left(B_{chemical}\right)_{ij} \tag{B-8}$$

Subscript F refers to the relatively "free" molecules (weak physical forces), and D refers to the "bound" or "dimerised" molecules ("chemical" forces).

Temperature-dependent corelations are used to calculate individual contributions to the second virial coefficient:

$$\left(B_{nonpolar}^{F}\right)_{ij} = b_{0ij}\left(0.94 - \frac{1.47}{T_{ij}^{*}} - \frac{0.85}{T_{ij}^{*2}} - \frac{1.015}{T_{ij}^{*3}}\right) \tag{B-9}$$

$$\left(B_{polar}^{F}\right)_{ij} = b_{0ij}\mu_{ij}^{*}\left(0.74 - \frac{3.0}{T_{ij}^{*}} - \frac{2.1}{T_{ij}^{*2}} - \frac{2.1}{T_{ij}^{*3}}\right) \tag{B-10}$$

$$\left(B_{metastable}\right)_{ij} + \left(B_{bond}\right)_{ij} = b_{0ij}A_{ij}\exp\left(\frac{\Delta h_{ij}}{T_{ij}^{*}}\right) \tag{B-11}$$

$$\left(B_{chemical}\right)_{ij} = b_{0ij}E_{ij}\left[1 - \exp\left(\frac{1500\eta_{ij}}{T}\right)\right] \tag{B-12}$$

$$\frac{1}{T_{ij}^{*'}} = \frac{1}{T_{ij}^{*}} - 1.6\omega_{ij} \tag{B-13}$$

$$T_{ij}^{*} = \frac{T}{\left(\frac{\varepsilon_{ij}}{k}\right)} \tag{B-14}$$

The temperature-independent parameters used in Equations B-9 to B-14 are:

$$b_{0ij} = 1.26184\sigma_{ij}^{3} \tag{B-15}$$

$$\begin{aligned} \mu_{ij}^{*'} &= \mu_{ij}^{*} && \mu_{ij}^{*} < 0.04 \\ &= 0 && 0.04 \le \mu_{ij}^{*} < 0.25 \\ &= \mu_{ij}^{*} - 0.25 && 0.25 \le \mu_{ij}^{*} \end{aligned} \tag{B-16}$$

$$A_{ij} = -0.3 - 0.05\mu_{ij}^{*} \tag{B-17}$$

$$\Delta h_{ij} = 1.99 + 0.2\mu_{ij}^{*2} \tag{B-18}$$

$$\mu_{ij}^{*} = \frac{7243.8\mu_i\,\mu_j}{\left(\frac{\varepsilon_{ij}}{k}\right)\sigma^{3}} \tag{B-19}$$

$$E_{ij} = \exp\left\{\eta_{ij}\left(\frac{650}{\left(\frac{\varepsilon_{ij}}{k}\right)+300} - 4.27\right)\right\} \qquad \text{for } \eta_{ij} < 4.5 \tag{B-20a}$$

or

$$E_{ij} = \exp\left\{\eta_{ij}\left[\frac{42800}{\left(\frac{\varepsilon_{ij}}{k}\right)+22400}-4.27\right]\right\} \qquad \text{for } \eta_{ij} \geq 4.5 \qquad \text{(B-20b)}$$

where

T	-	temperature (K)
$\left(\frac{\varepsilon_{ij}}{k}\right)$	-	characteristic energy for the *i-j* interaction (K)
σ_{ij}	-	molecular size (angstroms)
μ_{ij}	-	dipole moment of component *i* (Debye)
η_{ij}	-	association parameter ($i=j$); solvation parameter ($i\neq j$)
ω_{ij}	-	nonpolar acentric factor

For $i=j$, parameters $\left(\frac{\varepsilon_{ii}}{k}\right)$, σ_{ii} and ω_{ii} are predicted from the pure component properties:

$$\omega_{ii} = 0.006026R_{D_i} + 0.02096R_{D_i}^2 - 0.001366R_{D_i}^3 \qquad \text{(B-21)}$$

$$\left(\frac{\varepsilon_{ii}}{k}\right) = \left(\frac{\varepsilon_{ii}}{k}\right)^{'}\left\{1-\xi\, c_1\left[1-\frac{\xi(1+c_1)}{2}\right]\right\} \qquad \text{(B-22)}$$

$$\sigma_{ii} = \sigma_{ii}^{'}(1+\xi\, c_2)^{1/3} \qquad \text{(B-23)}$$

$$\left(\frac{\varepsilon_{ii}}{k}\right)^{'} = T_{ci}\left[0.748+0.91\omega_{ii}-\frac{0.4\eta_{ii}}{2+20\omega_{ii}}\right] \qquad \text{(B-24)}$$

$$\sigma_{ii}^{'} = (2.44-\omega_{ii})\left(1.0133\frac{T_{ci}}{P_{ci}}\right)^{1/3} \qquad \text{(B-25)}$$

$$\xi = 0 \qquad \text{for } \mu_i < 1.45 \tag{B-26a}$$

$$\xi = \frac{1.7941\times10^{7}\mu_i^{4}}{\left[\left(2.882-\frac{1.882\omega_{ii}}{0.03+\omega_{ii}}\right)T_{ci}\sigma_{ii}^{6}\left(\frac{\varepsilon_{ii}}{k}\right)\right]} \qquad \text{for } \mu_i \geq 1.45 \tag{B-26b}$$

$$c_1 = \frac{16+400\omega_{ii}}{10+400\omega_{ii}} \tag{B-27}$$

$$c_2 = \frac{3}{10+400\omega_{ii}} \tag{B-28}$$

Pure component properties that are required for Equations B-21 to B-28 are:

T_{ci}	-	critical temperature of component *i* (K)
P_{ci}	-	critical pressure of component *i* (bar)
R_{Di}	-	mean radius of gyration of component *i* (angstroms)

Cross parameters $\left(\frac{\varepsilon_{ij}}{k}\right)$, σ_{ij} and ω_{ij} $(i \neq j)$ are calculated using suitable mixing rules and pure component parameters given by Equations B-21 to B-28:

$$\omega_{ij} = \frac{1}{2}(\omega_{ii}+\omega_{jj}) \tag{B-29}$$

$$\left(\frac{\varepsilon_{ij}}{k}\right) = \left(\frac{\varepsilon_{ij}}{k}\right)'\left(1+\xi' c_1'\right) \tag{B-30}$$

$$\sigma_{ij} = \sigma_{ij}'\left(1-\xi' c_2'\right) \tag{B-31}$$

where

$$\left(\frac{\varepsilon_{ij}}{k}\right)' = 0.7\left[\left(\frac{\varepsilon_{ii}}{i}\right)\left(\frac{\varepsilon_{ij}}{k}\right)\right]^{1/2} + \frac{0.6}{\left[\frac{1}{\left(\frac{\varepsilon_{ii}}{k}\right)} + \frac{1}{\left(\frac{\varepsilon_{jj}}{k}\right)}\right]} \tag{B-32}$$

$$\sigma'_{ij} = \left(\sigma_{ii}\sigma_{jj}\right)^{1/2} \tag{B-33}$$

$$\xi' = \frac{\mu_i^2\left(\frac{\varepsilon_{jj}}{k}\right)^{2/3}\sigma_{ij}^4}{\left(\frac{\varepsilon_{ij}}{k}\right)'\sigma_{ij}'^6} \qquad for\ \mu_i \geq 2\ and\ \mu_j = 0 \tag{B-34a}$$

or

$$\xi' = \frac{\mu_j^2\left(\frac{\varepsilon_{kk}}{k}\right)^{2/3}\sigma_{ij}^4}{\left(\frac{\varepsilon_{ij}}{k}\right)'\sigma_{ij}'^6} \qquad for\ \mu_j \geq 2\ and\ \mu_i = 0 \tag{B-34b}$$

or

$$\xi' = 0.0 \text{ for all other values of } \mu_i \text{ and } \mu_\varphi \tag{B-34c}$$

$$c_1' = \frac{16 + 400\omega_{ij}}{10 + 400\omega_{ij}} \tag{B-35}$$

$$c_2' = \frac{3}{10 + 400\omega_{ij}} \tag{B-36}$$

B.4 OBJECTIVE FUNCTIONS

The objective function is defined as (Van Ness and Abott (1982)):

$$F = \sum \left(\frac{Y_{expt} - Y_{calc}}{Y_{expt}} \right)^2 \tag{B-37}$$

where Y is a measured variable. Models are fitted to the data by minimizing F. Below are some of the more common objective functions in use:

$$F = \sum \left(\frac{P_{expt} - P_{calc}}{P_{expt}} \right)^2 \tag{B-38}$$

$$F = \sum \left(\frac{y_{expt} - y_{calc}}{y_{expt}} \right)^2 \tag{B-39}$$

$$F = \sum \left(\frac{\frac{G^E}{RT}_{expt} - \frac{G^E}{RT}_{calc}}{\frac{G^E}{RT}_{expt}} \right)^2 \tag{B-40}$$

VLE data sets for which both pressure and vapour composition were measured can be regressed by minimising both the pressure and the vapour mole fraction functions simultaneously. The functions must be normalised if they are to be compatible for simultaneous treatment. This is accomplished with the aid of normalising factors (w) and the corresponding objective function is:

$$F = \sum \left(\frac{y_{expt} - y_{calc}}{w_y} \right)^2 + \sum \left(\frac{P_{expt} - P_{calc}}{w_P} \right)^2 \tag{B-41}$$

Van Ness and Abbott (1982) recommend that w_Y is usually set equal to the root-mean-square value of $(Y_{expt} - Y_{calc})$ resulting from the minimisation of $F = \sum \left(Y_{expt} - Y_{calc}\right)^2$.

APPENDIX

C

AUXILLARY CALCULATIONS

C.1 DETERMINATION OF IDAC BY THE METHOD OF MAHER AND SMITH (1979)

The use of the deviation pressure method for determining IDAC is discussed in Chapter Five. The plots of the linear function $\frac{P_D}{x_1 x_2}$ vs. x_1 or $\frac{x_1 x_2}{P_D}$ vs. x_1 are shown as follows:

- Hexane (1) + N-methylformamide (2) at 363.15 K [Figure C-1 and C-2],
- Benzene (1) + N-methylformamide (2) at 363.15 K [Figure C-3 and C-4],
- Chlorobenzene (1) + N-methylformamide (2) at 363.15 K [Figure C-5 and C-6], and,
- Acetonitrile + N-methylformamide (2) at 363.15 K [Figure C-7 and C-8].

Table C-1 lists the limiting values of $\left(\frac{P_D}{x_1 x_2}\right)_{x=0}$, $\left(\frac{P_D}{x_1 x_2}\right)_{x=1}$, $\left(\frac{x_1 x_2}{P_D}\right)_{x=0}$ or $\left(\frac{x_1 x_2}{P_D}\right)_{x=1}$ and the IDAC for the systems mentioned above.

Table C-2 compares the IDAC values calculated by the method of Maher and Smith (1979) with values calculated from the Wilson and NRTL regressed parameters.

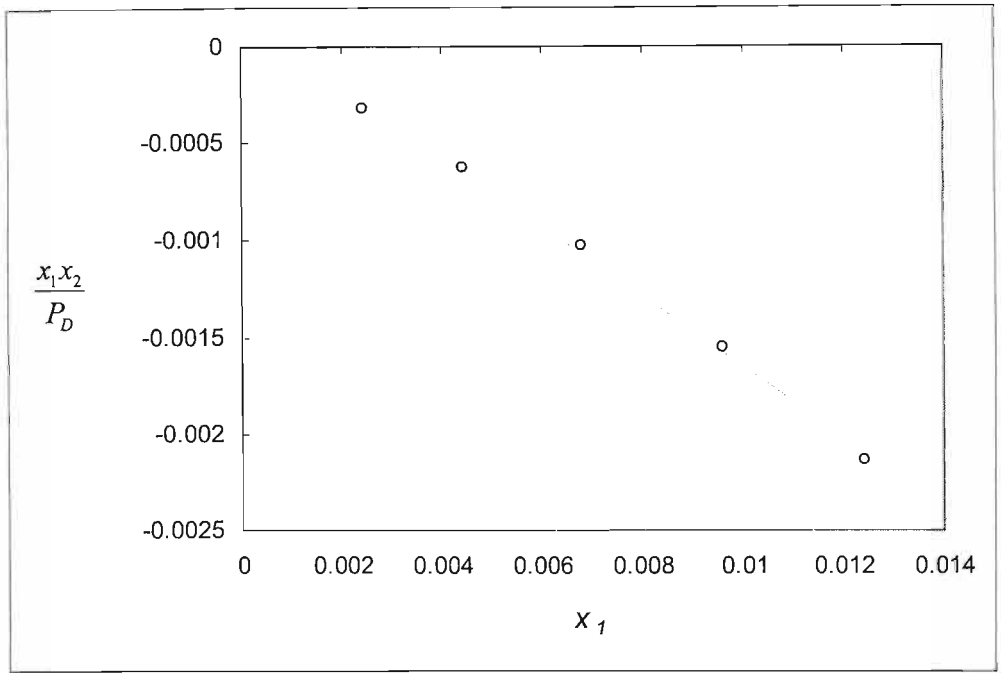

Figure C-1: $\frac{x_1x_2}{P_D}$ vs. x_1 as $x_1 \rightarrow 0$ for Hexane (1) + N-methylformamide (2) at 363.15 K.

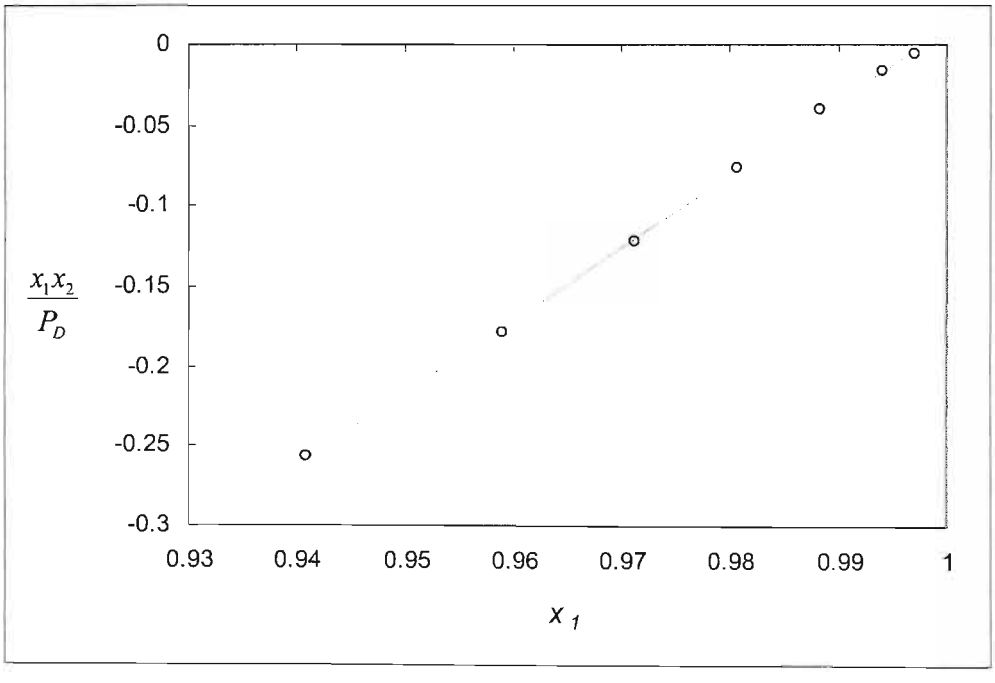

Figure C-2: $\frac{x_1x_2}{P_D}$ vs. x_1 as $x_1 \rightarrow 1$ for Hexane (1) + N-methylformamide (2) at 363.15 K.

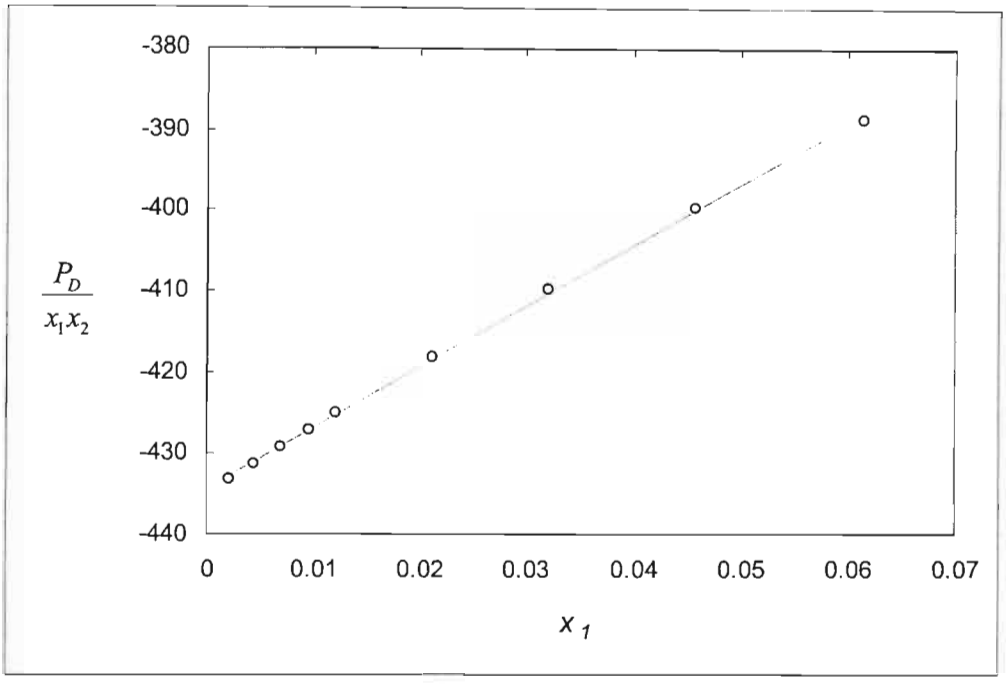

Figure C-3: $\frac{P_D}{x_1 x_2}$ vs. x_1 as $x_1 \rightarrow 0$ for Benzene (1) + N-methylformamide (2) at 363.15 K.

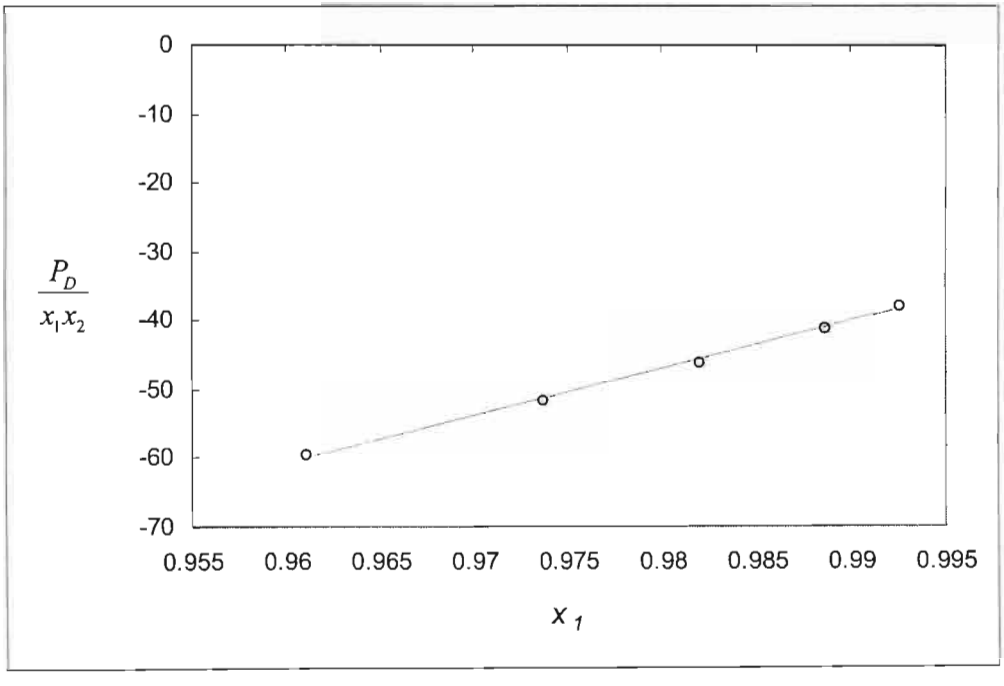

Figure C-4: $\frac{P_D}{x_1 x_2}$ vs. x_1 as $x_1 \rightarrow 1$ for Benzene (1) + N-methylformamide (2) at 363.15 K.

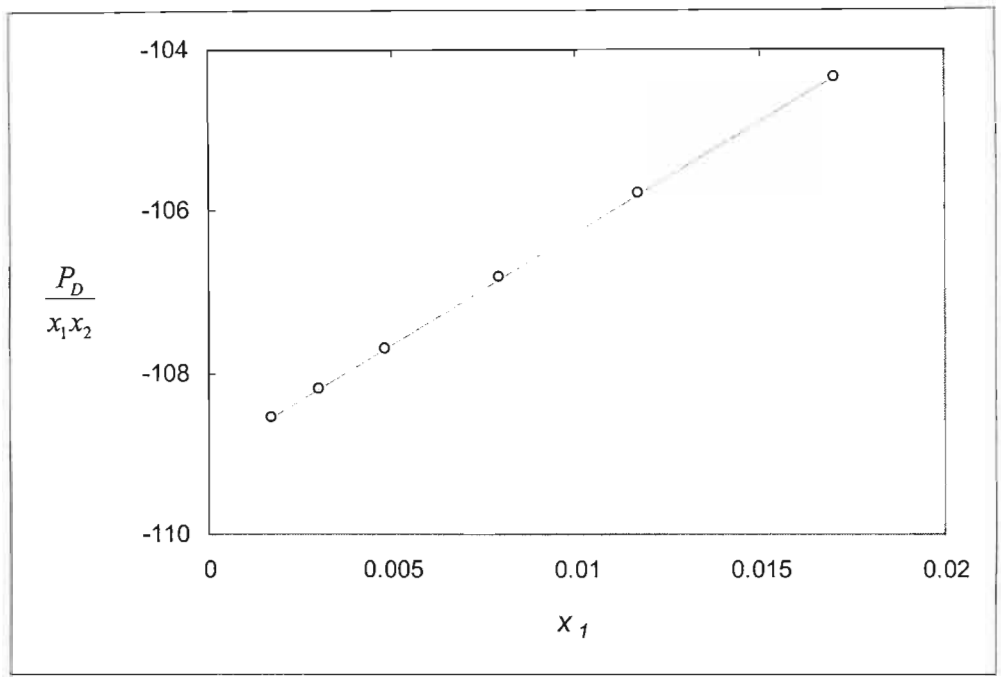

Figure C-5: $\frac{P_D}{x_1 x_2}$ vs. x_1 as $x_1 \rightarrow 0$ for Chlorobenzene (1) + N-methylformamide (2) at 363.15 K.

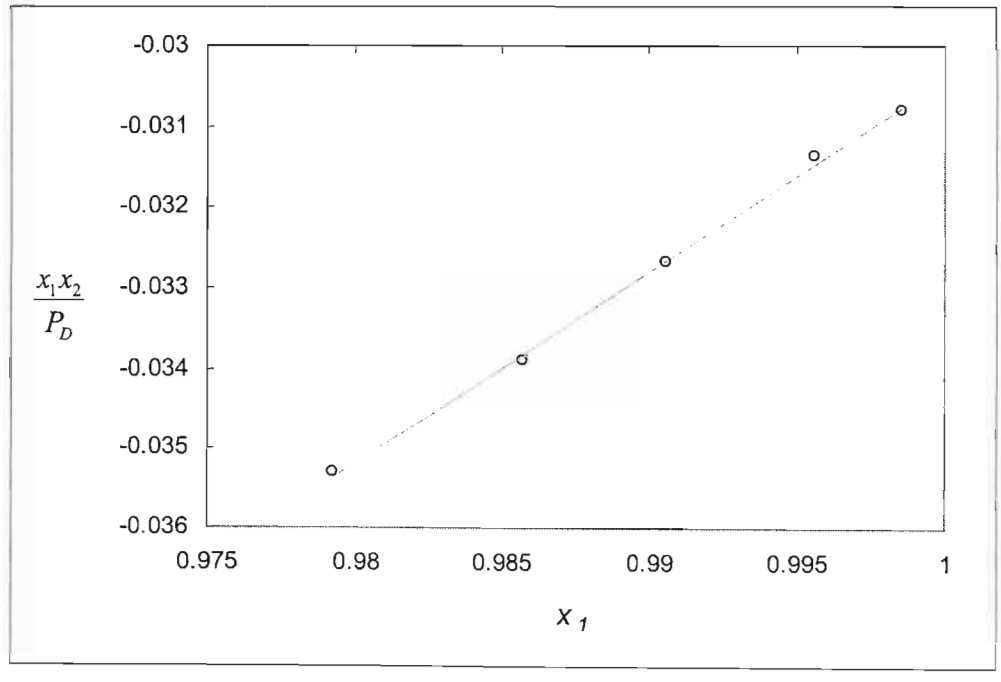

Figure C-6: $\frac{x_1 x_2}{P_D}$ vs. x_1 as $x_1 \rightarrow 1$ for Chlorobenzene (1) + N-methylformamide (2) at 363.15 K.

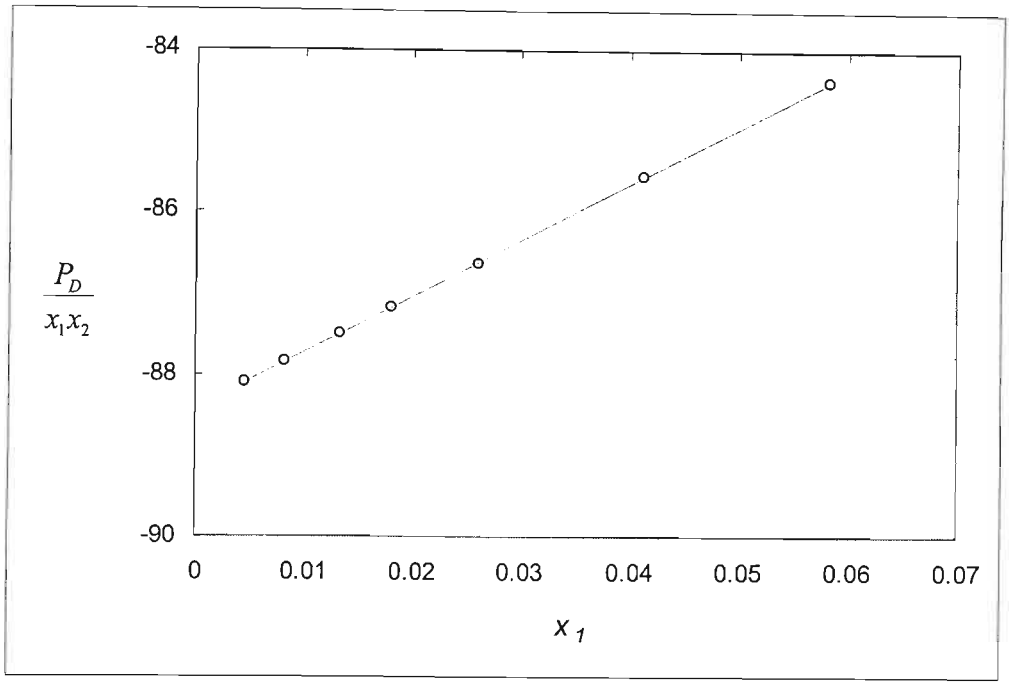

Figure C-7: $\frac{P_D}{x_1 x_2}$ vs. x_1 as $x_1 \rightarrow 0$ for Acetonitrile + N-methylformamide (2) at 363.15 K.

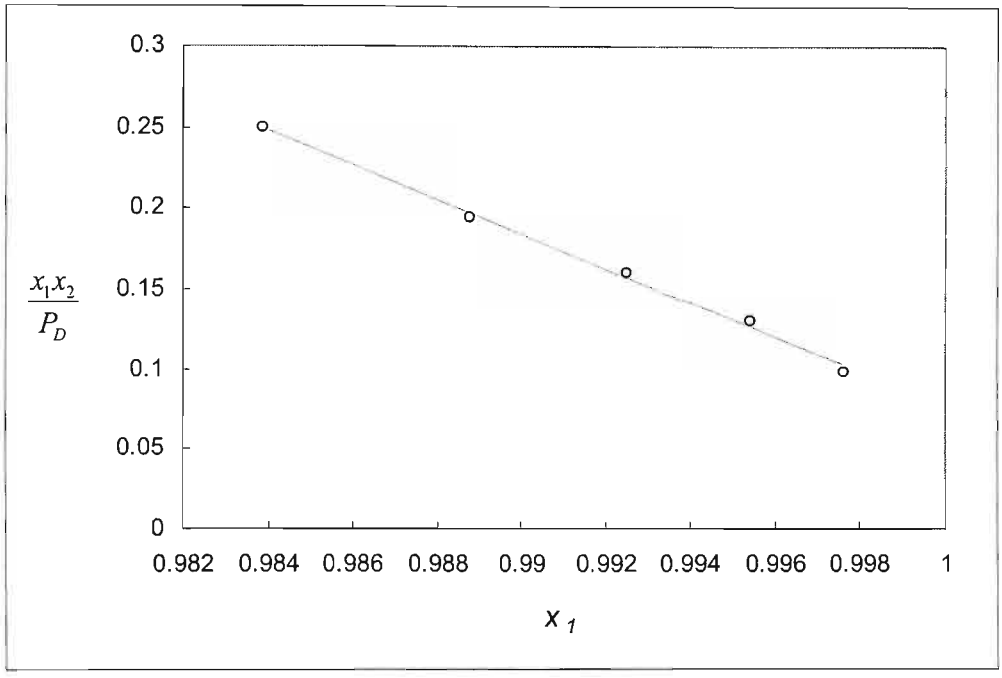

Figure C-8: $\frac{x_1 x_2}{P_D}$ vs. x_1 as $x_1 \rightarrow 1$ for Acetonitrile + N-methylformamide (2) at 363.15 K.

Table C-1 Limiting values obtained from the plots in Figures C-1 to C-8

System	$P_D/(x_1x_2)$		$(x_1x_2x)/P_D$	
	$x_1 = 0$	$x_1 = 1$	$x_1 = 0$	$x_1 = 1$
Hexane (1) + N-methylformamide (2)	-	-	0.000163	0.0104
Benzene (1) + N-methylformamide (2)	434.4	33.33	-	-
Chlorobenzene (1) + N-methylformamide (2)	109.0	-	-	0.0304
Acetonitrile (1) + N-methylformamide (2)	88.43	-	-	0.0770

Table C-2 γ^{∞} values for the four binary systems determined from VLE data at 363.15 K

System	γ_1^{∞} (a)	γ_1^{∞} (b)	γ_1^{∞} (c)
Hexane (1) + N-methylformamide (2)	43.6	30.9	33.6
Benzene (1) + N-methylformamide (2)	4.8	4.5	4.2
Chlorobenzene (1) + N-methylformamide (2)	5.1	5.1	4.9
Acetonitrile (1) + N-methylformamide (2)	1.8	1.9	1.7
System	γ_2^{∞} (a)	γ_2^{∞} (b)	γ_2^{∞} (c)
Hexane (1) + N-methylformamide (2)	523.0	96.9	48.8
Benzene (1) + N-methylformamide (2)	22.6	17.6	18.1
Chlorobenzene (1) + N-methylformamide (2)	16.2	13.8	16.7
Acetonitrile (1) + N-methylformamide (2)	2.4	2.3	7.1

d) Calculated using Wilson parameters

e) Calculated using NRTL parameters

f) Calculated using pressure deviation method

C.2 EXCESS THERMODYNAMIC PROPERTIES

The calculation of excess thermodynamic properties is explained in Chapter Five. The first step is to determine the G^E values from the regressed parameters. The G^E values are then used to plot the $\frac{G^E}{RT}$ vs. T relationship for several x1 values. The well-known Gibbs-Helmholtz equation

$$H^E = -RT^2 \left[\frac{\partial \left(G^E / RT \right)}{\partial T} \right]_{P, x_i} \tag{5-101}$$

is then used to calculate the H^E value where the slope of the $\frac{G^E}{RT}$ vs. T relationship gives the value of $\left[\frac{\partial \left(G^E / RT \right)}{\partial T} \right]$. TS^E values are calculated using Equation 5-102:

$$G^E = H^E - TS^E \tag{5-102}$$

The $\frac{G^E}{RT}$ vs. T relationship is plotted for CO_2 (1) + Naphthalene (2) and CO_2 (1) + Benzoic acid (2) in Figures C-9 and C-10 respectively. G^E, H^E and TS^E values for CO_2 (1) + Naphthalene (2) are given in Table C-3 and for CO_2 (1) + Benzoic acid (2) in Table C-4.

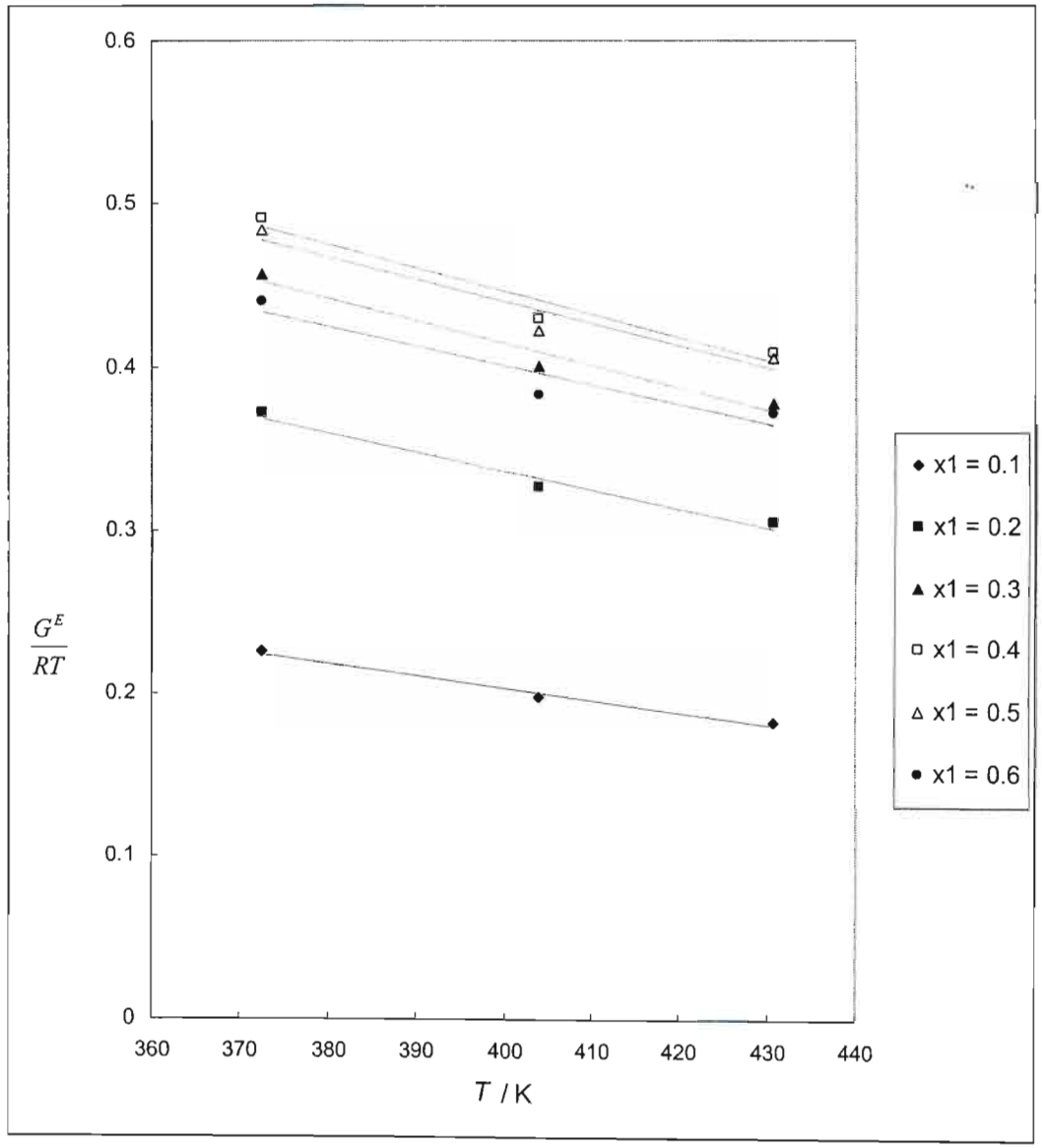

Figure C-9: $\frac{G^E}{RT}$ vs. T relationship for CO_2 (1) + Naphthalene (2).

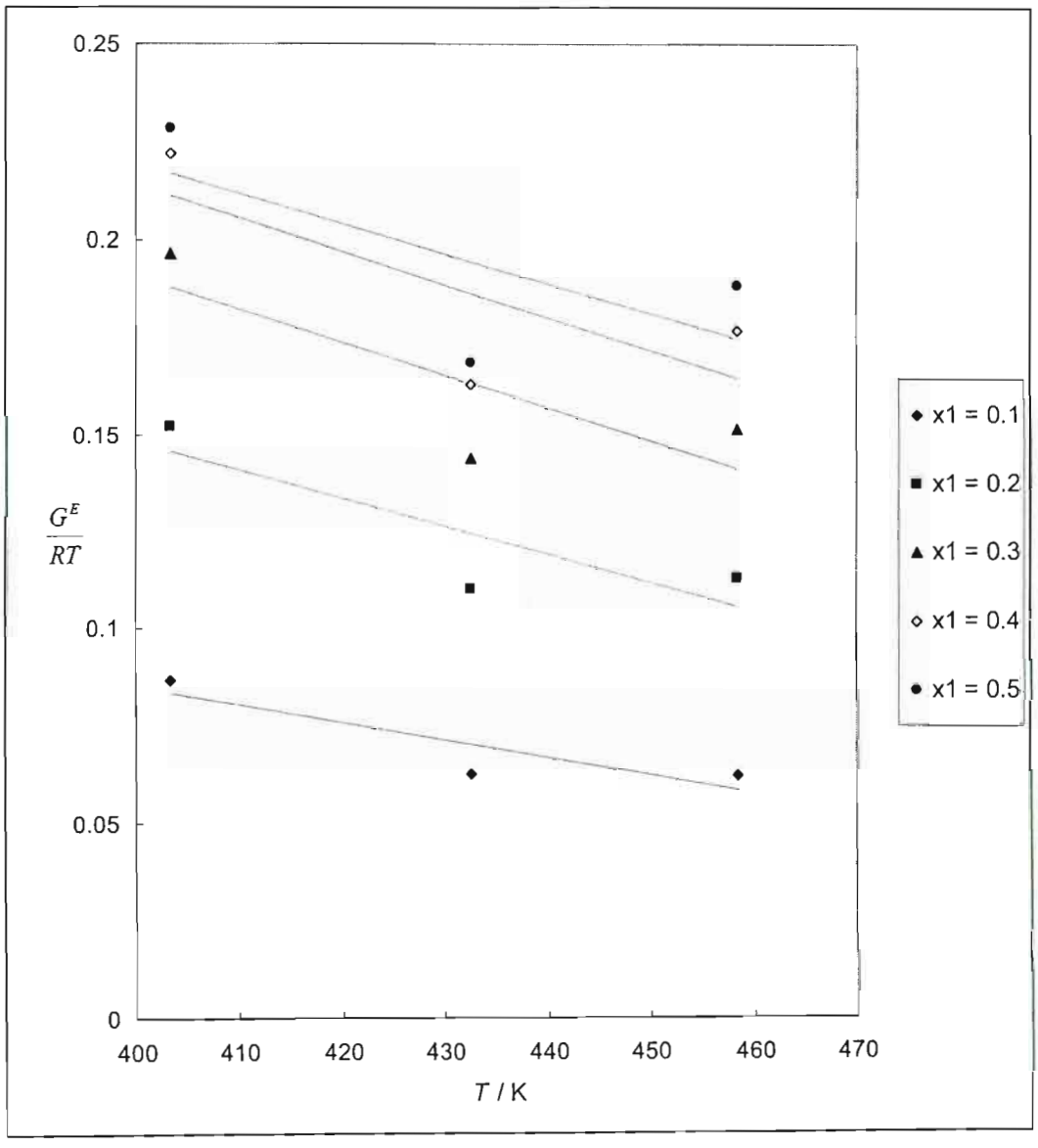

Figure C-10: $\frac{G^E}{RT}$ vs. T relationship for CO_2 (1) + Benzoic acid (2).

Table C-3 Calculated G^E, H^E and TS^E values for CO_2 (1) + Naphthalene (2)

x_1	Excess Properties / J.mol^{-1}		
	G^E	H^E	TS^E
T = 372.45 K			
0.0	0.0	0.0	0.0
0.1	697.6	858.1	160.4
0.2	1152.9	1348.2	195.3
0.3	1415.2	1581.2	166.0
0.4	1520.8	1630.8	110.0
0.5	1496.5	1545.4	49.0
0.6	1362.6	1360.9	-1.7
T = 403.85 K			
0.0	0.0	0.0	0.0
0.1	664.5	1008.8	344.4
0.2	1097.7	1585.1	487.4
0.3	1346.1	1859.0	512.9
0.4	1444.1	1917.3	473.2
0.5	1417.9	1817.0	399.1
0.6	1287.7	1600.0	312.4
T = 430.65 K			
0.0	0.0	0.0	0.0
0.1	652.4	1147.2	494.8
0.2	1091.1	1802.5	711.4
0.3	1353.2	2114.0	760.8
0.4	1467.1	2180.3	713.2
0.5	1454.7	2066.2	611.5
0.6	1333.5	1819.5	486.0

Table C-4 Calculated G^E, H^E and TS^E values for CO_2 (1) + Benzoic acid (2)

x_1	Excess Properties / J.mol^{-1}		
	G^E	H^E	TS^E
T = 403.28 K			
0.0	0.0	0.0	0.0
0.1	290.4	615.2	324.8
0.2	509.0	985.7	476.7
0.3	659.3	1150.7	491.4
0.4	744.2	1153.4	409.2
0.5	766.5	1034.4	267.9
T = 432.62 K			
0.0	0.0	0.0	0.0
0.1	225.0	708.0	483.0
0.2	396.6	1134.4	737.7
0.3	516.4	1324.2	807.8
0.4	585.8	1327.3	741.5
0.5	605.9	1190.4	584.4
T = 458.37 K			
0.0	0.0	0.0	0.0
0.1	236.3	794.8	558.5
0.2	429.0	1273.4	844.4
0.3	575.4	1486.5	911.1
0.4	672.5	1490.0	817.5
0.5	717.0	1336.3	619.3